Patterning of tissue stress responses by JNK and JAK/STAT

Dissertation der Fakultät für Biologie
der Ludwig-Maximilians-Universität München

Andrea Cosolo

München, 2019

Diese Dissertation wurde angefertigt

unter der Leitung von Dr. Anne-Kathrin Classen

im Fachbereich Biologie

an der Ludwig-Maximilians-Universität München

Erstgutachterin: Dr. Anne-Kathrin Classen
Zweitgutachter: Prof. Dr. Nicolas Gompel

Tag der Abgabe: 05.09.2019

Tag der mündlichen Prüfung: 21.11.2019

ERKLÄRUNG

Ich versichere hiermit an Eides statt, dass meine Dissertation selbständig und ohne unerlaubte Hilfsmittel angefertigt worden ist.

Die vorliegende Dissertation wurde weder ganz, noch teilweise bei einer anderen Prüfungskommission vorgelegt.

Ich habe noch zu keinem früheren Zeitpunkt versucht, eine Dissertation einzureichen oder an einer Doktorprüfung teilzunehmen.

München, den 05.09.2019

Andrea Cosolo

Contents

Contents

Abbreviations

Dcp-1	Death caspase-1
DIAP1	Death-associated inhibitor of apoptosis 1
Drice	Death related ICE-like caspase
Dronc	Death regulator Nedd2-like caspase
Egr	Eiger
G2	Gap 2
Hid	Head involution defective
JAK/STAT	Janus kinase/signal transducer and activator of transcription
JNK	Jun N-terminal kinase
MAPK	Mitogen-activated protein kinase
Nub	Nubbin
ROS	Reactive oxygen species
Rn	Rotund
Rpr	Reaper
SASP	Senescence-associated secretory phenotype
Stg	String
UPR	Unfolded protein response

List of publications and declaration of contribution as a co-author

The following list specifies my contribution to each publication, according to the CRediT taxonomy (Brand et al., 2015).

JNK-dependent cell cycle stalling in G2 promotes survival and senescence-like phenotypes in tissue stress
Cosolo A, Jaiswal J, Csordás G, Grass I, Uhlirova M, Classen AK
Elife. 2019 Feb 8;8. pii: e41036. doi: 10.7554/eLife.41036

My contribution includes: conceptualization, ideas and formulation of research goals; development of methodology and design of experimental strategy; performance of experiments and data collection for the entire paper, except for parts of figures 5 I-K, 6 J-M, S7.1 E-K, S7.2 C-J; formal analysis for all figures; validation; data curation; visualization and preparation of all the figures; writing of the original draft, review and editing.

JAK/STAT signalling mediates cell survival in response to tissue stress
La Fortezza M, Schenk M, Cosolo A, Kolybaba A, Grass I, Classen AK
Development. 2016 Aug 15;143(16):2907-19. doi: 10.1242/dev.132340

My contribution includes: ideas; methodology, investigation, formal analysis and visualization of the data presented in Figure S2 A-B',D; manuscript review and editing.

München, 05.09.2019
Andrea Cosolo

Supervisor: Dr. Anne-Kathrin Classen

Summary

The restoration of tissue homeostasis upon injury relies on the spatial and temporal coordination of multiple processes, including damage-induced apoptosis and compensatory proliferation of the surviving neighboring cells. In Drosophila, the JNK pathway plays a central role in tissue stress responses and promotes both apoptosis and proliferation. How activation of the same signaling cascade results in these alternative outcomes and how these responses are spatially patterned is still unclear. We address these questions by studying two distinct regions around the site of injury in Drosophila imaginal discs. Cells at the wound margin, which experience high JNK levels, undergo a JNK-dependent extension of the G2 cell cycle phase. While acute stress conditions induce a transient and reversible G2 stalling that protects from JNK-induced apoptosis, chronic stress results in G2 arrest and promotes paracrine proliferation. We also show that, in cells located at the periphery of the injury site, activation of JAK/STAT plays an essential role by promoting survival of JNK-signaling cells, thereby allowing the execution of JNK-dependent compensatory proliferation. Together, we propose that the apoptotic and proliferative outputs of JNK signaling are balanced in domains proximal to the wound site via G2 stalling and in more distal areas via activation of JAK/STAT.

Zusammenfassung

Die Wiederherstellung der Gewebehomöostase nach einer Verwundung beruht auf räumlicher und zeitlicher Koordination mehrerer Prozesse, einschließlich der verletzungsinduzierten Apoptose und der kompensatorischen Proliferation der überlebenden Nachbarzellen. In Drosophila Imaginalscheiben, ein epitheles Modellsystem, spielt der JNK Signalweg eine zentrale Rolle in der Wundantwort und fördert sowohl Apoptose, als auch Proliferation. Wie die Aktivierung einer Signalkaskade zu unterschiedlichen zellulären Antworten führt und wie diese Antworten räumlich und zeitlich koordiniert werden, ist unklar. Wir haben diese Frage untersucht, indem wir zwei unterschiedliche Regionen in der Umgebung einer in der Imaginalscheibe induzierten Verletzung untersuchten. Zellen, welche sich am Rand der Wunde befinden und hohe JNK Aktivität aufweisen, reagieren mit einer JNK-abhängigen Verlängerung der G2-Phase des Zellzyklus. Während akuter Stress zu einem transienten und reversiblen Anhalten in der G2-Phase führt, welches vor JNK-induzierter Apoptose schützt, führt chronischer Stress zu einem Stillstand in der G2-Phase und einer Überaktivierung parakriner Signale, die die Proliferation der umliegenden Zellen anregt. Zusätzlich konnten wir nachweisen, dass in diesen wund-peripheren, proliferierenden Zellen JAK/STAT Aktivität eine essentielle Rolle spielt, indem es das Überleben der JNK-signalübertragenden Zellen fördert und damit die Ausführung der JNK-abhängigen kompensatorischen Proliferation erlaubt. Wir schlagen ein Modell vor, in dem apoptotische und proliferative Reaktionen auf JNK in wund-proximalen Regionen durch ein Anhalten der G2-Phase balanciert werden und in wund-distalen Regionen durch Aktivierung der JAK/STAT Signalkaskade.

Introduction

Sensing the environment and responding to altered conditions are crucial properties of any biological system. From a single cell integrated in a tissue, to a whole multicellular organism, the maintenance of homeostasis relies on the ability to respond to environmental stress in order to maintain internal stable conditions, thus ensuring proper integrity and function. Cell and tissue homeostasis is continuously challenged by a variety of stressors, including mechanical tissue injury, reactive oxygen species (ROS), ultraviolet irradiation, or oncogenic genetic lesions. At the cellular level, a multitude of conserved stress response mechanisms have evolved, ranging from heat shock response, to protein unfolding response, DNA damage response, or oxidative stress response. While these protective mechanisms can relieve the cellular stress and repair the damage to promote cell survival, excessive cellular damage can also result in the activation of programmed cell death (Fulda et al., 2010). At the tissue scale, cellular stress responses need to be precisely coordinated in space and time to restore tissue homeostasis. The recovery of tissue integrity relies on the controlled balance of cell death, cell survival, cell cycle arrest and cell proliferation. Impairment in the coordination of these processes can result in tissue dysfunction and chronic stress (Eming et al., 2014; Park et al., 2017; Sandoval-Guzman and Currie, 2018). How the activation of cellular stress response pathways results in coordinated spatial and temporal gradients of tissue responses and how these are dynamically interacting is still not completely understood.

1   Models of epithelial stress responses

1.1   Wing imaginal discs: an epithelial model system

Drosophila wing imaginal discs provide a useful epithelial model to study tissue stress responses and regeneration. Thanks to the simple epithelial structure and their high accessibility, combined with the extensive genetic tractability and broad genetic toolkit available in *Drosophila*, imaginal discs are an established platform to study the interactions of

conserved signaling pathways during tissue stress responses (Ahmed-de-Prado and Baonza, 2018; Aldaz and Escudero, 2010; Beira and Paro, 2016; Bergantinos et al., 2010b; Hariharan and Serras, 2017; Worley et al., 2012).

Imaginal discs are larval tissues, and thus precursors of adult epidermal appendages such as wings, legs or eyes. In the larva, a wing imaginal disc presents as a single epithelial layer, closed in a flat sac-like shape. This consists of the disc proper on one side – a densely packed pseudo-stratified epithelium which generates, after metamorphosis, the adult wing blade, hinge and notum – in continuity with the peripodial membrane, on the other side – a squamous epithelium which provides little contribution to the adult cuticle (see also Figure1—figure supplement 1A in Cosolo et al. (2019)). Such relatively simple morphology confers a great advantage for imaging and monitoring of morphological alterations upon tissue damage (Beira and Paro, 2016).

During larval development, wing imaginal discs undergo exponential growth and proliferation. Originating from a cluster of about 50 cells in the embryo, the cell number increases 1000-fold by the end of the larval stages (Garcia-Bellido and Merriam, 1971). The cell-doubling time ranges from about 10 h during the second instar to more than 14 h at the end of the third and last instar (Buttitta et al., 2007; Johnston and Sanders, 2003). Additionally, developmental patterning in this highly proliferative tissue progressively restricts cell identity to region-specific fates (Beira and Paro, 2016).

Decades of work on imaginal discs allowed not only to have an in-depth characterization of its growth parameters and to study the conserved signaling pathways and morphogen gradients involved in development and homeostasis, but also led to the discovery of their capacity to regenerate upon tissue injury (Worley et al., 2012).

1.2   Tissue injury and regeneration paradigms

Classical studies involved the use of technically challenging and laborious microsurgical transplantation techniques, whereby imaginal discs were cut into fragments and cultured *in vivo* by implantation in the abdomen of a larva or an adult female host, where regeneration occurred (Hadorn et al., 1949; Hadorn and Buck, 1962; Schubiger, 1971; Ursprung, 1959). These studies revealed that, when cultured for a sufficient time, fragmented imaginal discs could generate additional tissue by localized cell proliferation, reminiscent of the blastema observed during vertebrate appendage regeneration. The cell fate potential of the cultured fragment could only be tested by its subsequent transplantation into a larval host, analyzing the differentiated structures after metamorphosis.

An alternative method to study imaginal discs regeneration in a more physiological context consists in the bisection of the imaginal disc *in situ* in the intact larvae, by applying

pressure on the disc from outside the cuticle, allowing for wound repair and regeneration to occur in the same living animal (Bryant, 1971). While extremely challenging in its original implementation, the recent usage of genetically encoded fluorescent proteins to directly identify the wing imaginal disc *in vivo* and guide the procedure has dramatically improved the processing time and increased its reproducibility (Diaz-Garcia and Baonza, 2013; Pastor-Pareja et al., 2008; Yoo et al., 2016).

The study of imaginal disc regeneration, however, has been revolutionized in the last decade by the introduction of genetic techniques to induce tissue ablation (Bergantinos et al., 2010a; Herrera et al., 2013; Smith-Bolton et al., 2009). These approaches allow to precisely target the expression of pro-apoptotic genes (*e.g. egr*, *rpr*, *hid*) in specific regions of the wing imaginal discs, for a defined period of time. This is obtained by combining the *Gal4/UAS* system, which allows tissue-specific transgene expression, with a temperature-sensitive allele of the *Gal80* repressor, that enables temporal control over transgene expression by shifting the temperature. Bypassing the need for surgical procedures, these methods have become very popular and have been widely applied to the study of tissue stress responses, including early stress signaling events, wound healing responses, systemic responses, apoptotic and proliferative responses, epigenetic control of plasticity and tissue re-patterning (Brock et al., 2017; Garelli et al., 2012; Harris et al., 2016; Herrera et al., 2013; Herrera and Morata, 2014; Khan et al., 2017; Martin et al., 2017; Repiso et al., 2013; Schuster and Smith-Bolton, 2015; Sun and Irvine, 2011; Worley et al., 2018).

Increased reproducibility, precision of ablation, flexibility in the time of induction and scalability are just some of the advantages of genetic ablation techniques compared to genuine surgical injury methods. However, we are just starting to appreciate also some important differences between the two approaches, *e.g.* in terms of intensity and duration of the stress applied to the tissue. While surgical injury disrupts tissue integrity instantaneously, genetically-induced apoptosis requires a longer time (16-40 h) to cause loss of epithelial integrity and may result in aberrantly high activity levels of stress signaling pathways. In the current work, we took advantage of these differences to explore distinct scenarios of tissue stress responses (acute *vs*. chronic) by using both surgical and genetic techniques. This combination of methods was instrumental to reveal the function of JAK/STAT-dependent cell survival and JNK-dependent cell cycle arrest during tissue stress responses.

2 Signaling responses to tissue stress

2.1 The JNK pathway plays a fundamental role in tissue stress responses

A crucial mediator of tissue stress responses is Jun N-terminal kinase (JNK), an evolutionarily conserved member of the mitogen-activated protein kinase (MAPK) family. In *Drosophila*, JNK protein is encoded by *basket* (*bsk*) and is activated by the JNK kinase (JNKK) Hemipterous (Hep) (Glise et al., 1995; Sluss et al., 1996). This is a substrate of several upstream JNKK kinases, that are activated by a number of intra- and extracellular stimuli. JNK activation results in the phosphorylation the transcription factor AP-1, formed by Jun-related antigen (Jra) and Kayak (Kay) homo- or heterodimers, as well as a variety of other intracellular substrates. AP-1 binds to *TRE* motifs and regulates the transcription of genes responsible for the cellular effects of JNK signaling, including the phosphatase Puckered (Puc) which regulates JNK in a negative feedback loop (Figure 1) (reviewed in Igaki, 2009).

The JNK pathway is triggered by a variety of stresses such as tissue wounding (Bosch et al., 2005; Ramet et al., 2002), apoptosis (Kuranaga et al., 2002; Ryoo et al., 2004; Shlevkov and Morata, 2012), or loss of epithelial polarity (Brumby and Richardson, 2003; Igaki et al., 2009) and has been implicated in a multitude of processes: stress-dependent JNK activation triggers on the one hand the apoptotic cascade to eliminate damaged cells (Moreno et al., 2002; Shlevkov and Morata, 2012), while on the other hand it is important to promote compensatory proliferation during tissue regeneration (Bosch et al., 2008; Martin et al., 2017; Sun and Irvine, 2011). Additionally, it facilitates tissue repair by delaying the larval-pupal transition, via Dilp8 secretion (Colombani et al., 2012; Garelli et al., 2012; Katsuyama et al., 2015). Furthermore, JNK is involved in cytoskeletal rearrangements, tissue remodeling and cell invasion, in various contexts: in development, for example during embryonic dorsal closure (Sluss et al., 1996), imaginal disc eversion and thorax closure (Agnes et al., 1999; Pastor-Pareja et al., 2004; Zeitlinger and Bohmann, 1999); during homeostasis, for example in epidermal wound healing in the adult fly (Ramet et al., 2002) and in imaginal discs (Bosch et al., 2005; Herrera et al., 2013; Mattila et al., 2005); as well as during cancer progression and metastasis (Kulshammer and Uhlirova, 2013; Uhlirova and Bohmann, 2006). Moreover, JNK activity has been associated with both tumor suppression and tumor promoting functions (Ballesteros-Arias et al., 2014; Enomoto et al., 2015; Gerlach et al., 2018; Igaki et al., 2006; Igaki et al., 2009; Perez et al., 2017; Pinal et al., 2018). How activation of the same signaling module can lead to distinct outcomes and how these are balanced is a very active area of research (Pinal et al., 2019).

2.2   Amplification and propagation of JNK signaling and apoptosis

Known targets of JNK signaling include the pro-apoptotic genes *head involution defective* (*hid*) and *reaper* (*rpr*) (Luo et al., 2007; Moreno et al., 2002). Stress stimuli, such as surgical injury or irradiation, result in JNK-dependent apoptosis, which leads to elimination of damaged cells (Bosch et al., 2005). Apoptosis, the main form of programmed cell death, is initiated in *Drosophila* by the activation of pro-apoptotic genes (*hid*, *rpr*, *grim*), which block the activity of the apoptotic inhibitor Diap1. This results in activation of the initiator caspase Dronc, which targets the effector caspases Dcp-1 and Drice, that execute the apoptotic program (Figure 1) (Hay and Guo, 2006).

Strikingly, activation of the apoptotic cascade results in a Dronc-dependent positive feedback loop that increases JNK and p53 activity, which in turn enhance caspase activity and amplify the apoptotic response (Shlevkov and Morata, 2012; Wells et al., 2006). Therefore, stress-induced JNK signaling is self-sustained cell-autonomously via the initiator caspase Dronc (Figure 1).
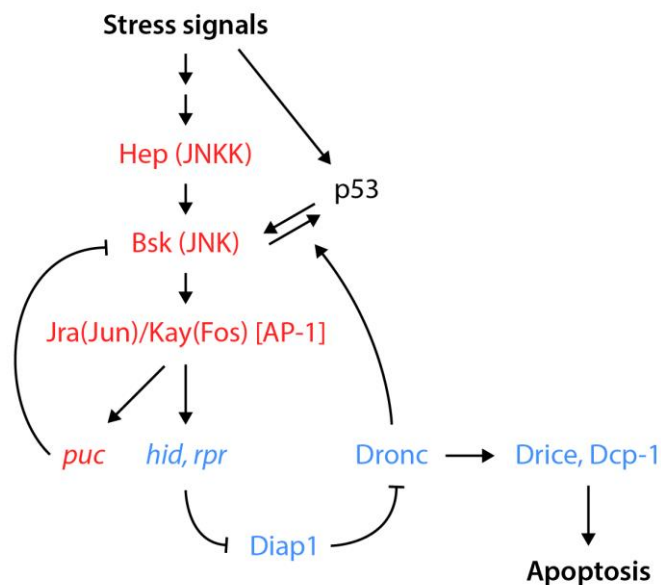
Figure 1: JNK pathway activation leads to apoptosis

The JNK pathway (red) is activated in response to stress signals, leading to the JNK-mediated phosphorylation of the transcription factor AP-1. The target gene *puc* encodes for a phosphatase that negatively regulates JNK. AP-1 also targets the pro-apoptotic genes *hid* and *rpr*, leading to activation of the apoptotic cascade (blue). A positive feedback loop, dependent on the initiator caspase Dronc, amplifies JNK signaling and the apoptotic response.

Importantly, reporters of JNK activity are observed not only in the apoptotic cells, but spread from sites of injury to neighboring cells (Bergantinos et al., 2010a; Bosch et al., 2008; Wu et al., 2010). One mechanism responsible of paracrine activation of JNK is the secretion of

the TNFα homolog Eiger (Egr) (Igaki et al., 2002; Moreno et al., 2002). This pro-inflammatory cytokine is produced by apoptotic cells and is capable of inducing paracrine JNK-dependent apoptosis, a process termed Apoptosis-induced Apoptosis (Figure 2) (Perez-Garijo et al., 2013).

Another upstream trigger of JNK signaling is ROS, which are released at high levels upon tissue damage by dying cells and taken up by the living cells at the wound edge (Brock et al., 2017; Santabarbara-Ruiz et al., 2015). Remarkably, JNK has been shown to induce *moladiez* (*mol*), a Duox maturation factor necessary for ROS production (Khan et al., 2017), thus sustaining JNK signaling in another positive feedback loop. Notably, this process is not dependent on apoptosis. Therefore, upon tissue stress, intracellular ROS participate in sustaining cell-autonomous activation of JNK via *mol*, while extracellular ROS released by dying cells can spread at the wound edge and contribute to non-cell autonomous expansion of JNK signaling (Figure 2).

Taken together, these results show that JNK self-amplifies both cell-autonomously and non-cell autonomously. How this signal amplification is modulated and prevented from excessive and uncontrolled spreading during stress responses is currently not completely understood.

2.3   JNK promotes proliferation

Besides its pro-apoptotic function, JNK has also the ability to stimulate cell-autonomous and non-cell autonomous proliferation, by activating conserved growth pathways and promoting the secretion of mitogenic signals (Figure 2) (Bergantinos et al., 2010a; Grusche et al., 2011; Huh et al., 2004; Katsuyama et al., 2015; Perez-Garijo et al., 2009; Ryoo et al., 2004). Indeed, lineage tracing studies revealed that most of the regenerated tissue comprises cells that activated JNK (Bosch et al., 2008; Katsuyama et al., 2015). How JNK activation results in either cell death or cell proliferation and how this decision is regulated is still unclear (Morata et al., 2011; Pastor-Pareja and Xu, 2013; Perez-Garijo, 2018; Sun and Irvine, 2014). One current view suggests that JNK-dependent apoptosis and proliferation may occur simultaneously and which of these is predominant might depend on the cellular context (Pinal et al., 2019).

One such context where JNK-dependent proliferation is particularly evident is the 'undead' model, where cells are subject to apoptotic stimuli but are artificially kept alive, *e.g*. by expressing the inhibitor of effector caspases *P35*. Undead cells experience high levels of JNK, likely due to the Dronc-dependent positive feedback loop described above, and keep secreting mitogenic factors, which ultimately lead to hyperplastic tissue overgrowths. This phenotype is critically dependent on JNK and is mediated by the conserved ligands Wingless (Wg)/Wnt and Decapentaplegic (Dpp)/TGFβ. Importantly, overgrowth occurs also in non-

apoptotic contexts (*e.g*. *Dronc* mutants) when JNK is activated directly, further highlighting that this effect is strictly dependent on JNK signaling (Perez-Garijo et al., 2009; Ryoo et al., 2004). Remarkably, *wg* and *dpp* are also upregulated upon surgical injury or genetic cell ablation and play an essential role in tissue regeneration (Figure 2) (Katsuyama et al., 2015; McClure et al., 2008; Smith-Bolton et al., 2009).

Another growth pathway implicated in imaginal discs regeneration is Hippo. The JNK-dependent activation of the Hippo pathway effector Yorkie (Yki) is observed not only when JNK is directly activated, but also upon surgical injury, genetic cell ablation, or in tumor contexts (Grusche et al., 2011; Sun and Irvine, 2011, 2013). Upon tissue damage, it occurs both in surviving cells at the wound site and in neighboring cells and is essential for compensatory cell proliferation and wing disc regeneration (Figure 2) (Sun and Irvine, 2011).
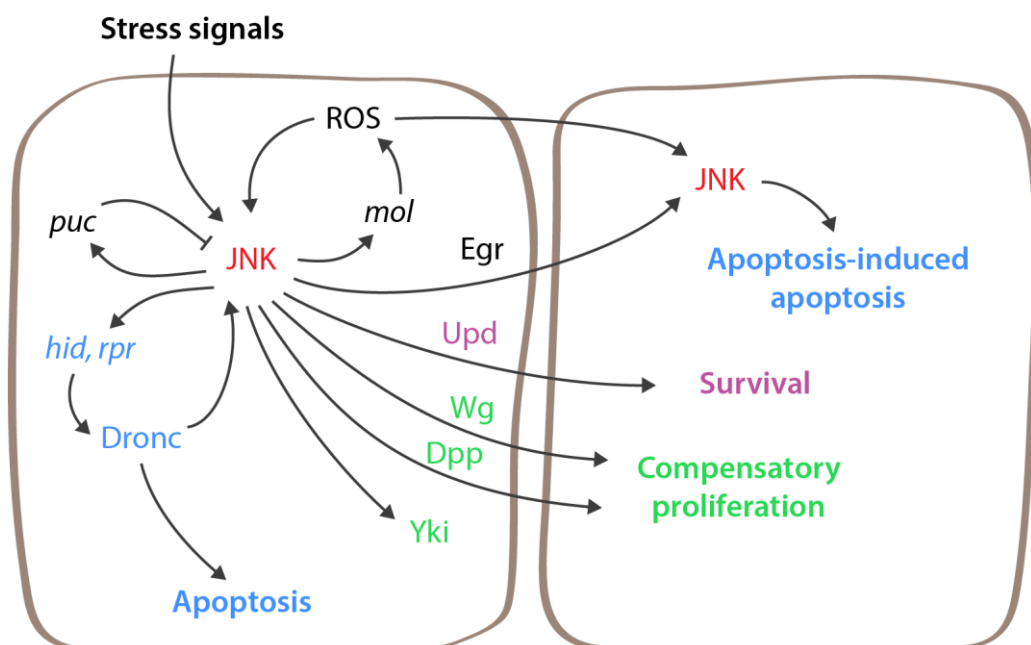
Figure 2: JNK coordinates wing imaginal disc regeneration.

JNK pathway is activated in response to stress signals and is amplified via cell-autonomous and non-cell autonomous mechanisms. JNK activation at the wound site results not only in apoptosis of the damaged cells, but also in cell survival and compensatory proliferation of neighboring cells.

2.4   The role of JAK/STAT during stress responses

Also the JAK/STAT pathway plays a central role in tissue stress responses and regeneration. JNK-dependent expression of cytokine-like ligands of the Unpaired (Upd) family is detected upon tissue injury and cell ablation (Katsuyama et al., 2015; Pastor-Pareja et al.,

2008; Santabarbara-Ruiz et al., 2015) and has both autocrine and paracrine functions (Ahmed-de-Prado et al., 2018; Herrera and Bach, 2019; Katsuyama et al., 2015; Santabarbara-Ruiz et al., 2015; Worley et al., 2018). JAK/STAT activity has been linked to proliferation in the context of development (Bach et al., 2003), neoplastic growth (Classen et al., 2009; Wu et al., 2010) and tissue damage (Pastor-Pareja et al., 2008; Santabarbara-Ruiz et al., 2015; Wu et al., 2010). However, little is known about the targets mediating the proliferative function of JAK/STAT.

With the present work we show evidence supporting a model where JAK/STAT function upon cell ablation is to protect JNK-signaling cells from apoptosis, thereby allowing their survival and the execution of JNK-dependent compensatory functions.

3   Cell cycle regulation during tissue damage and regeneration

As described above, stress-induced removal of damaged cells by apoptosis and compensatory proliferation of the neighboring cells are two essential processes for tissue homeostasis, intimately related. However, cellular stress response pathways do not always induce the elimination of a damaged cell, if the cellular damage is not detrimental or if it can be resolved (Fulda et al., 2010). In the case of a proliferating tissue like the larval imaginal discs, cells can stop proliferating and exit the cell cycle in response to developmental or injury signals. Such cell cycle arrest can either be permanent or transitory, followed by cell cycle re-entry once the damage is repaired (Sun and Buttitta, 2017). How the neighboring tissue responds to localized cell cycle arrest is little understood.

Cellular senescence, a process originally described in mammalian tissue culture cells, is a physiological stress response mechanism characterized by permanent cell cycle arrest in G0 and apoptosis resistance (He and Sharpless, 2017; Hernandez-Segura et al., 2018). Importantly, senescent cells maintain an active role in the tissue, interacting with the local environment by secreting a heterogeneous spectrum of soluble and insoluble proteins, including cytokines, chemokines, growth factors, tissue remodeling factors, collectively referred to as Senescence-Associated Secretory Phenotype (SASP) (Coppe et al., 2010; Czarkwiani and Yun, 2018; Pawlikowski et al., 2013). Although initially thought to represent only an aberrant byproduct of stress responses (Baker et al., 2011), recent reports have highlighted an essential role for senescent cells both during vertebrate development (Davaapil et al., 2017; Munoz-Espin et al., 2013; Storer et al., 2013) and during tissue injury repair (Demaria et al., 2014; Ritschka et al., 2017). In *Drosophila*, although one study described cells with senescent-like properties (Nakamura et al., 2014), the mechanism of cell cycle regulation and the general implications for tissue stress responses are still poorly understood.

While compensatory proliferation in response to tissue damage in imaginal discs is an established concept, a more detailed understanding of the dynamics of cell cycle regulation upon tissue stress is still lacking. Using either surgical injury or genetic ablation techniques, previous reports identified a JNK-dependent localized increase in the proliferation rate (Bergantinos et al., 2010a; Bosch et al., 2008; Herrera et al., 2013; Smith-Bolton et al., 2009; Sustar et al., 2011), as evaluated by the mitotic marker phospho-Histone 3 (pH3) or the incorporation of nucleotide analogs (*e.g*. BrdU, EdU), labeling cells in S-phase. However, a precise spatial and temporal description of the cell cycle progression upon injury is still missing. Moreover, some differences in the extent to which proliferation is localized and in the dynamics of the response have been reported (Herrera et al., 2013), depending on which pro-apoptotic gene was used to induce cell ablation, possibly reflecting the rate of cell killing.

Here we use a combination of methods, including a novel set of cell cycle reporters, to identify a previously undetected cell cycle arrest in G2, occurring in the cells located at the wound site. This reversible cell cycle arrest, which we term 'G2 stalling', is JNK-dependent and promotes survival and mitogenic signaling, qualities reminiscent of senescent cells.

Aim of study

The overall aim of this study was to investigate the spatial and temporal gradients of cellular signals and the resulting cell behaviors in response to tissue stress. Specifically, we wanted to understand how the activation of JNK signaling, a crucial stress response pathway, results in distinct outcomes such as removal of the damaged cells by apoptosis and compensatory proliferation of the surviving neighboring cells. We addressed this question using different approaches to induce tissue damage in the wing imaginal discs of *Drosophila*, an established epithelial model system.

Having discovered that the cells at the wound site undergo a transient cell cycle arrest in G2 phase that is JNK-dependent, we first aimed to identify the cell cycle regulators implicated in this process, which then allowed us to experimentally interfere with G2 stalling and investigate its function. Since JNK is implicated both in acute and chronic stress responses, we also sought to elucidate whether JNK-dependent G2 stalling occurred in both conditions, allowing us to identify distinct functions of G2 stalling that include protection from apoptosis and paracrine mitogenic signaling.

To complement this study on cell behavior proximal to the wound site, we also focused on the cells located in domains distal to it, where JAK/STAT is known to play an important role. With the aim to elucidate the signaling crosstalk between JNK and JAK/STAT in this domain, we identified a novel function of JAK/STAT in promoting cell survival.

Results

4   JNK-dependent cell cycle stalling in G2 promotes survival and senescence-like phenotypes in tissue stress

Cosolo A, Jaiswal J, Csordás G, Grass I, Uhlirova M, Classen AK

Permission to reproduce the full article in this thesis has been obtained.

JNK-dependent cell cycle stalling in G2 promotes survival and senescence-like phenotypes in tissue stress

Andrea Cosolo[1,2], Janhvi Jaiswal[3], Gábor Csordás[4,5], Isabelle Grass[2,6,7], Mirka Uhlirova[4,5,8], Anne-Kathrin Classen[2,6,7]*

[1]Center for Biological Systems Analysis, University of Freiburg, Freiburg, Germany; [2]Faculty of Biology, Ludwig-Maximilians-University Munich, Munich, Germany; [3]Spemann Graduate School of Biology and Medicine (SGBM), University of Freiburg, Freiburg, Germany; [4]Cologne Excellence Cluster on Cellular Stress Responses in Aging-Associated Diseases (CECAD), University of Cologne, Cologne, Germany; [5]Institute for Genetics, University of Cologne, Cologne, Germany; [6]Centre for Biological Signalling Studies (BIOSS), University of Freiburg, Freiburg, Germany; [7]Centre for Integrative Biological Signalling Studies (CIBSS), University of Freiburg, Freiburg, Germany; [8]Center for Molecular Medicine Cologne, University of Cologne, Cologne, Germany

Abstract The restoration of homeostasis after tissue damage relies on proper spatial-temporal control of damage-induced apoptosis and compensatory proliferation. In *Drosophila* imaginal discs these processes are coordinated by the stress response pathway JNK. We demonstrate that JNK signaling induces a dose-dependent extension of G2 in tissue damage and tumors, resulting in either transient stalling or a prolonged but reversible cell cycle arrest. G2-stalling is mediated by downregulation of the G2/M-specific phosphatase String(Stg)/Cdc25. Ectopic expression of *stg* is sufficient to suppress G2-stalling and reveals roles for stalling in survival, proliferation and paracrine signaling. G2-stalling protects cells from JNK-induced apoptosis, but under chronic conditions, reduces proliferative potential of JNK-signaling cells while promoting non-autonomous proliferation. Thus, transient cell cycle stalling in G2 has key roles in wound healing but becomes detrimental upon chronic JNK overstimulation, with important implications for chronic wound healing pathologies or tumorigenic transformation.
DOI: https://doi.org/10.7554/eLife.41036.001

Introduction

Stress signaling pathways activated by tissue injury set up precise spatio-temporal patterns of apoptosis, proliferation and survival that are required to repair a tissue (*Fuchs and Steller, 2015*; *Sun and Irvine, 2014*). Accordingly, deregulation of injury-induced signals and cell behaviors are associated with ageing or pathologies, such as non-healing chronic wounds and cancer (*Martin and Nunan, 2015*; *Neves et al., 2015*; *Taniguchi and Karin, 2018*). However, how injury-induced signals precisely balance proliferation and apoptosis to restore a tissue of the correct size is still not fully understood.

Cell proliferation during tissue repair is regulated by controlling cell cycle progression, promoting re-entry of quiescent cells into the cell cycle or accelerating cell division rates. In contrast to acceleration, tissue stress can also induce cell cycle arrest. Excess cellular damage or deregulated signaling environments cause cells to arrest in G0 and enter senescence - a state characterized by resistance

to apoptosis and senescence-associated secretory phenotypes (SASP) (*Hernandez-Segura et al., 2018*; *Neves et al., 2015*; *Pluquet et al., 2015*; *Salama et al., 2014*). SASP is linked to persistent production of signaling molecules, secretion of ECM degrading enzymes, as well as an upregulation of autophagy, unfolded protein response (UPR), ROS and an increase in cell size (*Hernandez-Segura et al., 2018*; *Neves et al., 2015*; *Pluquet et al., 2015*; *Salama et al., 2014*). Strikingly, recent studies suggest that senescent cells are required at wound sites to promote wound closure and cell plasticity (*Demaria et al., 2014*; *Ritschka et al., 2017*) and in development to promote morphogenesis of embryonic structures (*Davaapil et al., 2017*; *Muñoz-Espín et al., 2013*). Thus, while cell cycle arrest and senescence are often considered to be an aberrant by-product of stress responses, it emerges that arrested cells interface in a little appreciated way with physiological events during tissue regeneration.

Drosophila imaginal discs (*Figure 1—figure supplement 1A*) have provided deep insights into stress signals and responses to tissue injury. The JNK/MAPK-cascade is among the earliest pathways activated by physical wounding (*Bosch et al., 2005*; *Rämet et al., 2002*), loss of epithelial polarity (*Igaki, 2009*; *Igaki, 2009*) or apoptosis (*Ryoo et al., 2004*; *Shlevkov and Morata, 2012*). JNK activates multiple transcription factors, such as AP-1 (*Eferl and Wagner, 2003*; *Külshammer et al., 2015*), and is required for wound closure (*Bosch et al., 2005*; *Ríos-Barrera and Riesgo-Escovar, 2013*), elimination of damaged cells (*Chen, 2012*; *Moreno et al., 2002*; *Shlevkov and Morata, 2012*) and compensatory proliferation replacing lost tissues (*Bergantiños et al., 2010*; *Bosch et al., 2008*; *Ryoo et al., 2004*; *Sun and Irvine, 2014*). Feed-back loops acting through ROS, p53 and the initiator caspase Dronc maintain JNK activity until tissue homeostasis is restored (*Brock et al., 2017*; *Khan et al., 2017*; *Shlevkov and Morata, 2012*; *Wells et al., 2006*). However, how JNK signaling is balanced to eliminate damaged cells and to promote compensatory proliferation is little understood.

Apoptotic cells stimulate compensatory proliferation of the surrounding tissue by JNK-dependent activation of growth and survival pathways including Hippo/Yorkie and JAK/STAT (*Fuchs and Steller, 2015*; *Pastor-Pareja and Xu, 2013*; *Sun and Irvine, 2011*; *Zielke et al., 2014*). Importantly, preventing execution of apoptosis in damaged, aberrant or tumorigenic cells causes chronic signaling and non-autonomous overgrowth in fly tissues (*Fuchs and Steller, 2015*; *Herz et al., 2006*; *Martín et al., 2009*; *Pastor-Pareja and Xu, 2013*; *Pérez-Garijo et al., 2004*; *Pérez-Garijo et al., 2009*; *Ryoo et al., 2004*; *Uhlirova et al., 2005*). However, which autonomous and non-autonomous mechanisms drive compensatory proliferation remains to be fully elucidated.

We employ surgical injury of wing imaginal discs (*Bryant, 1971*; *Yoo et al., 2016*) and cell ablation induced by pro-apoptotic transgenes (*Herrera et al., 2013*; *Smith-Bolton et al., 2009*) to study how injury-induced JNK signaling, compensatory proliferation and survival unexpectedly link to control of cell cycle progression. While stress-induced cell cycle arrest and senescence in flies are little understood (*Nakamura et al., 2014*; *Wells et al., 2006*), we propose that JNK-induced G2 stalling exhibits senescence-like qualities in *Drosophila*.

Results

Tissue injury induces a transient G2-shift

To investigate how imaginal disc regeneration may be regulated by cell cycle progression, we induced acute surgical injury of wing imaginal discs in situ. Consistent with previous reports (*Bosch et al., 2005*; *Mattila et al., 2005*; *Rämet et al., 2002*), we observed activation of the JNK reporter *puc*-LacZ near the wound site 6 hr post-injury (*Figure 1A–B*). Strikingly, upregulation of the JNK reporter coincided with a pronounced shift of cells towards a G2-dominated cell cycle profile visualized by the G2-specific FUCCI reporter mRFP-NLS-CycB$^{1-266}$ (*Figure 1A',B'*; *Figure 1—figure supplement 1B,C*) (*Zielke et al., 2014*). We confirmed this finding by flow cytometry, where cells from injured imaginal discs positive for the alternative JNK-reporter *TRE*-RFP (*Chatterjee and Bohmann, 2012*) exhibited a pronounced G2-shift (*Figure 1D,E*). This response could be narrowed down to the injured pouch domain by flow cytometry analysis of *rotund(rn)-GAL4, UAS-GFP* expressing cells, which normally have little *TRE*-activity (*Figure 1—figure supplement 1D-E'*). Importantly, injury-induced JNK-activity and the G2-profile were transient events, as both decreased by 16 hr post-injury (*Figure 1C,C'*). These observations suggest that JNK activity correlates with a G2 cell
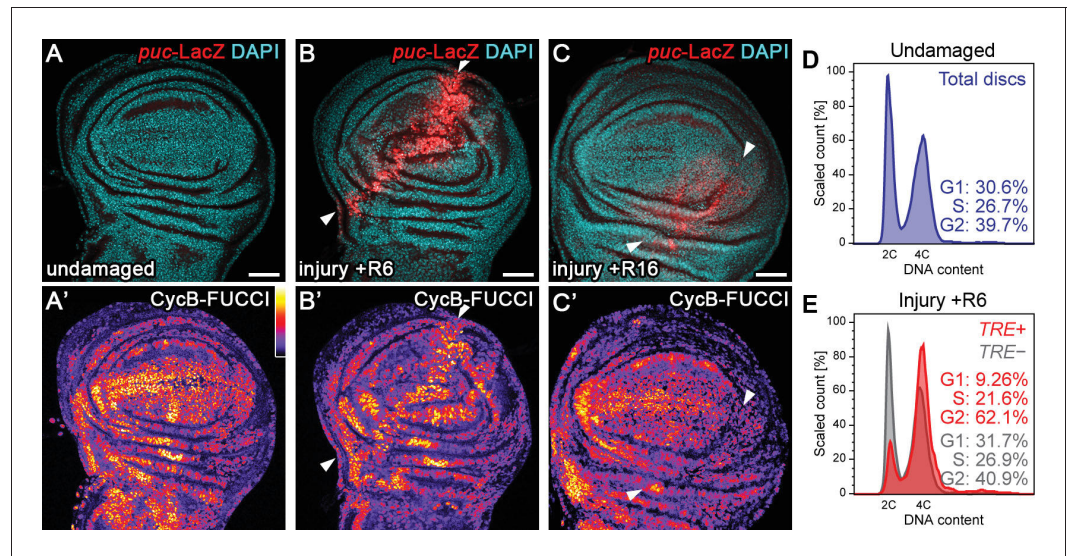
Figure 1. Tissue injury induces a transient G2-shift. (A–C') Undamaged control wing disc (A), a wing disc with surgical damage 6 hr (B) or 16 hr (C) into the recovery (R) period. Wing discs were counterstained with DAPI (cyan in A-C) and express the JNK-reporter *puc*-LacZ (red in A-C) as well as the G2-specific FUCCI reporter *ubi-mRFP-NLS-CycB*[1-266] (see **Figure 1—figure supplement 1B,C**) visualized using a thermal LUT (A'–C'). Arrows indicate injury axis (B,C). A quantification of JNK reporter (*TRE*-RFP) activity over time is presented in **Figure 5M**. (D–E) Flow cytometry analysis of DNA content in undamaged control wing discs (D) and wing discs with surgical damage 6 hr into the recovery period (E). JNK-signaling cells in damaged discs were detected by activation of *TRE*-RFP. *TRE*-RFP positive cells in undamaged control discs represent only a 2.5% of the total cell population and are thus not separately visualized. Detected events were plotted as counts scaled to mode against fluorescence intensity of the DNA stain Hoechst. Scale bars: 50 μm.
DOI: https://doi.org/10.7554/eLife.41036.002

The following figure supplement is available for figure 1:

Figure supplement 1. Tissue injury induces a transient G2-shift.
DOI: https://doi.org/10.7554/eLife.41036.003

cycle profile and that this correlation may be a transient component of physiological wound healing processes.

Stress-dependent JNK activity correlates with G2-stalling

To more quantitatively investigate this cell cycle shift, we turned to models of tissue injury and regeneration based on targeted expression of pro-apoptotic transgenes. We first induced expression of *TNFα/eiger* (*egr*) under the control of *rnGAL4* on developmental day 7, and limited expression to 24 hr by a temperature-sensitive GAL80-repressor (*rn^ts^>*) (**Figure 2—figure supplement 1A**). As described previously, we observed extensive cell death resulting in reduced adult wing sizes (**Herrera et al., 2013**; **La Fortezza et al., 2016**; **Smith-Bolton et al., 2009**) and broad activation of the JNK-reporter *TRE*-RFP in and around *egr*-expressing cells (**Figure 2—figure supplement 1B,C**) (**La Fortezza et al., 2016**). Importantly, FUCCI assays revealed a pronounced G2-shift of cells at the center of *egr*-expressing domains (**Figure 2A,B**). Flow cytometry analysis confirmed that cells positive for *TRE*-RFP (**Figure 2C,C'**), and particularly the GFP-labeled lineage of *egr*-expressing cells (**Figure 2—figure supplement 1B',C'**), exhibit a pronounced G2-profile. The marked cell cycle changes prompted us to investigate if JNK-signaling cells were actively cycling. EdU incorporation assays (**Figure 2A,B,D**) and staining for phospho-Histone 3 (pH3) (**Figure 2E,F**) revealed that DNA replication activity and mitotic cells were absent from G2-shifted, *TRE*-positive domains in *egr*-expressing discs. Of note, *TRE*-positive G2 cells were larger in size than G2 cells from undamaged control discs (**Figure 2—figure supplement 1D**). Combined, these observations confirm a pronounced correlation between injury-induced JNK activity and a G2-dominated cell cycle observed in surgically injured discs and suggest that the G2 profile represents a cell cycle arrest.
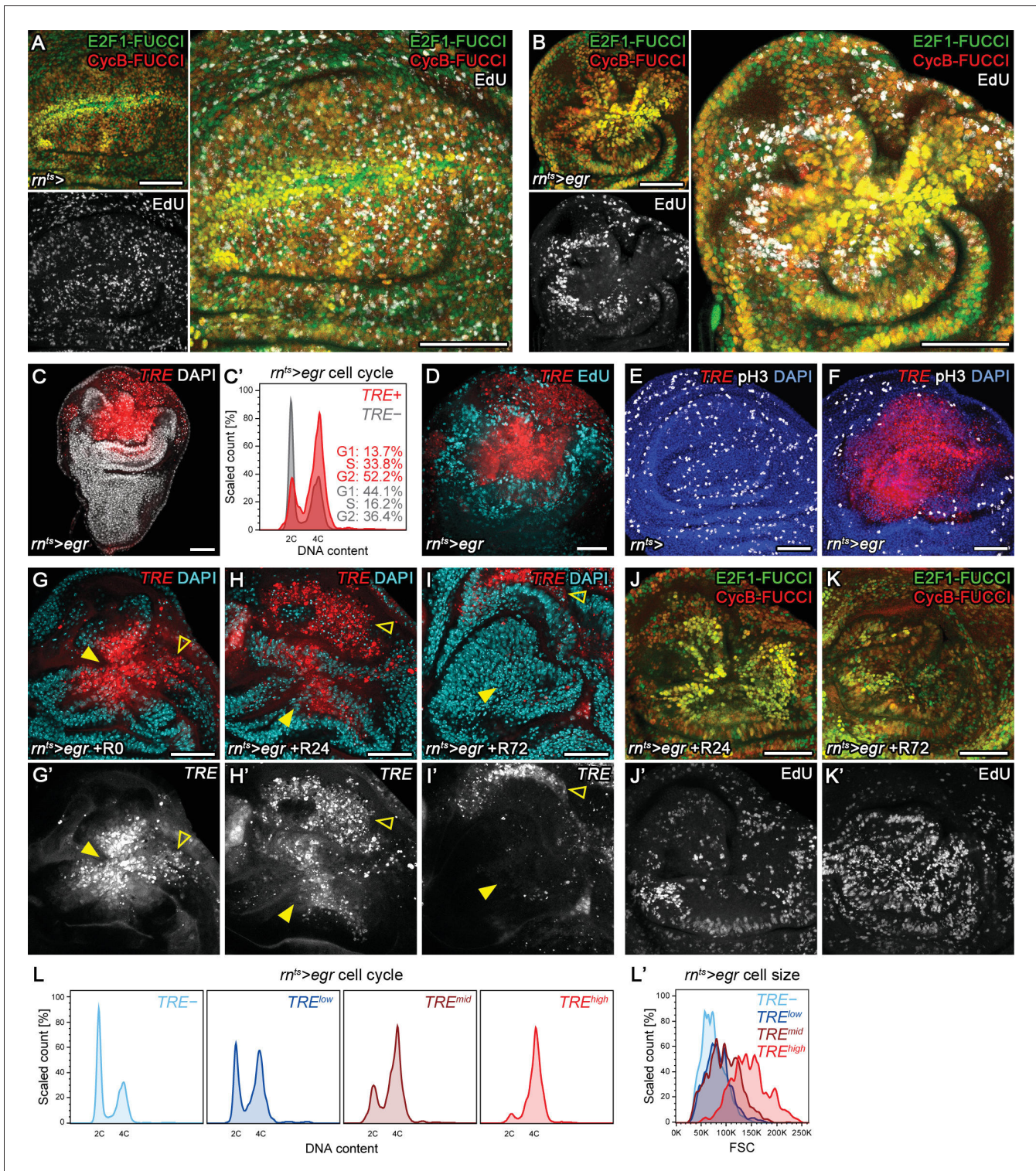
Figure 2. Stress-induced JNK activity correlates with G2-stalling. (**A,B**) Control wing disc (**A**) and a wing disc at 0 hr into the recovery period, after 24 hr of *egr*-expression in the pouch domain (**B**) (see *Figure 2—figure supplement 1A*). Discs also express the complete FUCCI reporter system consisting of *ubi*-mRFP-NLS-CycB$^{1-266}$ (red) and *ubi*-GFP-E2f1$^{1-230}$ (green) and were analyzed for EdU incorporation (grey) to reveal DNA replication activity. The field of view includes the pouch and hinge domain of the disc. The horizontal G1 and G2 pattern in control discs (**A**) represents normal developmental pattern at the dorsal-ventral compartment boundary. Note the intensely labeled G2-cells lacking EdU incorporation activity at the center of the folded pouch tissue in the *egr*-expressing disc (**B**). (**C**) JNK-signaling cells in *egr*-expressing discs were detected by activation of *TRE*-RFP (red). Discs were

Figure 2 continued on next page

We wanted to investigate the fate of G2-arrested cells and understand if they reversed to active cycling after *egr*-expression had ceased. Previous lineage tracing of *rnGAL4* positive cells surviving *egr*-expression indicated that mitotic rates increase 24 hr into the recovery period, which is followed by an increase in total volume of this population by 48 hr (please refer to Figure 1A,D,F in La Fortezza et al., 2016). To independently confirm that G2-arrested cells resume mitotic activity and cellular growth, we analyzed how JNK and cell cycle activity changed during the recovery period. When we analyzed *TRE*-activity in *egr*-expressing discs at 24 hr into the recovery period, we observed decreasing but still pronounced JNK activity (*Figure 2G-H'*). FUCCI analysis and EdU incorporation indicated the presence of G2 cells but also of isolated events of DNA replication activity at the center of the pouch (*Figure 2J,J'*). However, 72 hr into the recovery period, *TRE*-reporter activity was strongly reduced (*Figure 2I,I'*), and FUCCI as well as EdU incorporation assays revealed actively cycling cells (*Figure 2K,K'*). Combined, these results suggest that JNK-induced stalling of the cell cycle in G2 is reversible. However, unlike surgical injury where JNK-activity declined by 16 hr, stalling persisted much longer in *egr*-expressing discs. This temporal correlation between JNK activity and G2-stalling is also reflected by dose-sensitive responses. Specifically, *TRE*-reporter activity scaled with the proportion of cells in G2 and also with stalling-associated increase in cell size (*Figure 2L,L'*). We thus suggest that injury-induced stalling of cells in G2 represent a dose-dependent response to spatio-temporal JNK activity. For our study, we will use the term *stalling* to refer to a transient G2 shift induced by temporally limited JNK activation and use the term *arrest* when we want to emphasize prolonged stalling of G2 in response to high and persistent JNK activity.

JNK activity is necessary and sufficient for G2 stalling

The strong correlation between JNK-activity and a G2-dominated profile indicated a direct regulation of G2-stalling by JNK. To test this hypothesis, we transiently expressed a constitutively active form of JNKK Hemipterous (*hep^{ACT}*) in the disc pouch using *rnGAL4*. FUCCI analysis indeed revealed a cell cycle shift towards G2 and absence of DNA replication (*Figure 3A,A'*), indicating that JNK is sufficient to induce G2-stalling. Testing the necessity of JNK for G2-stalling in *egr*-expressing disc is challenging, because interference with JNK abolishes the apoptotic stimuli mediating *egr*-induced cell death (*La Fortezza et al., 2016*). To circumvent this issue, we applied acute surgical injury to wing imaginal discs expressing a dominant-negative form of the JNK Basket (*bsk^{DN}*) in the posterior compartment using *enGAL4*. As expected, inhibition of JNK blocked upregulation of the JNK-reporter *puc-LacZ* in the posterior compartment of injured discs (*Figure 3B*). Importantly, it also prevented a cell cycle shift towards G2 at the site of injury (*Figure 3B'*). Taken together, these data demonstrate that JNK-signaling in response to tissue damage is sufficient and necessary to induce G2-stalling.

To test if G2 stalling was a general response to JNK activation, we investigated if developmentally patterned JNK activity was associated with cell cycle changes. JNK in the wing peripodium is
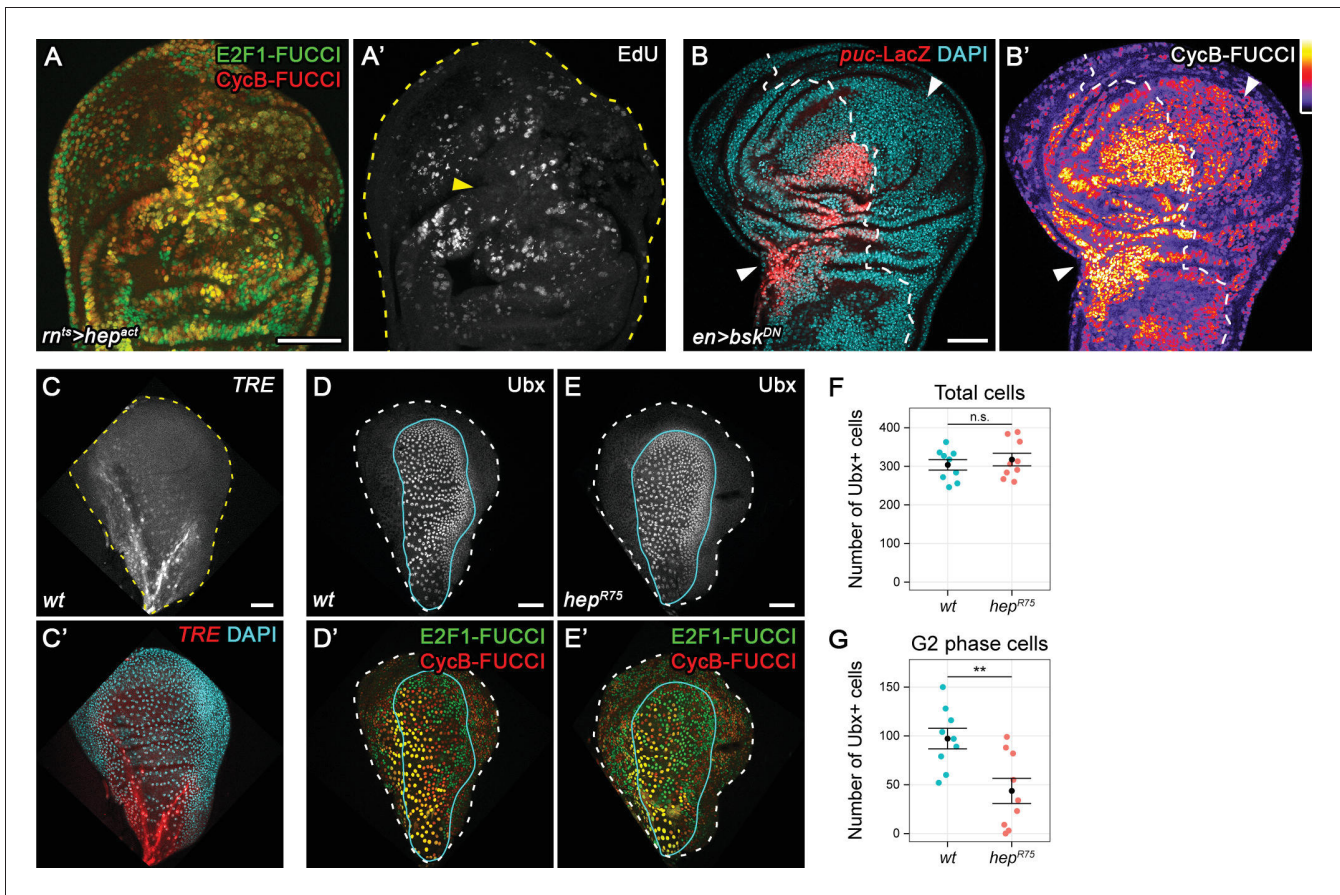
Figure 3. JNK activity is necessary and sufficient for G2-stalling. (**A,A'**) A wing disc expressing a constitutively active JNKK *hep*[ACT] in the pouch, assayed by FUCCI reporters (**A**) and EdU incorporation (**A'**) for cycling cells. At the center of the pouch, a G2-shifted cell population lacks EdU incorporation (arrow in **A'**). (**B,B'**) A wing disc with surgical damage 6 hr into the recovery period and expressing *bsk*[DN] in the posterior compartment (on the right-hand side of the dotted line) under control of *engrailed(en)GAL4*. Wing discs were counterstained with DAPI (cyan) and express the JNK-reporter *puc-LacZ* (red) as well as the G2-specific FUCCI reporter *mRFP-NLS-CycB*[1-266] (thermal LUT). Arrows indicate axis of surgical injury verified by tissue deformation in basal sections. (**C,C'**) The peripodium of a wild type disc counterstained with DAPI (cyan in **C'**) and expressing the JNK-reporter *TRE*-RFP (**C**, red in **C'**). JNK signaling in the wing peripodium is required for wing eversion at the larval-pupal transition (***Pastor-Pareja et al., 2004***). (**D–E'**) The peripodium of size-matched wild type (**D,D'**) and *hep*[R75] hemizygous mutant discs (**E,E'**) stained for Ubx (gray in **D,E**, outlined in cyan) and expressing both FUCCI reporters (**D',E'**). (**F–G**) Quantifications of the total number of Ubx-positive cells (**F**) and of the Ubx-positive cells in G2 (**G**) in wild type and *hep*[R75] hemizygous mutant discs. Graphs display mean ± SEM for *wt*, n = 9 and *hep*[R75], n = 9 discs. *U*-tests were performed to test for statistical significance, n.s. = non significant, **p=0.011. Maximum projections of multiple peripodial confocal sections are shown in **C-E'**. Scale bars: 50 μm.

DOI: https://doi.org/10.7554/eLife.41036.006

The following figure supplements are available for figure 3:

Figure supplement 1. JNK activity is necessary and sufficient for G2-stalling.

DOI: https://doi.org/10.7554/eLife.41036.007

Figure supplement 2. DNA damage is not rate-limiting for G2 stalling.

DOI: https://doi.org/10.7554/eLife.41036.008

required for disc eversion (***Pastor-Pareja et al., 2004***). Strikingly, *TRE* activity in the peripodium correlated with a G2 profile and absence of DNA replication (***Figure 3C, C'***, ***Figure 3—figure supplement 1A,A'***). To test if JNK was necessary for this developmentally regulated G2 profile, we suppressed JNKK activity in the entire larva by hemizygosity for *hep*[R75], a pupal lethal allele of *hep* (***Glise et al., 1995***). Indeed, the peripodium of size-matched *hep*[R75] discs displayed a significant reduction in the number of G2 cells and an increase in G1-phase cells, if compared to wild type discs (***Figure 3D-G***, ***Figure 3—figure supplement 1B-E***). Combined, these observations indicate that JNK

is at least partially necessary for one example of developmentally regulated G2-stalling in the absence of tissue damage.

The observation that JNKK was required for developmentally patterned G2 stalling suggested that JNK itself rather than tissue damage per se induces these cell cycle changes. In agreement with this hypothesis, we observed no correlation between the occurrence of γH2Av, a marker of dsDNA breaks (*Khurana and Oberdoerffer, 2015*), and G2-stalling in *egr*-expressing discs (*Figure 3—figure supplement 2A-A''*). Moreover, neither knock-down of the DNA damage sensing and relay components *chk1 (grp)*, *ATR (mei-41)*, nor organismal hemizygosity for *mei-41^{RT1}* prevented the appearance of a G2-dominated FUCCI profile in *egr*-expressing discs (*Figure 3—figure supplement 2B-D*). We conclude that DNA damage per se, normally a potent inducer of G2/M arrests (*Sancar et al., 2004*; *Song, 2005*), is not a rate-limiting driver of G2-stalling. Yet, DNA damage or damage of other cellular components could contribute to G2-stalling via activation of JNK. Importantly, however, activation of JNK could integrate both damage and developmental signals with cell cycle control.

Regulation of Cdc25/String and Tribbles is rate-limiting for G2 stalling

We next aimed to understand which cell cycle regulator may be targeted by JNK to promote G2-stalling. Knock-down of *Cdk1* in the wing pouch induced a dramatic shift of the FUCCI profile, resembling the shift observed in *egr*-expressing discs (*Figure 4—figure supplement 1A,B*). This suggests that a lack of Cdk1 activity may arrest JNK-signaling cells. A rate limiting activator of Cdk1 during the G2/M transition is the Cdc25-type phosphatase String (Stg) (*Edgar et al., 2001*; *Kimelman, 2014*; *Kiyokawa and Ray, 2008*), whose proteasomal degradation is regulated by Tribbles (Trbl) (*Mata et al., 2000*; *Seher and Leptin, 2000*). We first analyzed a GFP trap inserted in the *stg* locus (*Buszczak et al., 2007*). Of note, the *stg*-GFP chromosome is lethal and GFP expression fails to track with cell cycle phase in individual cells (*Figure 4—figure supplement 1E-E''*), suggesting that the trap disrupts *stg* function and does not give rise to a Stg-GFP fusion protein that is faithfully degraded during the cell cycle. However, expression of GFP from the locus reflects previously published tissue-level expression patterns of *stg* transcripts (*Figure 4—figure supplement 1F-G'''*) (*Johnston and Edgar, 1998*; *Thomas et al., 1994*), indicating that the trap behaves as a reporter of *stg* transcription. We observed that expression of the *stg*-GFP trap was dramatically downregulated in G2-shifted cells of *egr*-expressing discs (*Figure 4A-B'*) suggesting that *stg* transcription was reduced. A GFP-tagged Tribbles protein (*Nagarkar-Jaiswal et al., 2015*; *Otsuki and Brand, 2018*) was highly upregulated in *egr*-expressing and surgically injured discs (*Figure 4C-E*) in a manner that was dependent on JNK activity (*Figure 4E*). Thus, JNK-activity seperately impinges on *stg* transcription and Trbl availability, potentially underlying stalling of cells in G2 in parallel pathways.

We thus wanted to test, if targeted overexpression of *stg* or knockdown of *trbl* can suppress JNK-induced G2-stalling. While *stg* overexpression and *trbl* RNAi-mediated knockdown in the wild type disc reduces developmental G2-patterns at the dorsal-ventral compartment boundary (*Figure 4—figure supplement 1C,D*), we and previous studies (*Mata et al., 2000*; *Neufeld et al., 1998*; *Reis and Edgar, 2004*) failed to detect pronounced alterations in proliferation patterns (*Figure 4—figure supplement 1H-I''*) or adult wings (*Figure 4—figure supplement 1J-L*), suggesting that overexpression of *stg* or knockdown of *trbl* causes little changes to wing development. Importantly, overexpression of *stg* and or knockdown of *trbl* in *egr*-expressing cells re-established a heterogeneous FUCCI cell cycle profile (*Figure 4F-H*). Specifically, cycling cells in *egr,stg*-coexpressing domains could be detected by EdU incorporation and pH3 labeling (*Figure 4I-J'*). Combined, these observations suggest that *trbl* and *stg* are rate limiting for cell cycle progression in JNK-signaling cells and that overexpression of *stg* or knockdown of *trbl* is sufficient to override damage-induced cell cycle stalling in G2.

Chronic stalling in G2 interferes with proliferative capacity

Having identified two potent suppressors of G2-stalling, we asked what role stalling may have in tissue stress responses. We focus in the following experiments on *stg*, as a more direct cell cycle effector. *egr*-expressing discs normally present with a folded architecture (*Figure 5A,B*) and large G2-arrested cells at the center of the pouch (*Figure 2A,B*). In contrast, *egr,stg*-co-expressing discs presented with densely and regularly arranged columnar cells (*Figure 5A-C'*). Moreover, *stg* co-
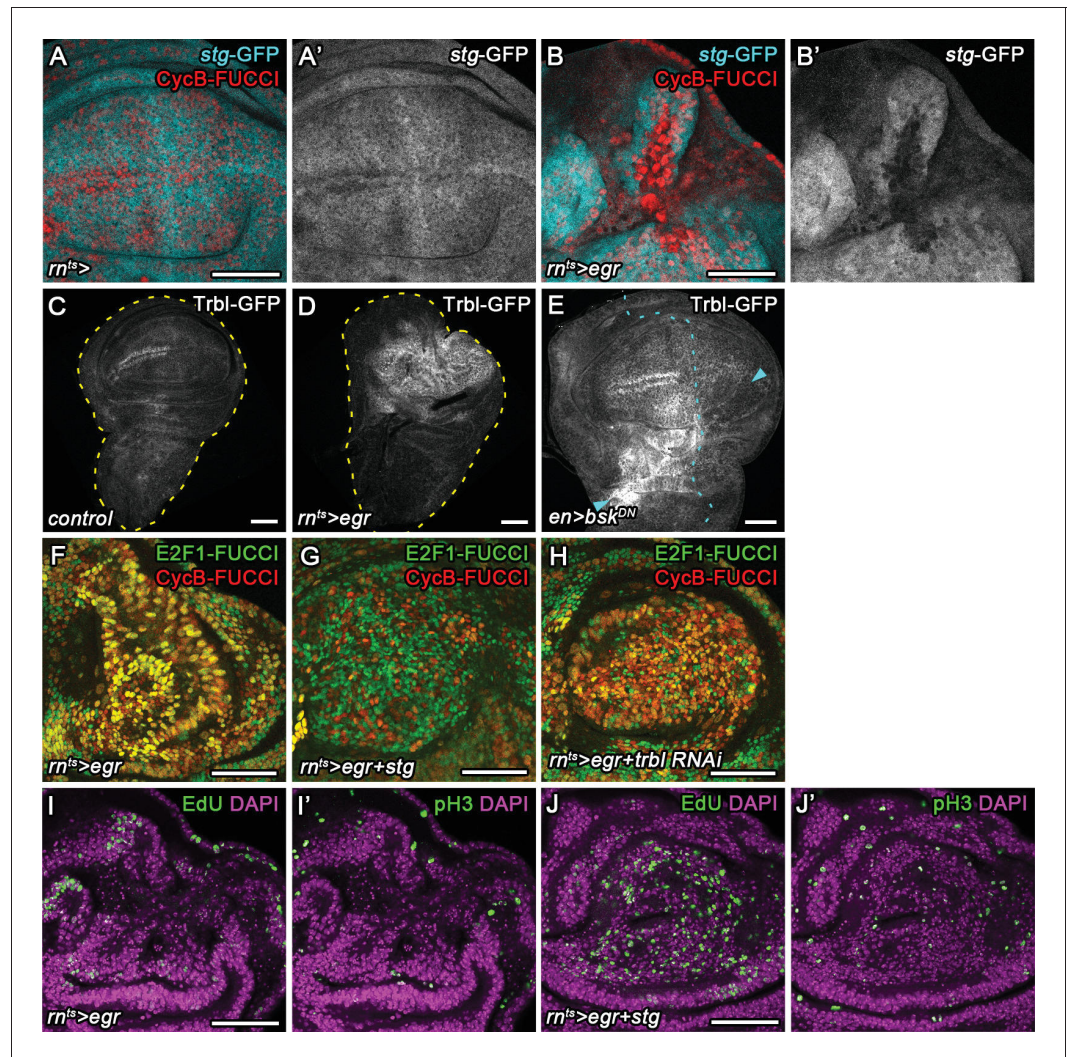
Figure 4. Cdc25/String and Tribbles regulate G2 stalling. (**A–B'**) Control wing disc (**A,A'**) and *egr*-expressing disc at 0 hr into the recovery period (**B,B'**) expressing a GFP trap element in the *stg* locus (**A',B'**, cyan in **A,B**) and the G2-specific FUCCI reporter *mRFP-NLS-CycB$^{1-266}$* (red in **A,B**). Note pronounced reduction of GFP expression in G2-arrested cells at the center of the pouch (**B,B'**). (**C–E**) Control wing disc (**C**), an *egr*-expressing disc at 0 hr into the recovery period (**D**), and a surgically damaged wing disc 6 hr into the recovery period expressing *bsk^{DN}* in the posterior compartment (on the right-hand side of the dotted line) under control of *enGAL4* (**E**). All discs also express a GFP-tagged Trbl protein expressed from the native locus (***Nagarkar-Jaiswal et al., 2015***). Arrows indicate axis of surgical injury verified by tissue deformation in basal sections. (**F–H**) An *egr*-expressing disc (**F**), an *egr,stg*-co-expressing disc (**G**) and an *egr,trbl RNAi*-co-expressing disc at 0 hr into the recovery period expressing the FUCCI reporters. Note increase in the frequency of G1 cells in (**G,H**). (**I–J'**) An *egr*-expressing disc (**I,I'**) and an *egr,stg*-co-expressing disc (**J,J'**) analyzed by EdU incorporation to reveal DNA replication activity (green in **I,J**) and by staining for phospho-Histone3 to reveal mitotic cells (pH3) (green in **I',J'**). Discs were counterstained with DAPI (magenta). Note increase in the frequency of S- and M-phase cells upon *egr,stg* co-expression. Maximum projections of multiple confocal sections are shown in **F-H**. Scale bars: 50 µm.
DOI: https://doi.org/10.7554/eLife.41036.009

The following figure supplement is available for figure 4:

Figure supplement 1. Cdc25/String and Tribbles regulate G2 stalling.
DOI: https://doi.org/10.7554/eLife.41036.010

expression improved tissue regeneration in *egr*-expressing discs, as assessed by size and
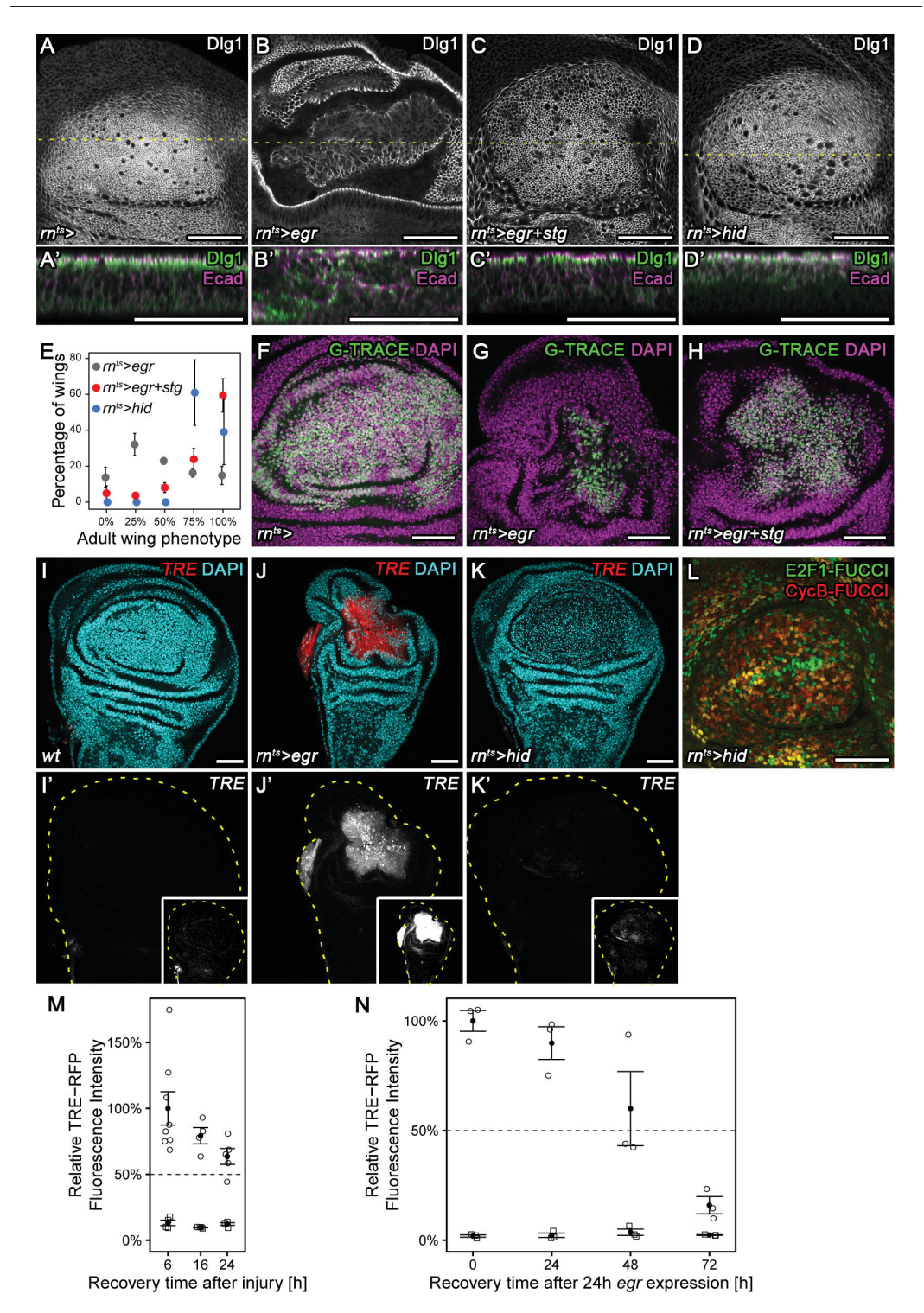
Figure 5. Chronic stalling in G2 interferes with proliferative capacity. (**A–D'**) X-Y view of a control wing disc (**A**), an *egr*-expressing (**B**), *egr,stg*-co-expressing (**C**) or *hid*-expressing disc (**D**) at 0 hr into the recovery period. Cross-sections through the tissue (**A'–D'**) were visualized along dotted yellow lines. Discs were stained for Discs large 1 (Dlg1, **A-D**, green in **A'-D'**) and E-cadherin (Ecad, magenta in **A'-D'**) to visualize cell outlines and cell polarity. (**E**) Adult wings developing from *egr*-expressing, *egr,stg*-co-expressing or *hid*-expressing discs were classified
Figure 5 continued on next page

Figure 5 continued

according to wing size and morphology (see Materials and methods, *Figure 5—figure supplement 1A-C*). Graphs display mean ± SEM of ≥3 independent experiments. Note the significantly improved wing regeneration of *rn^{ts}>egr+stg* (p<0.0001, *n* = 676 wings) and *rn^{ts}>hid* (p<0.0001, *n* = 514 wings) when compared to *rn^{ts}>egr* (*n* = 718 wings) by chi-squared tests. (F–H) Control wing disc (F), an *egr*-expressing (G) and *egr,stg*-co-expressing (H) disc at 0 hr into the recovery period where the surviving *rnGAL4*-lineage has been labeled by G-TRACE (green) (*Evans et al., 2009*). Discs were counterstained with DAPI (magenta). (I–K') Control wing disc (I), an *egr*-expressing (J) or *hid*-expressing (K) disc at 0 hr into the recovery period. Discs express the JNK-reporter *TRE*-RFP (I'-K', red in I-K) and were counterstained with DAPI (cyan in I-K). *TRE*-reporter activity was imaged at settings optimized to subsaturation in *egr*-expressing discs. Small insets in (I'–K') show the same images adjusted to the dynamic range in *hid*-expressing discs. Note that distinct DAPI dense particles seen in the pouch of *hid*-expressing discs represent remnants of apoptotic cells. (L) A *hid*-expressing disc at 0 hr into the recovery period expressing FUCCI reporters (compare to *Figure 2B*). (M,N) Quantifications of *TRE*-RFP fluorescence intensity at the wound site in surgically injured wing discs at 6 hr, 16 hr, and 24 hr after tissue damage (M, circles) and in *egr*-expressing discs at 0 hr, 24 hr, 48 hr and 72 hr into the recovery period (N, circles). Larvae with surgically injured wing discs pupariate at 24 hr so later time points could not be quantified. Note that TRE-RFP reporter activity declines faster in surgically injured discs. Fluorescence intensity in non-wound regions (squares) serves as baseline reference. Graphs display mean ± SEM for *n* = 8 (6 h), *n* = 4 (16 h), *n* = 5 (24 h) injured discs (M) or *n* = 3 (0 h), *n* = 3 (24 h), *n* = 3 (48 h), *n* = 3 (72 h) *egr*-expressing discs (N). Maximum projections of multiple confocal sections are shown in A-D, F-H. Scale bars: 50 μm.

DOI: https://doi.org/10.7554/eLife.41036.011

The following figure supplement is available for figure 5:

Figure supplement 1. Chronic stalling in G2 interferes with proliferative capacity.
DOI: https://doi.org/10.7554/eLife.41036.012

---

morphology of adult wings. 59% of adult wings developing from *egr,stg*-co-expressing discs were of wild type size, in contrast to just 14% of wings developing from *egr*-expressing discs (*Figure 5E*, *Figure 5—figure supplement 1A,B*). Importantly, *stg* expression did not interfere with activation of apoptosis (*Figure 5—figure supplement 1D-G*) or JNK activation (*Figure 5—figure supplement 1H*) in response to *egr* expression. Instead, the *egr,stg*-expressing cell population labelled by G-TRACE (*Evans et al., 2009*) was larger in size (*Figure 5F-H*). This suggests that *stg* overexpression did not interfere with cell ablation but specifically with arrest of the cell cycle and thus proliferative capacity in *egr*-expressing cells. *egr*-expressing discs had been previously reported to exhibit low regenerative potential, in contrast to discs expressing the pro-apoptotic gene *hid* (*Herrera et al., 2013*), an antagonist of *Diap1*-dependent inhibition of caspase activity (*Vaux and Silke, 2005*). Strikingly, preventing a G2-arrest in *egr*-expressing discs by *stg* overexpression phenocopied *hid*-induced regeneration, where discs display columnar morphology (*Figure 5D,D'*) and regenerate efficiently to normal-sized adult wings (*Figure 5E*, *Figure 5—figure supplement 1C*). Importantly, *hid*-expressing discs activated the *TRE*-reporter only at low levels and forwent the pronounced changes to FUCCI reporter activity observed in *egr*-expressing discs (*Figure 5I-L*). These observations indicate that persistent stalling and arrest of cells in G2 interferes with regeneration in *egr*-expressing discs by interfering with the ability of cells to divide and proliferate. Moreover, they highlight G2-stalling as dose-sensitive JNK-effector which determines the regenerative potential of different experimental regeneration models. Of note, *egr*-expression also induced TRE-reporter activity at much higher levels (Figure 7B,B',D,D') and at longer timescales than surgical injury (*Figure 5M,N*), supporting our conclusion that *egr*-expressing discs may experience extreme and possibly aberrant G2 stalling and arrest.

Stalling in G2 promotes survival by protecting cells from JNK-induced apoptosis

Our observation that G2-stalled cells reenter the cell cycle when JNK-signaling decreases suggests that G2-stalled cells can survive in high, potentially pro-apoptotic JNK-signaling environments. We therefore asked if G2-stalled cells are resistant to apoptosis. We thus suppressed G2-stalling in surgically injured discs by expressing *stg* using *rnGAL4*. Strikingly, 6 hr after injury, we observed a 2-fold increase in the apoptotic domain within injured discs (*Figure 6A-E*). Importantly, while *stg* overexpression also induced apoptosis primarily at the anterior D/V boundary in undamaged control discs,
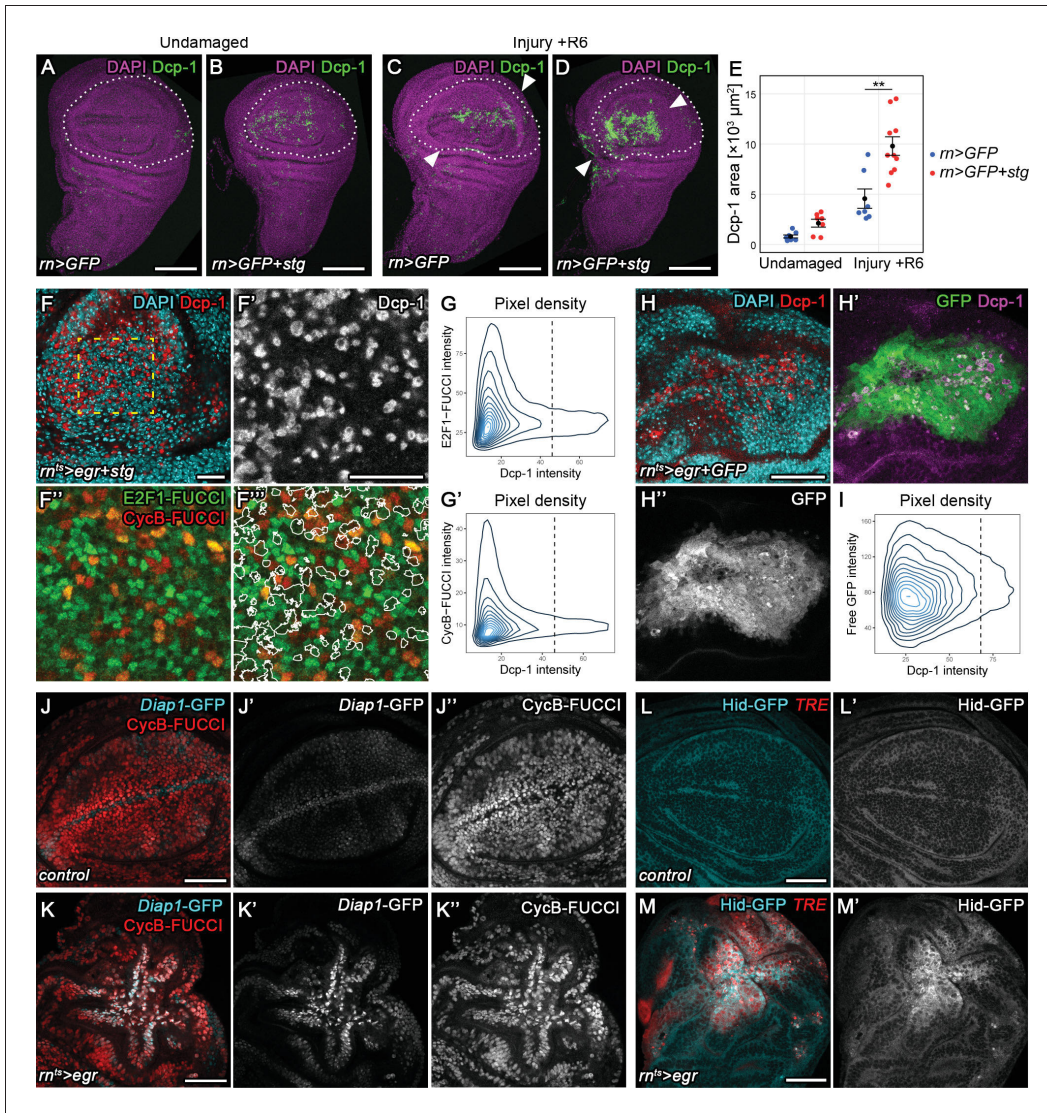
Figure 6. Transient stalling in G2 promotes survival by protecting cells from JNK-induced apoptosis. (A–E) Undamaged control (A) and an undamaged disc expressing *stg* under the control of *rnGAL4* (B). An injured control disc (C) and an injured *stg*-expressing disc (D), 6 hr into the recovery period. Dotted lines indicate the *rnGAL4* domain, arrows indicate injury axis. Wing discs were stained for the apoptotic marker Dcp-1 (green) and counterstained with DAPI (magenta). The area occupied by Dcp-1 in a maximum projection is quantified in (E). Graphs display mean ± SEM for undamaged *rn>GFP*, n = 8; undamaged *rn>GFP+stg*, n = 7; injured *rn>GFP*, n = 7; injured *rn>GFP+stg*, n = 10 discs. *U*-tests were performed to test for statistical significance, **p<0.01. (F–F''') An *egr,stg*-expressing disc analyzed for FUCCI activity (F'',F''') and the apoptotic marker Dcp-1 (F', red in F) or DAPI (cyan in F) at 0 hr into the recovery period. F'-F''' represent the area framed by broken line in F. White lines in F''' represent the Dcp-1 outline mask of F'. Note that masked cells generally express low levels of either FUCCI reporter. (G–G') The fluorescence intensities of Dcp-1 and the *GFP-E2f1^{1-230}* (G) or *mRFP-NLS-CycB^{1-266}* (G') FUCCI reporters for each pixel are plotted as 2D density graphs (see Materials and methods). The broken line represents a visually chosen Dcp-1 threshold defining apoptotic cells. Note that the surviving population expresses the entire range of FUCCI reporter intensities (left), in contrast to apoptotic cells (right). (H–I) An *egr,GFP*-expressing disc stained for the apoptotic marker Dcp-1 (red in H, magenta in H') and DAPI (cyan in H) at 0 hr into the recovery period. Graph (I) plots the 2D density of pixel fluorescence intensities for Dcp-1 and free GFP. The broken line represents a visually chosen Dcp-1 threshold defining apoptotic cells. Note that the surviving and apoptotic population use the GFP fluorescence spectrum symmetrically. (J–K'') Control (J–J'') and an *egr*-expressing (K–K'') disc at 0 hr into the recovery period expressing the *Diap1-GFP.3.5* reporter (J',K', cyan in J,K) and the G2-specific FUCCI reporter *mRFP-NLS-CycB^{1-266}* (J'',K'', red in J,K). Note the anti-correlation between *Diap1* promoter activity and G2-phase in control discs, in contrast to *egr*-expressing discs. (L–M') Control (L,L') and *egr*-expressing (M,M') discs at 0 hr into the recovery period expressing a Hid-GFP fusion protein under endogenous control (L',M', cyan in L,M). JNK-signaling cells were detected by activation of *TRE*-RFP (red in L,M). Maximum projections of multiple confocal sections are shown in A-D. Scale bars: 100 µm (A–D), 20 µm (F,F'''), 50 µm (H–M).

Figure 6 continued on next page

apoptosis in surgically injured discs was specifically increased near the wound site where JNK report-ers are expected to be activated (*Figure 6B,D*). This suggests that at transient time scales, G2-stall-ing is required to prevent apoptosis and thus promotes survival in injured tissues displaying potentially lethal levels of JNK activity.

If stalling in G2 protects cells from apoptosis, are JNK-signaling cells more susceptible to apopto-sis in other phases of the cell cycle? To test this idea, we first confirmed that actively cycling, JNK-signaling cells did not die in late G2 by demonstrating that Dcp-1 levels were highest in *egr*-express-ing cells with low levels of a co-expressed HA-tagged *stg* (*Figure 6—figure supplement 1A-A'''*). Stg-HA peaked in late G2 and mitotic cells but was absent in G1, S-phase and early G2 (*Figure 6—figure supplement 1B-B''*). To further narrow down the cell cycle phase at which JNK signaling cells died, we correlated levels of the apoptotic marker Dcp-1 with FUCCI reporter activity in *egr,stg*-co-expressing discs. We took care to specifically analyze confocal sections within the tissue to catch apoptotic cells before extrusion. We found that in actively cycling, JNK-signaling tissue, Dcp-1 could be specifically detected in cells with low intensity of either FUCCI reporter (*Figure 6F-G'*), suggest-ing that JNK-signaling cells preferentially died either early in G1 or late in S-phase. Importantly, low FUCCI reporter fluorescence was not due to apoptosis-dependent degradation of fluorophores, as levels of fluorescence intensity of an unrelated cytoplasmic GFP were independent of Dcp-1 levels in *egr,GFP*-co-expressing discs (*Figure 6H-I*). Additionally, the overall FUCCI profile of *egr,stg* and *stg*-expressing control discs was similar, confirming that FUCCI reporter intensities were not affected by apoptotic cells per se (*Figure 6—figure supplement 1C-C''*). To better understand when cycling JNK-signaling cells died, we allowed discs to incorporate EdU for at least 1 hr prior to fixation. We consistently failed to detect recent DNA replication in apoptotic cells (*Figure 6—figure supplement 1E-E''*) indicating that cells did not die in S-phase. Taken together, these results support a model where JNK-signaling cells are susceptible to apoptosis in G1 and protected from apoptosis by stall-ing in G2.

To understand how G2-stalled cells may be protected from apoptosis, we analyzed expression of *Diap1*, an inhibitor of the initiator caspases, as well as of *hid*, a potent IAP antagonist (*Vasudevan and Ryoo, 2015*; *Vaux and Silke, 2005*). A *Diap1*-GFP reporter encompassing enhancer elements sensitive to regulation by anti-apoptotic Hippo/Yorkie signaling (*Zhang et al., 2008*) was upregulated in *TRE*-positive (data not shown) and G2-stalled cells at the center of *egr*-expressing discs (*Figure 6J-K''*). Importantly, *Diap1*-GFP activity did not correlate with tissue pat-terns of G2 in undamaged control discs (*Figure 6J,J''*), suggesting that Yorkie activity at *Diap1* regu-latory elements was not controlled in a cell cycle-dependent manner per se, but likely reflected activation of Yorkie by JNK (*Sun and Irvine, 2011*; *Ríos-Barrera and Riesgo-Escovar, 2013*). A Hid-GFP fusion protein expressed under the control of endogenous regulatory elements (*Nagarkar-Jaiswal et al., 2015*) was also strongly upregulated in *TRE*-positive cells in *egr*-expressing discs (*Figure 6L-M'*). These observations align with previous reports of activation of anti-apoptotic Yorkie (*Sun and Irvine, 2011*; *Ríos-Barrera and Riesgo-Escovar, 2013*) or pro-apoptotic Hid (*Luo et al., 2007*; *Shlevkov and Morata, 2012*) by JNK in stressed cells. We highlight that the activation of anti-apoptotic and pro-apoptotic pathways occurs concomitantly in JNK-signaling G2-stalled cells. Taken together, these results suggest that transition from G2 to G1 represents the key switch in the cellular interpretation of opposing JNK-dependent signals with anti-apoptotic to pro-apoptotic consequences.

Chronic stalling in G2 promotes non-autonomous overgrowth

Cell cycle arrest and apoptosis resistance are hallmarks of senescence. Senescent cells affect their microenvironment through senescence-associated secretory phenotype (SASP) (*Hernandez-Segura et al., 2018*; *Neves et al., 2015*; *Pluquet et al., 2015*; *Salama et al., 2014*), which promotes tumorigenesis and contributes to tumor heterogeneity (*Hinds and Pietruska, 2017*;
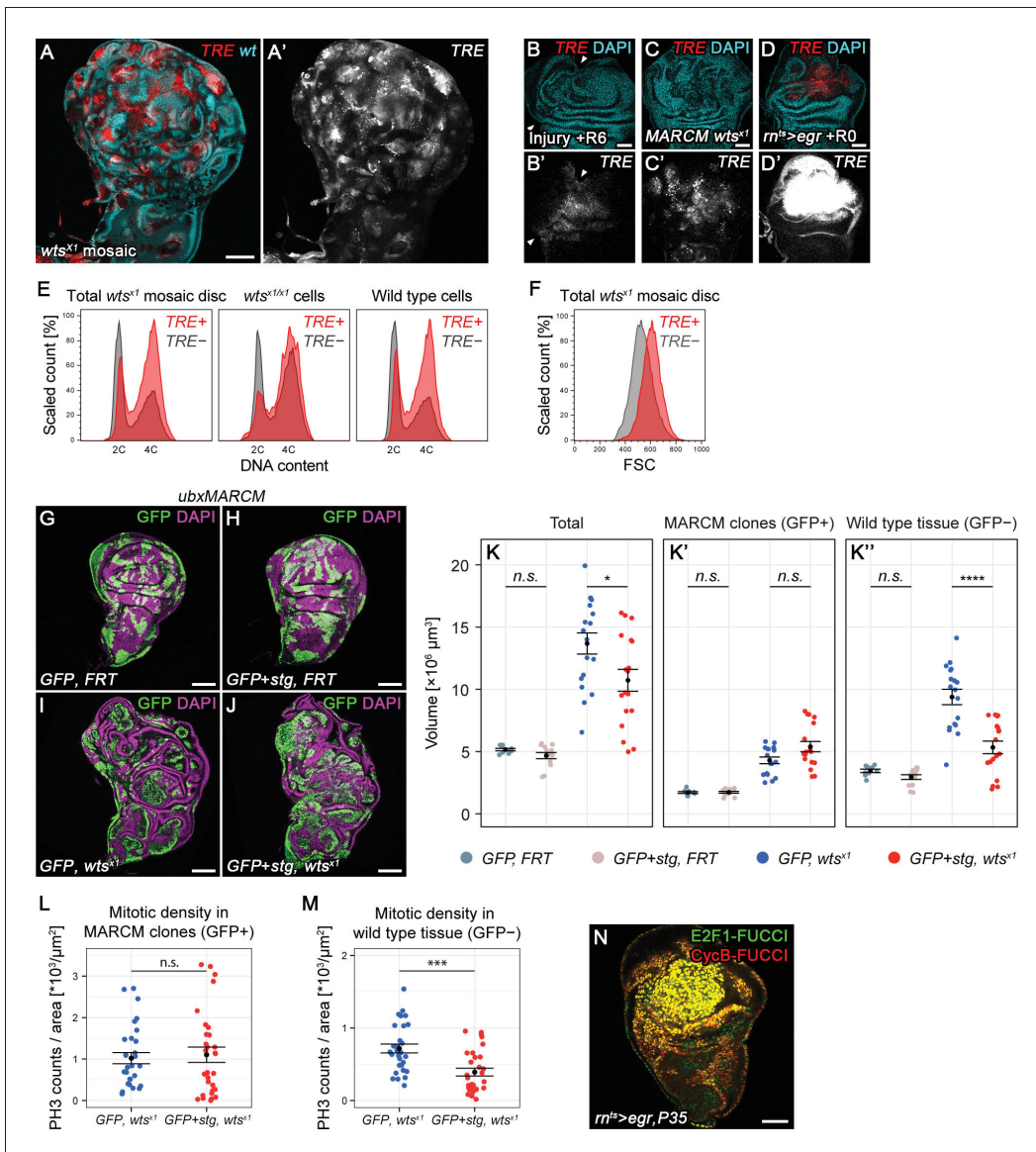
Figure 7. Chronic stalling in G2 promotes non-autonomous overgrowth. (A,A') A wing disc expressing *TRE*-RFP and carrying mosaic *wts^{x1/x1}* clones marked by the absence of GFP (cyan in **A**). (**B–D'**) A surgically damaged wing disc 6 hr into the recovery period (**B,B'**), a wing disc carrying *wts^{x1/x1}* MARCM clones (**C,C'**) and an *egr*-expressing disc at 0 hr into the recovery period (**D,D'**). Discs express the JNK-reporter *TRE*-RFP (**B'-D'**, red in **B-D**) and were counterstained with DAPI (cyan in **B-D**). *TRE*-reporter activity was imaged at settings optimized to subsaturation in *egr*-expressing discs. Panels (**B'–D'**) show the *TRE*-RFP fluorescence adjusted to the dynamic range of surgically injured discs. (**E–F**) Mosaic *wts^{x1/x1}* wing discs were analyzed for DNA content (**E**) and cell size (**F**) by flow cytometry. The total cell population of discs was plotted as *TRE*-positive or *TRE*-negative events (**E,F**). The same analysis was also applied separately to *wts^{x1/x1}* cells and wild type cells sub-populations (**E** only). Of note, previous cell cycle studies of Hippo-pathway mutant have not reported any alterations (*Harvey et al., 2003*; *Huang et al., 2005*; *Tapon et al., 2002*). Therefore, the mild cell cycle shift in TRE-negative *wts^{x1/x1}* cells appears to be specific to the *wts^{x1}* allele. (**G–J**) Wing imaginal discs carrying GFP-labeled MARCM clones (green) that are either wild type (**G**), *stg*-overexpressing (**H**), mutant for *wts^{x1}* (**I**) or *stg*-overexpressing and mutant for *wts^{x1}* (**J**). Discs were counterstained with DAPI (magenta). (**K–K''**) Volumes occupied by the total disc (**K**), the GFP-labeled fraction representing MARCM clones (**K'**) and the non-GFP-labeled fraction representing the surrounding wild type tissue (**K''**). Graphs display mean ± SEM for *tub>GFP, FRT*, n = 9; *tub>GFP+stg, FRT*, n = 13; *tub>GFP, FRT wts^{x1}*, n = 18; *tub>GFP+stg, FRT wts^{x1}*, n = 18 discs. *U*-tests were performed to test for statistical significance (*n.s.* not significant, *p<0.05, ****p<0.0001). (**L,M**) Quantification of phospho-Histone3 events identifying mitotic cells, normalized to the relevant tissue area. Mitotic cells were counted in GFP-positive MARCM clones that are either mutant for *wts^{x1}* (blue) or mutant for *wts^{x1}* and overexpressing *stg* (red) (**L**), and in the non-GFP-labeled fraction representing the wild type tissue surrounding clones mutant for *wts^{x1}* (blue) or mutant for *wts^{x1}* and overexpressing *stg* (red) (**M**). Graphs display mean ± SEM, n = 30 confocal sections from six discs per sample. *U*-tests were performed to test for statistical significance (*n.s.* not significant

Figure 7 continued on next page

Schosserer et al., 2017). Many studies report heterogenous activation of JNK in imaginal discs upon genetic loss of tumor suppressor function (*Richardson and Portela, 2018*). We thus tested if imaginal disc tumor models displayed any evidence of a JNK-induced G2-shift. We first analyzed *warts (wts^{x1})* mosaic clones (*Xu et al., 1995*) which promote Yorkie activity, in wing imaginal discs also expressing *TRE*-RFP (*Figure 7A*). Localized *TRE*-RFP expression increased in mosaic discs during larval stages (*Figure 7—figure supplement 1A*). Based on flow cytometry analysis, we estimated that 40.6% of *wts^{x1}* cells had at least elevated *TRE*-RFP reporter activity. Consistent with non-autonomous induction of JNK in response to tissue stress (*Bosch et al., 2005*; *Herrera et al., 2013*; *Wu et al., 2010*) 29.9% of wild type cells displayed *TRE*-RFP reporter activity. Importantly, *TRE*-RFP levels were comparable to levels induced by surgical injury but much lower than those induced by *egr*-expression (*Figure 7B-D'*). Flow cytometry analysis revealed that *TRE*-positive cells exhibited a strong G2 profile which correlated with an increase in cell size (*Figure 7E,F*). This effect was observed in *TRE*-positive *wts^{x1}* and wild type cells (*Figure 7E*). This relationship could also be observed in mosaic discs containing clones mutant for *scrib^{dt12}*, a hypomorphic tumor suppressor mutation in the key component of the Scrib/Lgl/Dlg epithelial polarity module (*Figure 7—figure supplement 1B-D*) (*Stephens et al., 2018*; *Zeitler et al., 2004*). Combined, these observations suggest that a pronounced shift towards G2 is associated with JNK activity in response to tissue stress imposed by the presence of abnormal or tumorigenic cells.

To understand if G2-stalling played a role in tumor growth or tumor microenvironment, we overexpressed *stg* in *wts^{x1}* or *dlg1^{G0342}* clones. Like *scrib*, *dlg1* is a tumor suppressor in the Scrib/Lgl/Dlg epithelial polarity module (*Stephens et al., 2018*) and mutant cells activate JNK (*Igaki, 2009*; *Igaki et al., 2009*). Overexpression of *stg* in mosaic *wts^{x1}* or *dlg1^{G0342}* clones did not significantly increase clone size (*Figure 7G-K"*, *Figure 7—figure supplement 1E-I''*). As division rates of cycling cells are not expected to be enhanced by *stg* overexpression alone (*Neufeld et al., 1998*), promoting cycling of a small fraction of arrested tumor cells may not significantly increase tumor mass.

Strikingly, however, when we further analyzed these mosaic discs, we found that *stg* overexpression in *wts^{x1}* and in *dlg1^{G0342}* cells strongly affected the surrounding wild type tissue. The absolute size of the wild type tissue in mosaic *wts^{x1}* or *dlg1^{G0342}* mutant discs is almost double of that in mosaic wild type control discs (*Figure 7K"*, *Figure 7—figure supplement 1I''*), a phenomenon ascribed to non-autonomous overgrowth stimulated by the chronic presence of tumorigenic cells (*Fuchs and Steller, 2015*; *Pastor-Pareja and Xu, 2013*; *Uhlirova et al., 2005*). However, *stg* overexpression strongly reduced the size of the surrounding wild type tissue in mosaic *wts^{x1}* and *dlg1^{G0342}* discs (*Figure 7K"*, *Figure 7—figure supplement 1I''*). Importantly, whereas mitotic activity in *wts^{x1}* clones was unaffected (*Figure 7L*), *stg*-overexpression strongly reduced mitotic activity in the wild type tissue surrounding *wts^{x1}* clones (*Figure 7M*). This strongly suggests that stalling of JNK-signaling cells in G2 directly promotes non-autonomous proliferation and thus causes non-autonomous overgrowth on prolonged timescales during imaginal disc tumor development.

Previous studies describe 'undead' cells as chronic drivers of non-autonomous overgrowth. Experimentally, undead cells are created by expression the anti-apoptotic factor p35 in apoptotic JNK-signaling cells (*Chen, 2012*; *Fuchs and Steller, 2015*; *Martín et al., 2009*; *Pérez-Garijo et al., 2009*; *Shlevkov and Morata, 2012*; *Wells et al., 2006*). We created undead cells by co-expressing p35 in *egr*-expressing disc. *Egr,p35*-coexpressing cells completely arrest in G2 (*Figure 7N*), confirming that G2-stalling is intimately associated with cellular states known to stimulate non-autonomous growth. Genetically, the initiator caspase Dronc is required to stimulate non-autonomous growth from dying and undead cells (*Enomoto et al., 2015*; *Fan and Bergmann, 2008a*; *Fan and Bergmann, 2008b*;
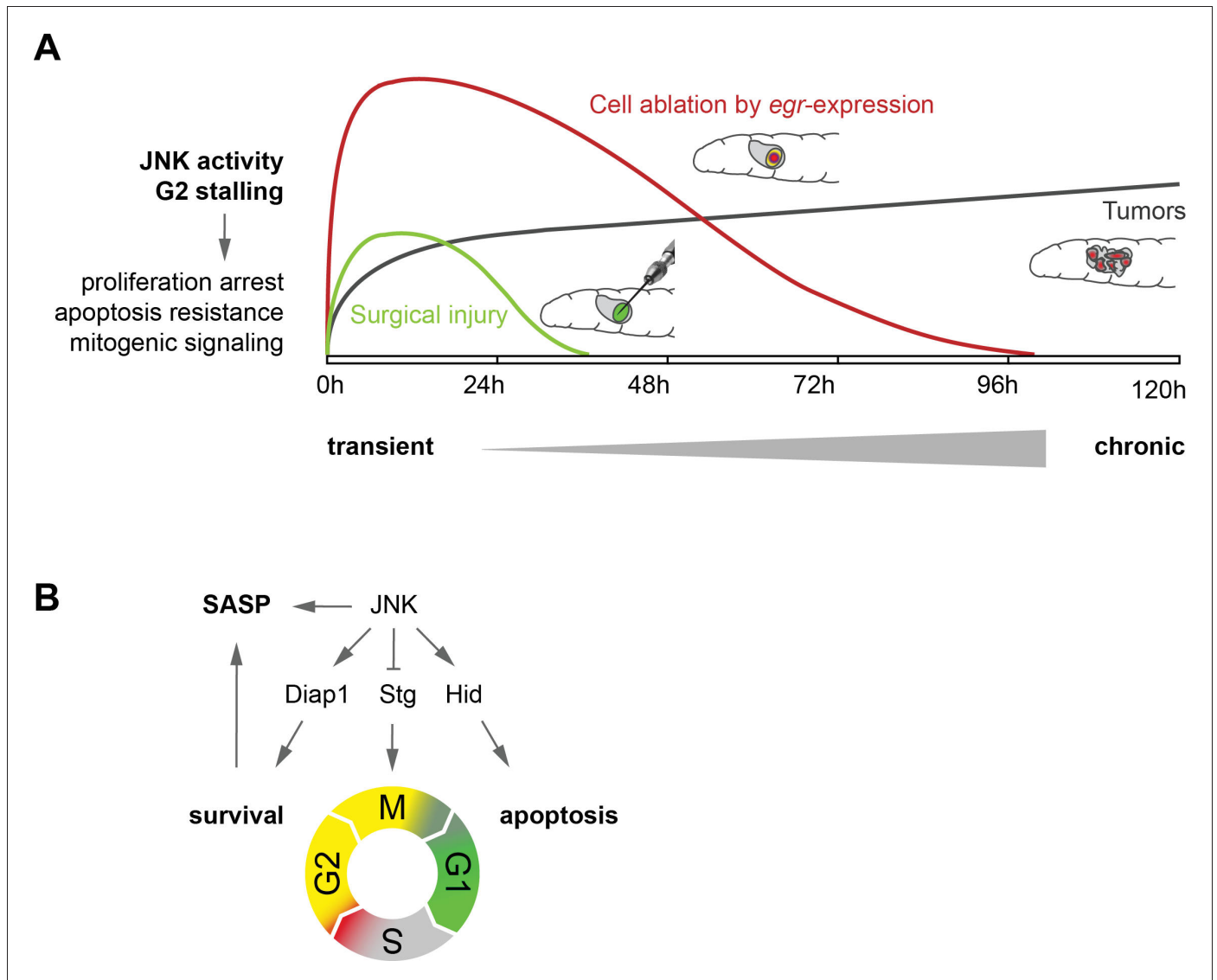
Figure 8. Model. (A) Transient (surgical injury), prolonged (*egr*-expression) and chronic (mosaic tumors) disruption of tissue homeostasis induces transient, prolonged and chronic JNK activity, thereby driving G2-stalling and senescence-like properties in a dose- and time-dependent manner. (B) JNK regulates SASP, Diap1, Stg and Hid. The transition between G2 and G1 acts as switch that prevents survival and SASP. The decision to arrest in G2 is JNK-dependent, which can integrate information about damage and has cell-protective functions. The decision to die in G1 may depend on additional information about the extent of cell and tissue damage.

DOI: https://doi.org/10.7554/eLife.41036.018

Kiyokawa and Ray, 2008; *Kondo et al., 2006*; *Wells et al., 2006*). To demonstrate that caspases are activated in G2 stalled cells and that G2 stalling may confer resistance to the execution of apoptosis, we analyzed the CasExpress sensor in surgically injured discs. CasExpress permanently labels anastatic cells, which have survived caspase activation (*Ding et al., 2016*; *Tang et al., 2012*). Strikingly, 24 hr after surgical injury, we observed many CasExpress-positive clones near the wound site (*Figure 7—figure supplement 2A,B*). This indicates that many wound-proximal cells survive caspase activation and subsequently proliferate. While we cannot demonstrate that these anastatic cells corresponded to G2-stalled cells, we suggest that G2 stalling could facilitate transient mitogenic signaling of Dronc-positive, JNK-activated cells at wound sites.

We wanted to understand if G2-arrested cells may affect their microenvironment not just via induction of mitogenic signaling, but also through upregulation of additional SASP-like markers. We

tested reporters for ECM degrading enzymes (MMP1), ROS response (*GstD*-GFP) and UPR (Xbp1-GFP), in addition to reporters for mitogenic signaling (*upd*-LacZ), for activation in *egr*-expressing discs. As expected from many studies previously linking upregulation of these markers to JNK (*Bunker et al., 2015*; *Fulda et al., 2010*; *Richardson and Portela, 2018*; *Santabárbara-Ruiz et al., 2015*; *Takino et al., 2014*; *Uhlirova and Bohmann, 2006*), we found all SASP-like markers, including cell size (*Figure 2—figure supplement 1D*), to be highly elevated (*Figure 7—figure supplement 2C-J*). The co-occurrence of G2-arrest, JNK activity and SASP-like markers suggests that a JNK-signaling induced G2-arrest in flies is linked to senescence-like phenotypes driven by JNK. Importantly, transient *upd*-LacZ and MMP1 upregulation is associated with transient JNK activity in surgical injuries (*Lin et al., 2010*; *McClure et al., 2008*), making it plausible that transient G2-stalling is linked to senescence-like properties promoting wound healing and regeneration, analogous to senescent cells observed in a mammalian wound model (*Demaria et al., 2014*).

Discussion

Here we uncover a mechanism whereby control of the cell cycle promotes survival and mitogenic signaling in JNK-dependent responses to tissue stress. We demonstrate that JNK signaling induces a dose-dependent extension of G2, which results in either transient stalling or prolonged arrest of cells in G2. Cells in G2 are protected from undergoing JNK-induced apoptosis and promote proliferative signaling to the surrounding tissue in a SASP-like manner (*Figure 8*).

At first sight, some results in our study appeared contradictory. Using *stg*-overexpression to force stalled cells to cycle, we observed (1) apoptosis of JNK-signaling cells in surgically damaged discs, (2) improvement of regenerative capacity in *egr*-expressing discs and (3) reduction of non-autonomous overgrowth in a mosaic tumor model. Our data support a model where any length of G2-stalling protects cells autonomously from JNK-induced apoptosis in G1. Stalled cells switch on a SASP-like phenotype, which when transient supports compensatory growth during regeneration. However, when cells stall chronically, proliferation is autonomously inhibited and chronic SASP-like phenotype drives non-autonomous overgrowth contributing to tumorigenesis. We suggest that our experimental models reveal a spectrum of cell-autonomous (survival, stalling of proliferation) and non-autonomous (mitogenic paracrine signaling) functions of G2-stalling. Importantly, this spectrum is defined by the intensity and length of JNK activity: whereas persistent stalling of tumor cells may cause persistent survival and non-autonomous overgrowth, transient stalling of wound site cells may promote survival transiently and facilitate transient induction of compensatory proliferation.

Surprisingly, both G2-stalling and survival as well as apoptosis directly link to JNK signaling in response to tissue stress. We find that JNK controls *stg/cdc25* transcription and Trbl availability as rate-limiting factors for stalling. Importantly, mouse JNK directly phosphorylates Cdc25C to stall G2/M transitions (*Goss et al., 2003*; *Gutierrez et al., 2010*). If JNK also phosphorylates Stg in flies remains to be determined. As reported before, JNK also regulates *hid* promoting apoptosis (*Shlevkov and Morata, 2012*) and activates Hippo/Yorkie promoting survival by upregulation of *Diap1* (*Sun and Irvine, 2011*; *Sun and Irvine, 2013*). This is analogous to mammalian models where tissue stress induces apoptosis but can also promote cell cycle arrest and survival through upregulation of cell-protective mechanisms. However, the switch between the anti- and pro-apoptotic consequences are not understood (*Fulda et al., 2010*). Importantly, our observations imply that cell cycle progression from G2 to G1 represents the switch between anti- and pro-apoptotic activity of JNK. We suggest that stalling the cell cycle is a protected state, which is dominated by pre-emptive protection from ROS damage through upregulation of the UPR, redox response and other repair pathways. Thus, G2-stalling is important to keep the pro-apoptotic branch of JNK signaling suppressed, a prerequisite of efficient regeneration (*La Fortezza et al., 2016*).

We propose that G2-stalling is induced by JNK itself, and thus only indirectly by cellular damage. While we have not excluded that, for example, proteotoxic stress induces G2-stalling (*Pluquet et al., 2015*), we find that, similar to a previous report (*Wells et al., 2006*), DNA damage is not rate-limiting for cell cycle arrest. In support of this hypothesis, we find that *stg* overexpression rescues architecture and proliferation in *egr*-expressing discs. This indicates that, despite the fact that many JNK-signaling cells die in G1 when bypassing stalling in G2, there are many JNK-signaling G1 cells, which survive, continue to cycle and are healthy enough to contribute to future adult tissues. Even more strikingly, we find that independent of any tissue damage, developmentally

regulated G2-stalling in the wing peripodium is dependent on JNK. Similarly, programmed cell arrest and senescence in mouse embryogenesis is independent of DNA damage or p53, but dependent on a general CDK-inhibitor (p21) and developmental signals of the TGF-β/SMAD or PI3K/FOXO pathways (*Davaapil et al., 2017*; *Muñoz-Espín et al., 2013*). Thus, cell cycle stalling and consequently, SASP or protection from apoptosis, may be under the control of signaling pathways which not always depend on tissue stress. Curiously, another developmentally regulated G2 arrest has already been reported to suppress apoptosis (*Qi and Calvi, 2016*).

At least one previous study has indicated the existence of senescent cells in flies, however their cell cycle stage was less well-defined (*Nakamura et al., 2014*; *Neves et al., 2015*). Many studies have demonstrated correlation of JNK with SASP-like characteristics in flies, such as mitogenic signaling, ECM remodeling or ROS production (*Brock et al., 2017*; *Khan et al., 2017*; *McClure et al., 2008*; *Nakamura et al., 2014*; *Neves et al., 2015*; *Pastor-Pareja and Xu, 2013*; *Ryoo et al., 2004*; *Uhlirova et al., 2005*). We speculate that G2-stalling may either represent a primitive version of a senescent cell cycle arrest that evolved to G0 in mammalian cells or that G2-stalling may also occur in mammals but is less well-defined. Recent studies implicate a role for cells with senescent markers in mammalian wounds and vertebrate development (*Davaapil et al., 2017*; *Demaria et al., 2014*; *Muñoz-Espín et al., 2013*; *Ritschka et al., 2017*) and an injury-induced G2 arrest has been found to interfere with restoration of epithelial homeostasis in a model of chronic kidney disease (*Bonventre, 2014*). Future studies thus need to address if senescence markers can also be found in G2-arrested mammalian cells. G2-stalling may offer an opportunity to protect cells from apoptosis, induce paracrine signals and, importantly, restore active cycling upon restoration of tissue homeostasis, instead of engaging permanent senescence in G0. Thus, more studies are needed to address how G2-stalling may be related to G2 quiescence in stem cells (*Otsuki and Brand, 2018*), to a reversible G2 arrest (*Gire and Dulic, 2015*) or G0 senescence in mammalian tissues.

Materials and methods

Key resources table

Reagent type (species) or resource	Designation	Source or reference	Identifiers	Additional information
Genetic reagent (*Drosophila melanogaster*)	Diap-1-GFP.3.5	PMID: 18258485		
Genetic reagent (*D. melanogaster*)	enGAL4, UAS-GFP			D.Bilder, UC Berekely
Genetic reagent (*D. melanogaster*)	'eyMARCM19A'; 'ey-FLP, FRT19A tub-GAL80; act5c>y[+]>GAL4, UAS-GFP[S56T]'	PMID: 29494583		
Genetic reagent (*D. melanogaster*)	'ubxMARCM82B'; 'Ubx-FLP, tubP-GAL4, UAS-GFP; FRT82B tubP-GAL80'	Bloomington Drosophila Stock Center	BDSC: 42734	
Genetic reagent (*D. melanogaster*)	FRT19A dlg[G0342]	Kyoto Stock Center	DGGR: 111872	
Genetic reagent (*D. melanogaster*)	FRT82B wts[x1]	Bloomington Drosophila Stock Center	BDSC: 44251	
Genetic reagent (*D. melanogaster*)	'G-TRACE'; 'UAS-FLP.Exel, Ubi-p63E(FRT.STOP)Stinger'	Bloomington Drosophila Stock Center	BDSC: 28282	
Genetic reagent (*D. melanogaster*)	gstD-GFP	PMID: 18194654		

Continued on next page

Continued

Reagent type (species) or resource	Designation	Source or reference	Identifiers	Additional information
Genetic reagent (*D. melanogaster*)	hep[R75]	Bloomington Drosophila Stock Center	BDSC: 6761	
Genetic reagent (*D. melanogaster*)	'hid-GFP'; 'hid[MI06452-GFSTF.1]'	Bloomington Drosophila Stock Center	BDSC: 65331	
Genetic reagent (*D. melanogaster*)	mei-41[RT1]	Bloomington Drosophila Stock Center	BDSC: 4169	
Genetic reagent (*D. melanogaster*)	'puc-LacZ'; 'puc[A251.1F3]'	Bloomington Drosophila Stock Center	BDSC: 11173	
Genetic reagent (*D. melanogaster*)	'rnGAL4'; 'rn[GAL4-DeltaS]'	Bloomington Drosophila Stock Center	BDSC: 8142	
Genetic reagent (*D. melanogaster*)	'rn(ts)>'; 'rn[GAL4-DeltaS], tubGAL80[ts]'	Bloomington Drosophila Stock Center	BDSC: 8142; BDSC: 7018	recombinant
Genetic reagent (*D. melanogaster*)	'rn(ts)>egr'; 'rn[GAL4-5], UAS-egr, tubP-GAL80[ts]'	Bloomington Drosophila Stock Center		
Genetic reagent (*D. melanogaster*)	'stg-GFP'; 'stg[YD0685]'	Bloomington Drosophila Stock Center	BDSC: 50879	
Genetic reagent (*D. melanogaster*)	'Trbl-GFP'; 'trbl[MI01025-GFSTF.2]'	Bloomington Drosophila Stock Center	BDSC: 61654	
Genetic reagent (*D. melanogaster*)	TRE-RFP	PMID: 22509270		
Genetic reagent (*D. melanogaster*)	UAS-bsk[DN]	Bloomington Drosophila Stock Center	BDSC: 6409	
Genetic reagent (*D. melanogaster*)	UAS-Cdk1 RNAi [TRiP.HMS01531]	Bloomington Drosophila Stock Center	BDSC: 36117	
Genetic reagent (*D. melanogaster*)	UAS-GFP S56T		BDSC: 1521	
Genetic reagent (*D. melanogaster*)	UAS-grp RNAi [TRiP.HMC05162]	Bloomington Drosophila Stock Center	BDSC: 62155	
Genetic reagent (*D. melanogaster*)	UAS-hep[act]	Bloomington Drosophila Stock Center	BDSC: 9306	
Genetic reagent (*D. melanogaster*)	UAS-hid			G. Morata, CBSMO Spain
Genetic reagent (*D. melanogaster*)	UAS-mei-41 RNAi [TRiP.GL00284]	Bloomington Drosophila Stock Center	BDSC: 35371	
Genetic reagent (*D. melanogaster*)	UAS-stg	Bloomington Drosophila Stock Center	BDSC: 4777	

Continued on next page

Continued

Reagent type (species) or resource	Designation	Source or reference	Identifiers	Additional information
Genetic reagent (*D. melanogaster*)	UAS-stg.HA	Bloomington Drosophila Stock Center	BDSC: 56562	
Genetic reagent (*D. melanogaster*)	UAS-Xbp1-GFP.HG	Bloomington Drosophila Stock Center	BDSC: 60731	
Genetic reagent (*D. melanogaster*)	'E2F1-FUCCI, CycB-FUCCI'; 'Ubi-GFP.E2f1.1–230, Ubi-mRFP1.NLS.CycB.1–266'	Bloomington Drosophila Stock Center	BDSC: 55123	
Genetic reagent (*D. melanogaster*)	'CycB-FUCCI'; 'Ubi-mRFP1.NLS.CycB.1–266'	PMID: 24726363		
Genetic reagent (*D. melanogaster*)	'ubx-flp;; FRT82B ubi-GFP'			I. Hariharan, UC Berkeley
Genetic reagent (*D. melanogaster*)	upd-lacZ (PD)	PMID: 8582614		
Genetic reagent (*D. melanogaster*)	UAS-trbl RNAi [TRiP.HMJ02089]	Bloomington Drosophila Stock Center	BDSC: 42523	
Genetic reagent (*D. melanogaster*)	UAS-P35	Bloomington Drosophila Stock Center	BDSC: 5072	
Genetic reagent (*D. melanogaster*)	GH146-QF, QUAS-mtdTomato-3xHA	Bloomington Drosophila Stock Center	BDSC: 30037	
Genetic reagent (*D. melanogaster*)	Ubi-CasExpress	Bloomington Drosophila Stock Center	BDSC: 65419	
Antibody	Rabbit anti-cleaved Dcp-1	Cell Signaling	Cat. #: 9578	(1:200)
Antibody	Mouse monoclonal anti-CycB	Developmental Studies Hybridoma Bank	Cat. #: F2F4	(1:20)
Antibody	Rat monoclonal anti-DE-cadherin	Developmental Studies Hybridoma Bank	Cat. #: DCAD2	(1:100)
Antibody	Mouse monoclonal anti-discs large	Developmental Studies Hybridoma Bank	Cat. #: 4F3	(1:100)
Antibody	Mouse anti-β-Galactosidase	Promega	Cat. #: Z3782	(1:1000)
Antibody	Chicken anti-GFP	Abcam	Cat. #: ab13970	(1:1000)
Antibody	Rabbit monoclonal anti-GFP	Invitrogen	Cat. #: G10362	(1:200)
Antibody	Rabbit anti-H2Av-pS137	Rockland	Cat. #: 600-401-914	(1:500)
Antibody	Mouse anti-H3-pS10	Abcam	Cat. #: ab14955	(1:2000)
Antibody	Rat monoclonal anti-HA	Monoclonal Antibody Core Facillity at the Helmholtz Zentrum München	Clone #: 3F10	(1:20)
Antibody	Mouse monoclonal anti-MMP1	Developmental Studies Hybridoma Bank	Cat. #: 3A6B4	(1:30)
Antibody	Mouse monoclonal anti-MMP1	Developmental Studies Hybridoma Bank	Cat. #: 3B8D12	(1:30)

Continued on next page

Continued

Reagent type (species) or resource	Designation	Source or reference	Identifiers	Additional information
Antibody	Mouse monoclonal anti-MMP1	Developmental Studies Hybridoma Bank	Cat. #: 5H7B11	(1:30)
Antibody	Mouse monoclonal anti-RFP	Abcam	Cat. #: ab65856	(1:100)
Antibody	Rat monoclonal anti-RFP	Monoclonal Antibody Core Facility at the Helmholtz Zentrum München	Clone #: 5F8	(1:20)
Antibody	Mouse monoclonal anti-Ultrabithorax	Developmental Studies Hybridoma Bank	Cat. #: Ubx FP3.38	(1:10)
Commercial assay or kit	Click-iT Plus EdU Alexa Fluor 647 Imaging Kit	Invitrogen	Cat. #: C10640	

Drosophila stocks and genetics

Flies were kept on standard food and raised at 18°C and 30°C (expression of pro-apoptotic transgenes), or 25°C. A list of strains, detailed genotypes and experimental conditions are provided in *Supplementary file 1* and in the key resources table.

Tissue injury models

In situ surgical wounding

Wounding of wing imaginal discs in situ was performed by quickly immobilizing L3 larvae in ice-cold PBS and applying pressure to the fluorescently-labeled wing imaginal disc with a 0.125 mm tungsten needle (Fine Science Tools, 10130–05) without perforating the larval cuticle, as described by *Bryant (1971)*; *Yoo et al. (2016)*. After wounding, the larvae were immediately placed in a new food vial and allowed to recover at 25°C for the indicated time. For each animal, only the right wing disc was wounded. The left wing disc was used as undamaged control. For each experiment involving functional genetics, a wild type control was included, and the wounding procedure was performed in blind. At least 15 larvae were wounded for each genotype.

Temporal and spatial control of pro-apoptotic transgene expression

To induce expression of *egr* or *hid*, experiments were carried out as described in *Smith-Bolton et al. (2009)* and *La Fortezza et al. (2016)* with few modifications. Briefly, larvae of genotype *rnGAL4, tub-GAL80^{ts}* (denoted as *rn^{ts}>*) and carrying the desired *UAS-transgenes* were staged by a 6 hr egg collection and raised at 18°C at the density of 50 larvae/vial. Overexpression of transgenes was induced by shifting the temperature to 30°C for 24 hr at day seven after egg deposition (AED) (*Figure 2—figure supplement 1A*). Larvae were subsequently allowed to recover at 18°C for the indicated time (recovery time R24-R72 hours, or adulthood), or dissected immediately (R0). All images are R0, unless noted otherwise. Control genotypes were either *rn^{ts}>*, or the siblings of the ablating animals (*+/TM6B, tubGAL80*) (*Smith-Bolton et al., 2009*). At least 16 discs were dissected for each genotype per replicate.

Mosaic tumor models

To obtain MARCM clones in the wing discs, larvae cultures were synchronized by a 6 hr egg collection and raised at 25°C at a density of 50 larvae/vial. Control larvae were analyzed 5 days AED, while larvae carrying *wts^{x1}* clones were analyzed 7 days AED, to account for developmental delay induced by the presence of tumorigenic cells. To obtain MARCM clones in the eye discs, equal crosses for all genotypes were set up in parallel and processed 6 days AED. Discs expressing and stained for HA-tagged Stg were mounted on the same slide as their respective control discs, to ensure comparability of volume quantifications.

Flow cytometry

Cell cycle analysis of wing imaginal discs by flow cytometry was performed as described (*de la Cruz and Edgar, 2008*). Wing imaginal discs from at least 10 larvae were dissected in PBS and incubated for 2 hr in PBS containing 9X Trypsin-EDTA (Sigma, T4174) and 0.5 µg/ml Hoechst 33342 (Invitrogen, H3570). Cells were analyzed with an LSRFortessa cell analyzer (BD Biosciences) or FACS Aria II cell sorter (BD Biosciences). Univariate cell cycle analysis was performed using the Watson Pragmatic algorithm in FlowJo v10 (FlowJo).

Immunohistochemistry

General comments

Where possible, control and experimental samples were fixed, processed and mounted together to ensure comparable staining and imaging conditions. The signals of the following fluorescent reporters were further amplified by anti-GFP or anti-RFP antibody staining: CycB-FUCCI, E2F1-FUCCI, G-TRACE, Hid-GFP, *stg*-GFP, Trbl-GFP, Xbp1-GFP.HG.

Immunohistochemistry

Larvae were dissected, and cuticles were fixed for 15 min at room temperature in 4% paraformaldehyde. Washing steps were performed in 0.1% Triton X-100/PBS (PBT), blocking in 5% NGS/PBT. The following antibodies were incubated overnight at 4°C: rabbit anti-cleaved Dcp-1 (Cell Signaling, 9578, 1:200), mouse anti-Cyclin B (DSHB, F2F4, 1:20), rat anti-DE-cadherin (DSHB, DCAD2, 1:100), mouse anti-discs large (DSHB, 4F3, 1:100), mouse anti-β-Galactosidase (Promega, Z3783, 1:1000), chicken anti-GFP (Abcam, ab13970, 1:1000), rabbit anti-GFP (Invitrogen, G10362, 1:200), rabbit anti-H2Av-pS137 (Rockland, 600-401-914, 1:500), mouse anti-H3-pS10 (Abcam, ab14955, 1:2000), rat anti-HA (MAB facility at the Helmholtz Zentrum München, 3F10, 1:20), mouse anti-MMP1 (DSHB, a mix of 3A6B4, 3B8D12 and 5H7B11, each 1:30), mouse anti-RFP (Abcam, ab65856, 1:100), rat anti-RFP (MAB facility at the Helmholtz Zentrum München, 5F8, 1:20), mouse anti-Ultrabithorax (DSHB, FP3.38, 1:10). EdU incorporation was performed for 15 min, unless noted otherwise, and detected using the Click-iT Plus EdU Alexa Fluor 647 Imaging Kit (Invitrogen, C10640) prior to primary antibody incubation, according to manufacturer's guidelines. Tissues were counterstained with DAPI (0.25 ng/µl, Sigma, D9542) during incubation with cross-adsorbed secondary antibodies coupled to Alexa Fluorophores (Invitrogen or Abcam) at room temperature for 2 hr. Tissues were mounted using SlowFade Gold Antifade (Invitrogen, S36936). Samples were imaged using Leica TCS SP5 or SP8 confocal microscopes.

Image analysis and quantification

General comments

Images were processed, analyzed and quantified using tools in Fiji (ImageJ v2.0.0) (*Schindelin et al., 2012*). Figure panels were assembled using Photoshop CS5 (Adobe). Statistical analyses were performed in R v3.3.3 (www.R-project.org).

Peripodial cell cycle quantification

A mask of the DAPI counterstain, obtained from total projections of confocal stacks containing the entire wing discs, was used to estimate the total disc size by measuring its area with the 'Analyze Particles' tool in Fiji. To analyze a defined population of cells in the peripodium of size-matched wing discs, Ubx +nuclei were identified with 'Analyze Particles' (size = 10.00–40.00 circularity = 0.50–1.00), after applying 'Unsharp Mask' (radius = 10 mask=0.4), Gaussian Blur (sigma = 0.2 scaled) and Watershed functions. The nuclei of the resulting mask were counted and displayed as total Ubx +cells. Automated determination of the cell cycle phase for each nucleus was obtained by measuring the average fluorescence intensity of both FUCCI reporters. The criteria to define each cell cycle phase are shown in *Figure 3—figure supplement 1E*.

TRE-RFP quantification

To measure the fluorescence intensity of *TRE*-RFP signals in injured, *egr*-expressing or tumor discs, a small circular ROI of fixed radius (25–30 µm) was placed in an area of high *TRE*-RFP signal of a single

confocal section for each stack, carefully chosen to capture maximal JNK activity in the disc proper, avoiding the peripodium and extruded cell debris. The mean intensity of each ROI was obtained using the 'Measure' function in Fiji.

Dcp-1 quantification in injured discs

Masks of Dcp-1 signals were obtained in Fiji from maximum intensity projections of confocal stacks by applying a fixed threshold (value = 75) and the 'Remove outliers' function (bright, radius = 1.5). Areas of the resulting masks were obtained using 'Analyze Particles'.

FUCCI and Dcp-1 intensity analysis in egr-expressing discs

A single confocal section for each stack was carefully chosen within the tissue to capture apoptotic cells before extrusion. An ROI corresponding to the pouch was selected using the 'Freehand Selection' tool in Fiji. Pixel fluorescence intensities for all channels were subsequently obtained using the 'Save XY Coordinates' function, after applying a 'Gaussian Blur' filter (radius = 0.3 µm) to reduce noise. Data from $n = 5$ (**Figure 6G**) and $n = 4$ discs (**Figure 6I**) were pooled and the distribution of fluorescence intensities of each pixel was represented as 2D density plots.

GFP volume and total disc size quantification (mosaic clone analysis)

Masks for GFP signals (positively labeled clones) and total volume were obtained in Fiji from entire confocal stacks by applying the functions 'Auto Threshold' (settings: 'Li' for GFP or 'Triangle' for total, white objects, stack histogram) and 'Remove Outliers' (settings: black and white pixels removal, radii = 2) to GFP signals or to the sum of DAPI and GFP signals, respectively. The resulting masks were analyzed using the '3D Objects Counter' function (settings: threshold = 128, min = 50 max=Inf). The sum of the resulting object volumes for each disc was used to describe the GFP and total volume of the disc. Non-GFP volumes were calculated by subtracting the GFP volume from the total disc volume.

Mitotic density

PH3-positive cells were counted in Fiji by applying 'Auto threshold' (settings: 'Yen') and 'Remove Outliers' (settings: black and white pixels removal, radii = 1) to single confocal sections. A total of 5 equally spaced (6 µm) confocal sections for each of 6 stacks per sample were analyzed. Masks for GFP signals were obtained by applying 'Auto threshold' (settings: 'Triangle) and 'Remove Outliers' (settings: dark, radius = 3; bright, radius = 1). GFP-negative areas were calculated by subtracting GFP-positive areas from the total tissue area.

Adult wing size analysis

Adult flies were collected 12 hr after eclosion and stored in 2-propanol. Wing sizes were indexed by binning into five different wing phenotypic classes: 0%, 25%, 50%, 75% or 100% of wild type size, as defined in *La Fortezza et al. (2016)*; *Smith-Bolton et al. (2009)*. Importantly, wings smaller than 100% of wild type size, typically present a range of morphological defects (*Smith-Bolton et al., 2009*). Of note, wings of 100% size but with notches or incomplete vein formation were classified as 75%.

Acknowledgements

Additional information

Author contributions

Andrea Cosolo, Conceptualization, Data curation, Formal analysis, Validation, Investigation, Visualization, Methodology, Writing—original draft, Writing—review and editing; Janhvi Jaiswal, Gábor Csordás, Data curation, Formal analysis, Validation, Investigation, Visualization, Writing—review and editing; Isabelle Grass, Validation, Investigation, Methodology; Mirka Uhlirova, Supervision, Writing—review and editing; Anne-Kathrin Classen, Conceptualization, Formal analysis, Supervision, Funding acquisition, Visualization, Writing—original draft, Writing—review and editing

Author ORCIDs

Andrea Cosolo http://orcid.org/0000-0003-3417-0713
Gábor Csordás http://orcid.org/0000-0001-6871-6839
Mirka Uhlirova https://orcid.org/0000-0002-5735-8287
Anne-Kathrin Classen http://orcid.org/0000-0001-5157-0749

Decision letter and Author response

Decision letter https://doi.org/10.7554/eLife.41036.028
Author response https://doi.org/10.7554/eLife.41036.029

Additional files

Supplementary files

• Supplementary file 1. Genotypes and experimental conditions. This table lists detailed genotypes and temperature conditions used to generate the data for each of the main and supplementary figures in this study.
DOI: https://doi.org/10.7554/eLife.41036.019
• Transparent reporting form
DOI: https://doi.org/10.7554/eLife.41036.020

Data availability

All data generated or analysed during this study are included in the manuscript and supporting files.

References

Bergantiños C, Corominas M, Serras F. 2010. Cell death-induced regeneration in wing imaginal discs requires JNK signalling. *Development* **137**:1169–1179. DOI: https://doi.org/10.1242/dev.045559, PMID: 20215351

Bonventre JV. 2014. Primary proximal tubule injury leads to epithelial cell cycle arrest, fibrosis, vascular rarefaction, and glomerulosclerosis. *Kidney International Supplements* **4**:39–44. DOI: https://doi.org/10.1038/kisup.2014.8, PMID: 26310195

Bosch M, Serras F, Martín-Blanco E, Baguñà J. 2005. JNK signaling pathway required for wound healing in regenerating Drosophila wing imaginal discs. *Developmental Biology* **280**:73–86. DOI: https://doi.org/10.1016/j.ydbio.2005.01.002, PMID: 15766749

Bosch M, Baguñà J, Serras F. 2008. Origin and proliferation of blastema cells during regeneration of Drosophila wing imaginal discs. *The International Journal of Developmental Biology* **52**:1043–1050. DOI: https://doi.org/10.1387/ijdb.082608mb, PMID: 18956337

Brock AR, Seto M, Smith-Bolton RK. 2017. Cap-n-Collar promotes tissue regeneration by regulating ROS and JNK signaling in the *Drosophila melanogaster* Wing Imaginal Disc. *Genetics* **206**:1505–1520. DOI: https://doi.org/10.1534/genetics.116.196832, PMID: 28512185

Bryant PJ. 1971. Regeneration and duplication following operations in situ on the imaginal discs of Drosophila melanogaster. *Developmental Biology* **26**:637–651. DOI: https://doi.org/10.1016/0012-1606(71)90146-1, PMID: 5002603

Bunker BD, Nellimoottil TT, Boileau RM, Classen AK, Bilder D. 2015. The transcriptional response to tumorigenic polarity loss in Drosophila. *eLife* **4**:e03189. DOI: https://doi.org/10.7554/eLife.03189

Buszczak M, Paterno S, Lighthouse D, Bachman J, Planck J, Owen S, Skora AD, Nystul TG, Ohlstein B, Allen A, Wilhelm JE, Murphy TD, Levis RW, Matunis E, Srivali N, Hoskins RA, Spradling AC. 2007. The carnegie protein trap library: a versatile tool for Drosophila developmental studies. *Genetics* **175**:1505–1531. DOI: https://doi.org/10.1534/genetics.106.065961, PMID: 17194782

Chatterjee N, Bohmann D. 2012. A versatile φc31 based reporter system for measuring AP-1 and Nrf2 signaling in Drosophila and in tissue culture. *PLOS ONE* **7**:e34063. DOI: https://doi.org/10.1371/journal.pone.0034063, PMID: 22509270

Chen F. 2012. JNK-induced apoptosis, compensatory growth, and cancer stem cells. *Cancer Research* **72**:379–386. DOI: https://doi.org/10.1158/0008-5472.CAN-11-1982, PMID: 22253282

Davaapil H, Brockes JP, Yun MH. 2017. Conserved and novel functions of programmed cellular senescence during vertebrate development. *Development* **144**:106–114. DOI: https://doi.org/10.1242/dev.138222, PMID: 27888193

de la Cruz AF, Edgar BA. 2008. Flow cytometric analysis of *Drosophila* cells. *Methods in Molecular Biology* **420**:373–389. DOI: https://doi.org/10.1007/978-1-59745-583-1_24, PMID: 18641961

Demaria M, Ohtani N, Youssef SA, Rodier F, Toussaint W, Mitchell JR, Laberge RM, Vijg J, Van Steeg H, Dollé ME, Hoeijmakers JH, de Bruin A, Hara E, Campisi J. 2014. An essential role for senescent cells in optimal wound healing through secretion of PDGF-AA. *Developmental Cell* **31**:722–733. DOI: https://doi.org/10.1016/j.devcel.2014.11.012, PMID: 25499914

Ding AX, Sun G, Argaw YG, Wong JO, Easwaran S, Montell DJ. 2016. CasExpress reveals widespread and diverse patterns of cell survival of caspase-3 activation during development in vivo. *eLife* **5**:e10936. DOI: https://doi.org/10.7554/eLife.10936, PMID: 27058168

Edgar BA, Britton J, de la Cruz AF, Johnston LA, Lehman D, Martin-Castellanos C, Prober D. 2001. Pattern- and growth-linked cell cycles in *Drosophila* development. *Novartis Foundation Symposium* **237**:3–12. PMID: 11444048

Eferl R, Wagner EF. 2003. AP-1: a double-edged sword in tumorigenesis. *Nature Reviews Cancer* **3**:859–868. DOI: https://doi.org/10.1038/nrc1209, PMID: 14668816

Enomoto M, Vaughen J, Igaki T. 2015. Non-autonomous overgrowth by oncogenic niche cells: cellular cooperation and competition in tumorigenesis. *Cancer Science* **106**:1651–1658. DOI: https://doi.org/10.1111/cas.12816, PMID: 26362609

Evans CJ, Olson JM, Ngo KT, Kim E, Lee NE, Kuoy E, Patananan AN, Sitz D, Tran P, Do MT, Yackle K, Cespedes A, Hartenstein V, Call GB, Banerjee U. 2009. G-TRACE: rapid Gal4-based cell lineage analysis in Drosophila. *Nature Methods* **6**:603–605. DOI: https://doi.org/10.1038/nmeth.1356, PMID: 19633663

Fan Y, Bergmann A. 2008a. Apoptosis-induced compensatory proliferation. the cell is dead. long live the cell!. *Trends in Cell Biology* **18**:467–473. DOI: https://doi.org/10.1016/j.tcb.2008.08.001, PMID: 18774295

Fan Y, Bergmann A. 2008b. Distinct mechanisms of apoptosis-induced compensatory proliferation in proliferating and differentiating tissues in the Drosophila eye. *Developmental Cell* **14**:399–410. DOI: https://doi.org/10.1016/j.devcel.2008.01.003, PMID: 18331718

Fuchs Y, Steller H. 2015. Live to die another way: modes of programmed cell death and the signals emanating from dying cells. *Nature Reviews Molecular Cell Biology* **16**:329–344. DOI: https://doi.org/10.1038/nrm3999, PMID: 25991373

Fulda S, Gorman AM, Hori O, Samali A. 2010. Cellular stress responses: cell survival and cell death. *International Journal of Cell Biology* **2010**:1–23. DOI: https://doi.org/10.1155/2010/214074

Gire V, Dulic V. 2015. Senescence from G2 arrest, revisited. *Cell Cycle* **14**:297–304. DOI: https://doi.org/10.1080/15384101.2014.1000134, PMID: 25564883

Glise B, Bourbon H, Noselli S. 1995. Hemipterous encodes a novel *Drosophila* MAP kinase kinase, required for epithelial cell sheet movement. *Cell* **83**:451–461. DOI: https://doi.org/10.1016/0092-8674(95)90123-X, PMID: 8521475

Goss VL, Cross JV, Ma K, Qian Y, Mola PW, Templeton DJ. 2003. SAPK/JNK regulates cdc2/cyclin B kinase through phosphorylation and inhibition of cdc25c. *Cellular Signalling* **15**:709–718. DOI: https://doi.org/10.1016/S0898-6568(03)00009-3, PMID: 12742231

Gutierrez GJ, Tsuji T, Cross JV, Davis RJ, Templeton DJ, Jiang W, Ronai ZA. 2010. JNK-mediated phosphorylation of Cdc25C regulates cell cycle entry and G(2)/M DNA damage checkpoint. *The Journal of Biological Chemistry* **285**:14217–14228. DOI: https://doi.org/10.1074/jbc.M110.121848, PMID: 20220133

Harvey KF, Pfleger CM, Hariharan IK. 2003. The Drosophila mst ortholog, hippo, restricts growth and cell proliferation and promotes apoptosis. *Cell* **114**:457–467. DOI: https://doi.org/10.1016/S0092-8674(03)00557-9, PMID: 12941274

Hernandez-Segura A, Nehme J, Demaria M. 2018. Hallmarks of cellular senescence. *Trends in Cell Biology* **28**: 436–453. DOI: https://doi.org/10.1016/j.tcb.2018.02.001, PMID: 29477613

Herrera SC, Martín R, Morata G. 2013. Tissue homeostasis in the wing disc of Drosophila melanogaster: immediate response to massive damage during development. *PLOS Genetics* **9**:e1003446. DOI: https://doi.org/10.1371/journal.pgen.1003446, PMID: 23633961

Herz HM, Chen Z, Scherr H, Lackey M, Bolduc C, Bergmann A. 2006. vps25 mosaics display non-autonomous cell survival and overgrowth, and autonomous apoptosis. *Development* **133**:1871–1880. DOI: https://doi.org/10.1242/dev.02356, PMID: 16611691

Hinds P, Pietruska J. 2017. Senescence and tumor suppression.In: *F1000Research* **6**:2121. DOI: https://doi.org/10.12688/f1000research.11671.1, PMID: 29263785

Huang J, Wu S, Barrera J, Matthews K, Pan D. 2005. The hippo signaling pathway coordinately regulates cell proliferation and apoptosis by inactivating yorkie, the Drosophila homolog of YAP. *Cell* **122**:421–434. DOI: https://doi.org/10.1016/j.cell.2005.06.007, PMID: 16096061

Igaki T. 2009. Correcting developmental errors by apoptosis: lessons from Drosophila JNK signaling. *Apoptosis* **14**:1021–1028. DOI: https://doi.org/10.1007/s10495-009-0361-7, PMID: 19466550

Igaki T, Pastor-Pareja JC, Aonuma H, Miura M, Xu T. 2009. Intrinsic tumor suppression and epithelial maintenance by endocytic activation of eiger/TNF signaling in Drosophila. *Developmental Cell* **16**:458–465. DOI: https://doi.org/10.1016/j.devcel.2009.01.002, PMID: 19289090

Johnston LA, Edgar BA. 1998. Wingless and notch regulate cell-cycle arrest in the developing Drosophila wing. *Nature* **394**:82–84. DOI: https://doi.org/10.1038/27925, PMID: 9665132

Khan SJ, Abidi SNF, Skinner A, Tian Y, Smith-Bolton RK. 2017. The Drosophila duox maturation factor is a key component of a positive feedback loop that sustains regeneration signaling. *PLOS Genetics* **13**:e1006937. DOI: https://doi.org/10.1371/journal.pgen.1006937, PMID: 28753614

Khurana S, Oberdoerffer P. 2015. Replication stress: a lifetime of epigenetic change. *Genes* **6**:858–877. DOI: https://doi.org/10.3390/genes6030858, PMID: 26378584

Kimelman D. 2014. Cdc25 and the importance of G2control. *Cell Cycle* **13**:2165–2171. DOI: https://doi.org/10.4161/cc.29537

Kiyokawa H, Ray D. 2008. In vivo roles of CDC25 phosphatases: biological insight into the anti-cancer therapeutic targets. *Anti-Cancer Agents in Medicinal Chemistry* **8**:832–836. PMID: 19075565

Kondo S, Senoo-Matsuda N, Hiromi Y, Miura M. 2006. DRONC coordinates cell death and compensatory proliferation. *Molecular and Cellular Biology* **26**:7258–7268. DOI: https://doi.org/10.1128/MCB.00183-06, PMID: 16980627

Külshammer E, Mundorf J, Kilinc M, Frommolt P, Wagle P, Uhlirova M. 2015. Interplay among Drosophila transcription factors Ets21c, fos and Ftz-F1 drives JNK-mediated tumor malignancy. *Disease Models & Mechanisms* **8**:1279–1293. DOI: https://doi.org/10.1242/dmm.020719, PMID: 26398940

La Fortezza M, Schenk M, Cosolo A, Kolybaba A, Grass I, Classen AK. 2016. JAK/STAT signalling mediates cell survival in response to tissue stress. *Development* **143**:2907–2919. DOI: https://doi.org/10.1242/dev.132340, PMID: 27385008

Lin G, Xu N, Xi R. 2010. Paracrine unpaired signaling through the JAK/STAT pathway controls self-renewal and lineage differentiation of Drosophila intestinal stem cells. *Journal of Molecular Cell Biology* **2**:37–49. DOI: https://doi.org/10.1093/jmcb/mjp028, PMID: 19797317

Luo X, Puig O, Hyun J, Bohmann D, Jasper H. 2007. Foxo and fos regulate the decision between cell death and survival in response to UV irradiation. *The EMBO Journal* **26**:380–390. DOI: https://doi.org/10.1038/sj.emboj.7601484, PMID: 17183370

Martín FA, Peréz-Garijo A, Morata G. 2009. Apoptosis in *Drosophila*: compensatory proliferation and undead cells. *The International Journal of Developmental Biology* **53**:1341–1347. DOI: https://doi.org/10.1387/ijdb.072447fm, PMID: 19247932

Martin P, Nunan R. 2015. Cellular and molecular mechanisms of repair in acute and chronic wound healing. *British Journal of Dermatology* **173**:370–378. DOI: https://doi.org/10.1111/bjd.13954, PMID: 26175283

Mata J, Curado S, Ephrussi A, Rørth P. 2000. Tribbles coordinates mitosis and morphogenesis in Drosophila by regulating string/CDC25 proteolysis. *Cell* **101**:511–522. DOI: https://doi.org/10.1016/S0092-8674(00)80861-2, PMID: 10850493

Mattila J, Omelyanchuk L, Kyttälä S, Turunen H, Nokkala S. 2005. Role of jun N-terminal kinase (JNK) signaling in the wound healing and regeneration of a Drosophila melanogaster wing imaginal disc. *The International Journal of Developmental Biology* **49**:391–399. DOI: https://doi.org/10.1387/ijdb.052006jm, PMID: 15968584

McClure KD, Sustar A, Schubiger G. 2008. Three genes control the timing, the site and the size of blastema formation in Drosophila. *Developmental Biology* **319**:68–77. DOI: https://doi.org/10.1016/j.ydbio.2008.04.004, PMID: 18485344

Moreno E, Yan M, Basler K. 2002. Evolution of TNF signaling mechanisms: jnk-dependent apoptosis triggered by eiger, the Drosophila homolog of the TNF superfamily. *Current Biology : CB* **12**:1263–1268. PMID: 12176339

Muñoz-Espín D, Cañamero M, Maraver A, Gómez-López G, Contreras J, Murillo-Cuesta S, Rodríguez-Baeza A, Varela-Nieto I, Ruberte J, Collado M, Serrano M. 2013. Programmed cell senescence during mammalian embryonic development. *Cell* **155**:1104–1118. DOI: https://doi.org/10.1016/j.cell.2013.10.019, PMID: 2423 8962

Nagarkar-Jaiswal S, Lee P-T, Campbell ME, Chen K, Anguiano-Zarate S, Cantu Gutierrez M, Busby T, Lin W-W, He Y, Schulze KL, Booth BW, Evans-Holm M, Venken KJT, Levis RW, Spradling AC, Hoskins RA, Bellen HJ.

2015. A library of MiMICs allows tagging of genes and reversible, spatial and temporal knockdown of proteins in *Drosophila*. *eLife* **4**:e05338. DOI: https://doi.org/10.7554/eLife.05338

Nakamura M, Ohsawa S, Igaki T. 2014. Mitochondrial defects trigger proliferation of neighbouring cells via a senescence-associated secretory phenotype in Drosophila. *Nature Communications* **5**:e5264. DOI: https://doi.org/10.1038/ncomms6264, PMID: 25345385

Neufeld TP, de la Cruz AF, Johnston LA, Edgar BA. 1998. Coordination of growth and cell division in the Drosophila wing. *Cell* **93**:1183–1193. DOI: https://doi.org/10.1016/S0092-8674(00)81462-2, PMID: 9657151

Neves J, Demaria M, Campisi J, Jasper H. 2015. Of flies, mice, and men: evolutionarily conserved tissue damage responses and aging. *Developmental Cell* **32**:9–18. DOI: https://doi.org/10.1016/j.devcel.2014.11.028, PMID: 25584795

Otsuki L, Brand AH. 2018. Cell cycle heterogeneity directs the timing of neural stem cell activation from quiescence. *Science* **360**:99–102. DOI: https://doi.org/10.1126/science.aan8795, PMID: 29622651

Pastor-Pareja JC, Grawe F, Martín-Blanco E, García-Bellido A. 2004. Invasive cell behavior during Drosophila imaginal disc eversion is mediated by the JNK signaling cascade. *Developmental Cell* **7**:387–399. DOI: https://doi.org/10.1016/j.devcel.2004.07.022, PMID: 15363413

Pastor-Pareja JC, Xu T. 2013. Dissecting social cell biology and tumors using Drosophila genetics. *Annual Review of Genetics* **47**:51–74. DOI: https://doi.org/10.1146/annurev-genet-110711-155414, PMID: 23988119

Pérez-Garijo A, Martín FA, Morata G. 2004. Caspase inhibition during apoptosis causes abnormal signalling and developmental aberrations in *Drosophila*. *Development* **131**:5591–5598. DOI: https://doi.org/10.1242/dev.01432, PMID: 15496444

Pérez-Garijo A, Shlevkov E, Morata G. 2009. The role of dpp and wg in compensatory proliferation and in the formation of hyperplastic overgrowths caused by apoptotic cells in the *Drosophila* wing disc. *Development* **136**:1169–1177. DOI: https://doi.org/10.1242/dev.034017, PMID: 19244279

Pluquet O, Pourtier A, Abbadie C. 2015. The unfolded protein response and cellular senescence. A review in the theme: cellular mechanisms of endoplasmic reticulum stress signaling in health and disease. *American Journal of Physiology-Cell Physiology* **308**:C415–C425. DOI: https://doi.org/10.1152/ajpcell.00334.2014, PMID: 25540175

Qi S, Calvi BR. 2016. Different cell cycle modifications repress apoptosis at different steps independent of developmental signaling in *Drosophila*. *Molecular Biology of the Cell* **27**:1885–1897. DOI: https://doi.org/10.1091/mbc.e16-03-0139, PMID: 27075174

Rämet M, Lanot R, Zachary D, Manfruelli P. 2002. JNK signaling pathway is required for efficient wound healing in Drosophila. *Developmental Biology* **241**:145–156. DOI: https://doi.org/10.1006/dbio.2001.0502, PMID: 11784101

Reis T, Edgar BA. 2004. Negative regulation of dE2F1 by cyclin-dependent kinases controls cell cycle timing. *Cell* **117**:253–264. DOI: https://doi.org/10.1016/S0092-8674(04)00247-8, PMID: 15084262

Richardson HE, Portela M. 2018. Modelling cooperative tumorigenesis in *Drosophila*. *BioMed Research International* **2018**:4258387:–. DOI: https://doi.org/10.1155/2018/4258387, PMID: 29693007

Ríos-Barrera LD, Riesgo-Escovar JR. 2013. Regulating cell morphogenesis: the Drosophila jun N-terminal kinase pathway. *Genesis* **51**:147–162. DOI: https://doi.org/10.1002/dvg.22354, PMID: 23109363

Ritschka B, Storer M, Mas A, Heinzmann F, Ortells MC, Morton JP, Sansom OJ, Zender L, Keyes WM. 2017. The senescence-associated secretory phenotype induces cellular plasticity and tissue regeneration. *Genes & Development* **31**:172–183. DOI: https://doi.org/10.1101/gad.290635.116, PMID: 28143833

Ryoo HD, Gorenc T, Steller H. 2004. Apoptotic cells can induce compensatory cell proliferation through the JNK and the wingless signaling pathways. *Developmental Cell* **7**:491–501. DOI: https://doi.org/10.1016/j.devcel.2004.08.019, PMID: 15469838

Salama R, Sadaie M, Hoare M, Narita M. 2014. Cellular senescence and its effector programs. *Genes & Development* **28**:99–114. DOI: https://doi.org/10.1101/gad.235184.113, PMID: 24449267

Sancar A, Lindsey-Boltz LA, Unsal-Kaçmaz K, Linn S. 2004. Molecular mechanisms of mammalian DNA repair and the DNA damage checkpoints. *Annual Review of Biochemistry* **73**:39–85. DOI: https://doi.org/10.1146/annurev.biochem.73.011303.073723, PMID: 15189136

Santabárbara-Ruiz P, López-Santillán M, Martínez-Rodríguez I, Binagui-Casas A, Pérez L, Milán M, Corominas M, Serras F. 2015. ROS-Induced JNK and p38 signaling is required for unpaired cytokine activation during *Drosophila* regeneration. *PLOS Genetics* **11**:e1005595. DOI: https://doi.org/10.1371/journal.pgen.1005595, PMID: 26496642

Schindelin J, Arganda-Carreras I, Frise E, Kaynig V, Longair M, Pietzsch T, Preibisch S, Rueden C, Saalfeld S, Schmid B, Tinevez JY, White DJ, Hartenstein V, Eliceiri K, Tomancak P, Cardona A. 2012. Fiji: an open-source platform for biological-image analysis. *Nature Methods* **9**:676–682. DOI: https://doi.org/10.1038/nmeth.2019, PMID: 22743772

Schosserer M, Grillari J, Breitenbach M. 2017. The dual role of cellular senescence in developing tumors and their response to cancer therapy. *Frontiers in Oncology* **7**:278. DOI: https://doi.org/10.3389/fonc.2017.00278, PMID: 29218300

Seher TC, Leptin M. 2000. Tribbles, a cell-cycle Brake that coordinates proliferation and morphogenesis during Drosophila gastrulation. *Current Biology* **10**:623–629. DOI: https://doi.org/10.1016/S0960-9822(00)00502-9, PMID: 10837248

Shlevkov E, Morata G. 2012. A dp53/JNK-dependant feedback amplification loop is essential for the apoptotic response to stress in Drosophila. *Cell Death & Differentiation* **19**:451–460. DOI: https://doi.org/10.1038/cdd.2011.113, PMID: 21886179

Smith-Bolton RK, Worley MI, Kanda H, Hariharan IK. 2009. Regenerative growth in *Drosophila* imaginal discs is regulated by wingless and myc. *Developmental Cell* **16**:797–809. DOI: https://doi.org/10.1016/j.devcel.2009.04.015, PMID: 19531351

Song YH. 2005. Drosophila melanogaster: a model for the study of DNA damage checkpoint response. *Molecules and Cells* **19**:167–179. PMID: 15879698

Stephens R, Lim K, Portela M, Kvansakul M, Humbert PO, Richardson HE. 2018. The scribble cell polarity module in the regulation of cell signaling in tissue development and tumorigenesis. *Journal of Molecular Biology* **430**:3585–3612. DOI: https://doi.org/10.1016/j.jmb.2018.01.011, PMID: 29409995

Sun G, Irvine KD. 2011. Regulation of hippo signaling by jun kinase signaling during compensatory cell proliferation and regeneration, and in neoplastic tumors. *Developmental Biology* **350**:139–151. DOI: https://doi.org/10.1016/j.ydbio.2010.11.036, PMID: 21145886

Sun G, Irvine KD. 2013. Ajuba family proteins link JNK to hippo signaling. *Science Signaling* **6**:ra81. DOI: https://doi.org/10.1126/scisignal.2004324, PMID: 24023255

Sun G, Irvine KD. 2014. Control of growth during regeneration. *Current Topics in Developmental Biology* **108**:95–120. DOI: https://doi.org/10.1016/B978-0-12-391498-9.00003-6, PMID: 24512707

Takino K, Ohsawa S, Igaki T. 2014. Loss of Rab5 drives non-autonomous cell proliferation through TNF and ras signaling in Drosophila. *Developmental Biology* **395**:19–28. DOI: https://doi.org/10.1016/j.ydbio.2014.09.003, PMID: 25224221

Tang HL, Tang HM, Mak KH, Hu S, Wang SS, Wong KM, Wong CS, Wu HY, Law HT, Liu K, Talbot CC, Lau WK, Montell DJ, Fung MC. 2012. Cell survival, DNA damage, and oncogenic transformation after a transient and reversible apoptotic response. *Molecular Biology of the Cell* **23**:2240–2252. DOI: https://doi.org/10.1091/mbc.e11-11-0926, PMID: 22535522

Taniguchi K, Karin M. 2018. NF-κB, inflammation, immunity and cancer: coming of age. *Nature Reviews Immunology* **18**:309–324. DOI: https://doi.org/10.1038/nri.2017.142, PMID: 29379212

Tapon N, Harvey KF, Bell DW, Wahrer DC, Schiripo TA, Haber D, Hariharan IK. 2002. Salvador promotes both cell cycle exit and apoptosis in *Drosophila* and is mutated in human cancer cell lines. *Cell* **110**:467–478. DOI: https://doi.org/10.1016/S0092-8674(02)00824-3, PMID: 12202036

Thomas BJ, Gunning DA, Cho J, Zipursky L. 1994. Cell cycle progression in the developing Drosophila eye: roughex encodes a novel protein required for the establishment of G1. *Cell* **77**:1003–1014. DOI: https://doi.org/10.1016/0092-8674(94)90440-5, PMID: 8020091

Uhlirova M, Jasper H, Bohmann D. 2005. Non-cell-autonomous induction of tissue overgrowth by JNK/Ras cooperation in a Drosophila tumor model. *PNAS* **102**:13123–13128. DOI: https://doi.org/10.1073/pnas.0504170102, PMID: 16150723

Uhlirova M, Bohmann D. 2006. JNK- and Fos-regulated Mmp1 expression cooperates with ras to induce invasive tumors in Drosophila. *The EMBO Journal* **25**:5294–5304. DOI: https://doi.org/10.1038/sj.emboj.7601401, PMID: 17082773

Vasudevan D, Ryoo HD. 2015. Regulation of cell death by IAPs and their antagonists. *Current Topics in Developmental Biology* **114**:185–208. DOI: https://doi.org/10.1016/bs.ctdb.2015.07.026, PMID: 26431568

Vaux DL, Silke J. 2005. IAPs, RINGs and ubiquitylation. *Nature Reviews Molecular Cell Biology* **6**:287–297. DOI: https://doi.org/10.1038/nrm1621, PMID: 15803136

Wells BS, Yoshida E, Johnston LA. 2006. Compensatory proliferation in *Drosophila* imaginal discs requires Dronc-dependent p53 activity. *Current Biology* **16**:1606–1615. DOI: https://doi.org/10.1016/j.cub.2006.07.046, PMID: 16920621

Wu M, Pastor-Pareja JC, Xu T. 2010. Interaction between ras(V12) and scribbled clones induces tumour growth and invasion. *Nature* **463**:545–548. DOI: https://doi.org/10.1038/nature08702, PMID: 20072127

Xu T, Wang W, Zhang S, Stewart RA, Yu W. 1995. Identifying tumor suppressors in genetic mosaics: the Drosophila lats gene encodes a putative protein kinase. *Development* **121**:1053–1063. PMID: 7743921

Yoo SK, Pascoe HG, Pereira T, Kondo S, Jacinto A, Zhang X, Hariharan IK. 2016. Plexins function in epithelial repair in both Drosophila and zebrafish. *Nature Communications* **7**:12282. DOI: https://doi.org/10.1038/ncomms12282, PMID: 27452696

Zeitler J, Hsu CP, Dionne H, Bilder D. 2004. Domains controlling cell polarity and proliferation in the Drosophila tumor suppressor scribble. *The Journal of Cell Biology* **167**:1137–1146. DOI: https://doi.org/10.1083/jcb.200407158, PMID: 15611336

Zhang L, Ren F, Zhang Q, Chen Y, Wang B, Jiang J. 2008. The TEAD/TEF family of transcription factor scalloped mediates hippo signaling in organ size control. *Developmental Cell* **14**:377–387. DOI: https://doi.org/10.1016/j.devcel.2008.01.006, PMID: 18258485

Zielke N, Korzelius J, van Straaten M, Bender K, Schuhknecht GF, Dutta D, Xiang J, Edgar BA. 2014. Fly-FUCCI: a versatile tool for studying cell proliferation in complex tissues. *Cell Reports* **7**:588–598. DOI: https://doi.org/10.1016/j.celrep.2014.03.020, PMID: 24726363
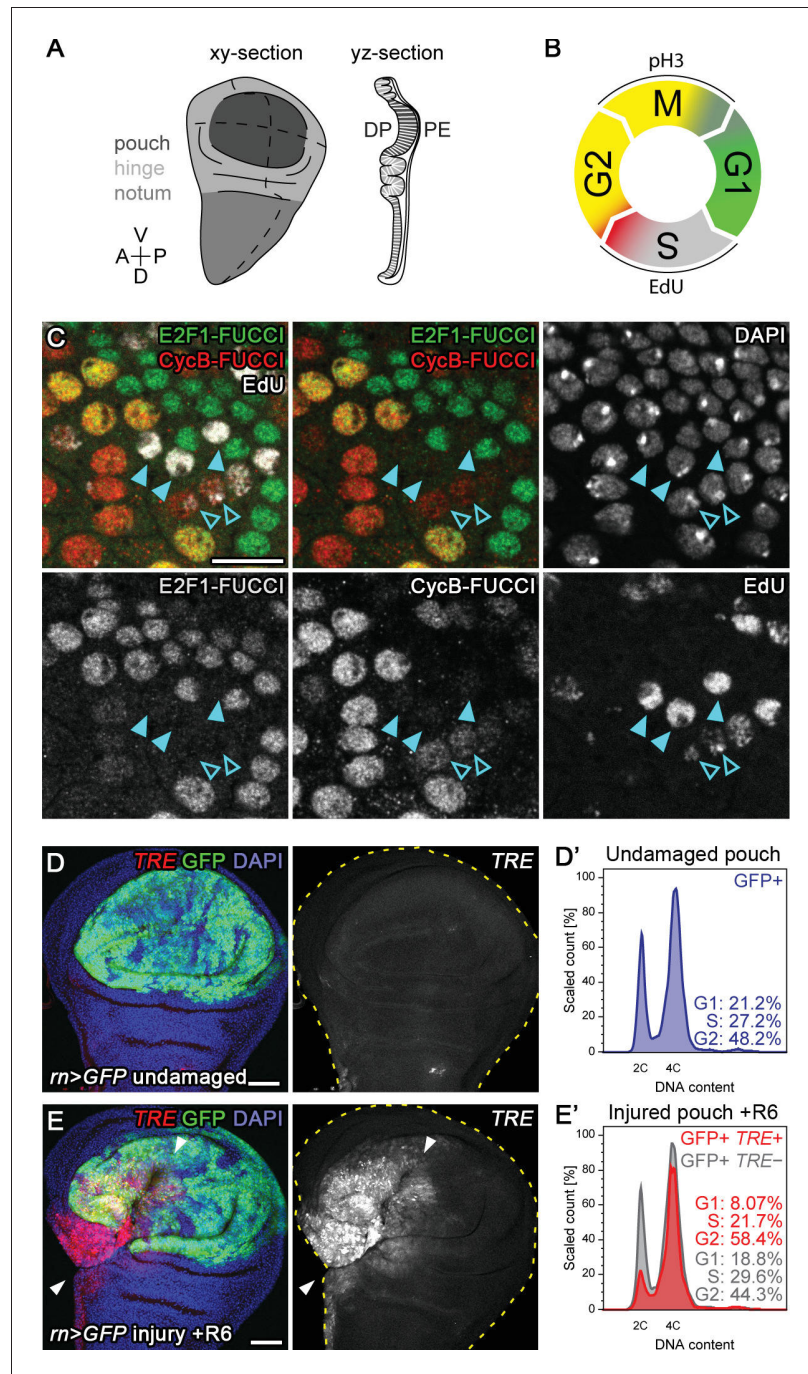
Figure 1—figure supplement 1. Tissue injury induces a transient G2-shift. (**A**) Scheme of a xy-section and yz-section through a wing imaginal disc. Gray shading in xy-view defines the disc subregions of *pouch*, *hinge* and *notum*. Broken lines represent the Anterior-Posterior and Dorsal-Ventral compartment boundaries. The yz-section scheme visualizes the 2 layers of the imaginal disc 'sac'. The columnar cells making up the pouch belong to the 'Disc Proper' whereas the overlying squamous cells belong to the 'Peripodial Epithelium'. Most images in this study represent xy-sections of the pouch and include domains of the hinge, unless noted otherwise. (**B**) Schematic representation of cell cycle phase identification using a combination of FUCCI reporters, EdU incorporation and mitotic markers, such as phospho-Histone 3 (pH3). (**C**) FUCCI reporter and EdU incorporation assays in the peripodium of a wild type wing disc. Identical results are observed in the densely packed epithelium of the disc proper. Wide-spread euchromatic incorporation of EdU (early S-phase) correlates with absence of fluorescence of

Figure 1—figure supplement 1 continued on next page

Figure 1—figure supplement 1 continued

both *mRFP-NLS-CycB*$^{1-266}$ (red) and *GFP-E2f1*$^{1-230}$ (green) FUCCI reporter (filled arrowheads). Heterochromatic incorporation of EdU (late S-phase) correlates with mild elevation of the G2-specific FUCCI reporter *mRFP-NLS-CycB*$^{1-266}$ (red) (open arrowheads). Cells with elevated levels of both FUCCI reporters (yellow) are in late G2 (*Zielke et al., 2014*) after which the FUCCI reporter *mRFP-NLS-CycB*$^{1-266}$ (red) is targeted for proteasomal degradation by APC/C during mitosis. The FUCCI reporter *GFP-E2f1*$^{1-230}$ (green) progressively accumulates in G1 until the onset of S-phase (*Zielke et al., 2014*). (**D–E'**) Flow cytometry analysis of DNA content (**D',E'**) from undamaged control wing discs (**D,D'**) and wing discs with surgical injury 6 hr into the recovery (R6) period (**E,E'**). The pouch of the wing disc was labeled by *rnGAL4*-driven expression of *UAS-GFP* (green in **D,E**). *TRE*-RFP (red in **D,E**) expression is almost undetectable in the pouch of undamaged control discs. JNK-signaling cells in damaged discs were detected by activation of *TRE*-RFP (**E,E'**). Arrowheads indicate axis of injury in (**E**). Only GFP-positive flow cytometry events were plotted in (**D',E'**). *TRE*-RFP positive cells in the undamaged pouch represent <0.1% of the total cell population and are thus not visualized. These plots are derived from the same dataset shown in *Figure 1*. Maximum projections of multiple confocal sections are shown in **D,E**. Scale bars: 10 μm (**C**) and 50 μm (**D,E**).

DOI: https://doi.org/10.7554/eLife.41036.003
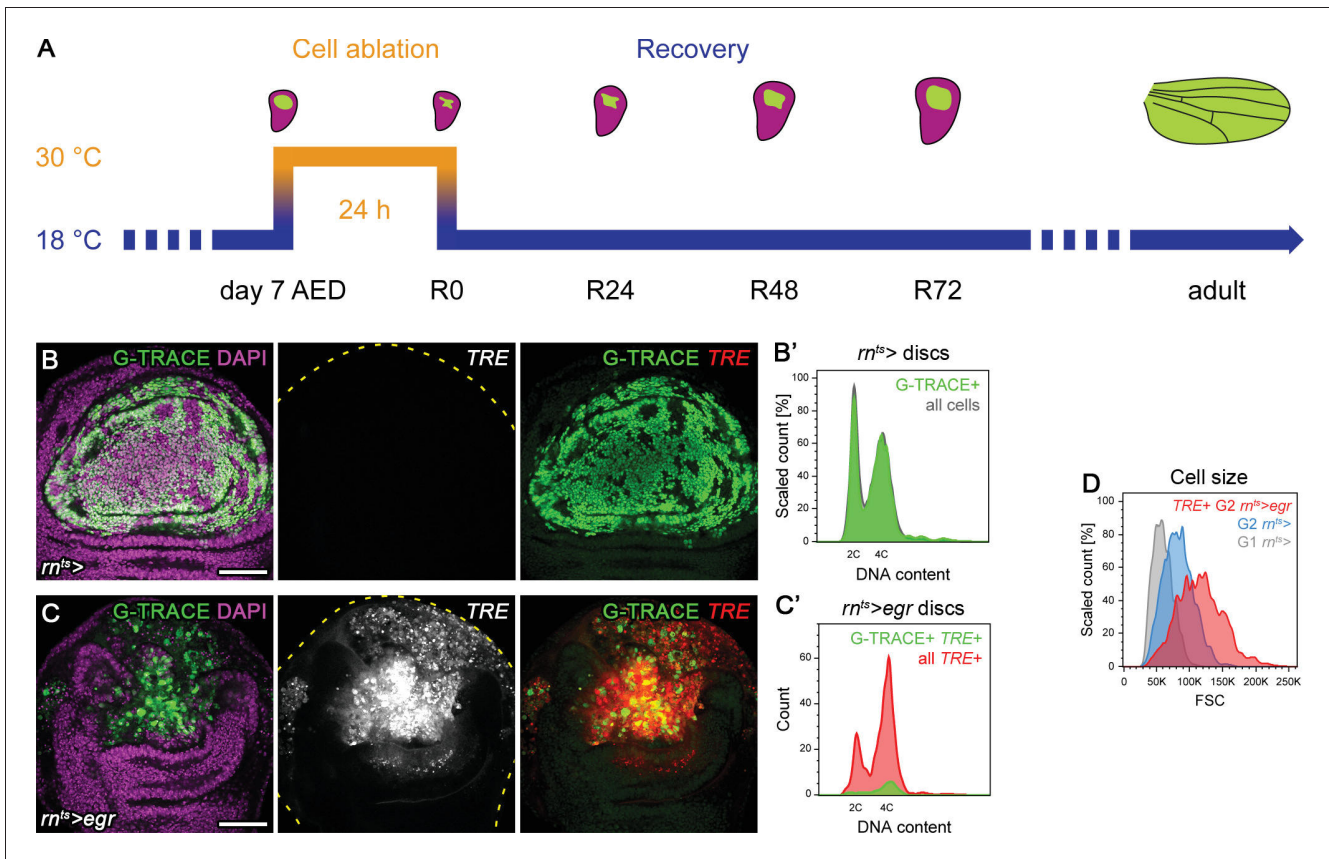
Figure 2—figure supplement 1. Stress-induced JNK activity correlates with G2-stalling. (A) Time line of development and induction of cell ablation by expression of pro-apoptotic transgenes as a function of rearing temperature. Larvae were raised at 18°C (blue) and transferred to 30°C (orange) for 24 hr to induce expression of pro-apoptotic transgenes in wing imaginal discs at day seven after egg deposition (AED). The wing pouch region (green) in third instar wild type disc (magenta) gives rise to future adult wings. Expression of pro-apoptotic transgenes under the control of *rnGAL4* in the pouch causes cell ablation and reduction in the size of the pouch. After expression of pro-apoptotic transgenes ceases by reducing the raising temperature to 18°C, the surviving pouch tissue increases in size between 0 hr to 72 hr of the recovery period (R0, R24, R48, R72). Analysis of adult wing sizes allows conclusion about the extent of the original injury and the success of the regenerative response. Most experiments utilizing expression of pro-apoptotic transgenes like *eiger* (*egr*) or *head involution defective* (*hid*) were visualized at R0, unless noted otherwise. Wing discs and adult wing depictions are not drawn at the same scale. (B–C') Control (B,B') and *egr*-expressing wing discs (C,C') at 0 hr into the recovery period. Cells of the *rnGAL4*-lineage were permanently labeled by expression of GFP (green in B,C) using the G-TRACE lineage labeling system (*Evans et al., 2009*). Discs were counterstained for DAPI (magenta in B,C) and express the JNK-reporter *TRE*-RFP (red in B,C). Note broad activation of *TRE*-RFP autonomous and non-autonomous to surviving *egr*-expressing cells (C). Flow cytometry events were plotted as counts scaled to mode (B') or absolute counts (C') against fluorescence intensity of the live DNA stain Hoechst for all cells (gray in B'), for cells of the *rnGAL4* G-TRACE labeled lineage (green in B'), for cells from *egr*-expressing discs positive for *TRE*-RFP (red in C'), and for the subpopulation of cells surviving *egr* expression in the *rnGAL4* lineage labeled by G-TRACE (green in C'). These plots are derived from the same dataset shown in *Figure 2*. *TRE*-RFP positive cells in undamaged control discs represent only a 2.5% of the total cell population and are thus not visualized separately. Please note that GFP-negative cells activating *TRE*-RFP non-autonomously to the *rnGAL4* lineage also experience a pronounced cell cycle shift if compared to non-ablated control wing discs. (D) Flow cytometry analysis of cell size in G1-phase (gray) and G2-phase (blue) populations of cells from *rn^ts>* control wing discs and in a G2-phase (red) population of *TRE*-RFP positive cells from *rn^ts>egr* discs. Note that *TRE*-positive G2-phase cells are larger than normally cycling cells in G2. Scale bars: 50 μm.
DOI: https://doi.org/10.7554/eLife.41036.005
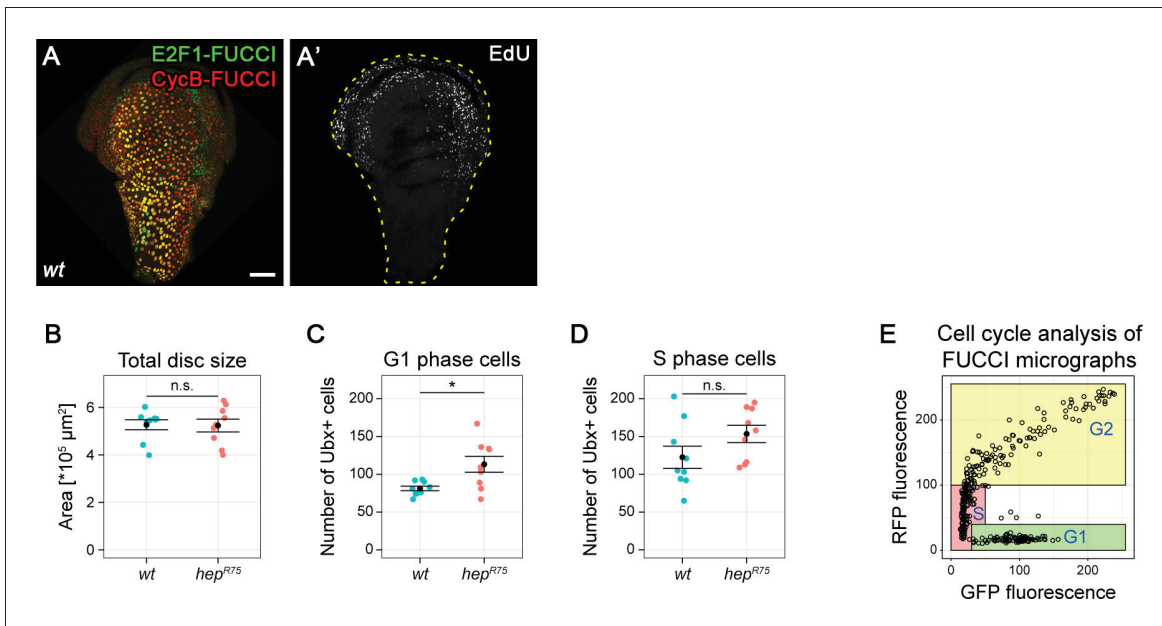
Figure 3—figure supplement 1. JNK activity is necessary and sufficient for G2-stalling. (A,A') The peripodium of a wild type disc expressing the FUCCI reporters (A) and assessed for cycling activity by EdU incorporation to reveal DNA replication activity (A'). (B–D) Quantification of the total disc area size (B), and the number of Ubx-positive cells in G1 phase (C) and S-phase (D) in wild type (blue) and hemizygous *hep*^{R75} (red) discs. These quantifications refer to the same dataset presented in **Figure 3**. Graphs display mean ± SEM for *wt*, n = 9 and *hep*^{R75}, n = 9 discs. *U*-tests were performed to test for statistical significance, n.s. = not significant, *p < 0.05. (E) Cell cycle analysis in a wing disc peripodium based on automated quantification of FUCCI fluorescence intensity in microscopy images (see Materials and methods). Each point represents one Ubx-positive cell and is classified as G1, S or G2 phase according to GFP and RFP fluorescence intensities of the FUCCI reporters. Maximum projections of multiple peripodial confocal sections are shown. Scale bar: 50 μm.

DOI: https://doi.org/10.7554/eLife.41036.007
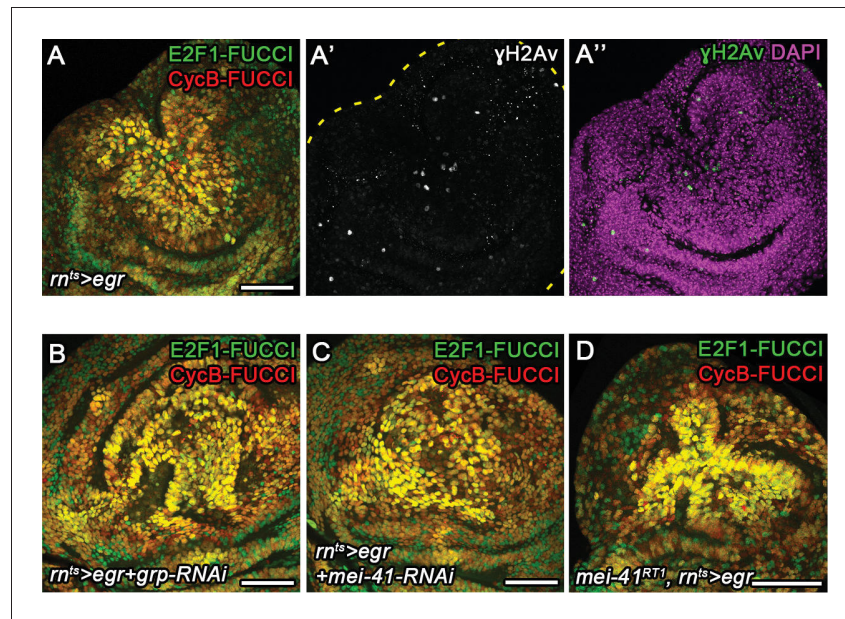
Figure 3—figure supplement 2. DNA damage is not rate-limiting for G2 stalling. (A–A'') *egr*-expressing disc at 0 hr into the recovery period expressing the FUCCI reporters (A) to visualize G2-stalled cells (yellow) was stained for phosphorylated H2Av (γH2Av, A', green in A'') a marker of dsDNA breaks (**Khurana and Oberdoerffer, 2015**). The disc was counterstained for DAPI (magenta in F''). Note lack of correlation between γH2Av and FUCCI patterns. (B–D) *egr*-expressing discs at 0 hr into the recovery period expressing the FUCCI reporters and also expressing RNAi transgenes targeting *grp* (*Drosophila* Chk1) (B) or *mei-41* (*Drosophila* ATR) (C) under the control of *rnGAL4,* or being hemizygous for an allele of *mei-41* (D). Compare FUCCI profiles in (B–D) to (A). Maximum projections of multiple confocal sections are shown. Scale bars: 50 μm.

DOI: https://doi.org/10.7554/eLife.41036.008
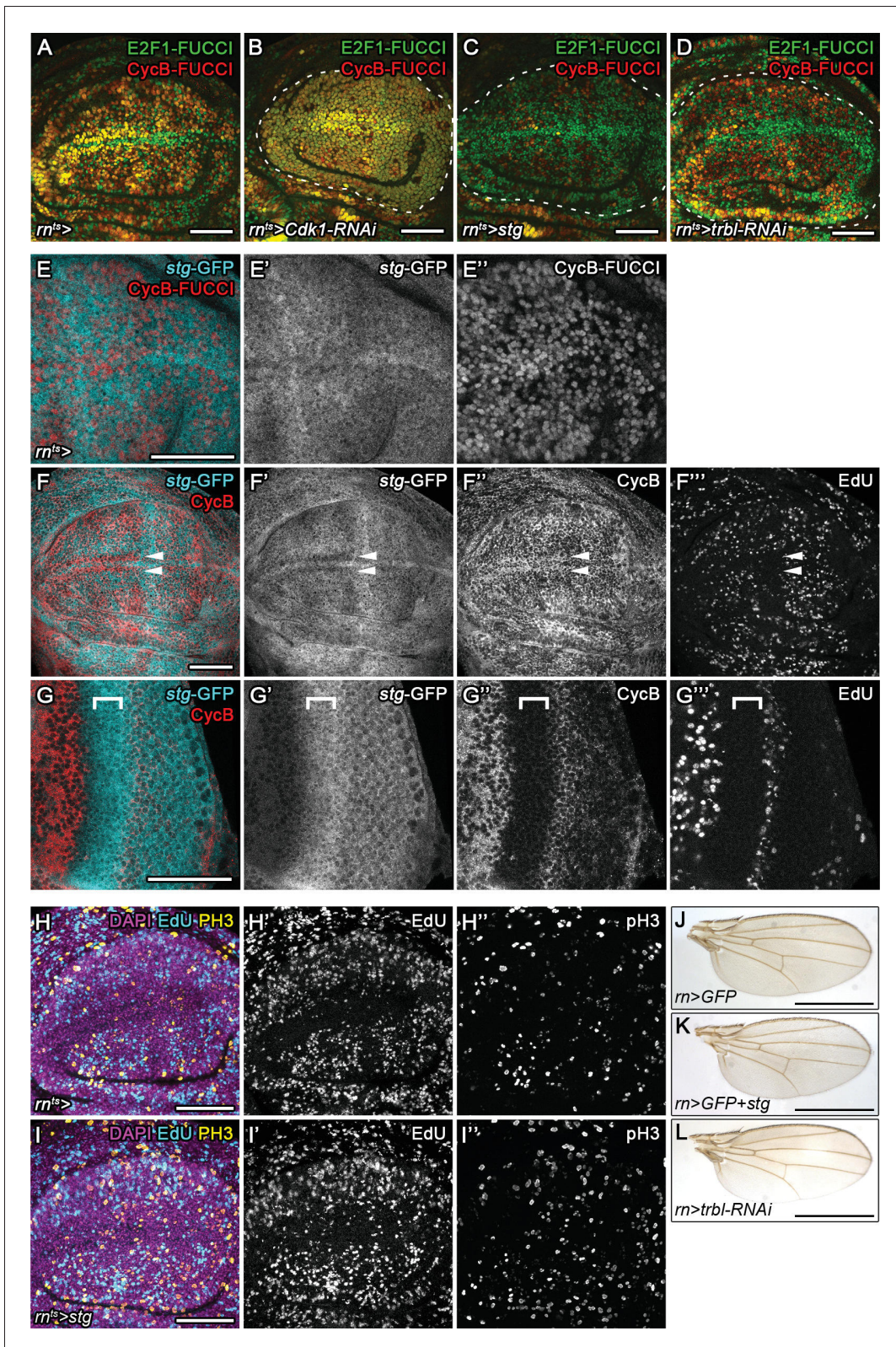
Figure 4—figure supplement 1. Cdc25/String and Tribbles regulate G2 stalling. (A–D) A wild type control disc (A) or wing discs expressing an RNAi transgene targeting *cdk1* (B), overexpressing *stg* (C) or expressing an RNAi transgene targeting *trbl* (D) under the control of *rnGAL4*. All discs express

Figure 4—figure supplement 1 continued on next page

Figure 4—figure supplement 1 continued

the FUCCI reporters. Note the shift towards G2-phase (**B**) or G1-phase (**C,D**) in the wing pouch (encircled by broken line) if compared to a wild type control disc. (**E–E''**) A wing disc expressing a GFP trap element in the *stg* locus (**E'**, cyan in **E**) and the G2-specific FUCCI reporter *mRFP-NLS-CycB$^{1-266}$* (**E''**, red in **E**). Note invariant GFP levels despite heterogeneous cell cycle profile of the tissue. Stg protein levels are expected to predominantly track with *mRFP-NLS-CycB$^{1-266}$*. (**F–G''**) A wing disc (**F–F'''**) and an eye disc (**G–G'''**) expressing a GFP trap element in the *stg* locus and labeled for EdU incorporation to detect DNA replication activity and stained for Cyclin B. Note reduction of GFP expression at the anterior D/V boundary in the wing (arrows in **F**) and elevated GFP expression in the posterior eye disc and morphogenetic furrow (bracket in **G**) as previously reported for *stg* (*Johnston and Edgar, 1998*; *Thomas et al., 1994*). (**H–I''**) Control wing disc (**H–H''**) and an *stg*-overexpressing disc (**I–I''**) under the control of *rnGAL4*. Discs were stained for DAPI (magenta in **H,I**) and assessed for cell cycle activity by EdU incorporation to reveal DNA replication (**H',I'**, cyan in **H,I**) and by staining for phospho-Histone3 to reveal mitotic cells (pH3) (**H'',I''**, yellow in **H,I**). (**J–L**) Representative adult wings arising from of wild type control discs overexpressing GFP (**J**) or from wing discs overexpressing *stg* (**K**) or an RNAi construct targeting *trbl* (**L**) under the control of *rnGAL4*. Maximum projections of multiple confocal sections are shown in **H-I**. Scale bars: 50 µm (**A–I**), 1.0 mm (**J–L**).
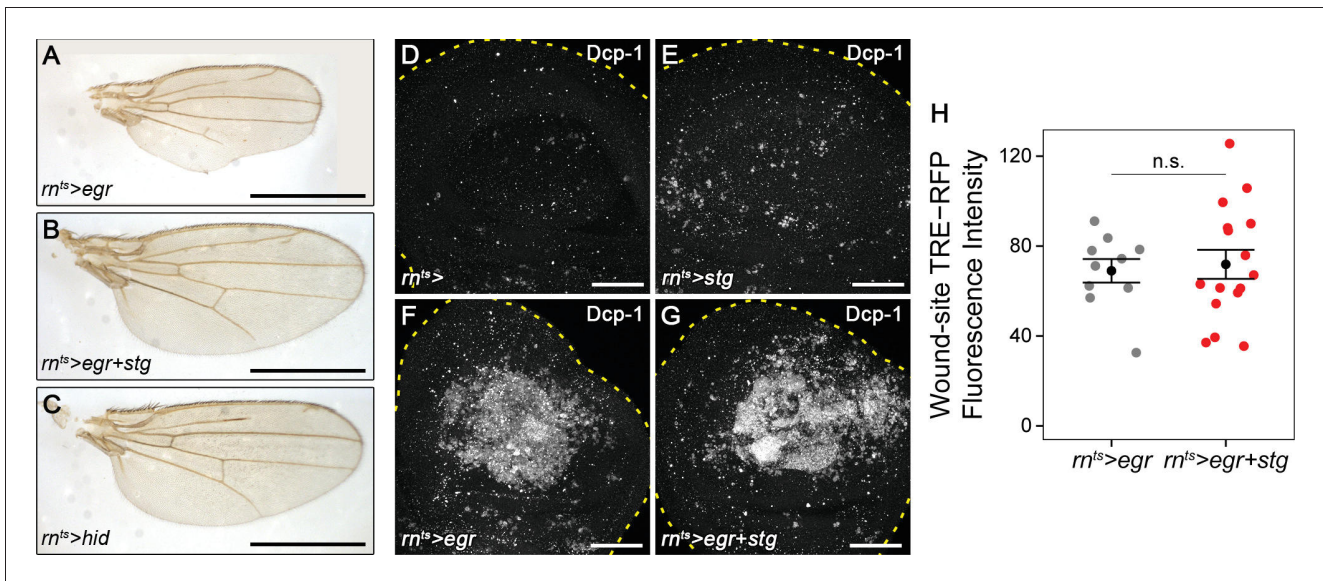
Figure 5—figure supplement 1. Chronic stalling in G2 interferes with proliferative capacity. (A–C) Representative adult wings arising from of *egr*-expressing (A), *egr,stg*-co-expressing (B) and *hid*-expressing discs (C) under the control of *rnGAL4*. (D–G) A control wing disc (D), a *stg*-expressing (E), an *egr*-expressing (F) and an *egr,stg*-co-expressing disc (G) at 0 hr into the recovery period. Discs were stained for the apoptotic marker Dcp-1. Dotted lines trace the outline of the wing disc. (H) Quantification of TRE-RFP fluorescence intensity in the central pouch domain of *egr*-expressing (gray) and *egr,stg*-co-expressing (red) at 0 hr into the recovery period. Graphs display mean ± SEM for *egr*-expressing, *n* = 10 and *egr,stg*-co-expressing, *n* = 16 discs. *U*-tests were performed to test for statistical significance, n.s. = non significant. Maximum projections of multiple confocal sections are shown. Scale bars: 1.0 mm (A–C), 50 μm (D–G).

DOI: https://doi.org/10.7554/eLife.41036.012
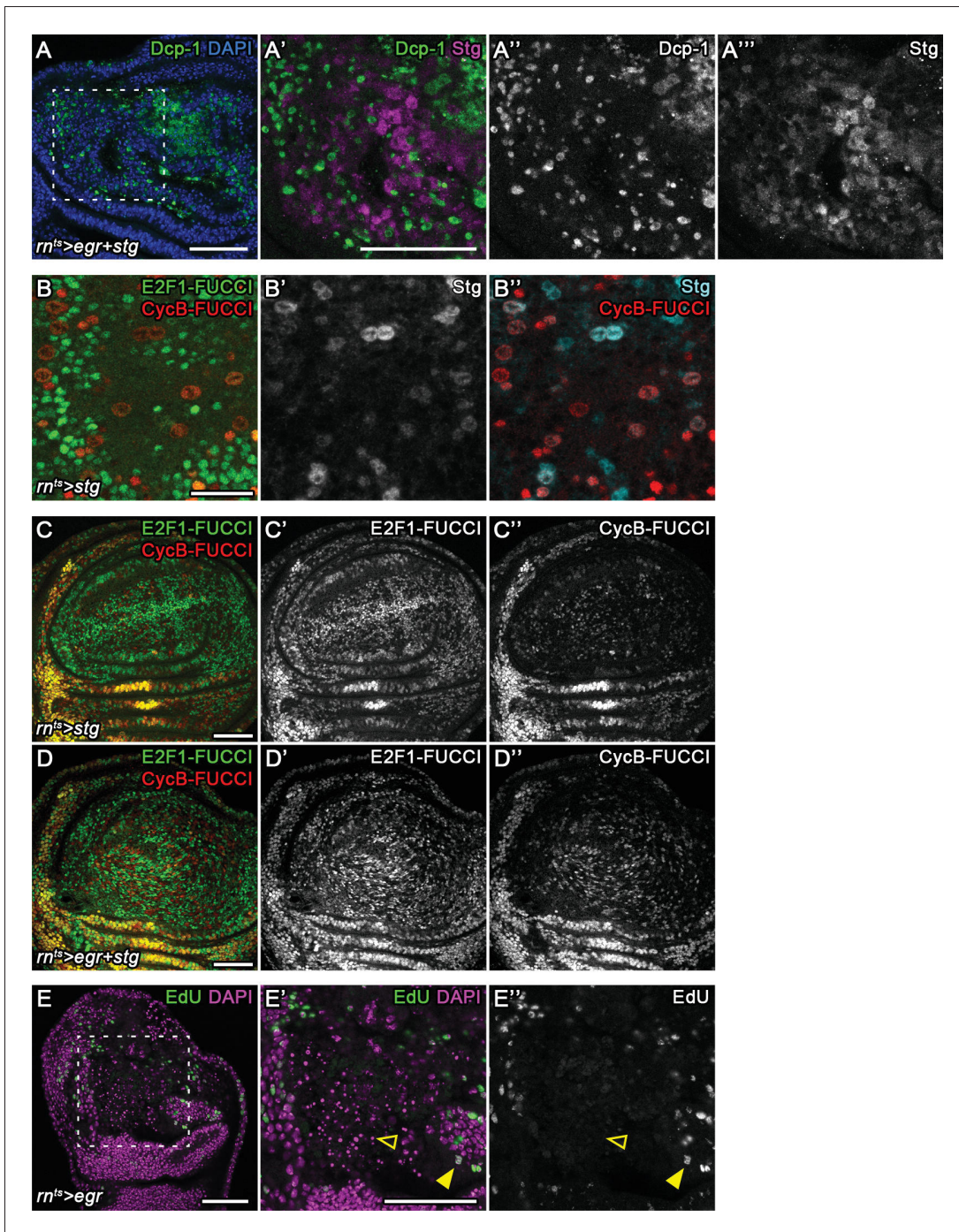
Figure 6—figure supplement 1. Stalling in G2 promotes survival by protecting cells from JNK-induced apoptosis. (**A–A′′′**) A *stg*-expressing disc at 0 hr into the recovery period stained for the apoptotic marker Dcp-1 (**A′′**, green in **A,A′**) and for the HA-tag to visualize overexpressed Stg-HA (**A′′′**, magenta in **A′**). Discs were stained for DAPI (blue in **A**). Note mutually exclusive detection of Dcp-1 and Stg-HA. (**B–B′′**) A FUCCI-expressing disc also expressing *stg-HA* under the control of *rn^{ts}GAL4*. The disc was stained for the HA-tag to visualize Stg-HA (**B′**, cyan in **B′′**). The apical section reveals high expression of Stg-HA in large mitotic cells also positive for *mRFP-NLS-CycB^{1-266}* (red). (**C–D′′**) A *stg*-expressing and an *egr,stg*-co-expressing disc also carrying the *GFP-E2f1^{1-230}* (**C′**, **D′**, green in **C,D**) and the *mRFP-NLS-CycB^{1-266}* (**C′′,D′′**, red in **C,D**) FUCCI reporters. Despite extensive cell death in the tissue upon *egr* co-expression, the distribution of *stg*-induced cell cycle profile does not extensively change, supporting the conclusion that low FUCCI reporter expression is not consequence of apoptotic cell death. (**E–E′′**) A single confocal section through basal domains of an *egr*-expressing disc (closed arrowhead) to visualize apoptotic cell debris (open arrowhead). The disc has been allowed to incorporate EdU for 1 hr to visualize a more

Figure 6—figure supplement 1 continued on next page

Figure 6—figure supplement 1 continued

historic footprint of DNA replication activity (**E''**, green in **E,E'**). The disc was stained for DAPI (magenta in **E,E'**). The broken line in **E** frames the region shown in **E',E''**. While the viable tissue has undergone EdU incorporation (closed arrowhead), none of the pyknotic nuclei show evidence of recent DNA replication activity (open arrowhead). Scale bars: 50 μm (**A–A''', C–E''**), 20 μm (**B**).
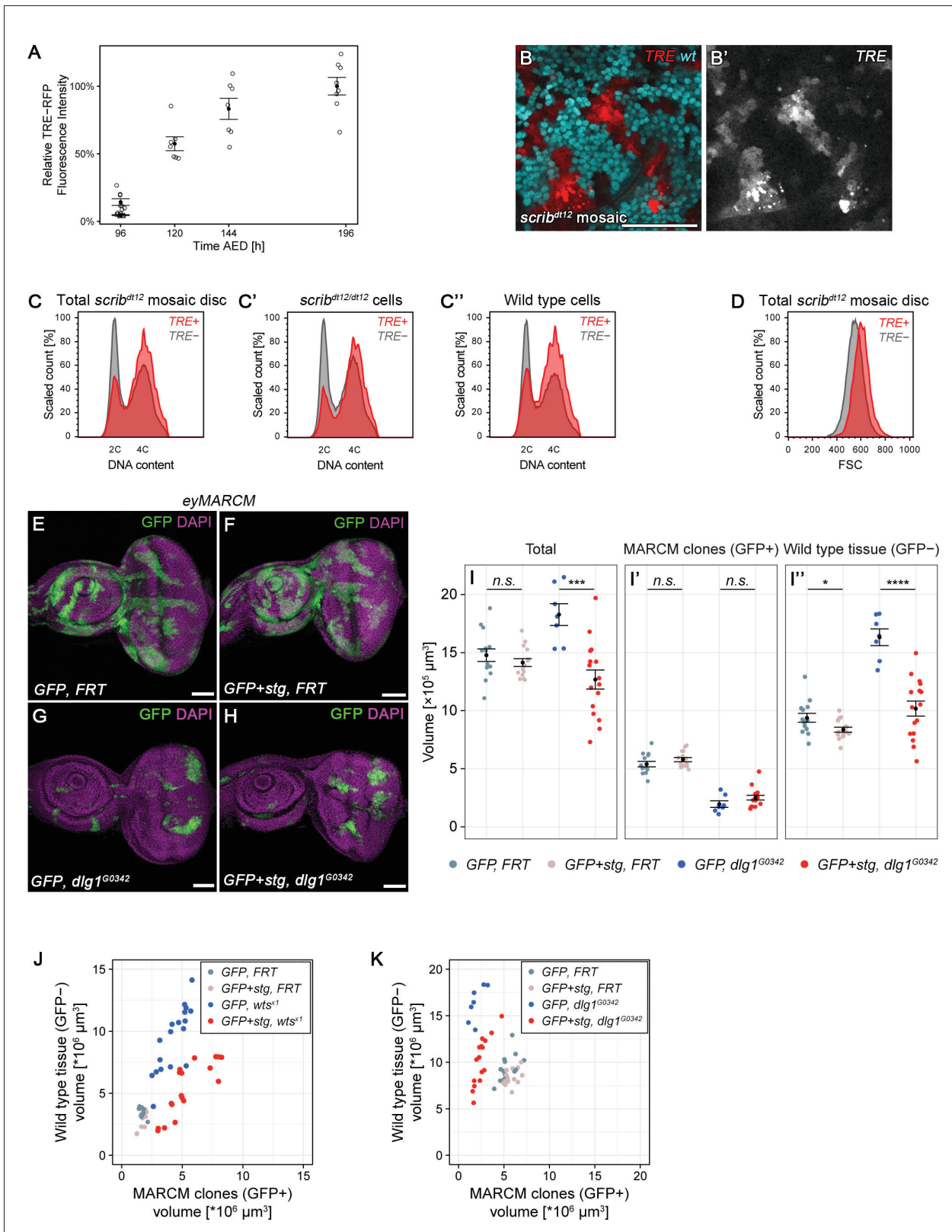
Figure 7—figure supplement 1. Chronic stalling in G2 promotes non-autonomous overgrowth. (**A**) Quantification of relative *TRE*-RFP fluorescence intensity in mosaic wing discs carrying *wts*^{X1} clones at 96 hr to 196 hr after egg deposition (AED) at 25°C (circles). Note that wild type larvae normally

Figure 7—figure supplement 1 continued on next page

Figure 7—figure supplement 1 continued

pupariate around 120 hr AED. Squares represent discs carrying wild type MARCM clones. Graphs display mean ± SEM for $n = 8$ (96 h), $n = 7$ (120 h), $n = 7$ (144 h), $n = 8$ (192 h), $n = 6$ (control) discs. (B–D′′) Wing discs expressing *TRE*-RFP (red) and carrying *scrib*$^{dt12/dt12}$ clones marked by the absence of GFP (cyan in B), were analyzed for DNA content (C–C′′) cell size (D) and by flow cytometry. The total cell population of discs was plotted as *TRE*-positive or *TRE*-negative events (C,D). The same analysis was also applied separately to GFP-negative (*scrib*$^{dt12/dt12}$ cells, C′) and GFP-positive (wild type cells, C′′) sub-populations. Detected events were plotted as counts scaled to mode against fluorescence intensity of the live DNA stain Hoechst. (E–H) Wing imaginal discs carrying GFP-labeled MARCM clones (green) that are either wild type (E), *stg*-overexpressing (F), mutant for *dlg1*^{G0342} (G) or *stg*-overexpressing and mutant for *dlg1*^{G0342} (H). Discs were counterstained with DAPI (magenta). (I–I′′) Volumes occupied by the total disc (I), the GFP-labeled fraction representing MARCM clones (I′) and the non-GFP-labeled fraction representing the surrounding wild type tissue (I′′). Graphs display mean ± SEM for *tub>GFP, FRT*, $n = 14$; *tub>GFP+stg, FRT*, $n = 15$; *tub>GFP, FRT dlg1*^{G0342}, $n = 7$; *tub>GFP+stg, FRT dlg1*^{G0342}, $n = 16$ discs. *U*-tests were performed to test for statistical significance (*n.s.* not significant, *$p<0.05$, ***$p<0.001$, ****$p<0.0001$). (J,K) Dot plots representing each of the discs analyzed in *Figure 7K* (J) and *Figure 7—figure supplement 1I* (K), pairing the data for the GFP-negative wild type tissue volume and the GFP-positive tissue volume they surround, which is either wild type (grey), *stg*-overexpressing (pink), mutant for *dlg1*^{G0342} or *wts*^{X1} (blue in J or K) or *stg*-overexpressing and mutant for *dlg1*^{G0342} or *wts*^{X1} (red in J or K).

DOI: https://doi.org/10.7554/eLife.41036.016
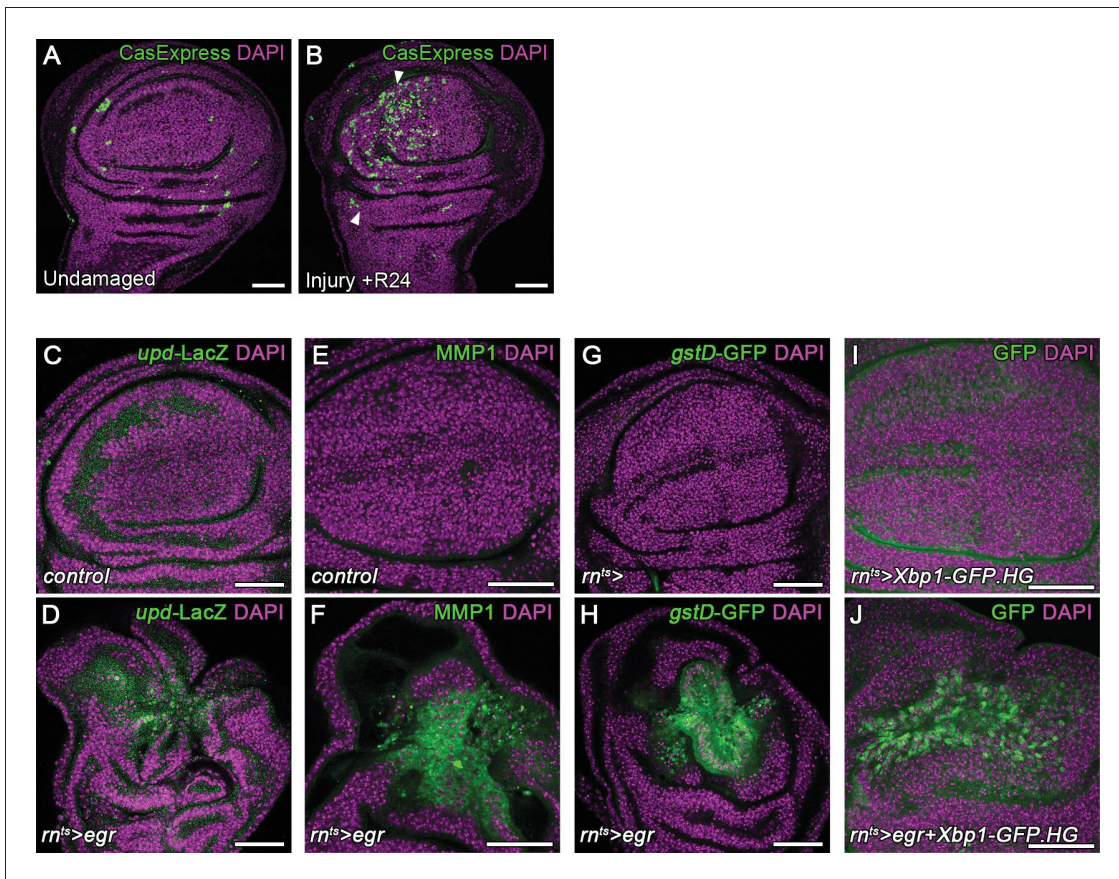
Figure 7—figure supplement 2. Chronic stalling in G2 promotes mitogenic signaling. (A,B) A control wing disc (A) and a surgically injured disc 24 hr after injury (B). Both discs use the CasExpress and G-TRACE reporter system to drive expression of GFP in cells that had experienced Caspase activity previously but survive. (C–J) Control wing discs (C,E,G,I) and *egr*-expressing discs (D,F,H,J) at 0 hr into the recovery period also analyzed for expression of *upd*-LacZ (C,D), MMP-1 (E,F), *GstD*-GFP (G,H) and spliced Xbp1 (I,J) (green in C-J). Discs were counterstained with DAPI (magenta). Maximum projections of multiple confocal sections are shown in I,J. Scale bars: 50 μm.

DOI: https://doi.org/10.7554/eLife.41036.017

Figure panel	Genotype	Raising temperature

Figure 1

A,B,C	en-GAL4, UAS-GFP/Ubi-GFP.E2f.1-230, Ubi-mRFP1.NLS.CycB.1-266; puc-LacZ	25°C
D,E	TRE-RFP/UAS-GFP S56T; rn-GAL4	25°C

Figure 1-figure supplement 1

B	Ubi-GFP.E2f.1-230, Ubi-mRFP1.NLS.CycB.1-266; rnGAL4, tub-GAL80ts	18°C until day 7 AED + 24h at 30°C
D-E'	TRE-RFP/UAS-GFP S56T; rn-GAL4	25°C

Figure 2

A	Ubi-GFP.E2f.1-230, Ubi-mRFP1.NLS.CycB.1-266; rn-GAL4, tub-GAL80(ts)	18°C until day 7 AED + 24h at 30°C
B	Ubi-GFP.E2f.1-230, Ubi-mRFP1.NLS.CycB.1-266; rn-GAL4, tub-GAL80(ts), UAS-egr	18°C until day 7 AED + 24h at 30°C
C,C',D,L,L'	TRE-RFP; rn-GAL4, tub-GAL80(ts), UAS-egr / UAS-Flp, ubi(FRT.STOP)-GFP	18°C until day 7 AED + 24h at 30°C
E	TRE-RFP; rn-GAL4, tub-GAL80(ts)	18°C until day 7 AED + 24h at 30°C
F,G	TRE-RFP; rn-GAL4, tub-GAL80(ts), UAS-egr	18°C until day 7 AED + 24h at 30°C
H	TRE-RFP; rn-GAL4, tub-GAL80(ts), UAS-egr	18°C until day 7 AED + 24h at 30°C + 24h at 18°C
I	TRE-RFP; rn-GAL4, tub-GAL80(ts), UAS-egr	18°C until day 7 AED + 24h at 30°C + 72h at 18°C
J	Ubi-GFP.E2f.1-230, Ubi-mRFP1.NLS.CycB.1-266; rn-GAL4, tub-GAL80(ts), UAS-egr	18°C until day 7 AED + 24h at 30°C + 24h at 18°C
K	Ubi-GFP.E2f.1-230, Ubi-mRFP1.NLS.CycB.1-266; rn-GAL4, tub-GAL80(ts), UAS-egr	18°C until day 7 AED + 24h at 30°C + 72h at 18°C

Figure 2-figure supplement 1

B,B'	TRE-RFP; rn-GAL4, tub-GAL80(ts) / UAS-Flp, ubi(FRT.STOP)-GFP	18°C until day 7 AED + 24h at 30°C
C,C',D	TRE-RFP; rn-GAL4, tub-GAL80(ts), UAS-egr / UAS-Flp, ubi(FRT.STOP)-GFP	18°C until day 7 AED + 24h at 30°C

Figure 3

A	Ubi-GFP.E2f.1-230, Ubi-mRFP1.NLS.CycB.1-266/UAS-hep[act]; rn-GAL4, tub-GAL80(ts)	18°C until day 7 AED + 24h at 30°C
B	UAS-bsk(DN); Ubi-GFP.E2f.1-230, Ubi-mRFP1.NLS.CycB.1-266/enGAL4, UAS-GFP; puc-LacZ	25°C
C	TRE-RFP	25°C
D,F,G	+/y; Ubi-GFP.E2f.1-230, Ubi-mRFP1.NLS.CycB.1-266	25°C
E,F,G	hep(R75)/y; Ubi-GFP.E2f.1-230, Ubi-mRFP1.NLS.CycB.1-266	25°C

Figure 3-figure supplement 1

A	Ubi-GFP.E2f.1-230, Ubi-mRFP1.NLS.CycB.1-266	25°C
B-E	+/y; Ubi-GFP.E2f.1-230, Ubi-mRFP1.NLS.CycB.1-266	25°C
B-D	hep(R75)/y; Ubi-GFP.E2f.1-230, Ubi-mRFP1.NLS.CycB.1-266	25°C

Figure 3-figure supplement 2

A	Ubi-GFP.E2f.1-230, Ubi-mRFP1.NLS.CycB.1-266; rn-GAL4, tub-GAL80(ts), UAS-egr	18°C until day 7 AED + 24h at 30°C
B	Ubi-GFP.E2f.1-230, Ubi-mRFP1.NLS.CycB.1-266/UAS-grp RNAi; rn-GAL4, tub-GAL80(ts), UAS-egr	18°C until day 7 AED + 24h at 30°C
C	Ubi-GFP.E2f.1-230, Ubi-mRFP1.NLS.CycB.1-266; rn-GAL4, tub-GAL80(ts), UAS-egr/UAS-mei-41 RNAi	18°C until day 7 AED + 24h at 30°C
D	mei-41[RT1]/y; Ubi-GFP.E2f.1-230, Ubi-mRFP1.NLS.CycB.1-266; rn-GAL4, tub-GAL80(ts), UAS-egr	18°C until day 7 AED + 24h at 30°C

Figure 4

A	Ubi-mRFP1.NLS.CycB.1-266; rn-GAL4, tub-GAL80(ts)/stg-GFP	18°C until day 7 AED + 24h at 30°C
B	Ubi-mRFP1.NLS.CycB.1-266; rn-GAL4, tub-GAL80(ts), UAS-egr/stg-GFP	18°C until day 7 AED + 24h at 30°C
C	trbl-GFP/TM6B, tub-GAL80	18°C until day 7 AED + 24h at 30°C
D	trbl-GFP/rn-GAL4, tub-GAL80(ts), UAS-egr	18°C until day 7 AED + 24h at 30°C
E	UAS-bsk(DN); en-GAL4; trbl-GFP/GH146-QF, QUAS-mtdTomato-3xHA	18°C until injury, 25°C during recovery
F	Ubi-GFP.E2f.1-230, Ubi-mRFP1.NLS.CycB.1-266; rn-GAL4, tub-GAL80(ts), UAS-egr	18°C until day 7 AED + 24h at 30°C
G	Ubi-GFP.E2f.1-230, Ubi-mRFP1.NLS.CycB.1-266/UAS-stg; rn-GAL4, tub-GAL80(ts), UAS-egr	18°C until day 7 AED + 24h at 30°C
H	'Ubi-GFP.E2f.1-230, Ubi-mRFP1.NLS.CycB.1-266/UAS-trbl RNAi (TRiP.HMJ02089); rn-GAL4, tub-GAL80(ts), UAS-egr	18°C until day 7 AED + 24h at 30°C
I	rn-GAL4, tub-GAL80(ts), UAS-egr	18°C until day 7 AED + 24h at 30°C
J	UAS-stg; rn-GAL4, tub-GAL80(ts), UAS-egr	18°C until day 7 AED + 24h at 30°C

Figure 4-figure supplement 1

A	Ubi-GFP.E2f.1-230, Ubi-mRFP1.NLS.CycB.1-266; rn-GAL4, tub-GAL80(ts)	18°C until day 7 AED + 24h at 30°C
B	Ubi-GFP.E2f.1-230, Ubi-mRFP1.NLS.CycB.1-266/UAS-Cdk1 RNAi (TRiP.HMS01531); rn-GAL4, tub-GAL80(ts)	18°C until day 7 AED + 24h at 30°C
C	Ubi-GFP.E2f.1-230, Ubi-mRFP1.NLS.CycB.1-266/UAS-stg; rn-GAL4, tub-GAL80(ts)	18°C until day 7 AED + 24h at 30°C
D	Ubi-GFP.E2f.1-230, Ubi-mRFP1.NLS.CycB.1-266/UAS-trbl RNAi (TRiP.HMJ02089); rn-GAL4, tub-GAL80(ts)	18°C until day 7 AED + 24h at 30°C
E	Ubi-mRFP1.NLS.CycB.1-266; rn-GAL4, tub-GAL80(ts)/stg[YD0685]-GFP	18°C until day 7 AED + 24h at 30°C
F,G	stg[YD0685]-GFP	25°C
H	rn-GAL4, tub-GAL80(ts)	18°C until day 7 AED + 24h at 30°C
I	UAS-stg; rn-GAL4, tub-GAL80(ts)	18°C until day 7 AED + 24h at 30°C
J	UAS-GFP; rn-GAL4	25°C
K	UAS-stg/UAS-GFP; rn-GAL4	25°C
L	UAS-trbl RNAi (TRiP.HMJ02089); rn-GAL4	25°C

Figure 5

A	rn-GAL4, tub-GAL80(ts)/UAS-Flp, ubi(FRT.STOP)-GFP	18°C until day 7 AED + 24h at 30°C
B	TRE-RFP; rn-GAL4, tub-GAL80(ts), UAS-egr	18°C until day 7 AED + 24h at 30°C
C	UAS-stg/TRE-RFP; rn-GAL4, tub-GAL80(ts), UAS-egr	18°C until day 7 AED + 24h at 30°C
D	UAS-hid; rn-GAL4, tub-GAL80(ts)/UAS-Flp, ubi(FRT.STOP)-GFP	18°C until day 7 AED + 24h at 30°C
E	rn-GAL4, tub-GAL80(ts), UAS-egr	18°C until day 7 AED + 24h at 30°C + 18°C until adulthood
E	UAS-stg; rn-GAL4, tub-GAL80(ts), UAS-egr	18°C until day 7 AED + 24h at 30°C + 18°C until adulthood
E	UAS-hid; rn-GAL4, tub-GAL80(ts)	18°C until day 7 AED + 24h at 30°C + 18°C until adulthood
F	TRE-RFP; rn-GAL4, tub-GAL80(ts)/ UAS-Flp, ubi(FRT.STOP)-GFP	18°C until day 7 AED + 24h at 30°C
G	rn-GAL4, tub-GAL80(ts), UAS-egr / UAS-Flp, ubi(FRT.STOP)-GFP	18°C until day 7 AED + 24h at 30°C
H	UAS-stg; rn-GAL4, tub-GAL80(ts), UAS-egr / UAS-Flp, ubi(FRT.STOP)-GFP	18°C until day 7 AED + 24h at 30°C
I	TRE-RFP; 10xStat92e-DGFP	18°C until day 7 AED + 24h at 30°C
J	TRE-RFP; 10xStat92e-DGFP/rn-GAL4, tub-GAL80(ts), UAS-egr	18°C until day 7 AED + 24h at 30°C
K	TRE-RFP/UAS-hid; 10xStat92e-DGFP/rn-GAL4, tub-GAL80(ts)	18°C until day 7 AED + 24h at 30°C
L	UAS-hid/Ubi-GFP.E2f.1-230, Ubi-mRFP1.NLS.CycB.1-266; rn-GAL4, tub-GAL80(ts)	18°C until day 7 AED + 24h at 30°C
M	TRE-RFP/UAS-GFP; rn-GAL4	25°C
N	TRE-RFP; rn-GAL4, tub-GAL80(ts), UAS-egr	18°C until day 7 AED + 24h at 30°C + 0/24/48/72h at 18°C

Figure 5-figure supplement 1

A	rn-GAL4, tub-GAL80(ts), UAS-egr	18°C until day 7 AED + 24h at 30°C + 18°C until adulthood
B	UAS-stg; rn-GAL4, tub-GAL80(ts), UAS-egr	18°C until day 7 AED + 24h at 30°C + 18°C until adulthood
C	UAS-hid; rn-GAL4, tub-GAL80(ts)	18°C until day 7 AED + 24h at 30°C + 18°C until adulthood
D	rn-GAL4, tub-GAL80(ts)	18°C until day 7 AED + 24h at 30°C
E	UAS-stg; rn-GAL4, tub-GAL80(ts)	18°C until day 7 AED + 24h at 30°C
F	rn-GAL4, tub-GAL80(ts), UAS-egr	18°C until day 7 AED + 24h at 30°C
G	UAS-stg; rn-GAL4, tub-GAL80(ts), UAS-egr	18°C until day 7 AED + 24h at 30°C

H	TRE-RFP; rn-GAL4, tub-GAL80(ts), UAS-egr	18°C until day 7 AED + 24h at 30°C
H	UAS-stg/TRE-RFP; rn-GAL4, tub-GAL80(ts), UAS-egr	18°C until day 7 AED + 24h at 30°C

Figure 6

A,C,E	UAS-GFP; rn-GAL4	25°C
B,D,E	UAS-GFP/UAS-stg.HA; rn-GAL4	25°C
F-G'	Ubi-GFP.E2f.1-230, Ubi-mRFP1.NLS.CycB.1-266/UAS-stg.HA; rn-GAL4, tub-GAL80(ts), UAS-egr	18°C until day 7 AED + 24h at 30°C
H,I	UAS-GFP; rn-GAL4, tub-GAL80(ts), UAS-egr	18°C until day 7 AED + 24h at 30°C
J	Diap1-GFP/Ubi-mRFP1.NLS.CycB.1-266; TM6b, tub-GAL80	18°C until day 7 AED + 24h at 30°C
K	Diap1-GFP/Ubi-mRFP1.NLS.CycB.1-266; rn-GAL4, tub-GAL80(ts), UAS-egr	18°C until day 7 AED + 24h at 30°C
L	TRE-RFP; Hid-GFP/TM6b, tub-GAL80	18°C until day 7 AED + 24h at 30°C
M	TRE-RFP; Hid-GFP/rn-GAL4, tub-GAL80(ts), UAS-egr	18°C until day 7 AED + 24h at 30°C

Figure 6-figure supplement 1

A	UAS-stg.HA/Diap1-GFP; rn-GAL4, tub-GAL80(ts), UAS-egr	18°C until day 7 AED + 24h at 30°C
B,C	Ubi-GFP.E2f.1-230, Ubi-mRFP1.NLS.CycB.1-266/UAS-stg.HA; rn-GAL4, tub-GAL80(ts)	18°C until day 7 AED + 24h at 30°C
D	Ubi-GFP.E2f.1-230, Ubi-mRFP1.NLS.CycB.1-266/UAS-stg.HA; rn-GAL4, tub-GAL80(ts), UAS-egr	18°C until day 7 AED + 24h at 30°C
E	Ubi-GFP.E2f.1-230, Ubi-mRFP1.NLS.CycB.1-266; rn-GAL4, tub-GAL80(ts), UAS-egr	18°C until day 7 AED + 24h at 30°C

Figure 7

A,E,F	ubx flp; TRE-RFP; FRT82B wts[x1]/FRT82B ubi-GFP	25°C
B	TRE-RFP/UAS-GFP; rn-GAL4	25°C
C	ubx-flp, tub-GAL4, UAS-GFP; TRE-RFP; FRT82B wts[x1]/FRT82B tub-GAL80	25°C
D	TRE-RFP; rn-GAL4, tub-GAL80(ts), UAS-egr	18°C until day 7 AED + 24h at 30°C
G,K-K''	ubx-flp, tub-GAL4, UAS-GFP; ; FRT82B/FRT82B tub-GAL80	25°C
H,K-K''	ubx-flp, tub-GAL4, UAS-GFP; UAS-stg.HA; FRT82B/FRT82B tub-GAL80	25°C
I,K-K'',L,M	ubx-flp, tub-GAL4, UAS-GFP; ; FRT82B wts[x1]/FRT82B tub-GAL80	25°C
J,K-K'',L,M	ubx-flp, tub-GAL4, UAS-GFP; UAS-stg.HA; FRT82B wts[x1]/FRT82B tub-GAL80	25°C
N	Ubi-GFP.E2f.1-230, Ubi-mRFP1.NLS.CycB.1-266/UAS-P35; rn-GAL4, tub-GAL80(ts), UAS-egr	18°C until day 7 AED + 24h at 30°C

Figure 7-figure supplement 1

A	ubx flp; TRE-RFP; FRT82B wts[x1]/FRT82B ubi-GFP	25°C
B-D	ubx flp; TRE-RFP; FRT82B scrib[dt12]/FRT82B ubi-GFP	25°C
E,I-I'',K	FRT19A/ey-FLP, FRT19A tub-GAL80; act5c>y[+]>GAL4, UAS-GFP[S56T]	25°C
F,I-I'',K	FRT19A/ey-FLP, FRT19A tub-GAL80; act5c>y[+]>GAL4, UAS-GFP[S56T]/UAS-stg	25°C
G,I-I'',K	FRT19A dlg1[G0342]/ey-FLP, FRT19A tub-GAL80; act5c>y[+]>GAL4, UAS-GFP[S56T]	25°C
H,I-I'',K	FRT19A dlg1[G0342]/ey-FLP, FRT19A tub-GAL80; act5c>y[+]>GAL4, UAS-GFP[S56T]/UAS-stg	25°C
J	ubx-flp, tub-GAL4, UAS-GFP; ; FRT82B/FRT82B tub-GAL80	25°C
J	ubx-flp, tub-GAL4, UAS-GFP; UAS-stg.HA; FRT82B/FRT82B tub-GAL80	25°C
J	ubx-flp, tub-GAL4, UAS-GFP; ; FRT82B wts[x1]/FRT82B tub-GAL80	25°C
J	ubx-flp, tub-GAL4, UAS-GFP; UAS-stg.HA; FRT82B wts[x1]/FRT82B tub-GAL80	25°C

Figure 7-figure supplement 2

A-B	ubi-CasExpress; UAS-Flp, ubi(FRT.STOP)-GFP/GH146-QF, QUAS-mtdTomato-3xHA	18°C until injury, 25°C during recovery
C	Upd-LacZ/X; TRE-RFP; TM6b, tub-GAL80	18°C until day 7 AED + 24h at 30°C
D	Upd-LacZ/X; TRE-RFP; rn-GAL4, tub-GAL80(ts), UAS-egr	18°C until day 7 AED + 24h at 30°C
E	TM6B, tub-GAL80	18°C until day 7 AED + 24h at 30°C
F	rn-GAL4, tub-GAL80(ts), UAS-egr	18°C until day 7 AED + 24h at 30°C
G	gstD-GFP; rn-GAL4, tub-GAL80(ts)	18°C until day 7 AED + 24h at 30°C
H	gstD-GFP; rn-GAL4, tub-GAL80(ts), UAS-egr	18°C until day 7 AED + 24h at 30°C
I	UAS-Xbp1-GFP.HG/ rn-GAL4, tub-GAL80(ts)	18°C until day 7 AED + 24h at 30°C
J	UAS-Xbp1-GFP.HG/ rn-GAL4, tub-GAL80(ts), UAS-egr	18°C until day 7 AED + 24h at 30°C

5 JAK/STAT signalling mediates cell survival in response to tissue stress

La Fortezza M, Schenk M, Cosolo A, Kolybaba A, Grass I, Classen AK

Development. 2016 Aug 15;143(16):2907-19. doi: 10.1242/dev.132340.

Permission to reproduce the full article in this thesis has been obtained.

JAK/STAT signalling mediates cell survival in response to tissue stress

Marco La Fortezza, Madlin Schenk, Andrea Cosolo, Addie Kolybaba, Isabelle Grass and Anne-Kathrin Classen*

ABSTRACT

Tissue homeostasis relies on the ability of tissues to respond to stress. Tissue regeneration and tumour models in *Drosophila* have shown that c-Jun amino-terminal kinase (JNK) acts as a prominent stress-response pathway promoting injury-induced apoptosis and compensatory proliferation. A central question remaining unanswered is how both responses are balanced by activation of a single pathway. Signalling through the Janus kinase/Signal transducers and activators of transcription (JAK/STAT) pathway, which is a potential JNK target, is implicated in promoting compensatory proliferation. While we observe JAK/STAT activation in imaginal discs upon damage, our data demonstrate that JAK/STAT and its downstream effector Zfh2 promote the survival of JNK signalling cells. The JNK component *fos* and the pro-apoptotic gene *hid* are regulated in a JAK/STAT-dependent manner. This molecular pathway restrains JNK-induced apoptosis and spatial propagation of JNK signalling, thereby limiting the extent of tissue damage, as well as facilitating systemic and proliferative responses to injury. We find that the pro-survival function of JAK/STAT also drives tumour growth under conditions of chronic stress. Our study defines the function of JAK/STAT in tissue stress and illustrates how crosstalk between conserved signalling pathways establishes an intricate equilibrium between proliferation, apoptosis and survival to restore tissue homeostasis.

KEY WORDS: JAK/STAT, JNK, Cell survival, Compensatory proliferation, Cancer, Injury-induced apoptosis, Eiger, Cell ablation

INTRODUCTION

Tissue homeostasis relies on the ability of tissues to respond to stress caused by damaging environmental insults. Physical wounding, toxins, reactive oxygen species and UV irradiation all induce cellular damage and thus disrupt tissue integrity. Mounting an appropriate response to these insults is essential for tissue repair and to prevent chronic cellular stress, which can lead to disease (Fulda et al., 2010). While much progress has been made to elucidate signalling pathways that seal wounds, remove damaged cells, promote regenerative proliferation or mediate patterning of regenerated tissue, little is known about how crosstalk between these pathways coordinates repair processes to restore homeostasis.

Studies on *Drosophila* progenitor organs called imaginal discs have provided deep insights into cellular adaptations to tissue stress. Surgical excision (Bryant, 1975; Haynie and Bryant, 1976;

Ludwig-Maximilians-University Munich, Faculty of Biology, Grosshaderner Strasse 2-4, Planegg-Martinsried 82152, Germany.

*Author for correspondence (classen@bio.lmu.de)

A.-K.C., 0000-0001-5157-0749

Katsuyama et al., 2015) or cell ablation induced by pro-apoptotic transgenes (Grusche et al., 2011; Herrera et al., 2013; Smith-Bolton et al., 2009) has revealed cellular responses that promote wound healing (Sun and Irvine, 2014; Kashio et al., 2014; Razzell et al., 2011). Disc size is restored by accelerated proliferation of cells proximal (Sustar et al., 2011; Bosch et al., 2008) and distal (Herrera et al., 2013) to the wound site. Lacking tissue-resident stem cells, fate plasticity displayed by parenchymal disc cells facilitates repatterning of replaced tissues (Herrera et al., 2013; Herrera and Morata, 2014; Repiso et al., 2013; Schuster and Smith-Bolton, 2015). In contrast, regeneration of the *Drosophila* adult midgut is driven by tissue-resident stem cells (Ohlstein and Spradling, 2006; Jiang et al., 2009; Osman et al., 2013; Staley and Irvine, 2010). Strikingly, while midgut and imaginal discs utilize stem cell-dependent and -independent repair processes, both tissues activate similar signalling pathways that underlie potentially highly conserved stress responses.

The c-Jun amino-terminal kinase (JNK)/mitogen-activated protein kinase (MAPK) cascade is one of the earliest pathways activated in damaged tissues and it is triggered by loss of epithelial polarity (Brumby and Richardson, 2003; Uhlirova et al., 2005; Igaki, 2009; Wu et al., 2010; Zhu et al., 2010), apoptosis (Ryoo et al., 2004; Shlevkov and Morata, 2012) or physical wounding (Bosch et al., 2005; Rämet et al., 2002; Lee et al., 2005). JNK regulates stress responses via activation of the transcription factor AP-1 (Eferl and Wagner, 2003), which comprises Jun and Fos homo- and heterodimers. JNK activation is required for cytoskeletal rearrangement during wound closure (Ríos-Barrera and Riesgo-Escovar, 2013; Bosch et al., 2005) and promotes elimination of damaged cells by injury-induced apoptosis (Bogoyevitch et al., 2010; Chen, 2012; Shlevkov and Morata, 2012; Luo et al., 2007; Moreno et al., 2002). Importantly, JNK drives compensatory proliferation to replace damaged tissues, through cell-autonomous (Bosch et al., 2008; Sun and Irvine, 2011; Grusche et al., 2011) and non-autonomous (Bergantinos et al., 2010; Mattila et al., 2005; Ryoo et al., 2004) mechanisms. A central question remaining unanswered is how these two different responses – proliferation and apoptosis – are brought into equilibrium downstream of JNK to restore tissue homeostasis.

Apoptotic JNK targets that facilitate clearing of damaged cells include the Diap1 inhibitors *reaper* (*rpr*), *head involution defective* (*hid*) and *p53* (Shlevkov and Morata, 2012; Luo et al., 2007; Moreno et al., 2002). Activation of *rpr*, *hid* and *p53* drives further activation of JNK via the initiator caspase Dronc (Shlevkov and Morata, 2012). JNK also activates the TNFα homologue Eiger (Pérez-Garijo et al., 2013), leading to activation of JNK in nearby cells (Pérez-Garijo et al., 2013; Bergantinos et al., 2010; Wu et al., 2010). This positive feedback could drive excessive cell elimination and therefore, needs to be restrained to prevent unlimited spatial propagation of pro-apoptotic JNK activity. It is not known how spatial constraints on JNK propagation are established.

Importantly, apoptosis of damaged cells stimulates compensatory proliferation by JNK-dependent activation of growth pathways including Wnt/β-catenin, TFGβ/SMAD, Janus kinase/Signal transducer and activator of transcription (JAK/STAT), Hippo/Yorkie and EGF (Sun and Irvine, 2011, 2014; Wells et al., 2006; Kondo et al., 2006; Huh et al., 2004; Morata et al., 2011; Pastor-Pareja and Xu, 2013). While the requirement for these pathways differs depending on context (Smith-Bolton et al., 2009; Herrera et al., 2013; Fan and Bergmann, 2008), many have been implicated in metazoan responses to stress (Sun and Irvine, 2014; Pahlavan et al., 2006; Chen, 2012). Importantly, prevention of apoptosis in damaged cells causes sustained proliferative signalling and eventual tumour formation in *Drosophila* (Kondo et al., 2006; Perez-Garijo et al., 2004, 2009; Ryoo et al., 2004; Huh et al., 2004; Martin et al., 2009), emphasizing how strongly apoptotic, survival and proliferative signals need to be balanced to re-establish normal tissue size.

Current models propose that JAK/STAT signalling is a major mediator of compensatory, cancerous and developmental proliferation. Cytokine-like ligands in *Drosophila* are encoded by *upd1* (*unpaired 1*), *upd2* and *upd3* and signal through conserved pathway components encoded by single genes, specifically the receptor Domeless (Dome), the Janus kinase Hopscotch (Hop) and the transcription factor Stat92E (Arbouzova and Zeidler, 2006). As in mammals, JAK/STAT plays diverse roles in fly development by regulating haemocyte activation (Myllymäki and Rämet, 2014), appendage patterning (Ayala-Camargo et al., 2013, 2007; Johnstone et al., 2013) and stem cell maintenance (Gregory et al., 2008). A proliferative function for JAK/STAT was suggested by early studies of tissue growth during disc development (Bach et al., 2003; Tsai and Sun, 2004; Mukherjee et al., 2005). Subsequently, JAK/STAT has been widely implicated in promoting proliferation of neoplastic cells (Classen et al., 2009; Wu et al., 2010; Davie et al., 2015; Bunker et al., 2015; Amoyel et al., 2014) and aberrant non-autonomous proliferation of wild-type cells in fly models of tumorigenesis (Vaccari and Bilder, 2005; Herz et al., 2006; Moberg et al., 2005). Activation of Upd gene transcription upon tissue damage has been linked to compensatory proliferation in imaginal discs and adult guts (Jiang et al., 2009; Pastor-Pareja et al., 2008; Katsuyama et al., 2015; Wu et al., 2010; Lin et al., 2009; Bunker et al., 2015; Santabárbara-Ruiz et al., 2015). Other studies suggest that JAK/STAT is involved in cell competition, where signalling either promotes 'winner' cell state (Schroeder et al., 2013; Rodrigues et al., 2012) or compensatory proliferation in response to 'loser' cell elimination (Kolahgar et al., 2015).

Despite this wealth of work, little is known about target genes mediating proliferative JAK/STAT function. In fly tumours, STAT-responsive enhancers have been mapped (Davie et al., 2015), but few target genes regulating tissue size have been described (Tsai and Sun, 2004; Betz et al., 2008; Hasan et al., 2015). However, several studies suggest that developmental functions of JAK/STAT are mediated by the transcriptional repressors Chinmo (Flaherty et al., 2010), Zfh1 (Ohayon et al., 2009; Leatherman and Dinardo, 2008) and Zfh2 (Perea et al., 2013; Guarner et al., 2014; Ayala-Camargo et al., 2013).

We wanted to better understand the precise role of JAK/STAT in cellular adaptations to stress and to gain further insight into how JAK/STAT might regulate compensatory proliferation after tissue damage. Because JAK/STAT is required for regeneration in tissues as diverse as the grasshopper leg to the mouse liver (Yamada et al., 1997; Bando et al., 2013; Cressman et al., 1996; Li et al., 2002; Wuestefeld et al., 2003; Zhao et al., 2014), dissecting the function of this highly conserved pathway is essential for our understanding of regenerative processes. To achieve this, we employed an imaginal disc model of tissue stress, which utilizes ectopic expression of the TNFα homologue Eiger (Smith-Bolton et al., 2009) (Fig. S1), triggering JNK activation (Igaki and Miura, 2014; Andersen et al., 2015) and apoptosis (Fig.S1D-D‴). This model has been previously used to study tissue regeneration in response to local cell ablation (Herrera et al., 2013; Smith-Bolton et al., 2009). Expression of Eiger induces multiple hallmarks of local and systemic stress responses, such as compensatory proliferation and dILP8-induced developmental delay (Fig. S1E,G) (Smith-Bolton et al., 2009). Because Eiger induces tissue stress in wild-type discs, it represents an ideal model to distinguish JAK/STAT functions in physiological stress from secondary effects incurred by developmental patterning or tumorigenic models. Instead of promoting compensatory proliferation, we found that JAK/STAT promotes survival of JNK-signalling cells, thereby acting as a central regulator of injury-induced apoptosis to restrain excessive tissue damage and facilitate initiation of compensatory responses.

RESULTS

Eiger-mediated JNK activation enables functional studies of JNK-dependent stress responses

We expressed Eiger under the control of *rotund* (*rn*)-*GAL4*, which drives expression in the wing disc pouch, fated to give rise to the future wing blade. We induced *eiger* expression on developmental day 7 and temporally limited *UAS-eiger* expression to 40 h by using a temperature-sensitive GAL80 repressor (Fig. S1A-C). In agreement with previous studies (Herrera et al., 2013; Smith-Bolton et al., 2009), we observed extensive cell ablation in discs (Fig. S1E-E′), which gave rise to a 50% reduction in adult wing size (Fig. S1H). G-trace lineage labelling (Evans et al., 2009) of *rn-GAL4*-expressing cells followed by FACS analysis revealed that about 85% of *rn-GAL4* lineage cells were eliminated after 40 h of Eiger stimulation (Fig. 1A,A′, Fig. S2A-A″). This correlated with an induction of a 2 day developmental delay at the larval-pupal transition (Fig. S1G).

In agreement with Eiger triggering JNK activation (Igaki and Miura, 2014), we found that Eiger-stimulated discs broadly activate the JNK-responsive *TRE* reporter (Fig. 1C) (Chatterjee and Bohmann, 2012). The *TRE* reporter was specifically activated at the wound site, whereas reporter activity is completely absent in control discs (Fig. 1B,C). Consistent with non-autonomous activation of JNK by Eiger (Pérez-Garijo et al., 2013) and tissue damage (Bosch et al., 2005; Herrera et al., 2013; Wu et al., 2010), *TRE* activation extended beyond a G-trace-labelled domain, in which *eiger* expression was induced (Fig. 1C and Fig. 2F). FACS analysis demonstrated that while 4.5% of cells in the disc belonged to the surviving *rn-GAL4* lineage, 29% of cells in the disc activated *TRE-GFP* (Fig. S2A-A′,B-B′).

We first wanted to quantify cell proliferation in Eiger-stimulated discs near the wound site, as well as in the whole disc between 0 h (R0) and 48 h (R48) into the recovery period after the end of cell ablation (Fig. S1A,E-E″). We used an image segmentation algorithm (Fiji) to specifically measure total disc size, the size of the surviving *rn-GAL4* lineage labelled by G-trace, the number of mitotic cells marked by phospho-Histone 3 (pH3) or the number of cells in S-phase marked by BrdU incorporation (Fig. 1D-G, Fig. S1F). We found that at R0, G-trace-labelled cells in the pouch account for about 3% of the total disc volume (Fig. 1D). This is in close agreement with FACS measurements (4.5%, Fig. S2A′), which also detect an additional subset of G-trace-labelled cells in
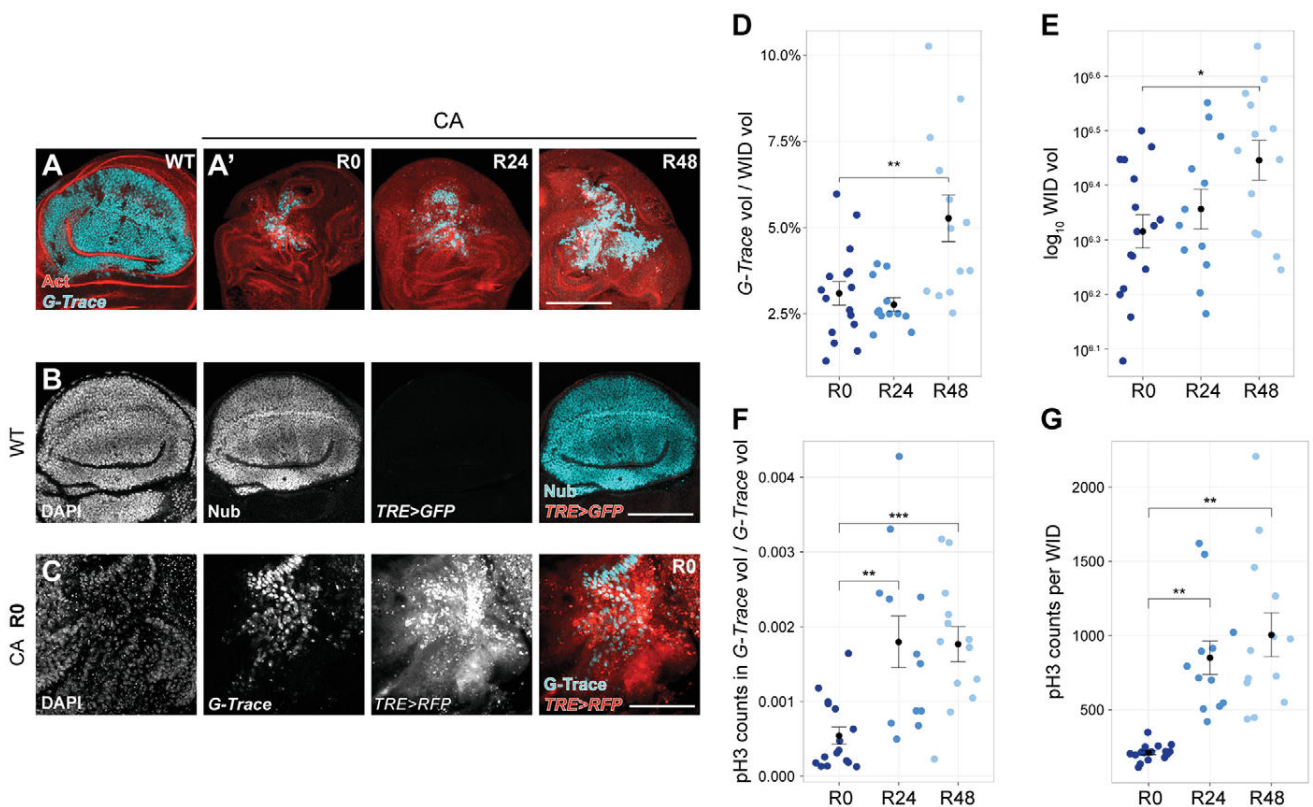
Fig. 1. Eiger expression enables functional studies of JNK stress responses. (A) G-trace labelling (cyan) visualizes the *rotund* (*rn*)*GAL4* cell lineage in wing discs. Actin labelling is red. (A′) Progeny of *rn-GAL4* G-trace-labelled cells (cyan) after 40 h of Eiger-mediated cell ablation (CA) at recovery points R0, R24, R48 h. (B) Wing pouch expressing the JNK reporter *TRE*>*GFP* (red in overlay), stained for DAPI and Nubbin (cyan in overlay) visualizing a lineage similar to *rn-GAL4*-derived cells. (C) Wing pouch after cell ablation (CA) expressing *TRE*>RFP (red in overlay) containing *rn-GAL4* G-trace-labelled cells (cyan in overlay) stained for DAPI. (D) Volume occupied by *rn-GAL4* G-trace-labelled cells and (E) total wing imaginal disc (WID) volumes at recovery time points R0, R24 and R48. (F) Normalized pH3-positive mitotic events within *rn-GAL4* G-trace-labelled volume and (G) within total disc volumes at R0, R24, R48. Graphs display mean±s.e.m. for R0, *n*=16; R24, *n*=12; R48, *n*=13 discs. *U*-tests were performed to test for statistical significance (*$P<0.05$, **$P<0.01$, ***$P<0.001$). Scale bars: 100 µm.

the notum. This analysis verified that volume quantifications of cell populations in Fiji accurately approximate cell counts. Our analysis revealed a marked increase in cell proliferation between R0 and R24, both near the wound site (Fig. 1F), as well as in the entire disc (Fig. 1G, Fig. S2E). Mitotic rates do not increase further between R24 and R48 (Fig. 1F,G). When we quantified the volume of the total disc and that of the G-trace-labelled population, we found that they increased in size by 36% and 126%, respectively (Fig. 1D,E).

While cell ablation can be induced more efficiently by expression of pro-apoptotic transgenes, such as *UAS-reaper* (Herrera et al., 2013), we did not observe broad activation of JNK in this context (Fig. S2C,D). Because Eiger-stimulated discs displayed broad activation and provided genetic access to JNK-signalling cells, we utilized expression of Eiger to investigate the role of JAK/STAT in JNK-mediated responses to tissue stress.

JAK/STAT is activated in response to Eiger-induced tissue damage

To understand if JAK/STAT plays a role in imaginal disc regeneration, we analysed JAK/STAT activity in response to *eiger* expression. JAK/STAT activation can be visualized using the *10xSTAT-dGFP* reporter (Bach et al., 2007), which is almost undetectable in wild-type discs (Fig. 2A). Analysis of the *10xSTAT-dGFP* reporter revealed that JAK/STAT is upregulated in response to *eiger* expression induced at day 5 or day 7 of development

(Fig. 2B,C). Reporter activation can also be observed upon *reaper* expression, suggesting that stress induced by ectopic cell death is sufficient to cause JAK/STAT activation (Fig. S3E). Importantly, in Eiger-stimulated discs, JAK/STAT activation was detected beyond the pouch periphery and thus extended beyond JNK domains marked by *TRE* activity (Fig. 2F). JAK/STAT signalling declined within the following 24 h suggesting that it is downregulated after *eiger* expression ceased (compare Fig. S3A-C with Fig. S3B′-C′). We furthermore examined JAK/STAT activation when *eiger* was induced at later stages of development. Surprisingly, JAK/STAT activity was almost undetectable when *eiger* was induced at day 8 (Fig. 2D, Fig. S3D-D′).

Unpaired ligands are upregulated upon Eiger-induced tissue damage

Previous reports and our studies demonstrate that the JAK/STAT ligands *upd1*, *upd2* and *upd3* are transcriptionally upregulated in response to stress from physical injury (Katsuyama et al., 2015; Pastor-Pareja et al., 2008) or tumorous growth (Wu et al., 2010; Bunker et al., 2015), indicating that pathway upregulation may be driven by JNK-dependent Upd gene transcription. We found that transcription of Upd genes is highly elevated in Eiger-stimulated discs, whereas transcription of *dome*, *hop* and *Stat92E* is not (Fig. 2E). Recapitulating the decline in *10xSTAT-dGFP* activity in response to *eiger* induction at day 8, Upd gene transcription was
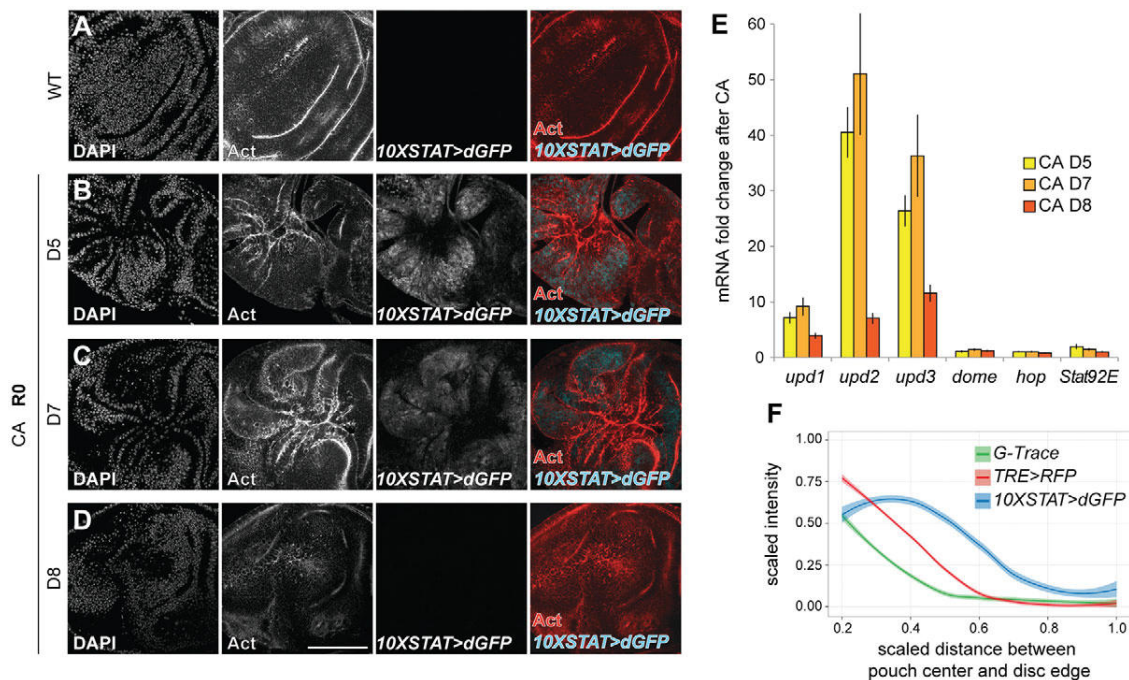
Fig. 2. JAK/STAT is activated in response to tissue damage. (A) Wing disc expressing the JAK/STAT-reporter *10XSTAT>dGFP* (cyan in overlay) stained for DAPI and Actin (red in overlay). (B-D) Wing pouch after cell ablation (CA) induced at day 5 (B), day 7 (C) or day 8 (D). Discs were stained for DAPI, Actin (red in overlay) and express *10XSTAT>dGFP* (cyan in overlay). (E) qRT-PCR analysis of *upd1*, *upd2*, *upd3*, *dome*, *hop* and *Stat92E* transcripts after cell ablation (CA) induced at day 5, day 7 or day 8. Fold induction relative to unablated controls is reported. Graphs display mean±s.e.m. for $n \geq 3$ biological replicates. (F) Fluorescence intensity of *rn-GAL4* G-trace (*n*=5 discs), *TRE>RFP* (*n*=6 discs) and *10XSTAT>dGFP* (*n*=12 discs) reporter signals at R0. Intensity plots are scaled to maximum measured values; interpolated averages are reported as a function of relative positions between pouch centre and disc edge. Graphs display interpolated mean±s.e.m. Scale bars: 100 µm.

strongest at day 5 and day 7 but decreased by more than half when *eiger* was induced at day 8 (Fig. 2E).

Loss of JAK/STAT activation at day 8 was not due to a decline in Eiger-mediated JNK activation, because *TRE* activity was as strong on day 8 as on day 7 (Fig. S3F,G). This suggests that even though JAK/STAT activation coincides with JNK activity (Katsuyama et al., 2015; Pastor-Pareja et al., 2008), JNK alone may not be sufficient to stimulate this pathway. This is supported by broader activation of JAK/STAT compared with JNK (Fig. 2F). Strikingly, the failure to activate JAK/STAT at late developmental stages correlated with a pronounced decline in the ability of larvae to induce a developmental delay at the larval-pupal transition (Fig. S3H) and with a strong reduction in recovered adult wing size (Fig. S3I). These correlations suggest that JAK/STAT may be a crucial mediator of JNK-induced compensatory responses in imaginal discs.

JAK/STAT activity is not required for compensatory proliferation

JAK/STAT has been reported to play a role in promoting cell proliferation in wild-type (Bach et al., 2003; Tsai and Sun, 2004; Mukherjee et al., 2005), tumorous (Classen et al., 2009; Wu et al., 2010; Davie et al., 2015; Bunker et al., 2015; Amoyel et al., 2014) and surgically injured discs (Katsuyama et al., 2015). To test whether JAK/STAT is generally required to drive compensatory proliferation, we quantified mitotic events after Eiger stimulation in discs with impaired JAK/STAT signalling. We genetically reduced JAK/STAT activity by two approaches: (1) we reduced gene dosage of JAK/STAT components in the entire animal by heterozygosity

for *dome*[G0441], *hop*[34] and *Stat92E*[85C9] alleles or (2) we interfered with JAK/STAT signalling exclusively in *eiger*-expressing cells through expression of RNAi constructs targeting JAK/STAT components (Fig. S5A), a dominant-negative *dome* (*dome*[Δcyt]) or the inhibitor *Socs36E* under the control of *rn-GAL4-tubGAL80*[ts].

Strikingly, even though 50% of the tissue in Eiger-stimulated discs activated JAK/STAT (Fig. 2B,C), discs heterozygous for *dome*[G0441], *hop*[34] and *Stat92E*[85C9] alleles did not show any evidence of a reduction in mitotic events or total disc size (Fig. 3A-F). Instead, we observed a mild increase in Eiger-stimulated discs heterozygous for *hop*[34]. These results are the opposite to what we would expect if JAK/STAT regulated compensatory proliferation. We thus wanted to confirm these findings by interfering with JAK/STAT specifically in Eiger-stimulated cells. *rn-GAL4*-driven co-expression of *dome-RNAi*, *dome*[Δcyt] or *Socs36E* did not reduce the number of mitotic events within surviving *eiger*-expressing cells (Fig. 3G-K). Instead, mitotic rates slightly increased, whereas they remained unchanged in the rest of the disc (Fig. 3K, Fig. S4A,C). Importantly, effects on *eiger*-expressing cells co-expressing transgenic constructs are strongest at R0 but decline as GAL4 activity decreased (Fig. 3K). Together, our results strongly argue against the previously assigned role of JAK/STAT in directly promoting compensatory proliferation in response to stress.

JAK/STAT is required for survival of JNK-signalling cells

While the total disc size of Eiger-stimulated discs was similar to that of discs with genetically impaired JAK/STAT activity (Fig. 3F, Fig. S4D), we were surprised to notice that the number of

DEVELOPMENT
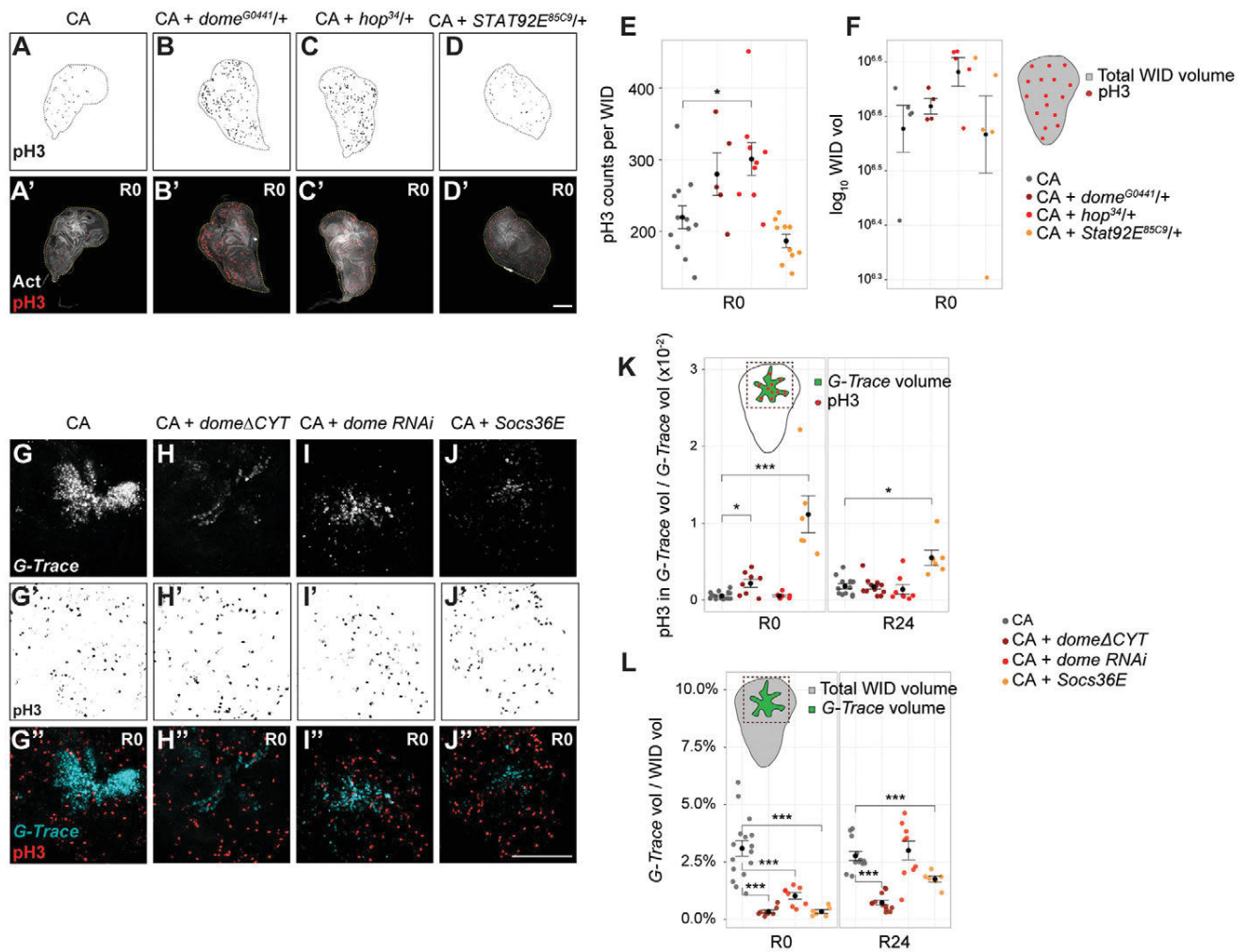
Fig. 3. JAK/STAT is not required for compensatory proliferation. (A) Wing disc after cell ablation (CA) stained for pH3 (A, red in A′, Actin in grey). (B-D) Wing disc heterozygous for $dome^{G0441}$ (B,B′), hop^{34} (C,C′) or $Stat92E^{85C9}$ (D,D′) after cell ablation (CA) stained for pH3 (B-D, red in B′-D′; Actin in grey). (E) pH3 events per disc or (F) total wild-type disc volume (n=12) and discs heterozygous for $dome^{G0441}$ (n=5), hop^{34} (n=9), or $Stat92E^{85C9}$ (n=10) after cell ablation (CA). (G-J) Wing pouch containing surviving rn-$GAL4$ G-trace-labelled cells (G-J, cyan in G″-J″), stained for pH3 (G′-J′, red in G″-J″). A wild-type disc (G) and discs with rn-$GAL4$-mediated co-expression of $dome^{\Delta cyt}$ (H), $dome$-$RNAi$ (I) or $Socs36E$ (J) in $eiger$-expressing cells are shown. (K) Normalized pH3 events within rn-$GAL4$ G-trace-labelled volume and (L) relative rn-$GAL4$ G-trace-labelled volume per disc at R0 and R24 in ablated discs (CA) (R0, n=16; R24, n=12 discs) or with rn-$GAL4$-mediated co-expression of $dome^{\Delta cyt}$ (R0, n=8; R24, n=12 discs), $dome$-$RNAi$ (R0, n=8; R24, n=9 discs), $Socs36E$ (R0, n=6; R24, n=6 discs) in $eiger$-expressing cells. Graphs display mean±s.e.m. U-tests were performed to test for statistical significance (*P<0.05, **P<0.01, ***P<0.001). Scale bars: 100 μm.

G-trace-labelled cells that survived $eiger$ expression was dramatically reduced when JAK/STAT signalling was inhibited. Specifically, we found that expression of $dome$-$RNAi$, $dome^{\Delta cyt}$ or $SOCS36E$ caused a 3- to 10-fold reduction in the volume of G-trace-labelled populations (Fig. 3L, Fig. S4B).

These observations suggested that more $eiger$-expressing cells die when JAK/STAT signalling is impaired. Indeed, we observed a 2-fold increase in the volume positive for activated Caspase-3 if JAK/STAT activity was exclusively reduced in $eiger$-expressing cells (Fig. 4A-E) and up to a 10-fold increase in the volume of Eiger-stimulated discs heterozygous for $dome^{G0441}$, hop^{34} or $Stat92E^{85C9}$ (Fig. 4F-I). The more pronounced effect observed for heterozygous tissues likely arises as a result of the tissue-wide reduction of JAK/STAT activity in this background. Reduction was also achieved in domains that display JAK/STAT and JNK activation but are located outside of the $rnGAL4$ lineage (Fig. 1C, Fig. 2B,C,F). Importantly, genetic reduction of JAK/STAT in developing wild-type discs under the same conditions does not

cause any elevation of apoptosis (Fig. S5B-E). Combined, these data highlight a specific role for JAK/STAT as an important mediator of cell survival, specifically in JNK-signalling cells.

JAK/STAT activity suppresses activation of JNK signalling

To understand how JAK/STAT promotes cell survival, we tested if genetically reducing JAK/STAT activity causes further elevation of JNK, which could divert JNK-dependent compensatory responses towards apoptosis. To this end, we monitored JNK activity using TRE reporters in $eiger$-expressing discs heterozygous for $dome^{G0441}$, hop^{34} and $Stat92E^{85C9}$ alleles. Our results suggested that after cell ablation, 14% of the wing pouch area activated the TRE reporter (Fig. 4J,N). In Eiger-stimulated discs heterozygous for $dome^{G0441}$, hop^{34} and $Stat92E^{85C9}$, we observed a 2- to 3-fold increase in the area positive for TRE activation (Fig. 4K-N). These results indicate that reduction of JAK/STAT signalling promotes non-autonomous expansion of JNK signalling beyond $eiger$-expressing cells and that this may underlie the observed increase
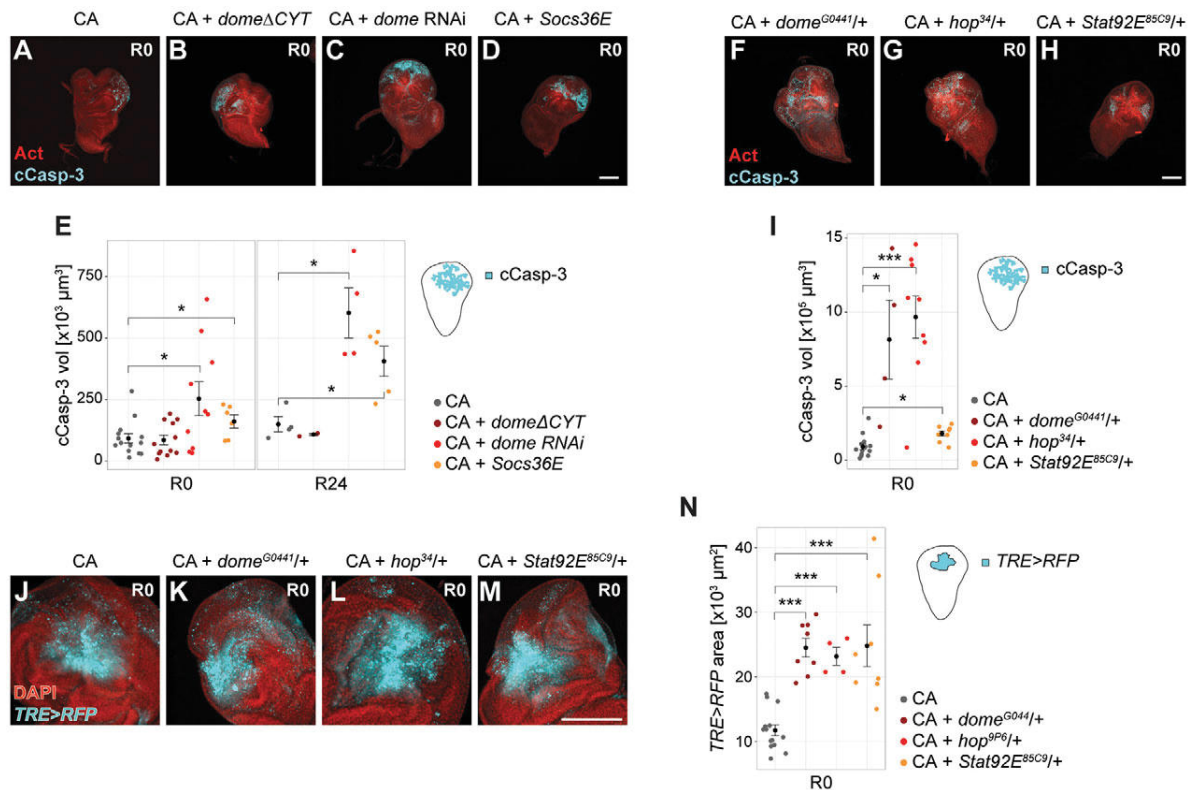
Fig. 4. JAK/STAT is required for survival of Eiger-stimulated cells. (A-D) Wing disc after cell ablation (CA) (A) and with *rn-GAL4*-mediated co-expression of *dome^{Δcyt}* (B), *dome-RNAi* (C) or *Socs36E* (D) in *eiger*-expressing cells stained for cleaved Caspase-3 to visualize apoptotic cells (cyan) and Actin (red). (E) Cleaved Caspase-3 volume in ablated discs (CA; R0, *n*=15; R24, *n*=4 discs) or with *rn-GAL4*-mediated co-expression of *dome^{Δcyt}* (R0, *n*=12; R24, *n*=3 discs), *dome-RNAi* (R0, *n*=10; R24, *n*=4 discs) or *Socs36E* (R0, *n*=6; R24, *n*=6 discs) in *eiger*-expressing cells at R0 and R24. (F-H) Ablated discs heterozygous for *dome^{G0441}* (F), *hop^{34}* (G) or *Stat92E^{85C9}* (H) stained for cleaved Caspase-3 (cyan) and Actin (red) at R0. (I) Quantification of cleaved Caspase-3-positive volume per disc after cell ablation (CA) (*n*=12 discs) or in discs heterozygous for *dome^{G0441}* (*n*=4 discs), *hop^{34}* (*n*=9 discs), or *Stat92E^{85C9}* (*n*=8 discs) at R0. (J-M) Disc expressing the JNK reporter *TRE>RFP* (cyan) after cell ablation (CA) (J) or if heterozygous for *dome^{G0441}* (K), *hop^{34}* (L) or *Stat92E^{85C9}* (M) at R0. (N) Quantification of *TRE>RFP*-positive area per disc after cell ablation (CA) (*n*=14 discs) and in discs heterozygous for *dome^{G0441}* (*n*=8 discs), *hop^{34}* (*n*=4 discs), or *Stat92E^{85C9}* (*n*=8 discs). Graphs display mean±s.e.m. *U*-tests were performed to test for statistical significance (**P*<0.05, ***P*<0.01, ****P*<0.001). Scale bars: 100 μm.

in the apoptotic index in JAK/STAT-impaired Eiger-stimulated discs (Fig. 4A-I).

Our observations prompted two important predictions. First, broad activation of JNK in JAK/STAT-impaired discs suggested that JAK/STAT acts as a suppressor of JNK signalling. Repression of JNK by JAK/STAT could either be mediated by direct transcriptional effects on JNK core components, or indirectly, by suppression of apoptosis and prevention of Dronc-driven positive feedback activation of JNK. This mechanism would restrain non-autonomous activation of JNK, excessive apoptosis and tissue damage. A second prediction implies that interfering with JAK/STAT increases the extent of tissue damage due to elevation of cell death. Thereby, the ability of discs to mount an appropriate regenerative response is reduced as cells required to drive regenerative responses are eliminated by excessive cell death.

A survival-promoting function of JAK/STAT is mediated by Zfh2

We did not find any evidence that negative JNK regulators are transcriptionally activated by Stat92E. We therefore wanted to understand if JAK/STAT regulates cell survival by impinging on pro-apoptotic JNK target genes *rpr* and *hid*, which act in combination with *grim* as inhibitors of IAP (inhibitor of

apoptosis) proteins. To this end, we first performed a bioinformatic Clover analysis of the promoter regions of *rpr*, *hid* and *grim* using highly stringent parameter selections (Frith et al., 2004). As previously suggested (Shlevkov and Morata, 2012; Luo et al., 2007; Moreno et al., 2002), we identified multiple AP-1 binding motifs associated with these loci (Fig. S7A, data not shown). In agreement with studies on JNK-induced apoptosis (Shlevkov and Morata, 2012; Luo et al., 2007; Moreno et al., 2002), we specifically observed induction of *hid* expression in Eiger-stimulated discs (Fig. 5A). The mild increase in *hid* levels is likely to be an underestimate because *eiger*-expressing cells make up only 4.5% of the entire disc used for qRT-PCR analysis (Fig. S2A,A′). *Eiger*-expressing discs heterozygous for *Df(3L)H99*, a deficiency removing *rpr*, *hid* and *grim* loci, displayed a pronounced 'undead cell' phenotype (Fig. S6A,B) (Perez-Garijo et al., 2009; Martin et al., 2009; Kondo et al., 2006), suggesting that upregulation of *hid* contributes to Eiger-mediated cell death. While one previous study reports that Eiger-mediated induction of apoptosis is independent of *hid* activation (Igaki et al., 2002), we suggest that the small adult eye phenotype observed upon *eiger* co-expression with the strong apoptosis inhibitor p35 is a consequence of epithelial tissue architecture disruption rather than a failure to prevent Eiger-induced cell death (Fig. S6L). Together, previous reports and our results support the notion that induction of cell death in *eiger*-
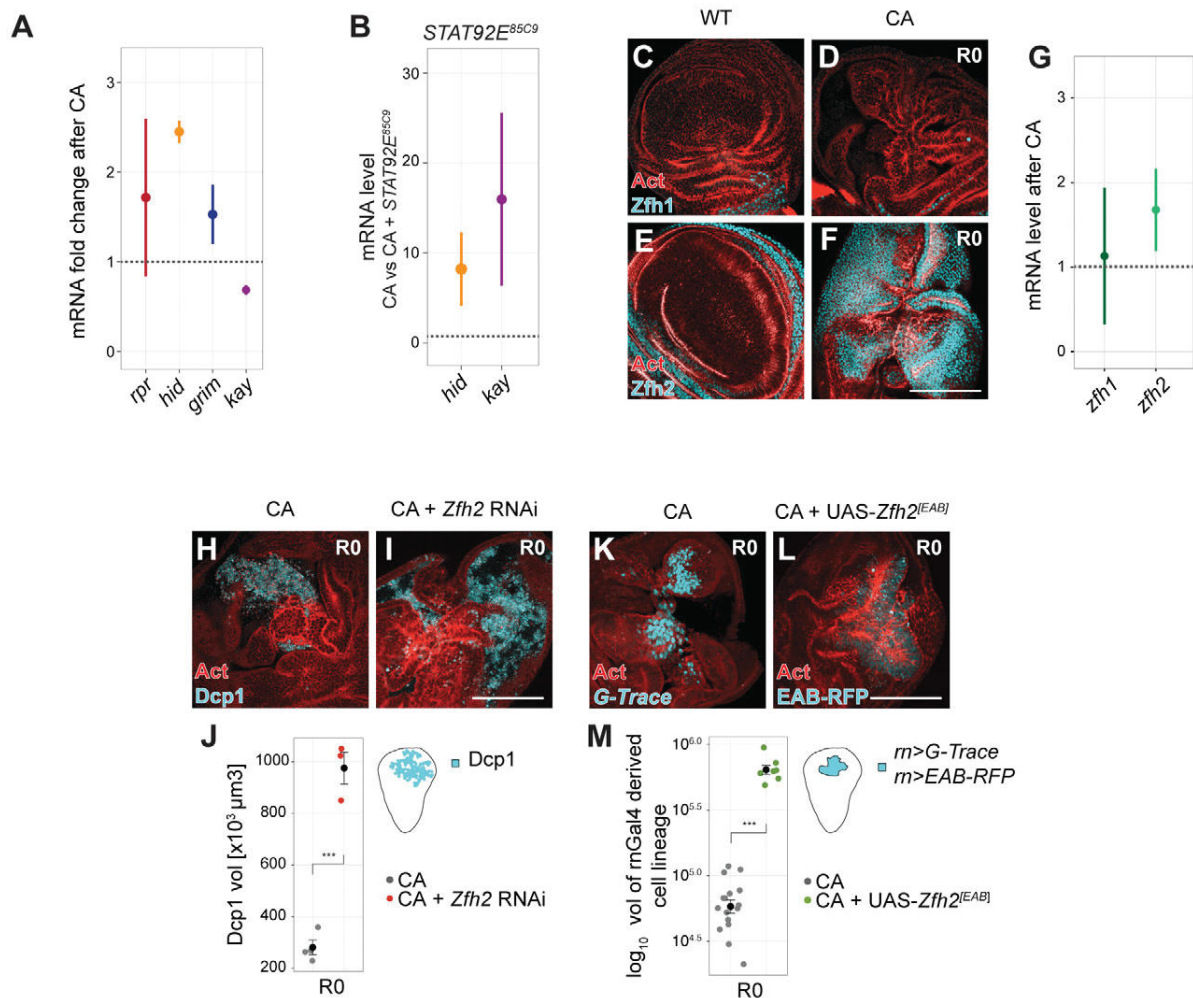
Fig. 5. A survival-promoting function of JAK/STAT is mediated by Zfh2. (A) qRT-PCR analysis of *rpr*, *hid*, *grim* and *fos* (*kay*) transcripts at R0. Fold induction relative to unablated discs is reported. Each graph shows mean±s.e.m. for *n*≥3 biological replicates. (B) qRT-PCT analysis of *hid* and *kay* at R0 in Eiger-expressing discs heterozygous mutant for *Stat92E85C9*. Fold induction relative to ablated discs. Each graph shows mean±s.e.m. for *n*=2 biological replicates. (C-F) Unablated discs (C,E) and ablated discs (D,F) stained for Zfh1 (C,D) or Zfh2 (E,F) at R0. (G) qRT-PCR analysis of *zfh1* and *zfh2* transcripts at R0. Fold induction relative to unablated discs is reported. Each graph shows mean±s.e.m. for *n*=3 biological replicates. (H,I) Disc after cell ablation (H) or with *rn-GAL4*-mediated co-expression of *zfh2-RNAi* (I) in *eiger*-expressing cells stained for Dcp-1 to visualize apoptotic cells (cyan) and Actin (red) at R0. (J) Dcp1-positive volume per disc after cell ablation (CA) (*n*=4 discs) or in discs with *rn-GAL4*-mediated co-expression of *zfh2-RNAi* (*n*=3 discs) in *eiger*-expressing cells at R0. (K,L) Disc after cell ablation (K) or discs with *rn-GAL4*-mediated co-expression of *UAS-zfh2* (L) in *eiger*-expressing cells stained for Dcp-1 (cyan) and Actin (red) at R0. (M) *rn-GAL4* G-trace-labelled volume in ablated discs (*n*=16 discs) and RFP-labelled volume in discs with *rn-GAL4*-mediated co-expression *UAS-Zfh2[EAB]* (*n*=7 discs) in *eiger*-expressing cells at R0. Graphs display mean±s.e.m. *U*-tests were performed to test for statistical significance (**P*<0.05, ***P*<0.01, ****P*<0.001). Scale bars: 100 μm.

expressing discs is specifically mediated by AP-1/JNK-dependent activation of *hid*.

Strikingly, our Clover analysis also revealed multiple, highly clustered mammalian ZEB1-binding motifs the *hid* promoter (Fig. S7A) as well as in the promoter of the *kay* gene coding for the AP-1 component dFos (Fig. S7B). ZEB1 binding motifs localized to highly conserved DNA sequences as shown by mVISTA analysis (Frazer et al., 2004; Bray et al., 2003) and to open chromatin regions, likely representing regulatory elements, as demonstrated by overlays with previously published ATAC-seq data sets (Fig. S7) (Davie et al., 2015). ZEB proteins are homologous to *Drosophila* Zfh1 and Zfh2 (Zinc-finger homeobox) proteins, which act as transcriptional repressors (Postigo et al., 1999; Postigo and Dean, 1999). Both Zfh1 and Zfh2 were previously identified to be downstream effectors of JAK/STAT (Leatherman and Dinardo,

2008; Ayala-Camargo et al., 2013). This is reflected by Zfh2 expression mirroring JAK/STAT activation patterns in developing wing discs (Fig. 5E) (Ayala-Camargo et al., 2013) and the ability of JAK/STAT to induce Zfh2 expression *de novo* (Fig. S6C,D). We hypothesized that *Drosophila* ZEB proteins could directly mediate repression of *kay* in Eiger-stimulated discs (Fig. 5A), thereby restraining JNK activation to promote cell survival. At the same time, ZEB proteins could compete with AP-1 for transcriptional repression of *hid*, thereby limiting AP-1/Hid-induced apoptosis to promote cell survival. Indeed, in *eiger*-expressing discs heterozygous for *Stat92E85C9*, the upstream regulator of Zfh proteins, we observed strong upregulation of *hid* and *kay* expression compared with discs expressing *eiger* alone (Fig. 5B).

To first understand if Zfh1 or Zfh2 expression was altered in tissue damage, we performed immunofluorescence and qRT-PCR

DEVELOPMENT

2913

analysis on Eiger-stimulated discs. We found that levels of Zfh2, but not Zfh1, are elevated in response to *eiger* expression (Fig. 5C-F). Zfh2 upregulation occurred specifically in regions with high levels of JAK/STAT activation (compare Fig. 2B,C with Fig. 5F). In addition, we found that transcripts of *zfh2* but not of *zfh1* were elevated (Fig. 5G). The observed mild increase in *zfh2* transcription represents a strong underestimate, as cells expressing *zfh-2 de novo* make up only a small portion of entire imaginal discs used for qRT-PCR analysis. In agreement with Zfh2 being a JAK/STAT effector, heterozygosity for $STAT92E^{85C9}$ reduces Zfh2 expression in Eiger-stimulated discs (Fig. S6E-G).

To test if Zfh2 in Eiger-stimulated discs is required to promote JAK/STAT-dependent survival by repressing *hid* and *kay* transcription, we performed genetic experiments to reduce or increase Zfh2 function. We found that expression of an RNAi construct targeting *zfh2* (Fig. S6H) increased apoptosis in *eiger*-expressing discs almost 4-fold (Fig. 5H-J). In contrast, overexpression of *UAS-zfh2* strongly promoted survival of *eiger*-expressing cells and resulted in a 10-fold increase in the size of surviving *rn-GAL4*-derived cell populations (Fig. 5K-M). While we found that Zfh1 levels were not upregulated in response to stimulation with Eiger, overexpression of *zfh1* also promoted survival of *eiger*-expressing cells, even phenocopying overexpression of the strong apoptosis inhibitor p35 (Fig. S6I-L). The survival-promoting function of either Zfh1 or Zfh2 suggests that both proteins can induce potent survival signals in stressed tissues, similar to developmental contexts (Ohayon et al., 2009; Guarner et al., 2014).

JAK/STAT activity prevents excessive tissue damage in response to tissue stress
We predicted that interfering with JAK/STAT signalling and therefore with Zfh2 function, increases the extent of tissue damage incurred by Eiger due to elevation of cell death. Consistent with these predictions, we found that Eiger-stimulated discs with genetically reduced JAK/STAT activity developed into significantly smaller adult wings (Fig. 6A,B). Expression of $dome^{\Delta cyt}$, *Socs36E* or RNAi constructs targeting multiple pathway components, including *zfh2*, as well as heterozygosity for $dome^{G0441}$, hop^{34} and $Stat92E^{85C9}$, caused a significant drop in adult wing size index by 30-90% (Fig. 6B). Importantly, genetic downregulation of JAK/STAT in wild-type discs at day 7 does not cause a comparable reduction in wing size (Fig. S8A), emphasizing that the survival-promoting function of JAK/STAT is specifically required during tissue stress responses.

Notably, *rn-GAL4*-driven overexpression of *upd1*, *upd2* or *zfh2* in *eiger*-expressing cells did not increase adult wing size (Fig. 6B). Extra Upd may not translate into JAK/STAT hyperactivation, because of pathway saturation in *eiger*-expressing cells. While *zfh2* overexpression promoted cell survival, it did not rescue other defects such as loss of epithelial polarity (Fig. 5L), which interferes with wing morphogenesis.

To test whether JAK/STAT was also required for stress responses induced by physical wounding, we analysed adult wings that developed from discs of surgically pinched larvae (Pastor-Pareja et al., 2008; Kashio et al., 2014). Reducing JAK/STAT function in the posterior compartment by expressing an RNAi construct targeting *hop* caused a pronounced reduction in adult wing sizes developing from discs, in which pinching had been targeted to the posterior compartment as visualized by co-expression of GFP (Fig. S8B). In contrast, no reduction in size of the posterior compartment was observed for adult wings derived from

undamaged control discs raised under the same conditions (not shown).

These data suggest that cellular responses to genetically or surgically induced damage critically rely on JAK/STAT activation to facilitate restoration of normal tissue homeostasis. Combined, our results strongly imply that a reduction in final tissue size upon JAK/STAT inhibition reflects an excessive loss of tissue due to cell death rather than a failure of the tissue to undergo compensatory proliferation.

JAK/STAT activity promotes efficient induction of compensatory responses
We wanted to investigate further if the observed reduction in adult wing sizes upon JAK/STAT inhibition is exclusively caused by a loss of tissue to cell death or if other regenerative processes may be disturbed. A process that contributes to successful tissue restoration is the induction of a dILP8-dependent developmental delay at the larval-pupal transition, which extends the time available for repair before metamorphosis (Colombani et al., 2012; Garelli et al., 2012). We found that interfering with JAK/STAT in *eiger*-expressing cells also caused a profound reduction in developmental delays induced by Eiger stimulation (Fig. 6C).

To understand if altered *Ilp8* expression caused this observation, we quantified expression of a *GFP*-reporter driven from the endogenous *Ilp8* locus (Garelli et al., 2012). We found that the reporter was strongly expressed in the pouch of Eiger-stimulated discs (Fig. S8C). In contrast, interfering with JAK/STAT by expression of *dome-RNAi* or $dome^{\Delta cyt}$ in *eiger*-expressing cells significantly reduced the area of GFP expression (Fig. 6D, Fig. S8D,E). This suggests that loss of *Ilp8* expression, caused by impaired JAK/STAT in JNK-signalling cells, underlies the observed failure to efficiently induce a developmental delay.

To test whether JAK/STAT signalling is sufficient to induce developmental delays, we expressed the JAK/STAT-ligands Upd1 or Upd2 in wild-type discs using *MS1096-GAL4*. However, no difference in pupariation timing between Upd-expressing and stage-matched wild-type larvae was observed (Fig. S8F). While a recent study links *Ilp8*-expression to JAK/STAT signalling (Katsuyama et al., 2015), our data implies that *Ilp8* is not a direct target gene of STAT92E. Instead, we suggest that cells that normally express *Ilp8* in response to JNK activation are more likely to die when JAK/STAT signalling is reduced, thereby preventing efficient expression of *Ilp8* and induction of a developmental delay. The failure to induce this important systemic response reduces the time available for repair and probably contributes to the decrease in recovered adult wing sizes that we observed upon genetic reduction of JAK/STAT signalling (Fig. 6B).

JAK/STAT regulates survival in a Ras^{V12}; $scrib^2$ tumour model
To understand if JAK/STAT generally acts as a survival-promoting pathway in the context of tissue stress, we revisited the role of JAK/STAT in established fly tumour models. Previous studies suggest that activation of JAK/STAT drives tumorous overgrowth in discs mutant for tumour suppressor genes, such as *scribbled* (*scrib*) or *Psc-Su(z)2* (Wu et al., 2010; Classen et al., 2009). *scrib* cells, similar to *eiger*-expressing cells, exhibit strong JNK activation, correlating with elevated transcription of Upd cytokines (Wu et al., 2010; Bunker et al., 2015; Leong et al., 2009; Brumby and Richardson, 2003). While *scrib* cells have a growth disadvantage if surrounded by wild-type cells, they efficiently cooperate with oncogenic Ras^{V12} to create invasive tumours in clonal assays
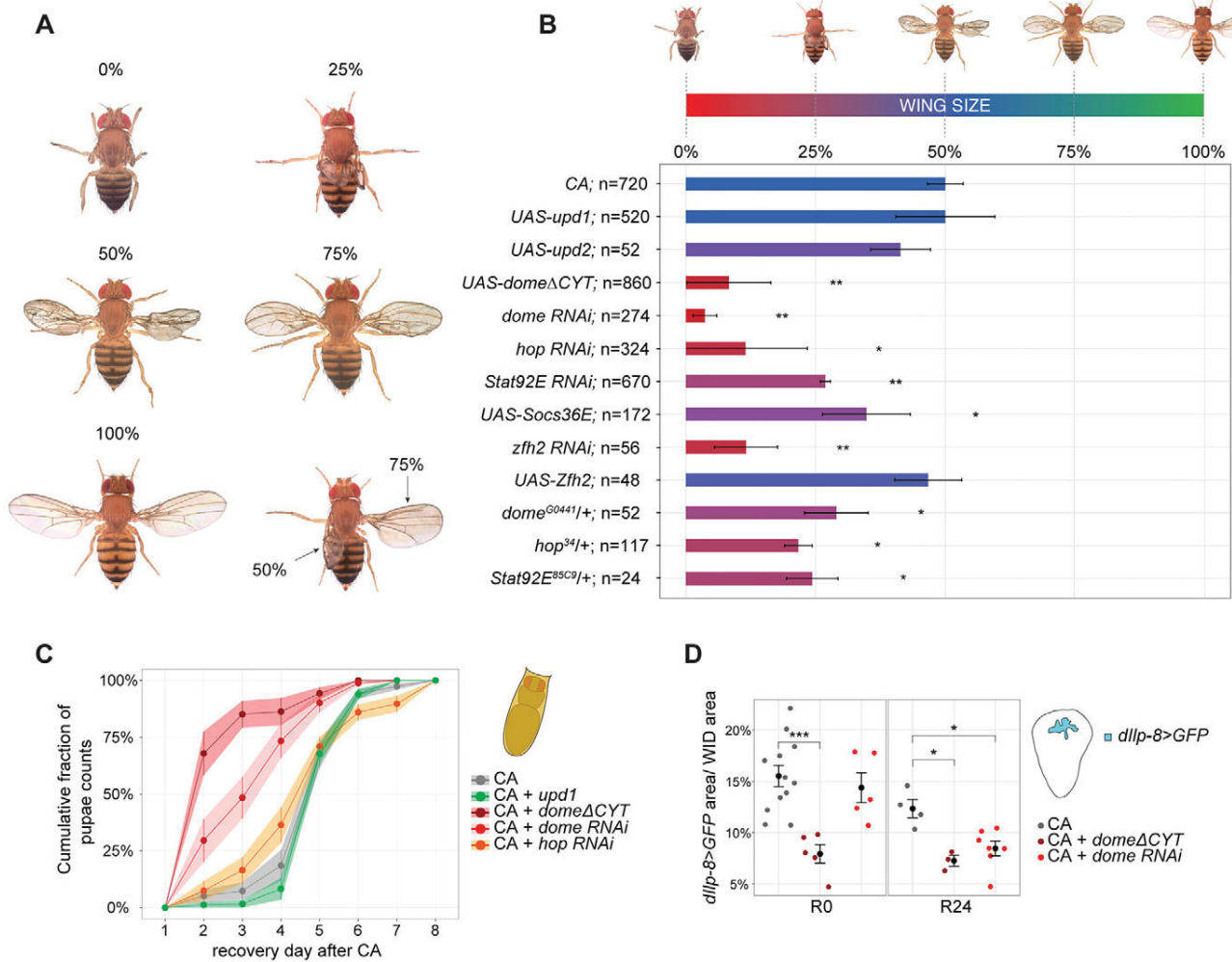
Fig. 6. JAK/STAT prevents excessive damage upon tissue stress. (A) Five adult wing size phenotypes were classified to score tissue damage after *eiger* expression at D7. (B) Average wing sizes developing from Eiger-stimulated disc (CA) or combined with *rn-GAL4*-mediated co-expression of UAS transgenes or in genetic backgrounds heterozygous for *dome^{G0441}*, *hop^{34}* or *Stat92E^{85C9}*. Graphs display mean±s.d. of average scores derived from ≥3 experiments. *t*-tests were performed to test for statistical significance (*$P<0.05$). *n*=number of wings scored. (C) Cumulative fraction of larvae undergoing larval-pupal transitions, which carry Eiger-stimulated discs (CA) (*n*=210) or were combined with *rn-GAL4*-mediated co-expression of *upd1* (*n*=213), *dome^{Δcyt}* (*n*=201), *dome-RNAi* (*n*=196), or *hop-RNAi* (*n*=230). Graphs display mean±s.e.m. of average scores from ≥3 experiments. (D) Relative disc area expressing *Ilp8>GFP* after cell ablation (CA) (R0, *n*=12; R24, *n*=4 discs) and in discs combined with *rn-GAL4*-mediated co-expression of *dome^{Δcyt}* (R0, *n*=5; R24, *n*=3 discs) or *dome-RNAi* (R0, *n*=5; R24, *n*=7 discs) in *eiger*-expressing cells. Graphs display mean±s.e.m. *U*-tests were performed to test for statistical significance (*$P<0.05$, **$P<0.01$, ***$P<0.001$).

(Brumby and Richardson, 2003; Wu et al., 2010). Larvae carrying MARCM-induced *Ras^{V12}; scrib^2* clones fail to pupariate (Fig. 7M), suggesting that *Ilp8* activation correlates with tumour load (Garelli et al., 2012). We found that *Ras^{V12}; scrib^2* clones covered about 47% of eye antennal discs, compared with 19% for wild-type clones (Fig. 7A,B,D). When we probed *Ras^{V12}; scrib^2* clones for activated Dcp-1, we did not observe any difference in apoptotic patterns compared with wild-type tissue (Fig. 7F,G).

When we completely removed JAK/STAT function in *Ras^{V12}; scrib^2* clones by homozygosity for a *Stat92E^{85C9}* allele, *Ras^{V12}; scrib^2* clone size was reduced from 47% to 28% of the eye disc area (Fig. 7B-D). Comparison of cell division rates within *Ras^{V12}; scrib^2* and *Ras^{V12}; scrib^2, Stat92E^{85C9}* clones did not reveal any significant changes upon loss of JAK/STAT function (Fig. 7B′,C′,E). However, in contrast to *Ras^{V12}; scrib^2* clones, *Ras^{V12}; scrib^2, Stat92E^{85C9}* clones displayed a 4.3-fold increase in areas of Dcp-1 activation (Fig. 7G,H,I), suggesting that increased

cell death of *Stat92E* mutant cells underlies the smaller sizes of *Ras^{V12}; scrib^2, Stat92E^{85C9}* clones (Fig. 7A-D). The reduction in *Ras^{V12}; scrib^2, Stat92E^{85C9}* clone size reduced total tumour load and allowed a significant proportion of host larvae to progress to pupal stages (Fig. 7M).

Strikingly, *Ras^{V12}; scrib^2* clones displayed ectopic activation of Zfh2 (Fig. 7J,K) but not of Zfh1 (not shown), indicating activation of a JNK-JAK/STAT-Zfh2 stress module by neoplastic transformation. Importantly, ectopic expression of Zfh2 was completely abolished within *Ras^{V12}; scrib^2, Stat92E^{85C9}* clones (Fig. 7L). These results support the notion that Zfh2 expression is regulated by JAK/STAT in multiple contexts of cellular stress and that stress-dependent Zfh2 activation in imaginal discs directly correlates with cell survival.

Altogether, our results support a model in which cellular stress caused by genetic cell ablation, physical wounding or tumorous growth drives activation of JAK/STAT to promote survival of
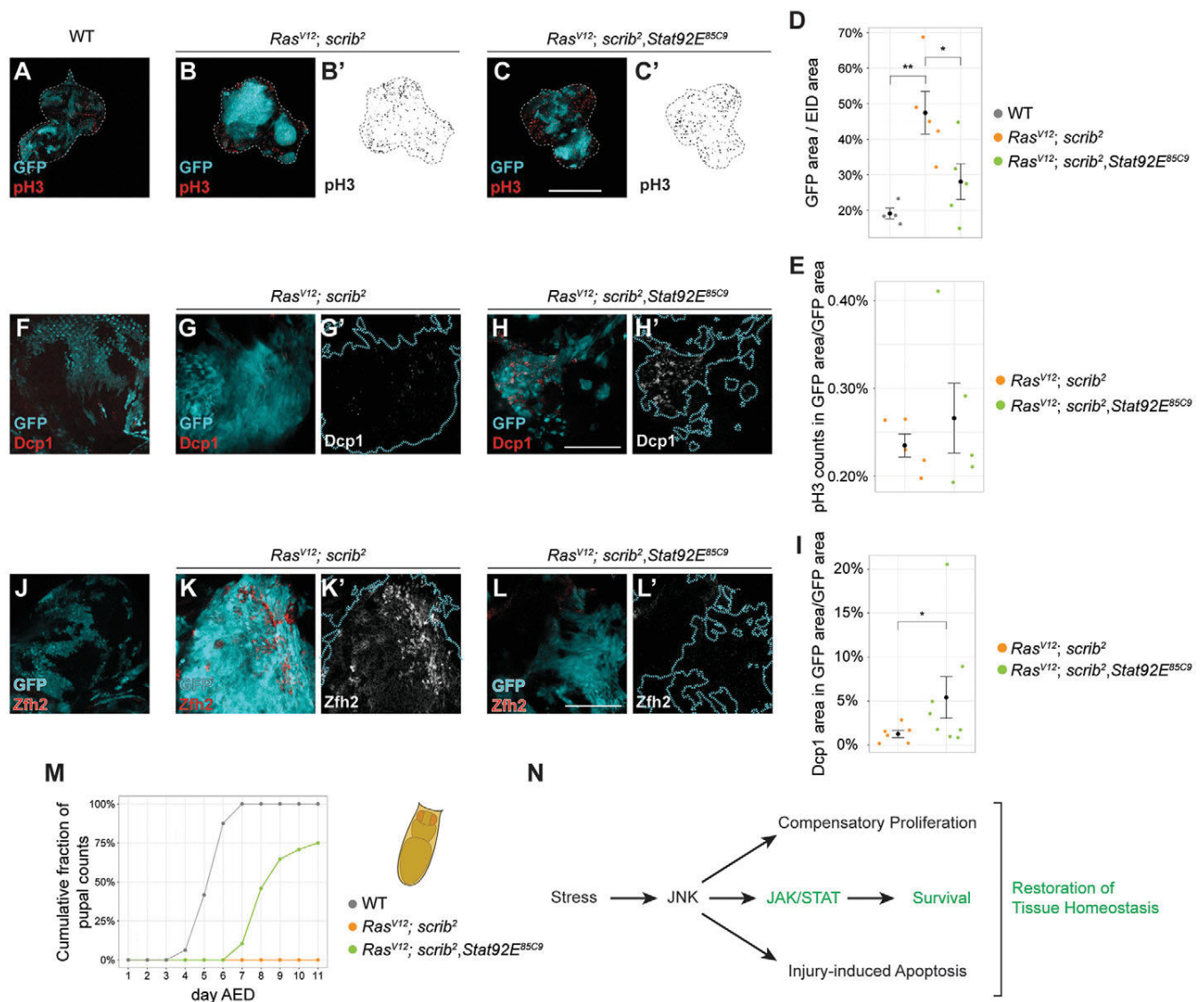
Fig. 7. JAK/STAT regulates survival in a *Ras^V12^; scrib²* tumour model. (A-C) Eye imaginal discs carrying neutral (A), *Ras^V12^; scrib²* (B,B′) or *Ras^V12^; scrib²*, *Stat92E^85C9^* (C,C′). GFP-marked MARCM clones (cyan in A-C) stained for pH3 (B′,C′, red in A-C). (D) Area occupied by neutral (*n*=4), *Ras^V12^; scrib²* (*n*=5) or *Ras^V12^; scrib²*, *Stat92E^85C9^* (*n*=5) clones, normalized to total eye imaginal disc (EID) area. (E) pH3-events in *Ras^V12^; scrib²* (*n*=5) or *Ras^V12^; scrib²*, *Stat92E^85C9^* (*n*=5) clones per eye disc normalized to total clone area per disc. (F-H) Eye discs carrying neutral (F), *Ras^V12^; scrib²* (G,G′) or *Ras^V12^; scrib²*, *Stat92E^85C9^* (H,H′) clones (cyan in F-H) stained for Dcp-1 (G′,H′, red in F-H). Clone borders indicated by outline in G′,H′. (I) Dcp-1-positive area within *Ras^V12^; scrib²* (*n*=6) or *Ras^V12^; scrib²*, *Stat92E^85C9^* (*n*=8) clones normalized to total clone area per disc. (J-L) Eye discs carrying neutral (J), *Ras^V12^; scrib²* (K,K′) or *Ras^V12^; scrib²*, *Stat92E^85C9^* (L,L′) clones (cyan in J-L) stained for Zfh2 (K′,L′, red in J-L). (M) Cumulative fraction of larvae undergoing larval-pupal transitions carrying *Ras^V12^; scrib²* or *Ras^V12^; scrib²*, *Stat92E^85C9^* clones. (N) Cells activating JNK in response to stress induce compensatory proliferation as well as injury-induced apoptosis. JAK/STAT suppresses apoptosis, thereby limiting the extent of tissue damage and promoting compensatory responses, such as induction of development delays. Graphs display mean±s.e.m. *U*-tests were performed to test for statistical significance (*P<0.05, **P<0.01, ***P<0.001). Scale bars: 100 μm.

JNK-signalling cells. Activation of JAK/STAT signalling thereby facilitates the induction and execution of local and systemic compensatory responses, rather than promoting compensatory cell proliferation directly (Fig. 7N).

DISCUSSION

JNK activation during tissue stress drives elimination of damaged cells by apoptosis (Bogoyevitch et al., 2010; Chen, 2012; Shlevkov and Morata, 2012; Luo et al., 2007; Moreno et al., 2002) and compensatory proliferation necessary to replace lost tissues (Bosch et al., 2005; Bergantinos et al., 2010; Mattila et al., 2005; Ryoo et al., 2004; Sun and Irvine, 2011). Our work provides

an answer to the central question of how these Janus-faced responses can be balanced by JNK. We show that in contrast to prevalent models, JAK/STAT signalling downstream of JNK does not promote compensatory proliferation, but instead supports cell survival and thereby contributes to tissue growth (Fig. 7N). The decision between JAK/STAT-dependent survival and JNK-induced apoptosis may depend on a relative cellular ratio between JAK/STAT and JNK signalling, which is determined by the position of cells within respective signalling gradients (Fig. S9B,B′). As a consequence of its pro-survival function, JAK/STAT indirectly supports regenerative growth by allowing JNK to initiate dILP8-dependent developmental delays and,

DEVELOPMENT

possibly, by facilitating Hippo/Yorkie-driven proliferation (Sun and Irvine, 2014). In fact, JNK-dependent Yorkie activation (Sun and Irvine, 2011) may occur independent of Jun/Fos-mediated transcription (Sun and Irvine, 2013), therefore JAK/STAT and Zfh2-dependent repression of *kay/fos* could suppress induction of JNK-dependent apoptosis without suppressing activation of Yorkie and thus of Hippo/Yorkie-driven compensatory proliferation. Hippo/Yorkie signalling, in turn, may sustain activation of *unpaired* and JAK/STAT signalling (Staley and Irvine, 2010; Bunker et al., 2015; Sarikaya and Extavour, 2015) even if JNK signalling is low. This signalling crosstalk would facilitate the stabilisation of a wound-proximal tissue domain supporting compensatory survival and proliferation.

Our new interpretation of JAK/STAT in promoting cell survival in response to tissue damage and in tumours can be reconciled with previous studies: JAK/STAT mutations frequently reduced tissue size. This was interpreted as a reduction in growth (Classen et al., 2009; Wu et al., 2010; Mukherjee et al., 2005; Amoyel et al., 2014), but we suggest that it is a consequence of excessive cell death. Similarly, Upd overexpression has been previously reported to drive cell proliferation (Bach et al., 2003; Classen et al., 2009; Tsai and Sun, 2004). However, continuous overexpression of Upd can also induce apoptosis (not shown) and, thus potentially also sustained JNK-dependent compensatory proliferation, driving tissue growth. So far, only isolated studies have implicated JAK/STAT in cell survival (Betz et al., 2008; Hasan et al., 2015; Guarner et al., 2014; Ohayon et al., 2009). For example, the apoptosis inhibitor *IAP* has been suggested to be a positively regulated target of Stat92E, protecting cells from apoptosis (Betz et al., 2008; Hasan et al., 2015). We identify the JAK/STAT effector Zfh2 as a potential repressor of *kay* and *hid* activity – a molecular pathway expected to restrain excessive JNK-activity and induction of apoptosis (Fig. S9A). Similarly, Dpp/TGFβ-dependent repression of *rpr* by Schnurri has been reported to prevent JNK-mediated apoptosis. Curiously, this occurs in contexts where JNK function is required to mediate cell shape remodelling during development (Beira et al., 2014) and therefore bears conceptual similarities to a model where JAK/STAT-dependent repression of *kay* and *hid* prevents JNK-mediated apoptosis but not Hippo/Yorkie-dependent compensatory proliferation. Our work does not address whether JAK/STAT only promotes survival during stress or if this also occurs during development. Cells carrying JAK/STAT mutations are eliminated from developing wing discs (Rodrigues et al., 2012) by cell competition. However, in the light of recent studies, which implicate JNK signalling in competitive cell elimination (Kolahgar et al., 2015), more studies are clearly needed to dissect the functional contribution of stress signals in this context. Combined, these studies and our work suggest that JNK-dependent apoptosis can be counteracted by multiple molecular pathways impinging on anti- and pro-apoptotic genes.

While the role of mammalian IL-6/STAT3 in regeneration needs to be further investigated, much evidence points to JNK and JAK/STAT pathways as crucial mediators of compensatory responses and tumorigenesis in mammalian tissues (Chen, 2012). A previous report suggests that JAK/STAT activation during mouse liver regeneration potentially confers a cell-protective function, similarly facilitating initiation of compensatory responses, rather then directly promoting cell proliferation (Wuestefeld et al., 2003). Therefore, the dominant pro-survival function of JAK/STAT in response to tissue stress, which we find to be essential for successful restoration of tissue homeostasis, appears highly

relevant to human contexts of cellular stress in physiological or pathological conditions.

MATERIALS AND METHODS

Drosophila stocks
For a detailed list of genotypes used in all experiments and shown in figures, refer to Table S1.

Temporal and spatial control of *eiger* expression
Fly crosses were carried out as described in supplementary Materials and Methods and *eiger* expression was induced as described in Smith-Bolton et al. (2009) and Fig. S1.

Immunohistochemistry
Larval cuticles were fixed in 4% PFA/PBS for 15 min at room temperature. Washing steps were performed in 0.1% Triton X-100/PBS (PBT), blocking in 5% NGS/PBT. Tissue samples were incubated in the following primary antibodies overnight at 4°C: mouse anti-Nub (1:100, S. Cohen, University of Copenhagen), rabbit anti-GFP (1:1000, Immunokontakt, cat. no. 210-PS-1GFP), mouse anti-H3S10p (1:2000, Abcam, cat. no. ab14955), rabbit anti-cCasp-3 (1:500, Cell Signaling, cat. no. 9661), rabbit anti-Dcp1 (1:500, Cell Signaling, cat. no. 9578), rabbit anti-β-Gal (1:500, Cappel, cat. no. 559762), rat anti-Zfh1 (1:500, R. Lehmann, NYU School of Medicine), rat anti-Zfh2 (1:300, C. Doe, HHMI/Institute of Molecular Biology). Secondary antibodies (Molecular Probes), DAPI and phalloidin-TRITC (Sigma) were applied and samples were incubated for 2 h at room temperature.

Flow cytometry and BrdU labelling
Flow cytometry of wing imaginal disc cells and labelling of fixed cuticle tissue with BrdU was carried out using standard techniques as described in supplementary Materials and Methods.

Real-time qPCR
RNA was extracted from ∼80 wing discs using Qiagen RNAlater and RNeasy protocols. cDNA libraries were prepared using standard protocols, including Ambion TurboDNase and Invitrogen Superscript III kits. qPCR was performed using Fast SYBR Green (Applied Biosystems) on a CFX-96 Real-Time machine (Bio-Rad). Data were analysed using the $\Delta\Delta C_t$ method and normalized to at least two housekeeping genes (Table S2).

Transcription factor binding site prediction
Bioinformatic analysis for potential transcription factor binding sites was performed using the program Clover (cis-element over-representation) (Frith et al., 2004) in combination with position-weighted matrices (PWM) obtained from the JASPAR collection (Mathelier et al., 2014) as detailed in supplementary Materials and Methods.

Adult wing size analysis
Wing size index (Ws) was calculated as the mean of five different wing phenotypes (*w*) (Fig. 5A) weighted with the frequencies at which they occurred (*f*) (Ws=$\Sigma w_i \times f_i / \Sigma f_i$). Samples were compared in a paired manner to control wings from the same experimental replicate (Wilcoxon signed rank test, α=0.05, $n \geq 3$ sample populations).

Author contributions
Designed the experiments: M.L.F., A.-K.C. Performed the experiments: M.L.F., M.S., A.C., A.K., I.G., A.-K.C. Data analysis: M.L.F., M.S., A.C., A.-K.C. Wrote the paper: M.L.F., A.-K.C.

DEVELOPMENT

Supplementary information
Supplementary information available online at
http://dev.biologists.org/lookup/doi/10.1242/dev.132340.supplemental

References

Amoyel, M., Anderson, A. M. and Bach, E. A. (2014). JAK/STAT pathway dysregulation in tumors: a Drosophila perspective. *Semin. Cell Dev. Biol.* **28**, 96-103.

Andersen, D. S., Colombani, J., Palmerini, V., Chakrabandhu, K., Boone, E., Röthlisberger, M., Toggweiler, J., Basler, K., Mapelli, M., Hueber, A.-O. et al. (2015). The Drosophila TNF receptor Grindelwald couples loss of cell polarity and neoplastic growth. *Nature* **522**, 482-486.

Arbouzova, N. I. and Zeidler, M. P. (2006). JAK/STAT signalling in Drosophila: insights into conserved regulatory and cellular functions. *Development* **133**, 2605-2616.

Ayala-Camargo, A., Ekas, L. A., Flaherty, M. S., Baeg, G. -H. and Bach, E. A. (2007). The JAK/STAT pathway regulates proximo-distal patterning in Drosophila. *Dev. Dyn.* **236**, 2721-2730.

Ayala-Camargo, A., Anderson, A. M., Amoyel, M., Rodrigues, A. B., Flaherty, M. S. and Bach, E. A. (2013). JAK/STAT signaling is required for hinge growth and patterning in the Drosophila wing disc. *Dev. Biol.* **382**, 413-426.

Bach, E. A., Vincent, S., Zeidler, M. P. and Perrimon, N. (2003). A sensitized genetic screen to identify novel regulators and components of the Drosophila janus kinase/signal transducer and activator of transcription pathway. *Genetics* **165**, 1149-1166.

Bach, E. A., Ekas, L. A., Ayala-Camargo, A., Flaherty, M. S., Lee, H., Perrimon, N. and Baeg, G.-H. (2007). GFP reporters detect the activation of the Drosophila JAK/STAT pathway in vivo. *Gene Expr. Patterns* **7**, 323-331.

Bando, T., Ishimaru, Y., Kida, T., Hamada, Y., Matsuoka, Y., Nakamura, T., Ohuchi, H., Noji, S. and Mito, T. (2013). Analysis of RNA-Seq data reveals involvement of JAK/STAT signalling during leg regeneration in the cricket Gryllus bimaculatus. *Development* **140**, 959-964.

Beira, J. V., Springhorn, A., Gunther, S., Hufnagel, L., Pyrowolakis, G. and Vincent, J. -P. (2014). The Dpp/TGFbeta-dependent corepressor Schnurri protects epithelial cells from JNK-induced apoptosis in drosophila embryos. *Dev. Cell* **31**, 240-247.

Bergantinos, C., Corominas, M. and Serras, F. (2010). Cell death-induced regeneration in wing imaginal discs requires JNK signalling. *Development* **137**, 1169-1179.

Betz, A., Ryoo, H. D., Steller, H. and Darnell, J. E., Jr. (2008). STAT92E is a positive regulator of Drosophila inhibitor of apoptosis 1 (DIAP/1) and protects against radiation-induced apoptosis. *Proc. Natl. Acad. Sci. USA* **105**, 13805-13810.

Bogoyevitch, M. A., Ngoei, K. R. W., Zhao, T. T., Yeap, Y. Y. C. and Ng, D. C. H. (2010). c-Jun N-terminal kinase (JNK) signaling: recent advances and challenges. *Biochim. Biophys. Acta* **1804**, 463-475.

Bosch, M., Serras, F., Martín-Blanco, E. and Baguñà, J. (2005). JNK signaling pathway required for wound healing in regenerating Drosophila wing imaginal discs. *Dev. Biol.* **280**, 73-86.

Bosch, M., Bagun, J. and Serras, F. (2008). Origin and proliferation of blastema cells during regeneration of Drosophila wing imaginal discs. *Int. J. Dev. Biol.* **52**, 1043-1050.

Bray, N., Dubchak, I. and Pachter, L. (2003). AVID: a global alignment program. *Genome Res.* **13**, 97-102.

Brumby, A. M. and Richardson, H. E. (2003). scribble mutants cooperate with oncogenic Ras or Notch to cause neoplastic overgrowth in Drosophila. *EMBO J.* **22**, 5769-5779.

Bryant, P. J. (1975). Regeneration and duplication in imaginal discs. *Ciba Found. Symp.* **0**, 71-93.

Bunker, B. D., Nellimoottil, T. T., Boileau, R. M., Classen, A. K. and Bilder, D. (2015). The transcriptional response to tumorigenic polarity loss in Drosophila. *eLife* **4**, e03189.

Chatterjee, N. and Bohmann, D. (2012). A versatile PhiC31 based reporter system for measuring AP-1 and Nrf2 signaling in Drosophila and in tissue culture. *PLoS ONE* **7**, e34063.

Chen, F. (2012). JNK-induced apoptosis, compensatory growth, and cancer stem cells. *Cancer Res.* **72**, 379-386.

Classen, A.-K., Bunker, B. D., Harvey, K. F., Vaccari, T. and Bilder, D. (2009). A tumor suppressor activity of Drosophila Polycomb genes mediated by JAK-STAT signaling. *Nat. Genet.* **41**, 1150-1155.

Colombani, J., Andersen, D. S. and Leopold, P. (2012). Secreted peptide Dilp8 coordinates Drosophila tissue growth with developmental timing. *Science* **336**, 582-585.

Cressman, D. E., Greenbaum, L. E., Deangelis, R. A., Ciliberto, G., Furth, E. E., Poli, V. and Taub, R. (1996). Liver failure and defective hepatocyte regeneration in interleukin-6-deficient mice. *Science* **274**, 1379-1383.

Davie, K., Jacobs, J., Atkins, M., Potier, D., Christiaens, V., Halder, G. and Aerts, S. (2015). Discovery of transcription factors and regulatory regions driving in vivo tumor development by ATAC-seq and FAIRE-seq open chromatin profiling. *PLoS Genet.* **11**, e1004994.

Eferl, R. and Wagner, E. F. (2003). AP-1: a double-edged sword in tumorigenesis. *Nat. Rev. Cancer* **3**, 859-868.

Evans, C. J., Olson, J. M., Ngo, K. T., Kim, E., Lee, N. E., Kuoy, E., Patananan, A. N., Sitz, D., Tran, P., Do, M.-T. et al. (2009). G-TRACE: rapid Gal4-based cell lineage analysis in Drosophila. *Nat. Methods* **6**, 603-605.

Fan, Y. and Bergmann, A. (2008). Distinct mechanisms of apoptosis-induced compensatory proliferation in proliferating and differentiating tissues in the Drosophila eye. *Dev. Cell* **14**, 399-410.

Flaherty, M. S., Salis, P., Evans, C. J., Ekas, L. A., Marouf, A., Zavadil, J., Banerjee, U. and Bach, E. A. (2010). chinmo is a functional effector of the JAK/STAT pathway that regulates eye development, tumor formation, and stem cell self-renewal in Drosophila. *Dev. Cell* **18**, 556-568.

Frazer, K. A., Pachter, L., Poliakov, A., Rubin, E. M. and Dubchak, I. (2004). VISTA: computational tools for comparative genomics. *Nucleic Acids Res.* **32**, W273-W279.

Frith, M. C., Fu, Y., Yu, L., Chen, J.-F., Hansen, U. and Weng, Z. (2004). Detection of functional DNA motifs via statistical over-representation. *Nucleic Acids Res.* **32**, 1372-1381.

Fulda, S., Gorman, A. M., Hori, O. and Samali, A. (2010). Cellular stress responses: cell survival and cell death. *Int. J. Cell Biol.* **2010**, 214074.

Garelli, A., Gontijo, A. M., Miguela, V., Caparros, E. and Dominguez, M. (2012). Imaginal discs secrete insulin-like peptide 8 to mediate plasticity of growth and maturation. *Science* **336**, 579-582.

Gregory, L., Came, P. J. and Brown, S. (2008). Stem cell regulation by JAK/STAT signaling in Drosophila. *Semin. Cell Dev. Biol.* **19**, 407-413.

Grusche, F. A., Degoutin, J. L., Richardson, H. E. and Harvey, K. F. (2011). The Salvador/Warts/Hippo pathway controls regenerative tissue growth in Drosophila melanogaster. *Dev. Biol.* **350**, 255-266.

Guarner, A., Manjón, C., Edwards, K., Steller, H., Suzanne, M. and Sánchez-Herrero, E. (2014). The zinc finger homeodomain-2 gene of Drosophila controls Notch targets and regulates apoptosis in the tarsal segments. *Dev. Biol.* **385**, 350-365.

Hasan, S., Hétié, P. and Matunis, E. L. (2015). Niche signaling promotes stem cell survival in the Drosophila testis via the JAK–STAT target DIAP1. *Dev. Biol.* **404**, 27-39.

Haynie, J. L. and Bryant, P. J. (1976). Intercalary regeneration in imaginal wing disk of Drosophila melanogaster. *Nature* **259**, 659-662.

Herrera, S. C. and Morata, G. (2014). Transgressions of compartment boundaries and cell reprogramming during regeneration in Drosophila. *eLife* **3**, e01831.

Herrera, S. C., Martín, R. and Morata, G. (2013). Tissue homeostasis in the wing disc of Drosophila melanogaster: immediate response to massive damage during development. *PLoS Genet.* **9**, e1003446.

Herz, H. -M., Chen, Z., Scherr, H., Lackey, M., Bolduc, C. and Bergmann, A. (2006). vps25 mosaics display non-autonomous cell survival and overgrowth, and autonomous apoptosis. *Development* **133**, 1871-1880.

Huh, J. R., Guo, M. and Hay, B. A. (2004). Compensatory proliferation induced by cell death in the Drosophila wing disc requires activity of the apical cell death caspase Dronc in a nonapoptotic role. *Curr. Biol.* **14**, 1262-1266.

Igaki, T. (2009). Correcting developmental errors by apoptosis: lessons from Drosophila JNK signaling. *Apoptosis* **14**, 1021-1028.

Igaki, T. and Miura, M. (2014). The Drosophila TNF ortholog Eiger: emerging physiological roles and evolution of the TNF system. *Semin. Immunol.* **26**, 267-274.

Igaki, T., Kanda, H., Yamamoto-Goto, Y., Kanuka, H., Kuranaga, E., Aigaki, T. and Miura, M. (2002). Eiger, a TNF superfamily ligand that triggers the Drosophila JNK pathway. *EMBO J.* **21**, 3009-3018.

Jiang, H., Patel, P. H., Kohlmaier, A., Grenley, M. O., Mcewen, D. G. and Edgar, B. A. (2009). Cytokine/Jak/Stat signaling mediates regeneration and homeostasis in the Drosophila midgut. *Cell* **137**, 1343-1355.

Johnstone, K., Wells, R. E., Strutt, D. and Zeidler, M. P. (2013). Localised JAK/STAT pathway activation is required for Drosophila wing hinge development. *PLoS ONE* **8**, e65076.

Kashio, S., Obata, F. and Miura, M. (2014). Interplay of cell proliferation and cell death in Drosophila tissue regeneration. *Dev. Growth Differ.* **56**, 368-375.

Katsuyama, T., Comoglio, F., Seimiya, M., Cabuy, E. and Paro, R. (2015). During Drosophila disc regeneration, JAK/STAT coordinates cell proliferation with Dilp8-mediated developmental delay. *Proc. Natl. Acad. Sci. USA* **112**, E2327-E2336.

Kolahgar, G., Suijkerbuijk, S. J. E., Kucinski, I., Poirier, E. Z., Mansour, S., Simons, B. D. and Piddini, E. (2015). Cell competition modifies adult stem cell and tissue population dynamics in a JAK-STAT-dependent manner. *Dev. Cell* **34**, 297-309.

Kondo, S., Senoo-Matsuda, N., Hiromi, Y. and Miura, M. (2006). DRONC coordinates cell death and compensatory proliferation. *Mol. Cell. Biol.* **26**, 7258-7268.

DEVELOPMENT

Leatherman, J. L. and Dinardo, S. (2008). Zfh-1 controls somatic stem cell self-renewal in the Drosophila testis and nonautonomously influences germline stem cell self-renewal. Cell Stem Cell 3, 44-54.

Lee, N., Maurange, C., Ringrose, L. and Paro, R. (2005). Suppression of Polycomb group proteins by JNK signalling induces transdetermination in Drosophila imaginal discs. Nature 438, 234-237.

Leong, G. R., Goulding, K. R., Amin, N., Richardson, H. E. and Brumby, A. M. (2009). Scribble mutants promote aPKC and JNK-dependent epithelial neoplasia independently of Crumbs. BMC Biol. 7, 62.

Li, W., Liang, X., Kellendonk, C., Poli, V. and Taub, R. (2002). STAT3 contributes to the mitogenic response of hepatocytes during liver regeneration. J. Biol. Chem. 277, 28411-28417.

Lin, G., Xu, N. and Xi, R. (2009). Paracrine unpaired signaling through the JAK/STAT pathway controls self-renewal and lineage differentiation of drosophila intestinal stem cells. J. Mol. Cell Biol 2, 37-49.

Luo, X., Puig, O., Hyun, J., Bohmann, D. and Jasper, H. (2007). Foxo and Fos regulate the decision between cell death and survival in response to UV irradiation. EMBO J. 26, 380-390.

Martin, F. A., Perez-Garijo, A. and Morata, G. (2009). Apoptosis in Drosophila: compensatory proliferation and undead cells. Int. J. Dev. Biol. 53, 1341-1347.

Mathelier, A., Zhao, X., Zhang, A. W., Parcy, F., Worsley-Hunt, R., Arenillas, D. J., Buchman, S., Chen, C. Y., Chou, A., Ienasescu, H. et al. (2014). JASPAR 2014: An extensively expanded and updated open-access database of transcription factor binding profiles. Nucleic Acids Res. 42, D142-D147.

Mattila, J., Omelyanchuk, L., Kyttala, S., Turunen, H. and Nokkala, S. (2005). Role of Jun N-terminal Kinase (JNK) signaling in the wound healing and regeneration of a Drosophila melanogaster wing imaginal disc. Int. J. Dev. Biol. 49, 391-399.

Moberg, K. H., Schelble, S., Burdick, S. K. and Hariharan, I. K. (2005). Mutations in erupted, the Drosophila ortholog of mammalian tumor susceptibility gene 101, elicit non-cell-autonomous overgrowth. Dev. Cell 9, 699-710.

Morata, G., Shlevkov, E. and Pérez-Garijo, A. (2011). Mitogenic signaling from apoptotic cells in Drosophila. Dev. Growth Differ. 53, 168-176.

Moreno, E., Yan, M. and Basler, K. (2002). Evolution of TNF signaling mechanisms: JNK-dependent apoptosis triggered by Eiger, the Drosophila homolog of the TNF superfamily. Curr. Biol. 12, 1263-1268.

Mukherjee, T., Hombría, J. C.-G. and Zeidler, M. P. (2005). Opposing roles for Drosophila JAK/STAT signalling during cellular proliferation. Oncogene 24, 2503-2511.

Myllymäki, H. and Rämet, M. (2014). JAK/STAT pathway in Drosophila immunity. Scand. J. Immunol. 79, 377-385.

Ohayon, D., Pattyn, A., Venteo, S., Valmier, J., Carroll, P. and Garces, A. (2009). Zfh1 promotes survival of a peripheral glia subtype by antagonizing a Jun N-terminal kinase-dependent apoptotic pathway. EMBO J. 28, 3228-3243.

Ohlstein, B. and Spradling, A. (2006). The adult Drosophila posterior midgut is maintained by pluripotent stem cells. Nature 439, 470-474.

Osman, D., Buchon, N., Chakrabarti, S., Huang, Y. -T., Su, W.-C., Poidevin, M., Tsai, Y.-C. and Lemaitre, B. (2013). Autocrine and paracrine unpaired signaling regulate intestinal stem cell maintenance and division. J. Cell Sci. 125, 5944-5949.

Pahlavan, P. S., Feldmann, R. E., Jr., Zavos, C. and Kountouras, J. (2006). Prometheus' challenge: molecular, cellular and systemic aspects of liver regeneration. J. Surg. Res. 134, 238-251.

Pastor-Pareja, J. C. and Xu, T. (2013). Dissecting social cell biology and tumors using Drosophila genetics. Annu. Rev. Genet. 47, 51-74.

Pastor-Pareja, J. C., Wu, M. and Xu, T. (2008). An innate immune response of blood cells to tumors and tissue damage in Drosophila. Dis. Model. Mech. 1, 144-154; discussion 153.

Perea, D., Molohon, K., Edwards, K. and Díaz-Benjumea, F. J. (2013). Multiple roles of the gene zinc finger homeodomain-2 in the development of the Drosophila wing. Mech. Dev. 130, 467-481.

Pérez-Garijo, A., Martín, F. A. and Morata, G. (2004). Caspase inhibition during apoptosis causes abnormal signalling and developmental aberrations in Drosophila. Development 131, 5591-5598.

Perez-Garijo, A., Shlevkov, E. and Morata, G. (2009). The role of Dpp and Wg in compensatory proliferation and in the formation of hyperplastic overgrowths caused by apoptotic cells in the Drosophila wing disc. Development 136, 1169-1177.

Pérez-Garijo, A., Fuchs, Y. and Steller, H. (2013). Apoptotic cells can induce non-autonomous apoptosis through the TNF pathway. eLife 2, e01004.

Postigo, A. A. and Dean, D. C. (1999). Independent repressor domains in ZEB regulate muscle and T-cell differentiation. Mol. Cell. Biol. 19, 7961-7971.

Postigo, A. A., Ward, E., Skeath, J. B. and Dean, D. C. (1999). zfh-1, the Drosophila homologue of ZEB, is a transcriptional repressor that regulates somatic myogenesis. Mol. Cell. Biol. 19, 7255-7263.

Rämet, M., Lanot, R., Zachary, D. and Manfruelli, P. (2002). JNK signaling pathway is required for efficient wound healing in Drosophila. Dev. Biol. 241, 145-156.

Razzell, W., Wood, W. and Martin, P. (2011). Swatting flies: modelling wound healing and inflammation in Drosophila. Dis. Model. Mech. 4, 569-574.

Repiso, A., Bergantinos, C. and Serras, F. (2013). Cell fate respecification and cell division orientation drive intercalary regeneration in Drosophila wing discs. Development 140, 3541-3551.

Ríos-Barrera, L. D. and Riesgo-Escovar, J. R. (2013). Regulating cell morphogenesis: the Drosophila Jun N-terminal kinase pathway. Genesis 51, 147-162.

Rodrigues, A. B., Zoranovic, T., Ayala-Camargo, A., Grewal, S., Reyes-Robles, T., Krasny, M., Wu, D. C., Johnston, L. A. and Bach, E. A. (2012). Activated STAT regulates growth and induces competitive interactions independently of Myc, Yorkie, Wingless and ribosome biogenesis. Development 139, 4051-4061.

Ryoo, H. D., Gorenc, T. and Steller, H. (2004). Apoptotic cells can induce compensatory cell proliferation through the JNK and the Wingless signaling pathways. Dev. Cell 7, 491-501.

Santabárbara-Ruiz, P., López-Santillán, M., Martínez-Rodríguez, I., Binagui-Casas, A., Pérez, L., Milán, M., Corominas, M. and Serras, F. (2015). ROS-Induced JNK and p38 signaling is required for unpaired cytokine activation during Drosophila regeneration. PLoS Genet. 11, e1005595.

Sarikaya, D. P. and Extavour, C. G. (2015). The Hippo pathway regulates homeostatic growth of stem cell niche precursors in the Drosophila ovary. PLoS Genet. 11, e1004962.

Schroeder, M. C., Chen, C.-L., Gajewski, K. and Halder, G. (2013). A non-cell-autonomous tumor suppressor role for Stat in eliminating oncogenic scribble cells. Oncogene 32, 4471-4479.

Schuster, K. J. and Smith-Bolton, R. K. (2015). Taranis protects regenerating tissue from fate changes induced by the wound response in Drosophila. Dev. Cell 34, 119-128.

Shlevkov, E. and Morata, G. (2012). A dp53/JNK-dependant feedback amplification loop is essential for the apoptotic response to stress in Drosophila. Cell Death Differ. 19, 451-460.

Smith-Bolton, R. K., Worley, M. I., Kanda, H. and Hariharan, I. K. (2009). Regenerative growth in Drosophila imaginal discs is regulated by Wingless and Myc. Dev. Cell 16, 797-809.

Staley, B. K. and Irvine, K. D. (2010). Warts and Yorkie mediate intestinal regeneration by influencing stem cell proliferation. Curr. Biol. 20, 1580-1587.

Sun, G. and Irvine, K. D. (2011). Regulation of Hippo signaling by Jun kinase signaling during compensatory cell proliferation and regeneration, and in neoplastic tumors. Dev. Biol. 350, 139-151.

Sun, G. and Irvine, K. D. (2013). Ajuba family proteins link JNK to Hippo signaling. Sci. Signal. 6, ra81.

Sun, G. and Irvine, K. D. (2014). Control of growth during regeneration. Curr. Top. Dev. Biol. 108, 95-120.

Sustar, A., Bonvin, M., Schubiger, M. and Schubiger, G. (2011). Drosophila twin spot clones reveal cell division dynamics in regenerating imaginal discs. Dev. Biol. 356, 576-587.

Tsai, Y.-C. and Sun, Y. H. (2004). Long-range effect of upd, a ligand for Jak/STAT pathway, on cell cycle in Drosophila eye development. Genesis 39, 141-153.

Uhlirova, M., Jasper, H. and Bohmann, D. (2005). Non-cell-autonomous induction of tissue overgrowth by JNK/Ras cooperation in a Drosophila tumor model. Proc. Natl. Acad. Sci. USA 102, 13123-13128.

Vaccari, T. and Bilder, D. (2005). The Drosophila tumor suppressor vps25 prevents nonautonomous overproliferation by regulating notch trafficking. Dev. Cell 9, 687-698.

Wells, B. S., Yoshida, E. and Johnston, L. A. (2006). Compensatory proliferation in Drosophila imaginal discs requires Dronc-dependent p53 activity. Curr. Biol. 16, 1606-1615.

Wu, M., Pastor-Pareja, J. C. and Xu, T. (2010). Interaction between Ras(V12) and scribbled clones induces tumour growth and invasion. Nature 463, 545-548.

Wuestefeld, T., Klein, C., Streetz, K. L., Betz, U., Lauber, J., Buer, J., Manns, M. P., Muller, W. and Trautwein, C. (2003). Interleukin-6/glycoprotein 130-dependent pathways are protective during liver regeneration. J. Biol. Chem. 278, 11281-11288.

Yamada, Y., Kirillova, I., Peschon, J. J. and Fausto, N. (1997). Initiation of liver growth by tumor necrosis factor: deficient liver regeneration in mice lacking type I tumor necrosis factor receptor. Proc. Natl. Acad. Sci. USA 94, 1441-1446.

Zhao, X. -F., Wan, J., Powell, C., Ramachandran, R., Myers, M. G., Jr. and Goldman, D. (2014). Leptin and IL-6 family cytokines synergize to stimulate Muller glia reprogramming and retina regeneration. Cell Rep. 9, 272-284.

Zhu, M., Xin, T., Weng, S., Gao, Y., Zhang, Y., Li, Q. and Li, M. (2010). Activation of JNK signaling links lgl mutations to disruption of the cell polarity and epithelial organization in Drosophila imaginal discs. Cell Res. 20, 242-245.

DEVELOPMENT

Supplementary experimental procedures

Temporal and spatial control of Eiger-expression

To induce expression of *eiger*, experiments were carried out as described in (Smith-Bolton et al., 2009) and in Fig.S1. Briefly, *rnGal4, UASegr, tubGal80[TS]/TM6B, tubGal80* lines were outcrossed to a w[1118] wild type strain or strains carrying indicated alleles or transgenes. Larvae were staged by collecting 50 1st instar larvae per vial 24 h after a 6 h egg collection. Larvae were raised at 18°C and shifted to 30°C for 40h at day 7 after egg deposition (D7 AED), unless noted otherwise. Genetic cell ablation experiments using *UASrpr; ptcGAL4, tubGAL80[TS]* or *rnGal4, UASrpr, tubGal80[TS]* were induced by a 16 h or a 24 h shift to 30°C at day 8 AED, respectively.

Flow cytometry

Flow cytometry analysis of wing imaginal disc cells was performed as described (de la Cruz and Edgar, 2008). Briefly, 20-30 dissected wing imaginal discs were dissociated in PBS with 9XTrypsin-EDTA (Sigma) supplemented with 1.5 µg/ml Hoechst 33342 for 2-3 h at room temperature. Cell profiles were obtained using a FACS Aria II instrument (BD Biosciences) and analysed using FlowJo 8.8.7 (Tree Star) software.

BrdU labelling

Larvae were dissected in Shields and Sang M3 medium and incubated for 30 min with 100µg/µl BrdU (Sigma) at room temperature. Cuticles were fixed in 4% PFA for 15 minutes and subsequently washed with 0.5% Triton X-100/PBS in all washing steps. Fixed tissues were incubated for 45 min in 2N HCl and washed with 0.1M H_3BO_3 for 2 min twice. Antibody incubations, sample mounting and analysis was carried out as described above.

Transcription factor binding site prediction

Bioinformatic analysis for potential transcription factor binding sites was performed using the program Clover (Cis-eLement OVERrepresentation) (Frith et al., 2004) in combination with position-weighted-matrices (PWM) obtained from the JASPAR collection (Mathelier et al., 2014). The p-value threshold of all predictions was set to $p<0.05$. *Drosophila* chromosome 2R was used as background sequence in all calculations. For each gene, genomic sequences (dm6 genome version) of 2.5 kb upstream from the transcriptional start site (TSS) and the entire first intron, if present, were selected for analysis. For short genes with a sequence shorter than 2 kb (e.g. *rpr* and *grim*) or for genes without introns, a 2.5 kb sequence downstream of the 3'UTR was add to the analysis. All results are documented in Supplemental .wig files. Data was visualized using USCS genome browser tools. mVISTA conservation analysis (Frazer et al., 2004, Bray et al., 2003) was run on *kay* and *hid* genomic

region by comparing *D.melanogaster* to: *D.simulans, D. sechellia, D. erecta, D. yakuba, D. ananassae, D. pseudobscura, D. persimilis, D. willistoni, D. virilis, D. grimshawi.* Genomic sequences were obtained from FlyBase. ATAC-seq profiles were previously published (Davie et al., 2015) (GEO access number: GSE59078) and used in this work as predictors of open chromatin regions.

Image analysis and quantification

General Information
Images were taken using 20X or 63X objectives (without additional optical zoom). Stacks were imaged at 1024x1024 pixel resolution and a z-step size of 1μm. Control and experimental samples were prepared under the same conditions on the same day, as well as imaged using the same conditions on the same day.

GFP volume quantification (G-trace lineage labelling)
Masks of the GFP signal were generated applying the 'Threshold' (settings: 'Triangle', stack histogram, dark background) and 'Remove Outliers' (settings: black and white pixels removal with radii= 1-10 at a constant threshold of 50) function to entire image stacks in FIJI. The resulting masks were analysed using the '3D Object Counter' function (settings: threshold= 128, min=10 max=Inf, Exclude Object On Edges=FALSE). Measured volumes for each disc were summed up and used to describe total GFP volume per disc.

pH3 and BrdU counts
Masks of pH3 (or BrdU) events per disc were generated by applying the 'Threshold' (settings: 'Li', stack histogram, dark background) and 'Remove Outliers' (settings: black and white pixels removal with radii= 1-5 at a constant threshold of 50) function to entire image stacks in FIJI. The resulting masks were analysed using the '3D Object Counter' function (settings: threshold= 128, min=10 max=Inf, Exclude Object On Edges=FALSE). The total number of counted particles was considered to represent mitotic or DNA replication events per disc.

pH3-positive mitotic events in G-trace lineage labelled cells (volumetric method)
To count the number of cells marked by pH3 within the GFP-positive, G-trace volume, the pH3 mask was 'Subtracted' (FIJI function) from the GFP mask. The resulting mask was analysed using the '3D Object Counter' function (settings: threshold= 128, min=10 max=Inf, Exclude Object On Edges=FALSE). The new total counts of particles were considered to be mitotic events in GFP-positive cells.

pH3-positive mitotic events in G-trace lineage labelled cells (absolute counts)
Nuclei of GFP-positive, cells were counted manually using the '*multi-point selection*' tool across stacks with z-step size of 2 μm. In the same disc, pH3-positive mitotic events within

the G-trace labelled region were manually counted across the entire stack. pH3 and nuclei counts were paired and ratios compared between genotypes.

TRE-reporter quantifications

Image stacks were manually curated to eliminate TRE-reporter activity signals arising from the peripodial membrane. The peripodium shows extensive TRE-reporter activity, which was not subject of this study. Maximum projections of the final image stacks were obtained in FIJI and

masks of the area with active reporter were generated using the 'Threshold' (settings: 'IsoData', stack histogram, dark background) and 'Remove Outliers' (settings: black and white pixels removal with radii=1-10 at a constant threshold of 50) function. The areas of resulting masks were quantified using the ROI analyzer in FIJI.

Supplementary Figures

Supplementary Figure 1. Experimental procedures
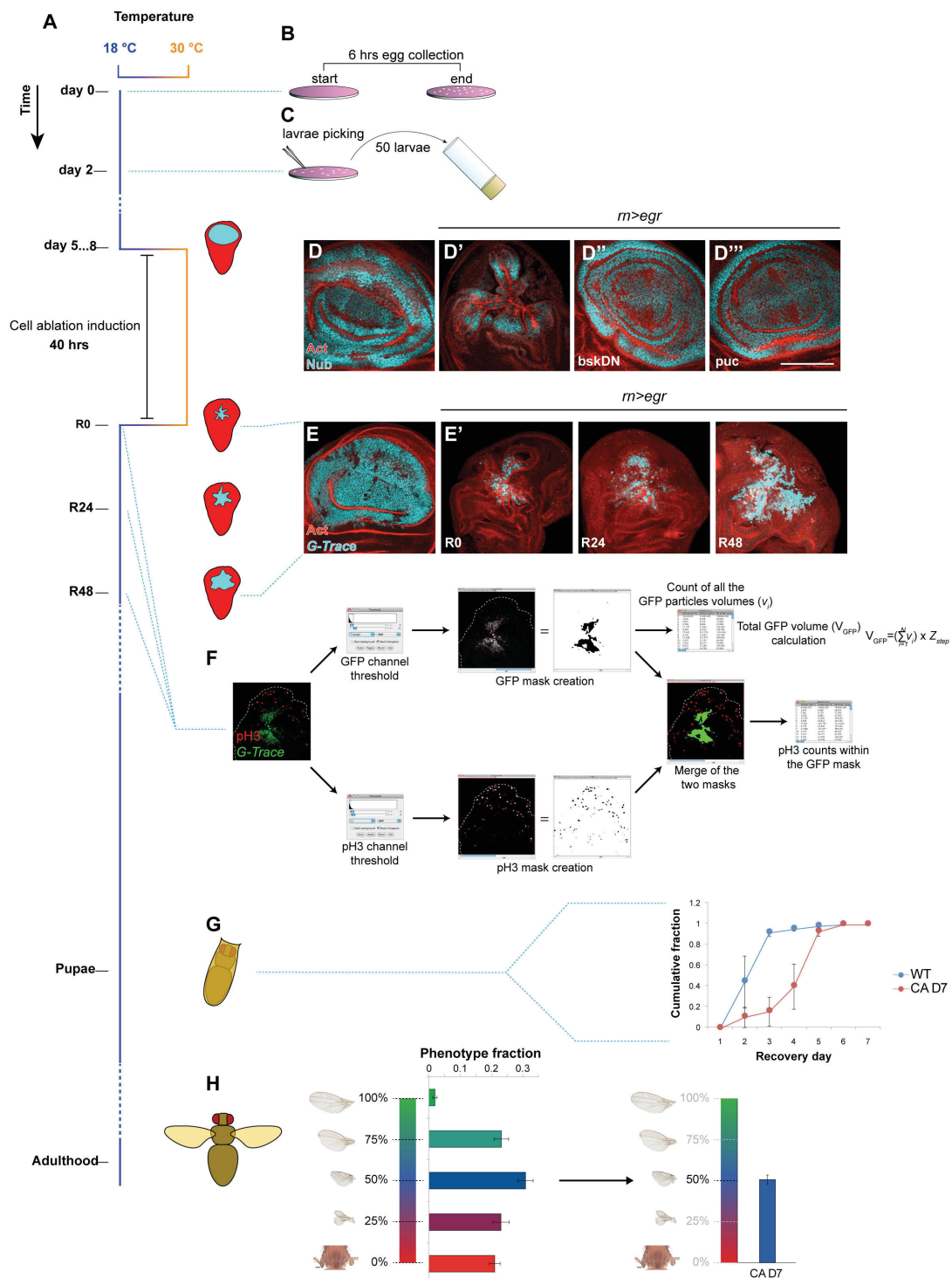
(A) Time line of development and induction of cell ablation by *eiger*-expression as a function of rearing temperature. Flies were raised at 18°C (blue) and transferred to 30°C (orange) for 40 hours to induce *eiger*-expression and cell ablation (CA) in wing imaginal discs. CA was

induced at different stages of development: 5 days (D5) after egg deposition (AED) or at day 6 (D6), day (D7) or day (D8). Unless otherwise noted, experiments were performed at D7.

(B) 6 hour egg collections were performed on grape juice plates (D0).

(C) 2 days after egg deposition (D2) 50 first instar larvae were collected in a vial.

(D) Wing pouch region in third instar wild type disc (D), wing disc after Eiger-mediated cell ablation at D7 (D'), wing disc after induction of *eiger*-expression with *rotund(rn)GAL4*-mediated co-expression a dominant-negative JNK (bskDN) (D'') or of the JNK-inhibitor Puckered (puc) (D''') stained for Actin (red) and for Nubbin (cyan) to visualize a lineage similar to *rnGAL4*-derived cells. Note that inhibition of JNK prevents Eiger-induced cell ablation.

(E) Wing pouch of a wild type disc, where cells of the *rnGAL4*-lineage were permanently labelled by GFP-expression using the GFP-lineage labelling system (*G-trace*). (E') *rnGAL4, G-trace* labelled cells which survived *eiger*-expression at recovery time point 0 hrs (R0), 24 hours (R24) and 48 hours (R48). Active proliferation of cells surviving *eiger*-expression contributes to compensatory proliferation.

(F) Schematic representation of automated workflows in Fiji to quantify volumes and particle counts in Eiger-stimulated discs.

(G) Cumulative fraction of larvae undergoing larval-pupal transitions, which carry wild type wing discs (WT) or wing discs that experienced *eiger*-expression for 40 h at D7 (CA). Compensatory responses to tissue stress induced by Eiger-mediated cell ablation induce a 2-day developmental delay at the larval to pupal transition.

(H) Quantification of average adult wing sizes developing from disc after Eiger-mediated cell ablation at D7. By scoring five different wing size phenotypes, quantifications were summarised as weighted averages of all different phenotypes (see Experimental procedures).

Supplementary Figure 2. Eiger-expression enables functional studies of JNK-dependent tissue stress responses
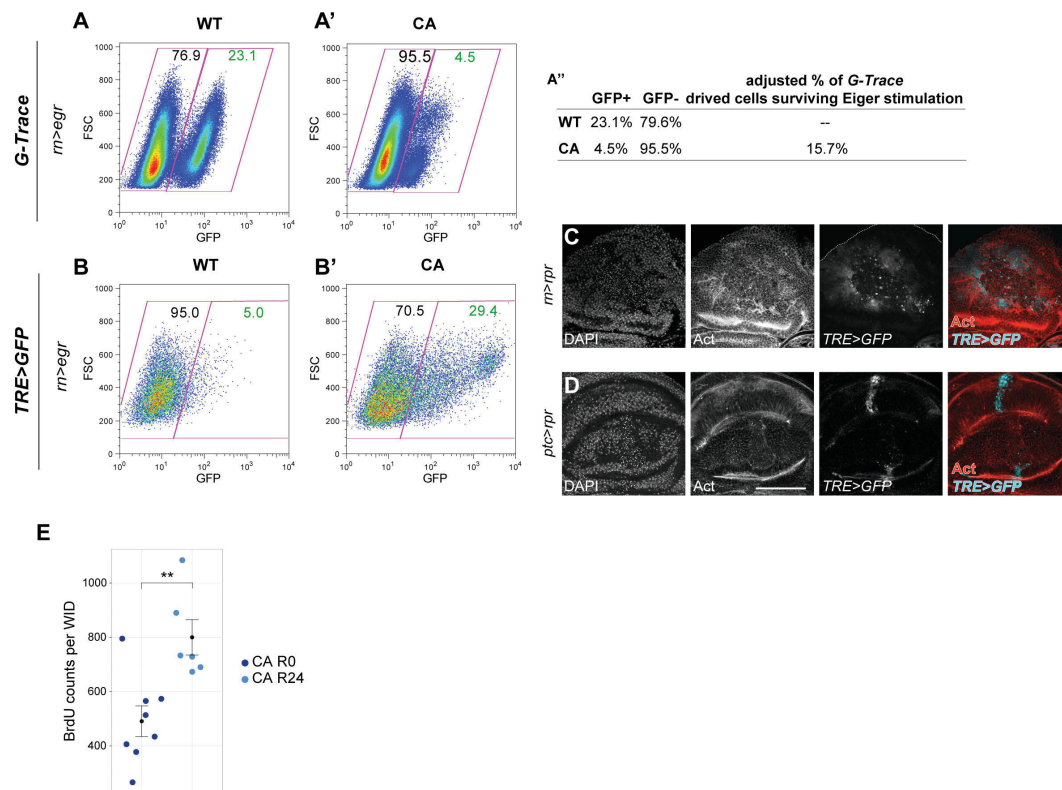
(A) FACS analysis of *rnGAL4,* G-trace-labelled cells expressing GFP in wild type (A) and in wing disc after Eiger-mediated cell ablation (A'). Data is plotted as a function of GFP-levels and forward scatter (FCS). To quantify the relative number of *rnGAL4,* G-trace-labelled cells that survive (A''), we made use of the following equation $X = (CA_{GFP+} * WT_{GFP-}) / (CA_{GFP-} * WT_{GFP+})$.

(B) FACS analysis of cells expressing the JNK reporter *TRE*-GFP in a wild type disc (B) and a wing disc after Eiger-mediated cell ablation (B'). Data is plotted as a function of GFP-levels and forward scatter (FCS).

(C, D) Wing pouch of discs expressing the JNK-reporter *TRE*-GFP (cyan in overlay), co-stained for DAPI or Actin (red in overlay). Discs were subjected to transient cell ablation driven by *rnGAL4, UAS-reaper* (rn>rpr) (C) or by *patched(ptc)GAL4, UAS-reaper* (ptc>rpr) (D). Compare to Fig.1B, C.

(E) Quantification of BrdU-positive events within Eiger-stimulated discs at R0 (n= 8 discs) and R24 (n= 6 discs).

Graphs display mean ± S.E.M. U-tests were performed to test for statistical significance (* *p<0.05, ** p<0.01, *** p<0.001*).

All scale bars: 100 μm.

Supplementary Figure 3. Eiger-induced tissue damage activates JAK/STAT signalling and tissue stress responses
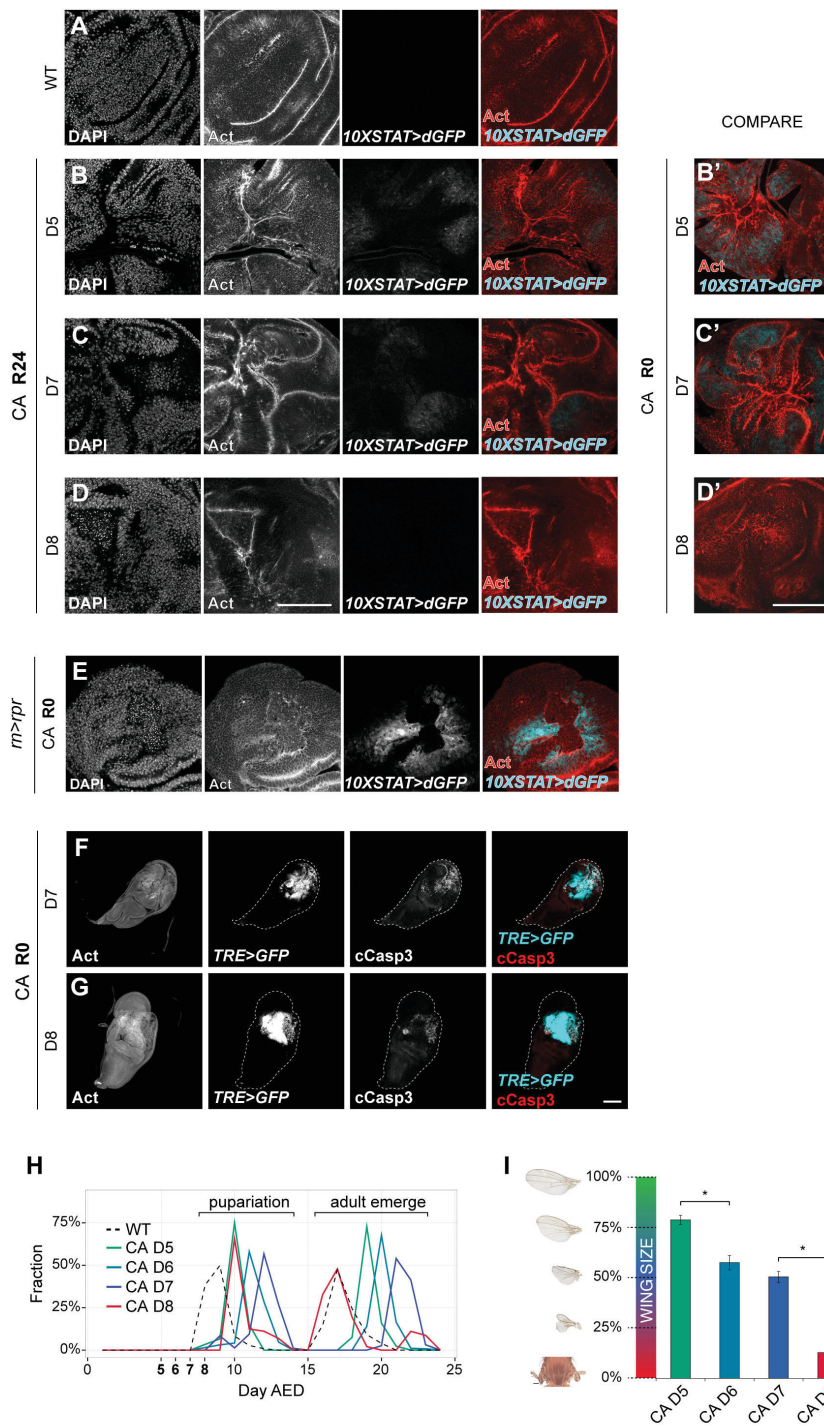
(A) Wing pouch in Eiger-stimulated discs (CA) expressing the JAK/STAT-reporter *10XSTAT*-dGFP (cyan in overlay), stained for DAPI or Actin (red in overlay).

(B-D) Wing pouch after *eiger*-expression was induced at developmental day 5 (B), day 7 (C) or day 8 (D) and imaged at R24. Discs express the JAK/STAT-reporter *10XSTAT*-dGFP (cyan

in overlay) and were stained for DAPI or Actin (red in overlay). Overlay images obtained at R0 are shown for comparison (B'-D').

(E) Wing pouch after transient cell ablation (CA) was induced by *rnGAL4, UAS-reaper* (rn>rpr). Disc expresses the JAK/STAT-reporter *10XSTAT*-dGFP (cyan in overlay), and was stained for DAPI and Actin (red in overlay). Compare to Fig. 2A.

(F, G) Wing discs after Eiger-stimulated cell ablation (CA) induced on D7 (F) or D8 (G). Discs expressing the JNK reporter *TRE*-GFP (cyan in overlay) were stained for Actin and for Cleaved Caspase-3 (cCasp3, red in overlay) to visualize apoptotic cells.

(H) Incident analysis of larva-to-pupal transition timing as well as adult eclosion timing in wild type animals and in animals where *eiger*-mediated CA was induced at D5, D6, D7 or D8.

(I) Quantification of average adult wing sizes developing from disc after *eiger*-mediated cell ablation was induced at D5, D6, D7 or D8.

All scale bars: 100 µm.

Supplementary Figure 4. JAK/STAT activation is not required for compensatory proliferation
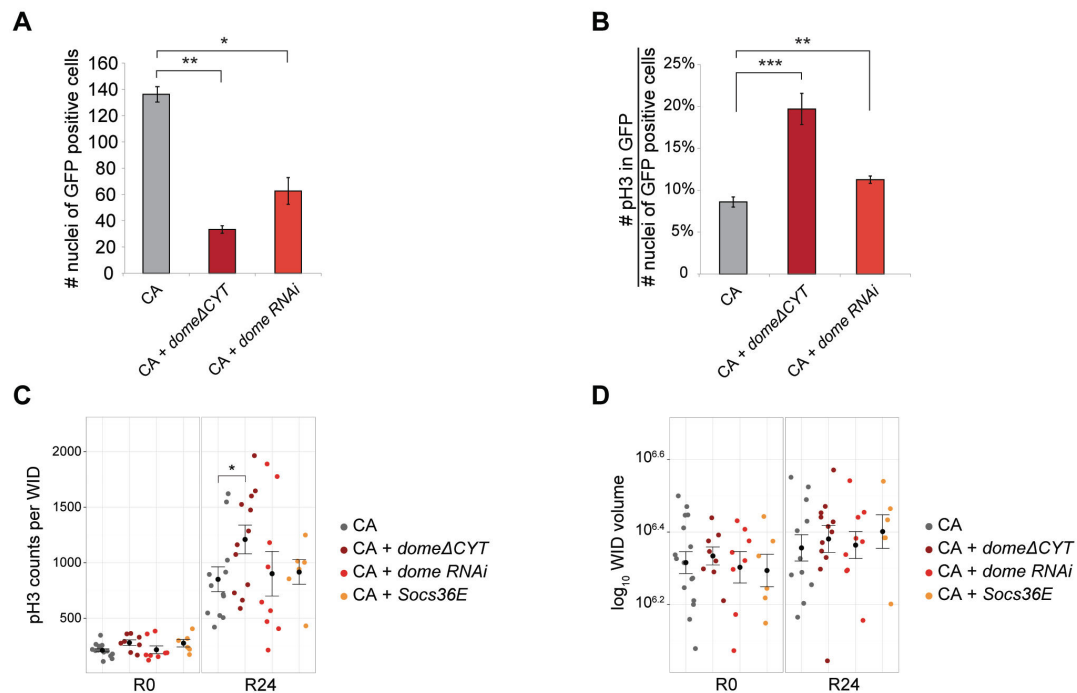
(A, B) Nuclear counts of G-trace labelled cells (B) and quantification of pH3-positive mitotic events within G-trace labelled cells (A) in ablated discs (CA) and ablated discs with *rnGAL4*-mediated co-expression of *dome*$^{\Delta cyt}$ or *dome* RNAi at R0 (for all samples n=3) in *eiger*-expressing cells.

(C, D) Quantification of pH3-positive, mitotic events per disc (A) and of total wing disc (WID) volume (B) at R0 and R24 after Eiger-stimulation. Wild type discs (CA) (R0 n=16, R24 n=12 discs) and discs with *rnGAL4*-mediated co-expression of *dome*$^{\Delta cyt}$ (R0 n= 8, R24 n=12 discs), *dome* RNAi (R0 n=8, R24 n= 9 discs) or *Socs36E* (R0 n= 6, R24 n= 6 discs) in *eiger*-expressing cells were quantified.

Graphs display mean ± S.E.M. U-test was run to check for statistical significance (* *p<0.05 ;* ** *p<0.01 ;* *** *p<0.001*).

Supplementary Figure 5. JAK/STAT activity is required for survival of Eiger-stimulated cells
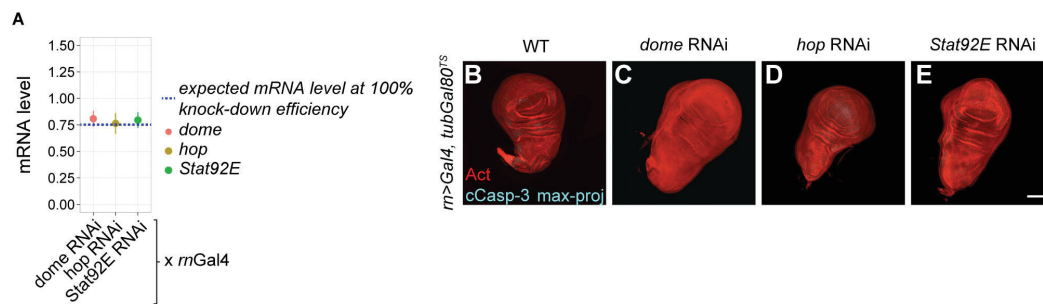
(A) Knock-down efficiency of UAS-RNAi transgenes targeting *dome, hop* and *Stat92E* was quantified by qRT-PCR. Wing imaginal discs expressing the constructs continuously under the control of *rnGAL4* were compared to wild type wing discs. Only about 25% of the total discs used for this analysis drives expression by *rnGAL4* (see Fig. S2A). Therefore the maximum expected reduction of transcript levels at 100% RNAi efficiency is only 25% (blue dashed line). Each graph shows mean ± S.E.M for n=2 biological replicates.

(B-E) Wild type wing disc (B) and wing discs with *rnGAL4*-driven expression of *dome* RNAi (C), *hop* RNAi (D) or *Stat92E* RNAi (E) induced at D7 for 40 hours were stained for Actin (red) and for Cleaved Caspase-3 (cyan) to visualize apoptotic cells. Maximum projections of entire image stacks are shown.

Graphs display mean ± S.E.M. U-tests were performed to test for statistical significance (* $p<0.05$, ** $p<0.01$, *** $p<0.001$).

All scale bars: 100 μm.

Supplementary Figure 6. A survival-promoting function of JAK/STAT is mediated by Zfh2
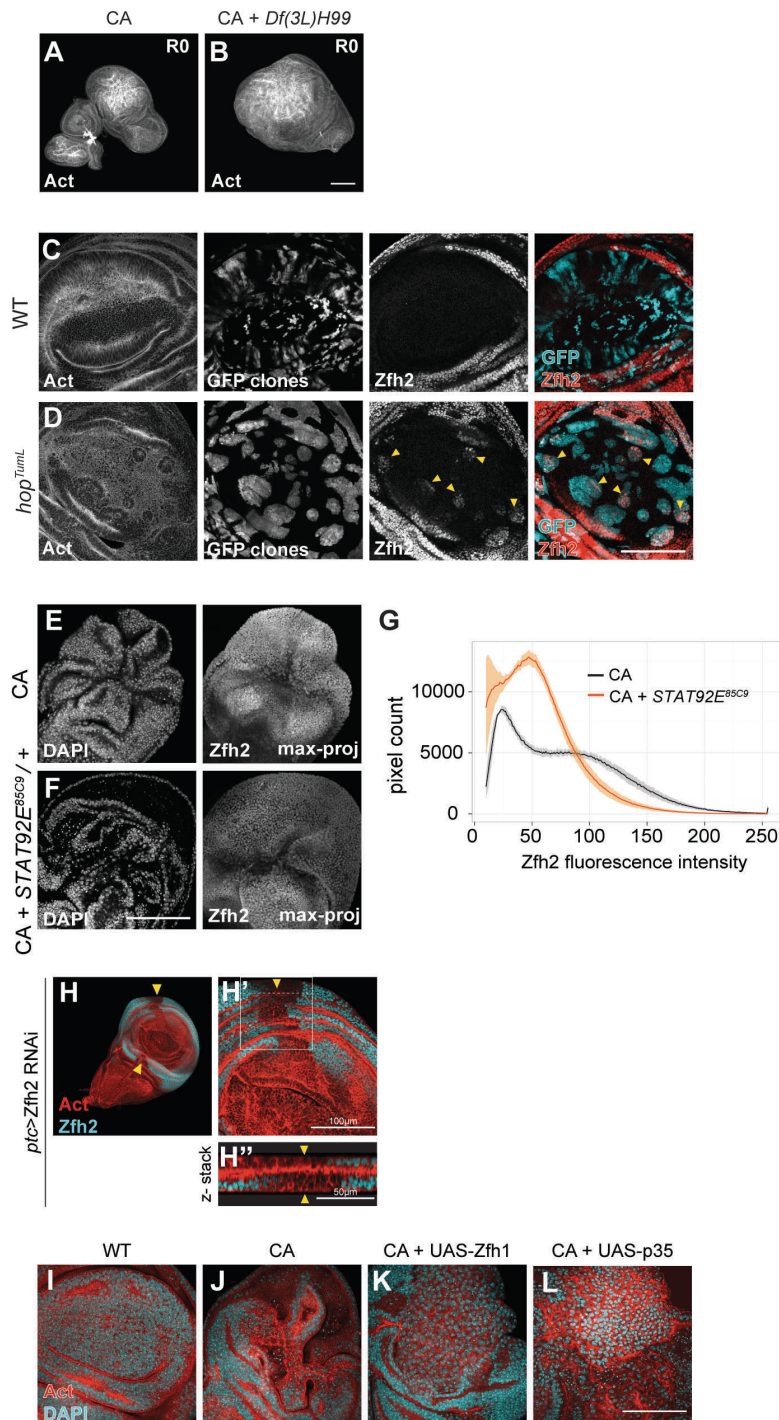
(A-B) Wild type wing disc (A) and wing disc heterozygous for *Df(3L)H99* (B) after Eiger-stimulated cell ablation were stained for Actin. Image in (A) also displays haltere and leg discs associated with the larger wing disc on the right.

(C-D) 'Flip-out' clones positively marked by expression of UAS-GFP under the control of Act5C-GAL4 (GFP clones, cyan in overlay) in wing discs stained for Zfh2 (red in overlay).

Clones were either wild type (C) or expressed a dominant active form of Hop (UAS-hop^{TumL}) (D). Yellow arrowheads indicate ectopic expression of Zfh2 in Hop^{TumL} expressing clones.

(E-F) Ablated discs (E) and ablated discs also heterozygous for $STAT92E^{85c9}$ (F) were stained for DAPI and Zfh2. Maximum-projection images of the confocal stacks are shown.

(G) Pixel counts of Zfh2 fluorescence intensity quantified in stainings on ablated discs (gray line) and ablated discs also heterozygous for $STAT92E^{85c9}$ (orange line). Each curve represents the average of n=3 independent measurements ± S.E.M.

(H) Wing disc expressing a RNAi construct targeting *zfh2* under the control of *ptcGAL4*. The disc was stained for Zfh2, confirming that Zfh2 signals disappeared in the *ptc* domain (yellow arrowheads, H, H'). Transverse section confirms loss of Zfh2 in the *ptc* domain (H'').

(I-L) Wild type wing disc (H), wing disc after Eiger-stimulation (I) and wing disc after Eiger-stimulation with *rnGAL4*-mediated co-expression of *Zfh1* (J) and *p35* (K) stained for DAPI (cyan) and Actin (red).

All scale bars: 100 µm unless otherwise noted.

Supplementary Figure 7. Prediction of AP-1 and ZFH binding sites on *hid* and *kay* loci.
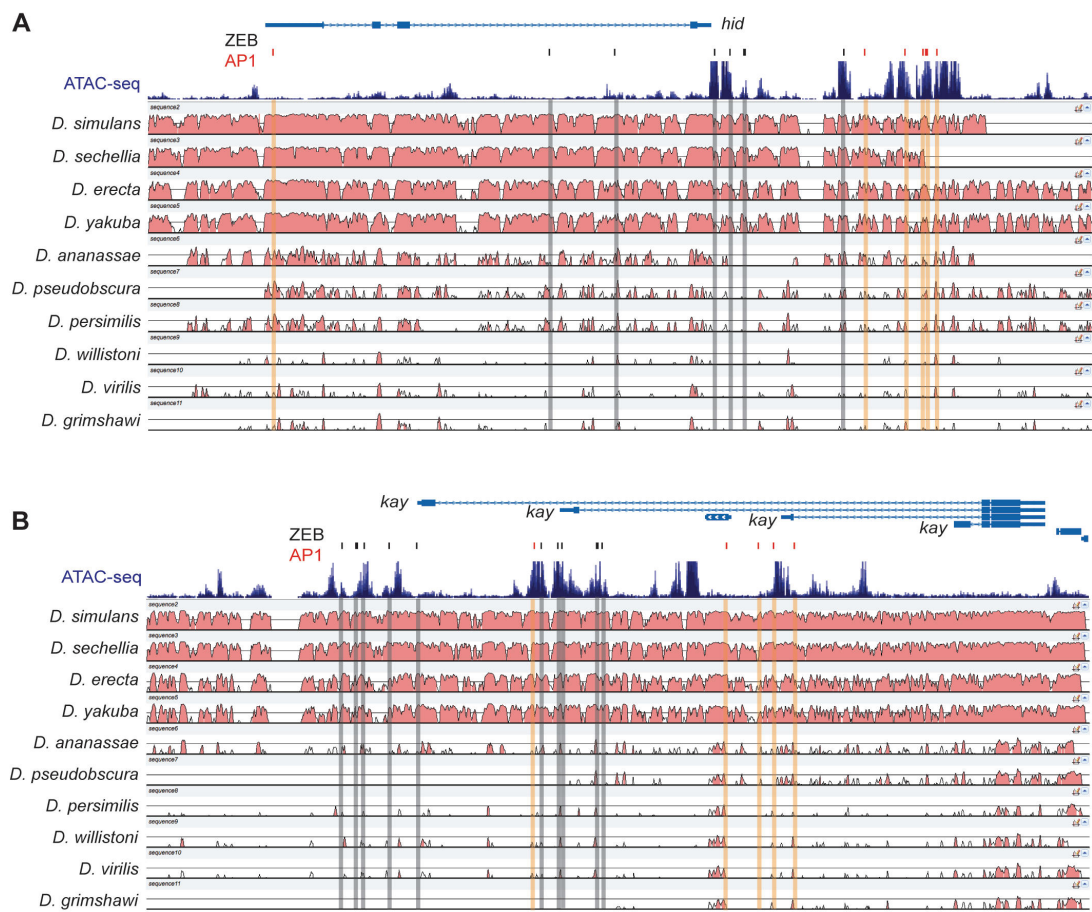
(A, B) Visualisation of AP-1 and ZEB/Zfh binding sites in regulatory regions of *hid* (A) *and fos (kay)* (B) predicted by bioinformatic analysis using Clover. ATAC-seq data (blue profile) from *D. mel.* wild type tissue, indicates open chromatin (Davie et al., 2015). mVISTA plots (red profiles) visualize conservation among *D. mel.* and species listed in the figure. Positions of predicted ZEB binding sites are shown in black/grey, predicted AP-1 binding sites in red/orange.

Supplementary Figure 8. JAK/STAT activity prevents excessive tissue damage in response to tissue stress
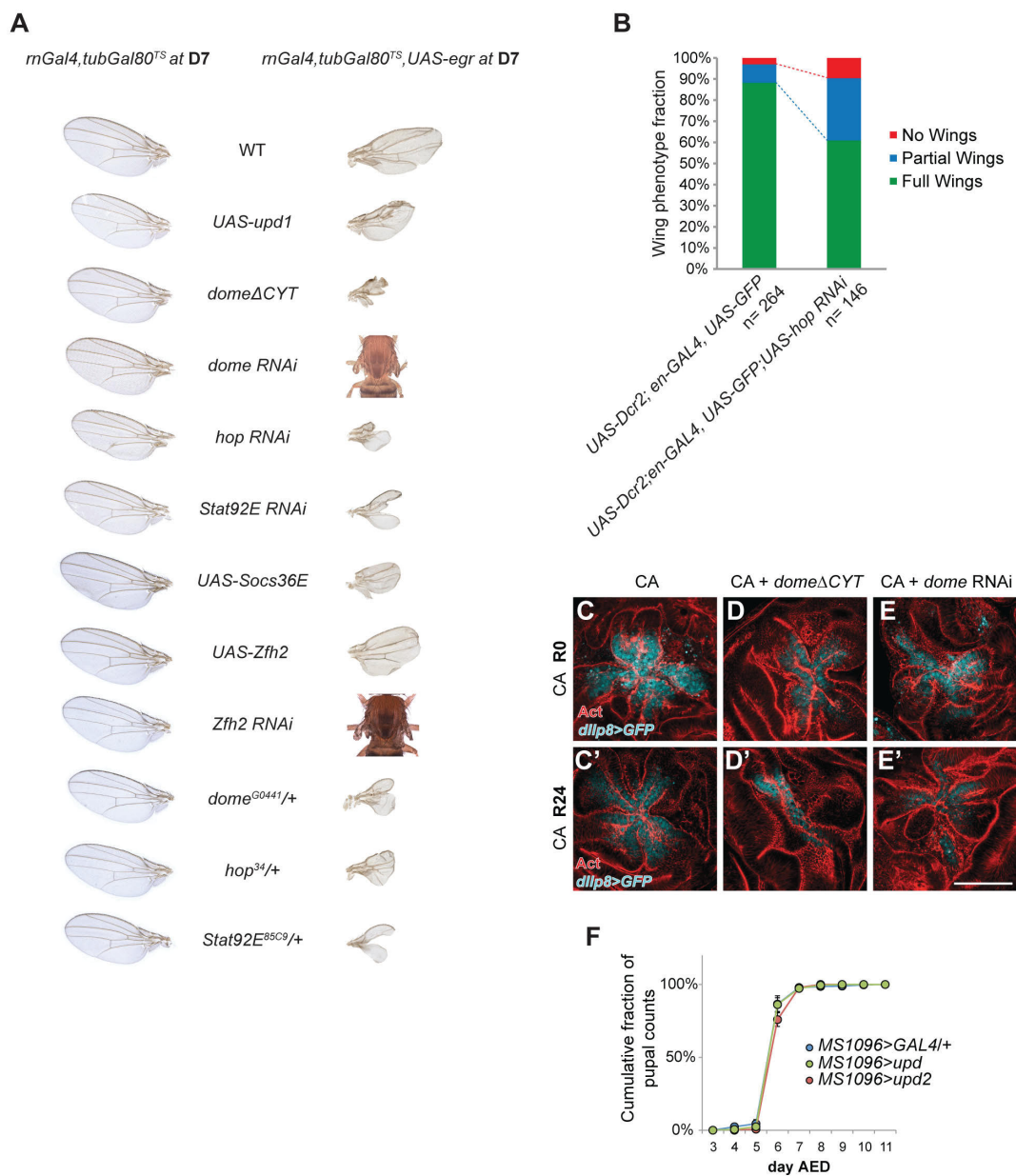
(A) Representative adult wings developing from wing discs having driven *rnGAL4*-mediated expression of UAS-transgenes at D7 or in genetic backgrounds heterozygous for *dome^G0441^*, *hop^34^*, or *Stat92E^85C9^* alleles (left column). Representative adult wings developing from wing disc having driven *eiger*-expression and *rnGAL4*-mediated co-expression of UAS-transgenes at D7 or in genetic backgrounds heterozygous for *dome^G0441^*, *hop^34^*, or *Stat92E^85C9^* alleles (right column).

(B) Quantification of 3 adult wing size classes developing from wing discs expressing GFP or GFP together with an RNAi-construct targeting *hop* in the posterior compartment. All wing discs were injured during larval development by targeted pinching using forceps.

(C-E) Wing disc after after Eiger-mediated cell ablation (CA) (C) and discs combined with *rnGAL4*-mediated co-expression of *dome$^{\Delta cyt}$* (B) or *dome* RNAi (C) in *eiger*-expressing cells, imaged at R0 (C-D) and R24 (C'-E') expressing the *dILP8*-GFP reporter (cyan) and stained for Actin (red).

(F) Cumulative fraction of larvae undergoing larval-pupal transitions, which carry control discs (MS1096GAL4/+) and discs expressing *upd* or *upd2* under the control of *MS1096*GAL4. Graph shows mean ± S.D. for average scores from at least 3 independent experiments.

Supplementary Figure 9. Models of how a survival-promoting function of JAK/STAT contributes to restoration of tissue homeostasis
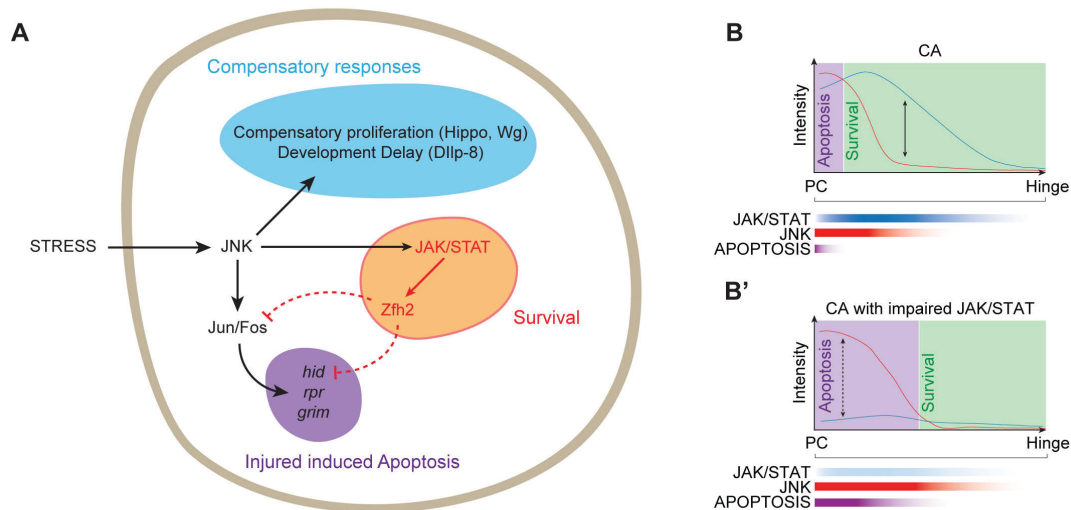
(A) Cells that activate JNK signalling in response to tissue stress induce compensatory responses as well as injured-induced apoptosis. JAK/STAT activates Zfh-2 to repress *hid* and *fos (kay),* thereby limiting strong JNK-activation and Hid-induced apoptosis. Suppression of apoptosis limits the extent of tissue damage and promotes compensatory responses by cells surviving JNK activation. This facilitates activation of compensatory proliferation and induction of development delays.

(B) Non-autonomous activation of JNK and of JAK/STAT creates two differently sloped signalling gradients from the site of damage (cell ablation (CA) in the pouch centre (PC)). A low JNK/JAKSTAT ratio induces apoptosis, whereas a high low JNK/JAKSTAT ratio promotes survival.

(B') If the JAK/STAT signalling gradient is disturbed (f.e. by heterozygosity for JAK/STAT components) all cells with JNK signalling have a low JNK/JAKSTAT ratio, making them more likely to die. Higher levels of apoptosis near the site of damage (PC) induce stronger non-autonomous activation of JNK, which in turn induces apoptosis at sites more distant to the initial damage. This feed-forward loop, unrestrained by loss of JAK/STAT activity, drives spatial expansion of JNK signalling and apoptosis, thereby increasing the extent of tissue damage and limiting the ability of the tissue to induce regenerative responses.

References

BRAY, N., DUBCHAK, I. & PACHTER, L. 2003. AVID: A global alignment program. *Genome Res,* 13**,** 97-102.

DAVIE, K., JACOBS, J., ATKINS, M., POTIER, D., CHRISTIAENS, V., HALDER, G. & AERTS, S. 2015. Discovery of Transcription Factors and Regulatory Regions Driving In Vivo Tumor Development by ATAC-seq and FAIRE-seq Open Chromatin Profiling. *PLoS Genet,* 11**,** e1004994.

DE LA CRUZ, A. F. & EDGAR, B. A. 2008. Flow cytometric analysis of Drosophila cells. *Methods Mol Biol,* 420**,** 373-89.

FRAZER, K. A., PACHTER, L., POLIAKOV, A., RUBIN, E. M. & DUBCHAK, I. 2004. VISTA: computational tools for comparative genomics. *Nucleic Acids Res,* 32**,** W273-9.

FRITH, M. C., FU, Y., YU, L., CHEN, J. F., HANSEN, U. & WENG, Z. 2004. Detection of functional DNA motifs via statistical over-representation. *Nucleic Acids Res,* 32**,** 1372-81.

MATHELIER, A., ZHAO, X., ZHANG, A. W., PARCY, F., WORSLEY-HUNT, R., ARENILLAS, D. J., BUCHMAN, S., CHEN, C. Y., CHOU, A., IENASESCU, H., LIM, J., SHYR, C., TAN, G., ZHOU, M., LENHARD, B., SANDELIN, A. & WASSERMAN, W. W. 2014. JASPAR 2014: an extensively expanded and updated open-access database of transcription factor binding profiles. *Nucleic Acids Res,* 42**,** D142-7.

SMITH-BOLTON, R. K., WORLEY, M. I., KANDA, H. & HARIHARAN, I. K. 2009. Regenerative growth in Drosophila imaginal discs is regulated by Wingless and Myc. *Dev Cell,* 16**,** 797-809.

Table S1. Genotypes and experimental conditions. This table lists all fly lines, their sources and the derived genotypes used to generate the data for each of the main and supplementary figures in this study. Experimental conditions related to induction of Eiger-expression are listed to the right.

General information	Genotypes	Source
	w^{118}	
	rn-Gal4,UAS-egr,tub-GAL80^{TS}/TM6b, tub-GAL80^{TS}	I Hariharan, R Smith-Bolton
	UAS-FLP,Ubi-p63E.FRT>STOP>FRT-Stinger15F2	Bloomington
	TRE-RFP	D Bohmann
	TRE-GFP	D Bohmann
	UAS-Bsk^{DN}	Bloomington
	UAS-puc	Bloomington
	10XSTATdGFP/Cyo	E Bach
	dome^{G0441}/FM7, ubi-GFP	Bloomington
	hop^{34}/FM7, ubi-GFP	N Perrimon
	FRT82-Stat92E^{85C9}/TM6c	E Bach
	UAS-dome$^{\Delta CYT}$/Cyo, ubi-GFP	E Bach
	UAS-Socs36E	E Bach
	zfh2[EAB]	F. J. Díaz-Benjumea and E. Sánche
	UAS-upd1/Cyo, ubi-GFP	M Zeidler
	w; UAS-upd2/Cyo	M Zeidler
	dilp8-GFP	Bloomington
	w; FRT 82B	Bloomington
	yw, ey-FLP; act>y^{+}>GAL4, UAS-GFP/Cyo;FRT82B, tub-GAL80/TM6b	G Halder
	yw, ey-FLP; UAS-Ras^{V12}/Cyo,FRT82B, scrib^{2}/TM6b	G Halder
	UAS-Ras^{V12}/Cyo; FRT82B, scrib^{2}, Stat92E^{85C9}/Tm6b	G Halder
	UAS-p35	Bloomington
	UAS-domeRNAi /Cyo, ubi-GFP	VDRC-KK106071
	UAS-hopRNAi	BL-HMS00761
	UAS-hopRNAi	BL-JF01268
	UAS-Stat92ERNAi	BL-HMS00035
	UAS-zfh1.P	Bloomington
	UAS-zfh1RNAi/TM3, Sb	BL-JF02509
	UAS-zfh2RNAi/TM6b	VDRC-GD13305
	Df(3L)H99/TM3, Sb	Bloomington
	UAS-Dcr2/FM7i;en-Gal4,UAS-GFP	Bloomington
	MS1096-Gal4/FM7a;Sp/Cyo;Dr/TM6c	
	ex[e1]-lacZ/SM6	G Halder
	upd-LacZ/FM7a	
	UAS-Hop^{TumL}/CyO	N Perrimon
	STAT92E-GFP.FLAG/CyO;Dr/TM6c	Bloomington
	hsflp[122]/+; act>y[+]>GAL4,UAS-GFP/+	

Figures	Genotypes	raised at	temperature shift	AED
Figure 1				
1A	+/+;rn-Gal4,tub-Gal80^{TS}/UAS-FLP,Ubi-p63E-FRT>STOP>FRT-Stinger15F2	18°C	30°C, 40 h	7d
1A',1D,1F	+/+;rn-Gal4,UAS-egr,tub-Gal80^{TS}/UAS-FLP,Ubi-p63E-FRT>STOP>FRT-Stinger15F2	18°C	30°C, 40 h	7d
1B	TRE-GFP/+;+/+	18°C	30°C, 40 h	7d
1C	TRE-RFP/+;rn-Gal4,UAS-egr,tub-Gal80^{TS}/UAS-FLP,Ubi-p63E-FRT>STOP>FRT-Stinger15F2	18°C	30°C, 40 h	7d
1E,1G	+/+;rn-Gal4,UAS-egr,tub-Gal80^{TS}/+	18°C	30°C, 40 h	7d
Figure 2				
2A	10XSTATdGFP/+;+/+	18°C	30°C, 40 h	5d-7d-8d
2B-D	10XSTATdGFP/+;rn-Gal4,UAS-egr,tub-Gal80^{TS}/+	18°C	30°C, 40 h	5d-7d-8d
2E	+/+;rn-Gal4,UAS-egr,tub-Gal80^{TS}/+	18°C	30°C, 40 h	5d-7d-8d
Figure 3				
3A,3E-F	+/+;rn-Gal4,UAS-egr,tub-Gal80^{TS}/+	18°C	30°C, 40 h	7d
3B,3E-3F	dome^{G0441}/+;+/+;rn-Gal4,UAS-egr,tub-Gal80^{TS}/+	18°C	30°C, 40 h	7d + 6h
3C,3E-3F	hop^{34}/+;+/+;rn-Gal4,UAS-egr,tub-Gal80^{TS}/+	18°C	30°C, 40 h	7d + 6h
3D,3E-3F	+/+;rn-Gal4,UAS-egr,tub-Gal80^{TS}/FRT82-Stat92E^{85C9}	18°C	30°C, 40 h	7d + 12h

Figures	Genotypes	raised at	exp. conditions	
3G,3K-3L	+/+;rn-Gal4,UAS-egr,tub-Gal80^TS/UAS-FLP,Ubi-p63E-FRT>STOP>FRT-Stinger15F2	18°C	30°C, 40 h	7d
3H,3K-3L	UAS-domeΔCYT/+;rn-Gal4,UAS-egr,tub-Gal80^TS/UAS-FLP,Ubi-p63E-FRT>STOP>FRT-Stinger15F2	18°C	30°C, 40 h	7d
3I,3K-3L	UAS-domeRNAi/+;rn-Gal4,UAS-egr,tub-Gal80TS/UAS-FLP,Ubi-p63E-FRT>STOP>FRT-Stinger15F2	18°C	30°C, 40 h	7d
3J,3K-3L	UAS-Socs36E/+;rn-Gal4,UAS-egr,tub-Gal80TS/UAS-FLP,Ubi-p63E-FRT>STOP>FRT-Stinger15F2	18°C	30°C, 40 h	7d

Figure 4

Figures	Genotypes	raised at	exp. conditions	
4A,4E,4I	+/+;rn-Gal4,UAS-egr,tub-Gal80^TS/+	18°C	30°C, 40 h	7d
4B,4E	UAS-domeΔCYT/+;rn-Gal4,UAS-egr,tub-Gal80^TS/+	18°C	30°C, 40 h	7d
4C,4E	UAS-domeRNAi/+;rn-Gal4,UAS-egr,tub-Gal80TS/+	18°C	30°C, 40 h	7d
4D-E	+/+;rn-Gal4,UAS-egr,tub-Gal80TS/UAS-Socs36E	18°C	30°C, 40 h	7d
4F,4I	dome^{G0441}/+;+/+;rn-Gal4,UAS-egr,tub-Gal80^TS/+	18°C	30°C, 40 h	7d + 6h
4G,4I	hop^{34}/+;+/+;rn-Gal4,UAS-egr,tub-Gal80^TS/+	18°C	30°C, 40 h	7d + 6h
4H-I	+/+;rn-Gal4,UAS-egr,tub-Gal80^TS/FRT82-Stat92E^{85C9}	18°C	30°C, 40 h	7d + 12h
4J,4N	TRE-RFP/+;rn-Gal4,UAS-egr,tub-Gal80^TS/+	18°C	30°C, 40 h	7d
4K,4N	dome^{G0441}/+;TRE-RFP/+;rn-Gal4,UAS-egr,tub-Gal80^TS/+	18°C	30°C, 40 h	7d + 6h
4L,4N	hop^{34}/+;TRE-RFP/+;rn-Gal4,UAS-egr,tub-Gal80^TS/+	18°C	30°C, 40 h	7d + 6h
4M-N	TRE-RFP/+;rn-Gal4,UAS-egr,tub-Gal80^TS/FRT82-Stat92E^{85C9}	18°C	30°C, 40 h	7d + 12h

Figure 5

Figures	Genotypes	raised at	exp. conditions	
5A, 5C, 5E, 5G	w118			
5A-M	+/+;rn-Gal4,UAS-egr,tub-Gal80^TS/+	18°C	30°C, 40 h	7d
5B	+/+;rn-Gal4,UAS-egr,tub-Gal80^TS/FRT82-Stat92E^{85C9}	18°C	30°C, 40 h	7d
5I	+/+;rn-Gal4,UAS-egr,tub-Gal80TS/UAS-Zfh2RNAi	18°C	30°C, 40 h	7d
5K	+/+;rn-Gal4,UAS-egr,tub-Gal80^TS/UAS-FLP,Ubi-p63E-FRT>STOP>FRT-Stinger15F2	18°C	30°C, 40 h	7d
5L	+/+;rn-Gal4,UAS-egr,tub-Gal80^TS/+;Zfh2[EAB]	18°C	30°C, 40 h	7d

Figure 6

Figures	Genotypes	raised at	exp. conditions	
6A-D	+/+;rn-Gal4,UAS-egr,tub-Gal80^TS/+	18°C	30°C, 40 h	7d
6B-C	UAS-upd1/+;+/+;rn-Gal4,UAS-egr,tub-Gal80^TS/+	18°C	30°C, 40 h	7d
6B	UAS-upd2/+;+/+;rn-Gal4,UAS-egr,tub-Gal80^TS/+	18°C	30°C, 40 h	7d
6B-C	UAS-domeΔCYT/+;rn-Gal4,UAS-egr,tub-Gal80^TS/+	18°C	30°C, 40 h	7d
6B-C	UAS-domeRNAi/+;rn-Gal4,UAS-egr,tub-Gal80TS/+	18°C	30°C, 40 h	7d
6B-C	+/+;rn-Gal4,UAS-egr,tub-Gal80TS/UAS-hopRNAi	18°C	30°C, 40 h	7d
6B	+/+;rn-Gal4,UAS-egr,tub-Gal80TS/UAS-STAT92ERNAi	18°C	30°C, 40 h	7d
6B	+/+;rn-Gal4,UAS-egr,tub-Gal80TS/UAS-Socs36E	18°C	30°C, 40 h	7d
6B	+/+;rn-Gal4,UAS-egr,tub-Gal80TS/UAS-Zfh2RNAi	18°C	30°C, 40 h	7d
6B	+/+;rn-Gal4,UAS-egr,tub-Gal80^TS/+;Zfh2[EAB]	18°C	30°C, 40 h	7d
6B	dome^{G0441}/+;+/+;rn-Gal4,UAS-egr,tub-Gal80^TS/+	18°C	30°C, 40 h	7d + 6h
6B	hop^{34}/+;+/+;rn-Gal4,UAS-egr,tub-Gal80^TS/+	18°C	30°C, 40 h	7d + 6h
6B	+/+;rn-Gal4,UAS-egr,tub-Gal80^TS/FRT82-Stat92E^{85C9}	18°C	30°C, 40 h	7d + 12h
6D	+/+;rn-Gal4,UAS-egr,tub-Gal80^TS/dIlp8-GFP	18°C	30°C, 40 h	7d
6D	UAS-domeΔCYT/+;rn-Gal4,UAS-egr,tub-Gal80^TS/dIlp8-GFP	18°C	30°C, 40 h	7d
6D	UAS-domeRNAi/+;rn-Gal4,UAS-egr,tub-Gal80TS/dIlp8-GFP	18°C	30°C, 40 h	7d

Figure 7

Figures	Genotypes	raised at
7A,7D-E,7F,7I,7J,7M	yw,ey-FLP;act>y+>GAL4,UAS-GFP/+;FRT82B,tub-GAL80/FRT82B-iso	25°C
7B,7D-E,7G,7I,7K,7M	yw,ey-FLP;act>y+>GAL4,UAS-GFP/UAS-Ras^{V12};FRT82B, tub-GAL80/FRT82B,scrib^2	25°C
7C-E,7H-I,7L-M	yw,ey-FLP;act>y+>GAL4,UAS-GFP/UAS-Ras^{V12};FRT82B, tub-GAL80/FRT82B,scrib^2,Stat92E^{85C9}	25°C

Supplementary figures

Figures	Genotypes	raised at	exp. conditions	

Figure S1

Figures	Genotypes	raised at	exp. conditions	
S1D,S1G	w118	18°C	30°C, 40 h	7d
S1D',S1G-H	+/+;rn-Gal4,UAS-egr,tub-Gal80^TS/+	18°C	30°C, 40 h	7d
S1D"	UAS-bskDN/+;+/+;rn-Gal4,UAS-egr,tub-Gal80^TS/+	18°C	30°C, 40 h	7d
S1D'''	+/+;rn-Gal4,UAS-egr,tub-Gal80^TS/UAS-puc	18°C	30°C, 40 h	7d
S1E	+/+;rn-Gal4,tub-Gal80^TS/UAS-FLP,Ubi-p63E-FRT>STOP>FRT-Stinger15F2	18°C	30°C, 40 h	7d
S1E'-F	+/+;rn-Gal4,UAS-egr,tub-Gal80^TS/UAS-FLP,Ubi-p63E-FRT>STOP>FRT-Stinger15F2	18°C	30°C, 40 h	7d

Figure S2

S2A	+/+;rn-Gal4,tub-Gal80^{TS}/UAS-FLP,Ubi-p63E-FRT>STOP>FRT-Stinger15F2	18°C	30°C, 40 h	7d
S2A'	+/+;rn-Gal4,UAS-egr,tub-Gal80^{TS}/UAS-FLP,Ubi-p63E-FRT>STOP>FRT-Stinger15F2	18°C	30°C, 40 h	7d
S2B	TRE-GFP/+;+/+	18°C	30°C, 40 h	7d
S2B'	TRE-GFP/+;rn-Gal4,UAS-egr,tub-Gal80^{TS}/+	18°C	30°C, 40 h	7d
S2C	TRE-GFP/+;rn-Gal4,UAS-rpr,tub-Gal80^{TS}/+	18°C	30°C, 24 h	7d
S2D	UAS-rpr/+;ptc-Gal4,tub-Gal80^{TS}/TRE-GFP;+/+	18°C	30°C, 16 h	7d
S2E	+/+;rn-Gal4,UAS-egr,tub-Gal80^{TS}/+	18°C	30°C, 40 h	7d

Figure S3

S3A	10XSTATdGFP/+;+/+	18°C	30°C, 40 h	7d
S3B-D	10XSTATdGFP/+;rn-Gal4,UAS-egr,tub-Gal80^{TS}/+	18°C	30°C, 40 h	5d-7d-8d
S3E	10XSTATdGFP/+;rn-Gal4,UAS-rpr,tub-Gal80^{TS}/+	18°C	30°C, 24 h	7d
S3F-G	TRE-GFP/+;rn-Gal4,UAS-egr,tub-Gal80^{TS}/+	18°C	30°C, 40 h	7d-8d
S3H-I	+/+;rn-Gal4,UAS-egr,tub-Gal80^{TS}/+	18°C	30°C, 40 h	5d-6d-7d-8d

Figure S4

S4A-D	+/+;rn-Gal4,UAS-egr,tub-Gal80^{TS}/+	18°C	30°C, 40 h	7d
S4A-D	UAS-domeΔCYT/+;rn-Gal4,UAS-egr,tub-Gal80^{TS}/+	18°C	30°C, 40 h	7d
S4A-D	UAS-domeRNAi/+;rn-Gal4,UAS-egr,tub-Gal80TS/+	18°C	30°C, 40 h	7d
S4C-D	UAS-Socs36E/+;rn-Gal4,UAS-egr,tub-Gal80TS/+	18°C	30°C, 40 h	7d

Figure S5

S5A	+/+;rn-Gal4/+	21°C		
S5A	UAS-domeRNAi/+;rn-Gal4/+	21°C		
S5A	+/+;rn-Gal4/UAS-hopRNAi	21°C		
S5A	+/+;rn-Gal4/UAS-STAT92ERNAi	21°C		
S5B	+/+;rn-Gal4,tub-Gal80^{TS}/+	18°C	30°C, 40 h	7d
S5B	UAS-domeRNAi/+;rn-Gal4,tub-Gal80TS/+	18°C	30°C, 40 h	7d
S5B	+/+;rn-Gal4,tub-Gal80TS/UAS-hopRNAi	18°C	30°C, 40 h	7d
S5B	+/+;rn-Gal4,tub-Gal80TS/UAS-STAT92ERNAi	18°C	30°C, 40 h	7d

Figure S6

S6A,S6E, S6J	+/+;rn-Gal4,UAS-egr,tub-Gal80^{TS}/+	18°C	30°C, 40 h	7d
S6B	+/+;rn-Gal4,UAS-egr,tub-Gal80^{TS}/Df(3L)H99	18°C	30°C, 40 h	7d
S6C	hsflp [122]/+;+/+, ubi-GFP; act>y[+]>GAL4,UAS-GFP/+	21°C	37°C, 15 min	
S6D	hsflp [122]/+;UAS-Hop^{TumL}/+; act>y[+]>GAL4,UAS-GFP/+	21°C	37°C, 15 min	
S6H-H"	ptc-Gal4,tub-Gal80TS/+;UAS-Zfh2RNAi/+	18°C	30°C, 40 h	7d
S6F	+/+;rn-Gal4,UAS-egr,tub-Gal80^{TS}/FRT82-Stat92E^{85C9}	18°C	30°C, 40 h	7d
S6I	w118	18°C	30°C, 40 h	7d
S6K	UAS-Zfh1/+;rn-Gal4,UAS-egr,tub-Gal80^{TS}/+	18°C	30°C, 40 h	7d
S6L	UAS-p35/+;rn-Gal4,UAS-egr,tub-Gal80^{TS}/+	18°C	30°C, 40 h	7d

Figure S7

S7A	+/+;rn-Gal4,UAS-egr,tub-Gal80^{TS}/+	18°C	30°C, 40 h	7d
S7A	UAS-upd1/+;+/+;rn-Gal4,UAS-egr,tub-Gal80^{TS}/+	18°C	30°C, 40 h	7d
S7A	UAS-upd2/+;+/+;rn-Gal4,UAS-egr,tub-Gal80^{TS}/+	18°C	30°C, 40 h	7d
S7A	UAS-domeΔCYT/+;rn-Gal4,UAS-egr,tub-Gal80^{TS}/+	18°C	30°C, 40 h	7d
S7A	UAS-domeRNAi/+;rn-Gal4,UAS-egr,tub-Gal80TS/+	18°C	30°C, 40 h	7d
S7A	+/+;rn-Gal4,UAS-egr,tub-Gal80TS/UAS-hopRNAi	18°C	30°C, 40 h	7d
S7A	+/+;rn-Gal4,UAS-egr,tub-Gal80TS/UAS-STAT92ERNAi	18°C	30°C, 40 h	7d
S7A	+/+;rn-Gal4,UAS-egr,tub-Gal80TS/UAS-Socs36E	18°C	30°C, 40 h	7d
S7A	+/+;rn-Gal4,UAS-egr,tub-Gal80TS/UAS-Zfh2RNAi	18°C	30°C, 40 h	7d
S7A	+/+;rn-Gal4,UAS-egr,tub-Gal80^{TS}/+;Zfh2[EAB]	18°C	30°C, 40 h	7d
S7A	dome^{G0441}/+;+/+;rn-Gal4,UAS-egr,tub-Gal80^{TS}/+	18°C	30°C, 40 h	7d + 6h
S7A	hop^{34}/+;+/+;rn-Gal4,UAS-egr,tub-Gal80^{TS}/+	18°C	30°C, 40 h	7d + 6h
S7A	+/+;rn-Gal4,UAS-egr,tub-Gal80^{TS}/FRT82-Stat92E^{85C9}	18°C	30°C, 40 h	7d + 12h
S7A	+/+;rn-Gal4,tub-Gal80^{TS}/+	18°C	30°C, 40 h	7d
S7A	UAS-upd1/+;+/+;rn-Gal4,tub-Gal80^{TS}/+	18°C	30°C, 40 h	7d

S7A	*UAS-upd2/+;+/+;rn-Gal4,tub-Gal80^{TS}/+*	18°C	30°C, 40 h	7d
S7A	*UAS-domeΔCYT/+;rn-Gal4,tub-Gal80^{TS}/+*	18°C	30°C, 40 h	7d
S7A	*UAS-domeRNAi/+;rn-Gal4,tub-Gal80TS/+*	18°C	30°C, 40 h	7d
S7A	*+/+;rn-Gal4,tub-Gal80TS/UAS-hopRNAi*	18°C	30°C, 40 h	7d
S7A	*+/+;rn-Gal4,tub-Gal80TS/UAS-STAT92ERNAi*	18°C	30°C, 40 h	7d
S7A	*+/+;rn-Gal4,tub-Gal80TS/UAS-Socs36E*	18°C	30°C, 40 h	7d
S7A	*+/+;rn-Gal4,tub-Gal80TS/UAS-Zfh2RNAi*	18°C	30°C, 40 h	7d
S7A	*+/+;rn-Gal4,tub-Gal80^{TS}/+;Zfh2[EAB]*	18°C	30°C, 40 h	7d
S7A	*dome^{G0441}/+;+/+;rn-Gal4,tub-Gal80^{TS}/+*	18°C	30°C, 40 h	7d + 6h
S7A	*hop^{34}/+;+/+;rn-Gal4,tub-Gal80^{TS}/+*	18°C	30°C, 40 h	7d + 6h
S7A	*+/+;rn-Gal4,tub-Gal80^{TS}/FRT82-Stat92E^{85C9}*	18°C	30°C, 40 h	7d + 12h
S7B	*UAS-dcr2/+;en-Gal4,UAS-GFP/+;+/+*	25°C		
S7B	*UAS-dcr2/+;en-Gal4,UAS-GFP/+;UAS-hopRNAi/+*	25°C		
S7C	*+/+;rn-Gal4,UAS-egr,tub-Gal80^{TS}/dllp8-GFP*	18°C	30°C, 40 h	7d
S7D	*UAS-domeΔCYT/+;rn-Gal4,UAS-egr,tub-Gal80^{TS}/dllp8-GFP*	18°C	30°C, 40 h	7d
S7E	*UAS-domeRNAi/+;rn-Gal4,UAS-egr,tub-Gal80TS/dllp8-GFP*	18°C	30°C, 40 h	7d
S7F	*MS1096-Gal4/+;+/+;+/+*	25°C		
S7F	*MS1096-Gal4/UAS-upd1;+/+;+/+*	25°C		
S7F	*MS1096-Gal4/UAS-upd2;+/+;+/+*	25°C		

Table S2. Primers used for real--time qPCR analysis.

	Gene	Seq.	5' - 3'
	upd1	Fwr	TCGATATGCGCTTTGTGAAG
	upd1	Rev	TGCTGCTGCTGTAGCAACTT
	upd2	Fwr	TACAAGTTCCTGCCGAACATGAC
	upd2	Rev	ACAAGTGGCGATTCTATAAGGGAAAC
	upd3	Fwr	CCCCTGAAGCACCTACAGAA
	upd3	Rev	AGGATCCTTTGGCGTTTCTT
	dome	Fwr	ATCGCAAAGAATACAAAATAAATTACAAAC
	dome	Rev	TCTGGAATCTGGAAACTAGAAACCAC
	hop	Fwr	TATCCGGATTTGGTATGGATGAATG
	hop	Rev	TTTTTAAAACAACACAAGCCAGACC
	STAT92E	Fwr	CATGCAATGTGCTCTTCACA
	STAT92E	Rev	AGATCTGGACGTGCTTTGCT
	hid	Fwr	ACAACTTCTTCCGGCAGCAG
	hid	Rev	GAAGGGAGGGGAATGGTGTG
	rpr	Fwr	CGACTCTGTTGCGGGAGG
	rpr	Rev	GGCTTGCGATATTTGCCGGA
	grim	Fwr	GTCGGAGTTTGGATGCTGGG
	girm	Rev	AGTCACGTCGTCCTCATCGT
	zfh1	Fwr	ACGAGCAGAGCAACATGAGC
	zfh1	Rev	CGGCGACATTTTGTTAGCAC
	zfh2	Fwr	TGCACACACAACAGATGCGT
	zfh2	Rev	GCACAGCTGACAAAGGAGCA
	kay	Fwr	CGAATAGCAAGAATCAGCTGGAGTA
	kay	Rev	CTGTCGTTGCTGTTGTGGTTGT
Housekeeping	*Act5C*	Fwr	GGCGCAGAGCAAGCGTGGTA
Housekeeping	*Act5C*	Rev	GGGTGCCACACGCAGCTCAT
Housekeeping	*αTub84B*	Fwr	TGGGCCCGTCTGGACCACAA
Housekeeping	*αTub84B*	Rev	TCGCCGTCACCGGAGTCCAT
Housekeeping	*RpL32*	Fwr	AAGCGGCGACGCACTCTGTT
Housekeeping	*RpL32*	Rev	GCCCAGCATACAGGCCCAAG
Housekeeping	*RpL13A*	Fwr	AGCTGAACCTCTCGGGACAC
Housekeeping	*RpL13A*	Rev	TGCCTCGGACTGCCTTGTAG

Discussion

With this work, we addressed the long-standing question of how JNK signaling activity balances two opposing effects – damage-induced cell death and compensatory proliferation – in the context of tissue stress responses.

The main part of my PhD project focused in particular on the cells located directly at the wound, thus experiencing the highest levels of JNK activity. I described an unexpected transient arrest of the cell cycle in G2, that is JNK-dependent and correlates with the levels of activity of the pathway. My functional studies highlighted a pro-survival role of G2 stalling, prompting us to propose a model whereby cell cycle progression through mitosis might represent a key switch in the interpretation of JNK signaling, from pro-survival to pro-apoptotic. Additionally, I also found evidence that G2-stalled cells upregulate paracrine signaling and cell-protective functions, which are reminiscent of senescent cells.

In a second paper, investigating the JNK-dependent induction of JAK/STAT in cells at the wound vicinity, we showed that JAK/STAT does not directly promote compensatory proliferation, as predicted by the current models, but rather promotes cell survival through its target effector *Zfh2*. This transcriptional repressor is predicted to bind the pro-apoptotic gene *hid* and the JNK effector *kay*, thus providing a mechanism for a JNK-dependent negative feedback loop. By limiting expansion of JNK signaling and preventing apoptosis in JNK-signaling cells located at the wound vicinity, we propose that JAK/STAT signaling allows the surviving cells to execute JNK-dependent compensatory responses such as regenerative proliferation and induction of developmental delay.

Together, this work has helped to clarify two mechanisms whereby the apoptotic and proliferative outputs of JNK signaling are balanced in domains proximal to the wound site (via G2 stalling) and in more distal areas (via JAK/STAT) (Figure 3).
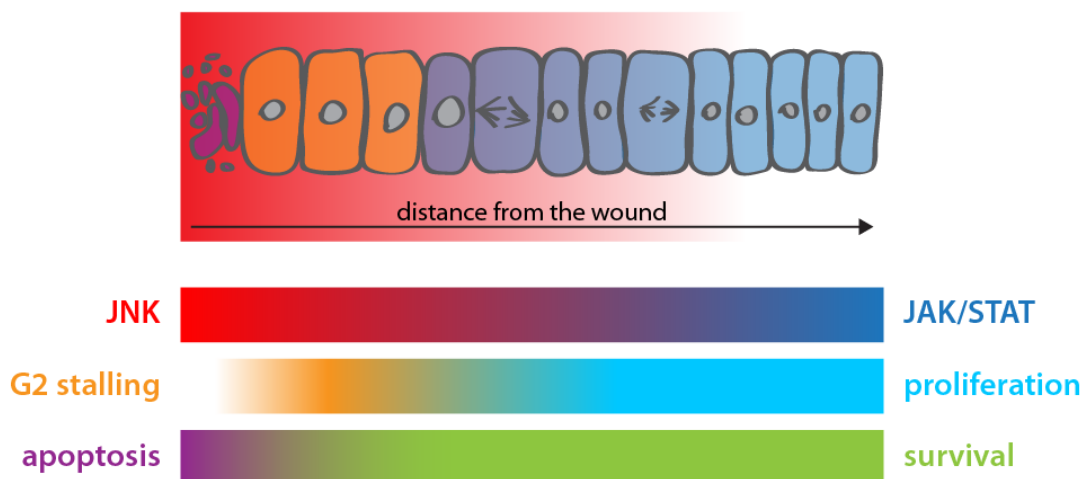
Figure 3: Spatial gradients of G2 stalling and JAK/STAT signaling, mediating survival of JNK–signaling cells.

At the wound site (left) the JNK signaling activity (red) is high and cells die by apoptosis (violet). JNK also induces a dose–dependent G2 stalling (orange), which has a pro–survival effect (green) in cells close to the wound. Also JAK/STAT (blue) mediates cell survival, by suppressing apoptosis and JNK gradient expansion, in more distal regions. Together, G2 stalling and JAK/STAT signaling promote survival of JNK–signaling cells, thereby facilitating the execution of JNK–dependent compensatory responses and regenerative processes.

6 Mechanism of cell cycle arrest

6.1 Stg/Cdc25 mediates G2 stalling

With the present work we identified the phosphatase Stg/Cdc25 as a central mediator of the JNK-dependent G2 stalling. Stg is a crucial cell cycle regulator at the G2/M transition, responsible of removing inhibitory phosphates on the activation loop of the mitotic cyclin-dependent kinase Cdk1 (Edgar and O'Farrell, 1989). We provided evidence that *stg* is downregulated in JNK-signaling cells upon *egr*-expression, and *stg*-overexpression is sufficient to prevent G2 stalling.

Our analysis of the molecular mechanism of cell cycle regulation responsible of the G2 stalling, however, was limited by the lack of good biochemical or genetic tools to faithfully detect endogenous levels of Stg protein in imaginal discs. We verified that the only antibody available is not sensitive enough in this tissue, whereas an in-depth characterization of the reporter line used (a GFP insertion in an intronic region of *stg*) led us conclude that this construct can only be used as a readout for transcriptional regulation, but is not producing a

functional tagged protein, therefore preventing us to gain further insight into the protein levels and distribution. Thus, in the absence of better tools to detect Stg protein, the mechanistic details underlying the G2 stalling remain to be clarified. Interestingly, however, we also found that *tribbles* (*trbl*), a mediator of the proteasomal degradation of Stg (Mata et al., 2000), is highly upregulated upon injury in a JNK-dependent manner. Strikingly, *trbl* was also implicated in the G2 quiescence of *Drosophila* Neuronal Stem Cells, through Stg degradation (Otsuki and Brand, 2018). Combined, the data presented here suggests that the JNK-mediated cell cycle regulation could occur at multiple levels, including *stg* transcriptional downregulation and protein degradation, thus providing a robust mechanism to control G2 stalling. Importantly, Stg represents a downstream bottleneck in this redundant system and its overexpression is sufficient to bypass G2 stalling.

Additional studies would be needed in order to investigate whether JNK is regulating Stg levels indirectly, for example by targeting upstream regulators such as Trbl, or also directly (either via AP-1-mediated transcription or direct phosphorylation). Importantly, in support of the latter hypothesis, studies in mammalian systems showed that JNK can directly phosphorylate the Stg homologs Cdc25B on Ser-101 upon stress, causing its proteasomal degradation (Uchida et al., 2009), and Cdc25C on Ser-168 in unperturbed G2 phase, negatively regulating its phosphatase activity (Goss et al., 2003; Gutierrez et al., 2010). While a preliminary analysis suggests that the regions containing these residues are not easy to align unequivocally, a more detailed bioinformatic study might further clarify whether this regulation is present also in *Drosophila* or has been acquired later during evolution.

Concerning the capacity of JNK to directly regulate the cell cycle, there is also evidence in *Drosophila* that the JNK effector Fos binds to AP-1 sites in the *cyclin B* (*CycB*) promoter, increasing its expression (Hyun et al., 2006). This result, implicating a positive role for JNK in promoting G2/M transition, further supports our model of transient G2 stalling, suggesting that JNK could transiently arrest the cell cycle in G2 by regulating Stg, but also prepare the cell to readily transition into mitosis once the stress is resolved by promoting *CycB* transcription.

6.2 G2 stalling as a response to JNK signaling

When investigating upstream regulators of G2 stalling, we initially focused our attention on DNA damage, given its role in triggering cell cycle checkpoints (Barnum and O'Connell, 2014). Among others, one of the known sources of DNA damage is oxidative stress (Cooke et al., 2003) and several reports highlighted the occurrence of reactive oxidative species upon wounding or cell ablation (Brock et al., 2017; Fogarty et al., 2016; Santabarbara-Ruiz et al., 2015). However, we did not find any evidence of DNA damage in G2-stalled cells, nor of

requirement of DNA damage response factors *chk1* (*grp*) or *ATR* (*mei-41*) for G2 stalling. Importantly, this result aligns with previous work on *hid+P35* undead cells, which upregulate JNK and arrest in G2 independently of DNA damage (Wells et al., 2006).

Therefore, we hypothesized that JNK-dependent G2 stalling does not necessarily require a stress stimulus such as DNA damage, but rather it could be directly linked to the signaling activity of the JNK pathway itself: independently on the upstream trigger, JNK signaling can lead to G2 stalling. Interestingly, in support of this idea, we also found one example of developmental JNK activity in the wing disc peripodium, which is linked to an increased fraction of G2 cells, suggesting that JNK signaling can promote G2 stalling also in the absence of cellular stress.

7 Temporal dynamics of JNK–dependent G2 stalling

7.1 G2 stalling is reversible

The concept of G2 stalling implies a dynamic definition, describing the cell cycle progression of a given cell over a period of time. Does it slow down or arrest? And is it reversible? While a snapshot on a single time point can provide information on the relative cell cycle distribution of a cell population, the possibility to follow the same cells with live imaging during recovery would allow a much deeper understanding of the dynamics of the process. Despite the recent technology advancements, for example in the imaging of wing discs *in vivo* (Heemskerk et al., 2014) or in *ex vivo* disc culturing and imaging (Dye et al., 2017), these approaches remain extremely challenging and are only suited for relatively short time scales. We overcame this limitation by combining cell cycle reporter analysis at multiple time points with genetic lineage tracing, demonstrating not only that G2 stalling declines in parallel with the decline in JNK-positive cells, but also that G2 stalling is transient and cells can re-enter the cell cycle. In particular, 48 h after *egr* expression has ceased, no G2 stalling is observed at the wound site, but the G-TRACE population (deriving from genetic labeling of *egr* expressing cells, that were stalled in G2 at 0 h of recovery) has expanded in number and constitutes a large portion of the wing pouch. This implies that at least some, if not all, of the previously G2-stalled cells, were healthy enough to survive, re-enter the cell cycle and proliferate to contribute to tissue regeneration.

We speculate that the same process happens in shorter time scales upon acute surgical injury, and that this could be important for stressed cells to survive and thus contribute to repopulating the tissue. Indeed, when preventing G2 stalling in surgically injured discs, we observe increased apoptosis (see also section 8.1).

7.2   The time scale of G2 stalling depends on JNK

By analyzing different models of tissue stress (surgical injury, genetic cell ablation, oncogenic genetic lesions), we provide evidence that JNK-dependent G2 stalling occurs on transient, prolonged and chronic time scales. A detailed and quantitative description of the temporal evolution of the JNK reporter TRE-RFP highlighted that JNK response is transient upon surgical injury, prolonged and extremely elevated upon egr expression, and lower but chronically increasing during tumor development. Strikingly, JNK-positive populations have an increased fraction of G2 cells in all of these conditions, as shown by flow cytometry and confirmed by FUCCI reporter assays. Moreover, we showed that not only G2 stalling correlates with the levels and temporal dynamics of JNK activity, but JNK is also necessary and sufficient to induce G2 stalling.

Collectively, the data presented support a model where any type of JNK signal, from transient to chronic, induces a stalling of the cell cycle in G2. We propose that JNK levels determine the fraction of G2-stalled cells, as suggested by the correlations measured by flow cytometry, and the length of the JNK stimulation regulates the duration of G2 stalling (Figure 4).
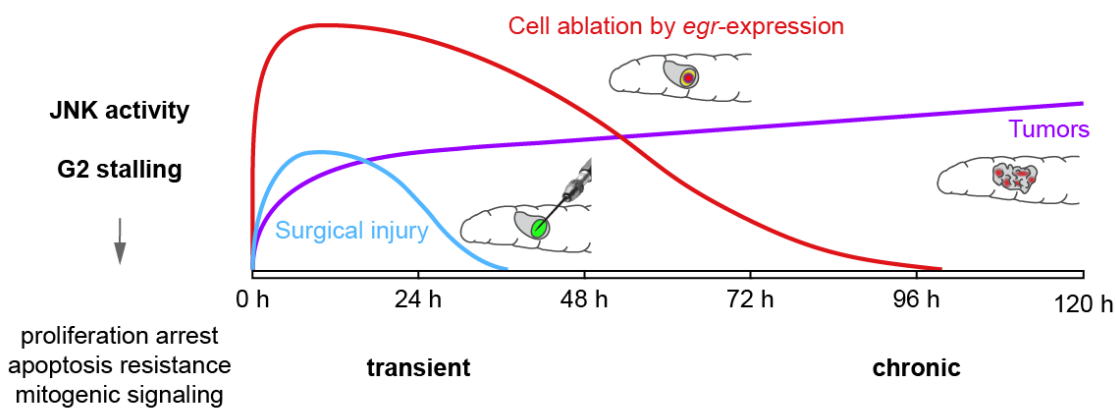

Figure 4: Dose- and time-dependent effects of JNK activity and G2 stalling.

Different models of tissue stress (surgical injury, cell ablation by *egr*-expression, or oncogenic genetic lesions) induce different levels and temporal dynamics of JNK activity, which can be transient, prolonged or chronic. Independently on the time length, JNK activation induces a reversible G2 stalling, which leads to proliferation arrest, resistance to apoptosis and paracrine mitogenic signaling. While we predict these effects occur for any length of G2 stalling, each is revealed only under certain circumstances. Together, they are essential for tissue repair and regeneration under physiological conditions, but become detrimental under extreme and potentially aberrant signaling conditions. Figure modified with permission from (Cosolo et al., 2019).

8 Different experimental models reveal distinct functions of G2 stalling

Interestingly, suppressing G2 stalling by *stg* expression revealed different aspects of the function of G2 stalling during tissue stress responses: apoptosis resistance, arrest of cell-autonomous proliferation and promotion of non-autonomous overgrowth. While each of these phenotypes becomes apparent in the tissue only under specific genetic conditions and timescales, we propose that they all occur in any condition, but the overall outcome depends on the duration of the stress and consequently of G2 stalling. In particular, we hypothesize that, during physiological tissue stress responses (*i.e.* upon surgical wounding), a transient cell cycle arrest protects a cell from JNK-induced apoptosis, allowing it to remain integrated in the tissue and contribute to tissue integrity. Additionally, a cell can perform JNK-dependent secretion of paracrine signals (Pastor-Pareja et al., 2008; Ryoo et al., 2004; Santabarbara-Ruiz et al., 2015), which induce regenerative growth to compensate for the tissue lost. Conversely, chronic G2 stalling is detrimental because it keeps chronically stressed cells alive and sustains persistent mitogenic signaling leading to non-autonomous overgrowth.

8.1 G2 stalling protects from apoptosis

Our functional experiments suggest that one important role of the G2 stalling is to promote the survival of cells at the wound site, which experience high JNK signaling levels. This is revealed by increased apoptosis in injured discs where G2 stalling is suppressed by targeted *stg* overexpression. Additionally, we could also show that cells which previously activated the executioner caspases, can survive and are integrated in the regenerated epithelium. Although we could not directly test whether these surviving cells are the same which transiently stalled in G2, the prediction would be that this is the case, given their proximity to the wound. Together, these results suggest that G2-stalled cells are protected from apoptosis and contribute to the regenerated tissue.

How is apoptosis resistance mediated in G2 stalled cells? The JNK-dependent activation of *yki*, which in turn upregulates the apoptosis inhibitor *Diap1*, could provide a possible mechanism (Sun and Irvine, 2011, 2013). However, we also observe concomitant JNK-dependent expression of pro-apoptotic *hid* (Shlevkov and Morata, 2012). Therefore, we speculate that JNK-positive cells at the wound site, experiencing both pro- and anti-apoptotic signals, require additional cues to shift this balance and adopt one fate rather than the other.

One such signal could be represented by the cell cycle regulation, inducing G2 stalling to promote cell survival. Indeed, our experiments support a model whereby cells in G1 are more likely to undergo apoptosis than cells in G2, as shown by increased caspase staining of

Discussion

JNK-activated cells in G1. Interestingly, it has already been suggested that G2-arrested follicle cells, either developmentally or experimentally induced, are more resistant to apoptosis when exposed to genotoxic stress (Qi and Calvi, 2016). The underlying molecular mechanism which could render G2 phase more protected from apoptosis compared to other cell cycle phases, however, remains to be explored. Moreover, further studies will also need to address whether G2 stalling increases the resistance to apoptotic signals, or actively alleviates the cellular stress.

8.2   The function of stalling the cell cycle progression

While promoting cell survival upon surgical injury, prolonged G2 stalling upon *egr* expression interferes with cell-autonomous compensatory proliferation. One potential function of stalling the cell cycle progression could be to allow time to repair cellular damage. Although our data on DNA damage response seem to rule out this hypothesis, other stress response pathways remain to be investigated.

Additionally, it is tempting to speculate that the alterations in the mechanical environment arising from the morphogenetic events required for wound healing, such as remodeling of cell-cell contacts and cell migration, are interfering with the cytoskeletal rearrangements occurring during cell cycle progression and mitosis, or vice versa (Cadart et al., 2014). Indeed, skin wound healing experiments in mouse models have shown that cell proliferation and cell migration, although interconnected and partially co-localizing, distribute in spatial counter-gradients, with cells at the migratory front that are spatially distinct from those actively proliferating in a more distal ring around the wound (Park et al., 2017).

8.3   G2 stalling promotes non-autonomous growth

Another function of G2 stalling, revealed by our *stg* overexpression data, is to promote non-autonomous growth. This is evident from experiments on tumors, experiencing chronic JNK signaling, where differences in tissue volume and mitotic counts can be consistently quantified. However, we speculate that transiently G2-stalled cells could similarly support regenerative growth upon surgical injury, although such transient effect would be more difficult to detect. Moreover, in physiological wound healing conditions, the extent of growth would be limited, since it would only compensate for the tissue lost, whereas in tumor models we observe extensive and aberrant tissue overgrowth.

These results raise the question on why specifically G2-stalled cells would have the peculiar ability to promote non-autonomous growth and what would be the mechanism. While we demonstrated that it could be prevented by forcing cell cycle progression via *stg* overexpression, we did not test whether a cell cycle arrest in G1, for example, would produce a

similar growth phenotype. This could be done by co-expressing *stg* to promote G2/M transition and *Cdk2* RNAi to prevent G1/S. If this were the case, it would indicate that transiently arrested cells in gap phases are more prone to produce and secrete paracrine signaling molecules, compared to cells that are forced to cycle under (chronic) stress conditions.

Additionally, it would be important to clarify whether JNK, apart from affecting cell cycle progression, is also altered by the cell cycle itself, in a feedback loop. If G2-stalled cells have higher JNK compared to cells forced to proliferate by *stg*, the non-autonomous growth phenotype could simply be a direct effect of the increased JNK activity. To partially address this question, we measured the levels of the TRE-RFP reporter and verified that, at least in the *egr* expression context, JNK levels are not significantly affected by *stg* co-expression.

But what are the mitogenic signals produced by G2-stalled tumor cells? Two major candidates are represented by the morphogens Wg and Dpp, which are known to have mitogenic activity in wing discs (Burke and Basler, 1996; Giraldez and Cohen, 2003): in the context of 'undead' cells, obtained by inducing apoptosis and simultaneously blocking its execution by expressing the caspase inhibitor *P35*, the induction of *wg* and *dpp* leads to tissue overgrowth (Huh et al., 2004; Perez-Garijo et al., 2004; Perez-Garijo et al., 2009; Ryoo et al., 2004). Genetic evidence suggests that this phenotype is dependent on JNK, therefore it would be interesting to test whether such signals are also produced in tumor models and in transient conditions.

Importantly, the temporal dynamics and intensity of JNK activity could play a role, since *wg* and *dpp* are not required for compensatory proliferation in more transient conditions such as the 'genuine' apoptosis models (*i.e.* without *P35*) (Perez-Garijo et al., 2009). Conversely, both *wg* and *dpp* are upregulated at the wound site upon *egr* expression (Smith-Bolton et al., 2009). Our unpublished analysis of the expression patterns revealed, however, that while the pattern of Wg correlates with G2 stalled cells, the increase in *dpp* transcription is restricted to the anterior compartment, where it is normally expressed. This indicates that G2 stalling is not sufficient to induce Dpp signaling, although it does not exclude that G2 cells could promote it, in domains that already have the ability to do so. Further experiments are needed in order to clarify whether these correlations depend on G2 stalling, or maybe on JNK.

9 Cell cycle responses to tissue stress

9.1 G2 arrest and senescence

Interestingly, we found that G2-stalled cells share many similarities with senescent cells in vertebrates. Besides the cell cycle arrest and apoptosis resistance, they also show

Discussion

increased cell size, secretion of signaling molecules and enzymes degrading the extracellular matrix, upregulation of stress response pathways such as autophagy, UPR, and antioxidant response, which are all markers of senescence (Hernandez-Segura et al., 2018).

Senescent cells have a dual-sided role in vertebrates. They are associated with several beneficial functions, including positive regulation of tissue remodeling and repair, both during development and adulthood, and tumor suppression owed to the proliferation arrest of abnormal cells. However, excessive accumulation of senescent cells in tissues during ageing is also negatively affecting the tissue's regenerative capacity and is associated with pro-inflammatory signaling and a pro-tumorigenic function (Czarkwiani and Yun, 2018; He and Sharpless, 2017). Intriguingly, also the phenotypes associated with G2 stalling can potentially be linked to both positive and negative effects for tissue homeostasis: we speculate that, while cell survival and mitogenic signaling could be beneficial for transient tissue stress responses, their prolonged effect on the tissue could be detrimental in chronic conditions, promoting aberrant tissue overgrowth.

Despite these apparent similarities, which may suggest a possible evolutionary or functional link between G2 stalling and senescence, it is important to underline that there are also some crucial differences. For example, senescence is often triggered by activation of a chronic DNA damage response, which we failed to detect in G2-stalled cells. Additionally, while the G2 stalling is transient and reversible, the cell cycle arrest of senescent cells is irreversible and occurs in G0 – although there are also reports of senescent cells in G0 with tetraploid DNA content, suggesting that in certain contexts senescence might also originate from a cell cycle arrest in G2, followed by mitotic skipping (Dikovskaya et al., 2015; Gire and Dulic, 2015; Restall et al., 2015). Therefore, additional studies are needed to further investigate whether there is an evolutionary relevant link between G2 stalling in *Drosophila* and vertebrate senescence, and whether a cell cycle arrest functionally similar to senescence can also occur in G2, rather than G0.

Interestingly, a cell cycle arrest in G2 was recently reported to occur in *Drosophila* Neuronal Stem Cells (NSCs), which were previously thought to exit the cell cycle in G0 (Otsuki and Brand, 2018). NSCs are known to become quiescent during late embryonic stages, transiently arresting their cell cycle, before restarting to proliferate in post-embryonic stages and give rise to neurons and glia. Otsuki and Brand (2018) found surprisingly that only 25% of quiescent NSCs are in G0, whereas the vast majority is in G2. Quiescence in G2 is induced by Trbl-mediated degradation of Stg and is maintained by Trbl-mediated inhibition of Akt. In this heterogeneous population of quiescent NSCs, those in G2 are reactivating faster than those in G0. The authors speculate that the function of G2 quiescence might be related to the possibility to perform homologous recombination-mediated repair of DNA after damage.

9.2 Endocycles and other cell cycle responses to tissue damage

It is interesting to note how other *Drosophila* organs, when subject to tissue damage, are repaired with different strategies in terms of cell cycle regulation. In the hindgut, for example, different cell cycle programs can be used to allow for efficient regeneration upon tissue damage, depending on the developmental stage when the damage occurs. Proliferating larval pyloric cells respond to acute damage by inducing mitosis, while post-mitotic adult pyloric cells perform endocycles (ploidy-increasing G/S cycles lacking mitosis) to repair the tissue (Cohen et al., 2018). Additionally, endocycles have also been implicated in the regeneration of adult Drosophila epidermis, accompanied by cell fusion and syncytium formation (Losick et al., 2013).

While all of these mechanisms regulating the cell cycle have the effect to increase tissue mass and efficiently cover the wound, either by increasing the cell number or by increasing cell size, our unpublished data in wing imaginal discs suggest that the *egr*-induced JNK signaling cells at the wound site do not undergo endoreplication. Of note, we do observe a moderate increase in size of the G2-stalled cells when compared to the size of normal proliferating cells in G2. Whether this provides an advantage to the epithelium to allow for successful wound healing, however, still remains to be tested.

10 Gradients of tissue damage responses

We showed that JNK-dependent G2 stalling occurs in cells immediately at the wound site, experiencing high levels of JNK activity. Given the protective role of G2 stalling against JNK-dependent apoptosis, we suggest that cell cycle stalling could help balancing the pro-apoptotic and pro-proliferative outputs of JNK signaling, preventing excessive cell death in cells close to the wound.

Another mechanism that protects from JNK-dependent apoptosis is the activation of JAK/STAT pathway, via JNK-dependent secretion of Upd ligands. The peak of JAK/STAT activity is shifted towards domains immediately more distal from the wound site, where no G2 stalling is observed (Figure 3). We showed that JAK/STAT limits the spatial propagation of JNK, promotes survival of JNK-signaling cells and execution of JNK-dependent compensatory functions in cells not directly at the wound site (Figure 5).

Discussion
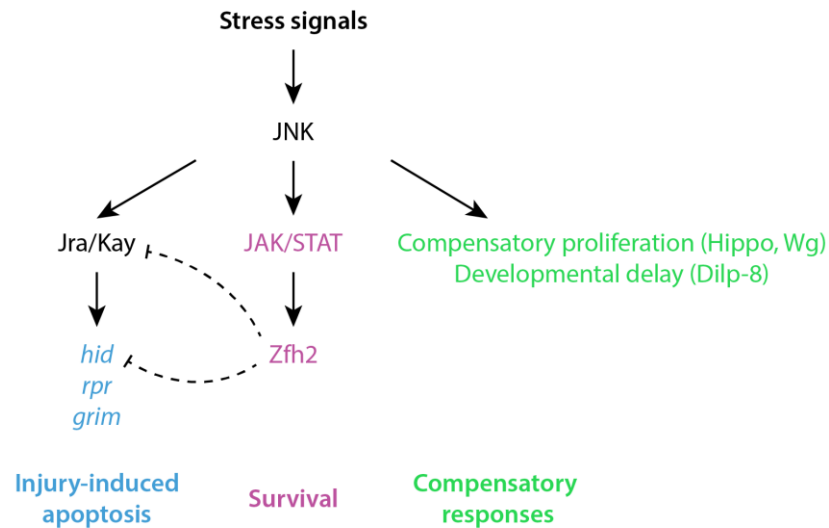
Figure 5: JAK/STAT signaling mediates survival and JNK-dependent compensatory responses

Upon cell ablation, stress-induced JNK signaling leads to JAK/STAT activation in cells not immediately at the wound. This promotes cell survival through *Zfh2*, a transcriptional repressor predicted to bind the pro-apoptotic gene *hid* and the JNK effector *kay*, thus providing a mechanism for a JNK-dependent negative feedback loop. By preventing apoptosis in JNK-signaling cells located in the wound vicinity, we propose that JAK/STAT indirectly allows the surviving cells to execute JNK-dependent compensatory responses such as regenerative proliferation and induction of developmental delay.

10.1   JNK and JAK/STAT form spatial counter-gradients

When analyzing the spatial distribution of JAK/STAT activity upon cell ablation, it is interesting to note that it peaks in the wound vicinity, in an area where the intensity of JNK signaling gradually declines (Figure 3). Therefore, while JNK activity self-propagates in the tissue by secretion of Egr and generation of ROS (see section 2.2), it also induces the non-autonomous activation of JAK/STAT by promoting the secretion of Upd ligands, which in turn limits the spatial propagation of JNK. This results in an anti-correlation of JNK and JAK/STAT signaling gradients.

We propose a model whereby in a cell located in intermediate position where both pathways are active, JAK/STAT suppresses JNK-dependent apoptosis, indirectly allowing for the execution of JNK-dependent compensatory responses. Of note, a recent paper confirms our observations, as apoptosis appeared to be increased upon impairment of JAK/STAT signaling in JNK-activating cells, thus supporting a pro-survival function of JAK/STAT (Ahmed-de-Prado et al., 2018).

On the other hand, in cells closer to the wound where there is no JAK/STAT activity, G2 stalling helps to suppress excessive JNK-dependent apoptosis by promoting cell survival.

Further studies will elucidate whether there is any direct link between G2 stalling and JAK/STAT activity, as suggested by the fact that both perform a pro-survival function, in adjacent but distinct domains.

10.2   Other examples of gradients

After our original publication, strikingly similar observations on the interplay between JNK and JAK/STAT pathways during wound healing were also reported to occur in the larval epidermis (Lee et al., 2017). Larval epidermal cells are highly polyploid and wounds in this tissue are repaired by JNK-dependent cell fusion, in order to close the epithelial gap and re-establish epidermal integrity (Wang et al., 2015). Lee et al. (2017) showed that the JAK/STAT ligands *upd2* and *upd3* are induced upon wounding and that JAK/STAT is required to suppress excessive cell fusion. Moreover, they describe mutually exclusive spatial gradients of activation of JNK and JAK/STAT pathways and provide genetic evidence that JNK is required to suppress JAK/STAT activation in the wound vicinity, thereby promoting efficient wound closure. Based on this antagonistic effect of JNK and JAK/STAT on cell fusion, the authors propose that epidermal cells sense the relative levels of the two pathways to determine whether or not to execute cell fusion during wound healing. The molecular mechanism responsible of how this is computed has yet to be elucidated.

These results further highlight that the interplay between JNK and JAK/STAT signaling in the context of wound healing responses is potentially a more general mechanism, not only important in larval imaginal discs, but at least in one other example of wound healing model. Given the established role of JNK signaling in tissue stress responses, ranging from development to adult stages, it is conceivable that similar signaling interactions could occur also in different contexts. Of note, the antagonistic interaction between JNK and JAK/STAT is not only acting on the decision between apoptosis and survival, but also on other processes related to tissue stress responses, such as cell fusion.

10.3   JAK/STAT is inhibited at the wound site

One question that remains still open concerns the mechanism of JAK/STAT activation upon cell ablation and in particular the reason why JAK/STAT is absent in cells at the wound site where JNK activation levels are high. Since the secretion of Upd is promoted by JNK, one would predict that JAK/STAT activity would be highest in those cells, however, this is not the case. This suggests the possible existence of a mechanism that inhibits JAK/STAT activation at the wound site. Such mechanism could also be essential to generate the asymmetry necessary

for gradient formation, as in its absence JAK/STAT could simply suppress JNK responses completely.

It is tempting to speculate that G2 stalling might have a role in suppressing JAK/STAT, however this idea has yet to be tested. In the context of larval epidermis wound healing, JNK itself is necessary to suppress JAK/STAT at the wound site (Lee et al., 2017). Another candidate mechanism could be the existence of a developmentally-regulated repressor. Indeed, during early larval development JAK/STAT is active throughout the wing imaginal disc, whereas at later stages it is excluded from the pouch by *nub* and *rn* (the same domain and developmental stage where *egr*-expression is induced for cell ablation). This restricts JAK/STAT activity to the surrounding area, where it plays a role for the development of the hinge (Ayala-Camargo et al., 2013). It is not surprising that forcing JAK/STAT activation through *upd1*, *upd2* or *Zfh2* overexpression in the pouch does not rescue the adult wing recovery after cell ablation, since ectopic activation of JAK/STAT in the pouch during development was reported to cause defects in the adult wing blade formation (Ayala-Camargo et al., 2013).

These developmental repressors suggest that JAK/STAT cannot be activated in the pouch during these developmental stages. However, there are also reports in the literature that show JAK/STAT upregulation in the pouch upon transient wounding (Pastor-Pareja et al., 2008) or in aberrant signaling conditions (Pinal et al., 2018; Worley et al., 2018). In addition, our knockdown experiments were based on the expression of RNAi constructs targeting components of the JAK/STAT pathway specifically in the pouch. The phenotypes observed suggest that at least part of the pouch activates JAK/STAT. Therefore, additional experiments are necessary in order to identify the mechanism of JAK/STAT activation with respect to the wound site.

References

Agnes, F., Suzanne, M., and Noselli, S. (1999). The Drosophila JNK pathway controls the morphogenesis of imaginal discs during metamorphosis. Development *126*, 5453-5462.

Ahmed-de-Prado, S., and Baonza, A. (2018). Drosophila as a Model System to Study Cell Signaling in Organ Regeneration. Biomed Res Int *2018*, 7359267.

Ahmed-de-Prado, S., Diaz-Garcia, S., and Baonza, A. (2018). JNK and JAK/STAT signalling are required for inducing loss of cell fate specification during imaginal wing discs regeneration in Drosophila melanogaster. Developmental biology *441*, 31-41.

Aldaz, S., and Escudero, L.M. (2010). Imaginal discs. Current biology : CB *20*, R429-431.

Ayala-Camargo, A., Anderson, A.M., Amoyel, M., Rodrigues, A.B., Flaherty, M.S., and Bach, E.A. (2013). JAK/STAT signaling is required for hinge growth and patterning in the Drosophila wing disc. Developmental biology *382*, 413-426.

Bach, E.A., Vincent, S., Zeidler, M.P., and Perrimon, N. (2003). A sensitized genetic screen to identify novel regulators and components of the Drosophila janus kinase/signal transducer and activator of transcription pathway. Genetics *165*, 1149-1166.

Baker, D.J., Wijshake, T., Tchkonia, T., LeBrasseur, N.K., Childs, B.G., van de Sluis, B., Kirkland, J.L., and van Deursen, J.M. (2011). Clearance of p16Ink4a-positive senescent cells delays ageing-associated disorders. Nature *479*, 232-236.

Ballesteros-Arias, L., Saavedra, V., and Morata, G. (2014). Cell competition may function either as tumour-suppressing or as tumour-stimulating factor in Drosophila. Oncogene *33*, 4377-4384.

Barnum, K.J., and O'Connell, M.J. (2014). Cell cycle regulation by checkpoints. Methods in molecular biology *1170*, 29-40.

Beira, J.V., and Paro, R. (2016). The legacy of Drosophila imaginal discs. Chromosoma *125*, 573-592.

Bergantinos, C., Corominas, M., and Serras, F. (2010a). Cell death-induced regeneration in wing imaginal discs requires JNK signalling. Development *137*, 1169-1179.

References

Bergantinos, C., Vilana, X., Corominas, M., and Serras, F. (2010b). Imaginal discs: Renaissance of a model for regenerative biology. BioEssays : news and reviews in molecular, cellular and developmental biology *32*, 207-217.

Bosch, M., Baguna, J., and Serras, F. (2008). Origin and proliferation of blastema cells during regeneration of Drosophila wing imaginal discs. The International journal of developmental biology *52*, 1043-1050.

Bosch, M., Serras, F., Martin-Blanco, E., and Baguna, J. (2005). JNK signaling pathway required for wound healing in regenerating Drosophila wing imaginal discs. Developmental biology *280*, 73-86.

Brand, A., Allen, L., Altman, M., Hlava, M., and Scott, J. (2015). Beyond authorship: Attribution, contribution, collaboration, and credit. Learn Publ *28*, 151-155.

Brock, A.R., Seto, M., and Smith-Bolton, R.K. (2017). Cap-n-Collar Promotes Tissue Regeneration by Regulating ROS and JNK Signaling in the Drosophila melanogaster Wing Imaginal Disc. Genetics *206*, 1505-1520.

Brumby, A.M., and Richardson, H.E. (2003). scribble mutants cooperate with oncogenic Ras or Notch to cause neoplastic overgrowth in Drosophila. The EMBO journal *22*, 5769-5779.

Bryant, P.J. (1971). Regeneration and duplication following operations in situ on the imaginal discs of Drosophila melanogaster. Developmental biology *26*, 637-651.

Burke, R., and Basler, K. (1996). Dpp receptors are autonomously required for cell proliferation in the entire developing Drosophila wing. Development *122*, 2261-2269.

Buttitta, L.A., Katzaroff, A.J., Perez, C.L., de la Cruz, A., and Edgar, B.A. (2007). A double-assurance mechanism controls cell cycle exit upon terminal differentiation in Drosophila. Developmental cell *12*, 631-643.

Cadart, C., Zlotek-Zlotkiewicz, E., Le Berre, M., Piel, M., and Matthews, H.K. (2014). Exploring the function of cell shape and size during mitosis. Developmental cell *29*, 159-169.

Classen, A.K., Bunker, B.D., Harvey, K.F., Vaccari, T., and Bilder, D. (2009). A tumor suppressor activity of Drosophila Polycomb genes mediated by JAK-STAT signaling. Nat Genet *41*, 1150-1155.

Cohen, E., Allen, S.R., Sawyer, J.K., and Fox, D.T. (2018). Fizzy-Related dictates A cell cycle switch during organ repair and tissue growth responses in the Drosophila hindgut. eLife *7*.

Colombani, J., Andersen, D.S., and Leopold, P. (2012). Secreted peptide Dilp8 coordinates Drosophila tissue growth with developmental timing. Science *336*, 582-585.

Cooke, M.S., Evans, M.D., Dizdaroglu, M., and Lunec, J. (2003). Oxidative DNA damage: mechanisms, mutation, and disease. FASEB J *17*, 1195-1214.

Coppe, J.P., Desprez, P.Y., Krtolica, A., and Campisi, J. (2010). The senescence-associated secretory phenotype: the dark side of tumor suppression. Annu Rev Pathol *5*, 99-118.

Cosolo, A., Jaiswal, J., Csordas, G., Grass, I., Uhlirova, M., and Classen, A.K. (2019). JNK-dependent cell cycle stalling in G2 promotes survival and senescence-like phenotypes in tissue stress. eLife *8*.

Czarkwiani, A., and Yun, M.H. (2018). Out with the old, in with the new: senescence in development. Current opinion in cell biology *55*, 74-80.

Davaapil, H., Brockes, J.P., and Yun, M.H. (2017). Conserved and novel functions of programmed cellular senescence during vertebrate development. Development *144*, 106-114.

Demaria, M., Ohtani, N., Youssef, S.A., Rodier, F., Toussaint, W., Mitchell, J.R., Laberge, R.M., Vijg, J., Van Steeg, H., Dolle, M.E., *et al*. (2014). An essential role for senescent cells in optimal wound healing through secretion of PDGF-AA. Developmental cell *31*, 722-733.

Diaz-Garcia, S., and Baonza, A. (2013). Pattern reorganization occurs independently of cell division during Drosophila wing disc regeneration in situ. Proceedings of the National Academy of Sciences of the United States of America *110*, 13032-13037.

Dikovskaya, D., Cole, J.J., Mason, S.M., Nixon, C., Karim, S.A., McGarry, L., Clark, W., Hewitt, R.N., Sammons, M.A., Zhu, J., *et al*. (2015). Mitotic Stress Is an Integral Part of the Oncogene-Induced Senescence Program that Promotes Multinucleation and Cell Cycle Arrest. Cell reports *12*, 1483-1496.

Dye, N.A., Popovic, M., Spannl, S., Etournay, R., Kainmuller, D., Ghosh, S., Myers, E.W., Julicher, F., and Eaton, S. (2017). Cell dynamics underlying oriented growth of the Drosophila wing imaginal disc. Development *144*, 4406-4421.

Edgar, B.A., and O'Farrell, P.H. (1989). Genetic control of cell division patterns in the Drosophila embryo. Cell *57*, 177-187.

Eming, S.A., Martin, P., and Tomic-Canic, M. (2014). Wound repair and regeneration: mechanisms, signaling, and translation. Sci Transl Med *6*, 265sr266.

Enomoto, M., Kizawa, D., Ohsawa, S., and Igaki, T. (2015). JNK signaling is converted from anti- to pro-tumor pathway by Ras-mediated switch of Warts activity. Developmental biology *403*, 162-171.

Fogarty, C.E., Diwanji, N., Lindblad, J.L., Tare, M., Amcheslavsky, A., Makhijani, K., Bruckner, K., Fan, Y., and Bergmann, A. (2016). Extracellular Reactive Oxygen Species Drive Apoptosis-Induced Proliferation via Drosophila Macrophages. Current biology : CB.

Fulda, S., Gorman, A.M., Hori, O., and Samali, A. (2010). Cellular stress responses: cell survival and cell death. Int J Cell Biol *2010*, 214074.

Garcia-Bellido, A., and Merriam, J.R. (1971). Parameters of the wing imaginal disc development of Drosophila melanogaster. Developmental biology *24*, 61-87.

References

Garelli, A., Gontijo, A.M., Miguela, V., Caparros, E., and Dominguez, M. (2012). Imaginal discs secrete insulin-like peptide 8 to mediate plasticity of growth and maturation. Science *336*, 579-582.

Gerlach, S.U., Eichenlaub, T., and Herranz, H. (2018). Yorkie and JNK Control Tumorigenesis in Drosophila Cells with Cytokinesis Failure. Cell reports *23*, 1491-1503.

Giraldez, A.J., and Cohen, S.M. (2003). Wingless and Notch signaling provide cell survival cues and control cell proliferation during wing development. Development *130*, 6533-6543.

Gire, V., and Dulic, V. (2015). Senescence from G2 arrest, revisited. Cell Cycle *14*, 297-304.

Glise, B., Bourbon, H., and Noselli, S. (1995). hemipterous encodes a novel Drosophila MAP kinase kinase, required for epithelial cell sheet movement. Cell *83*, 451-461.

Goss, V.L., Cross, J.V., Ma, K., Qian, Y., Mola, P.W., and Templeton, D.J. (2003). SAPK/JNK regulates cdc2/cyclin B kinase through phosphorylation and inhibition of cdc25c. Cell Signal *15*, 709-718.

Grusche, F.A., Degoutin, J.L., Richardson, H.E., and Harvey, K.F. (2011). The Salvador/Warts/Hippo pathway controls regenerative tissue growth in Drosophila melanogaster. Developmental biology *350*, 255-266.

Gutierrez, G.J., Tsuji, T., Cross, J.V., Davis, R.J., Templeton, D.J., Jiang, W., and Ronai, Z.A. (2010). JNK-mediated phosphorylation of Cdc25C regulates cell cycle entry and G(2)/M DNA damage checkpoint. The Journal of biological chemistry *285*, 14217-14228.

Hadorn, E., Bertani, G., and Gallera, J. (1949). Regulative capacity and field organization of male genital discs in Drosophila melanogaster. Wilhelm Roux Arch Entwickl Mech Org *144*, 31-70.

Hadorn, E., and Buck, D. (1962). On the differentiation of transplanted wing imaginal disc fragments of Drosophila melanogaster. Rev Suisse Zool *69*, 302-310.

Hariharan, I.K., and Serras, F. (2017). Imaginal disc regeneration takes flight. Current opinion in cell biology *48*, 10-16.

Harris, R.E., Setiawan, L., Saul, J., and Hariharan, I.K. (2016). Localized epigenetic silencing of a damage-activated WNT enhancer limits regeneration in mature Drosophila imaginal discs. eLife *5*.

Hay, B.A., and Guo, M. (2006). Caspase-dependent cell death in Drosophila. Annu Rev Cell Dev Biol *22*, 623-650.

He, S., and Sharpless, N.E. (2017). Senescence in Health and Disease. Cell *169*, 1000-1011.

Heemskerk, I., Lecuit, T., and LeGoff, L. (2014). Dynamic clonal analysis based on chronic in vivo imaging allows multiscale quantification of growth in the Drosophila wing disc. Development *141*, 2339-2348.

Hernandez-Segura, A., Nehme, J., and Demaria, M. (2018). Hallmarks of Cellular Senescence. Trends in cell biology.

Herrera, S.C., and Bach, E.A. (2019). JAK/STAT signaling in stem cells and regeneration: from Drosophila to vertebrates. Development *146*.

Herrera, S.C., Martin, R., and Morata, G. (2013). Tissue homeostasis in the wing disc of Drosophila melanogaster: immediate response to massive damage during development. PLoS genetics *9*, e1003446.

Herrera, S.C., and Morata, G. (2014). Transgressions of compartment boundaries and cell reprogramming during regeneration in Drosophila. eLife *3*, e01831.

Huh, J.R., Guo, M., and Hay, B.A. (2004). Compensatory proliferation induced by cell death in the Drosophila wing disc requires activity of the apical cell death caspase Dronc in a nonapoptotic role. Current biology : CB *14*, 1262-1266.

Hyun, J., Becam, I., Yanicostas, C., and Bohmann, D. (2006). Control of G2/M transition by Drosophila Fos. Molecular and cellular biology *26*, 8293-8302.

Igaki, T. (2009). Correcting developmental errors by apoptosis: lessons from Drosophila JNK signaling. Apoptosis *14*, 1021-1028.

Igaki, T., Kanda, H., Yamamoto-Goto, Y., Kanuka, H., Kuranaga, E., Aigaki, T., and Miura, M. (2002). Eiger, a TNF superfamily ligand that triggers the Drosophila JNK pathway. The EMBO journal *21*, 3009-3018.

Igaki, T., Pagliarini, R.A., and Xu, T. (2006). Loss of cell polarity drives tumor growth and invasion through JNK activation in Drosophila. Current biology : CB *16*, 1139-1146.

Igaki, T., Pastor-Pareja, J.C., Aonuma, H., Miura, M., and Xu, T. (2009). Intrinsic tumor suppression and epithelial maintenance by endocytic activation of Eiger/TNF signaling in Drosophila. Developmental cell *16*, 458-465.

Johnston, L.A., and Sanders, A.L. (2003). Wingless promotes cell survival but constrains growth during Drosophila wing development. Nat Cell Biol *5*, 827-833.

Katsuyama, T., Comoglio, F., Seimiya, M., Cabuy, E., and Paro, R. (2015). During Drosophila disc regeneration, JAK/STAT coordinates cell proliferation with Dilp8-mediated developmental delay. Proceedings of the National Academy of Sciences of the United States of America.

Khan, S.J., Abidi, S.N.F., Skinner, A., Tian, Y., and Smith-Bolton, R.K. (2017). The Drosophila Duox maturation factor is a key component of a positive feedback loop that sustains regeneration signaling. PLoS genetics *13*, e1006937.

Kulshammer, E., and Uhlirova, M. (2013). The actin cross-linker Filamin/Cheerio mediates tumor malignancy downstream of JNK signaling. Journal of cell science *126*, 927-938.

References

Kuranaga, E., Kanuka, H., Igaki, T., Sawamoto, K., Ichijo, H., Okano, H., and Miura, M. (2002). Reaper-mediated inhibition of DIAP1-induced DTRAF1 degradation results in activation of JNK in Drosophila. Nat Cell Biol *4*, 705-710.

Lee, J.H., Lee, C.W., Park, S.H., and Choe, K.M. (2017). Spatiotemporal regulation of cell fusion by JNK and JAK/STAT signaling during Drosophila wound healing. Journal of cell science *130*, 1917-1928.

Losick, V.P., Fox, D.T., and Spradling, A.C. (2013). Polyploidization and cell fusion contribute to wound healing in the adult Drosophila epithelium. Current biology : CB *23*, 2224-2232.

Luo, X., Puig, O., Hyun, J., Bohmann, D., and Jasper, H. (2007). Foxo and Fos regulate the decision between cell death and survival in response to UV irradiation. The EMBO journal *26*, 380-390.

Martin, R., Pinal, N., and Morata, G. (2017). Distinct regenerative potential of trunk and appendages of Drosophila mediated by JNK signalling. Development.

Mata, J., Curado, S., Ephrussi, A., and Rorth, P. (2000). Tribbles coordinates mitosis and morphogenesis in Drosophila by regulating string/CDC25 proteolysis. Cell *101*, 511-522.

Mattila, J., Omelyanchuk, L., Kyttala, S., Turunen, H., and Nokkala, S. (2005). Role of Jun N-terminal Kinase (JNK) signaling in the wound healing and regeneration of a Drosophila melanogaster wing imaginal disc. The International journal of developmental biology *49*, 391-399.

McClure, K.D., Sustar, A., and Schubiger, G. (2008). Three genes control the timing, the site and the size of blastema formation in Drosophila. Developmental biology *319*, 68-77.

Morata, G., Shlevkov, E., and Perez-Garijo, A. (2011). Mitogenic signaling from apoptotic cells in Drosophila. Dev Growth Differ *53*, 168-176.

Moreno, E., Yan, M., and Basler, K. (2002). Evolution of TNF signaling mechanisms: JNK-dependent apoptosis triggered by Eiger, the Drosophila homolog of the TNF superfamily. Current biology : CB *12*, 1263-1268.

Munoz-Espin, D., Canamero, M., Maraver, A., Gomez-Lopez, G., Contreras, J., Murillo-Cuesta, S., Rodriguez-Baeza, A., Varela-Nieto, I., Ruberte, J., Collado, M.*, et al*. (2013). Programmed cell senescence during mammalian embryonic development. Cell *155*, 1104-1118.

Nakamura, M., Ohsawa, S., and Igaki, T. (2014). Mitochondrial defects trigger proliferation of neighbouring cells via a senescence-associated secretory phenotype in Drosophila. Nature communications *5*, 5264.

Otsuki, L., and Brand, A.H. (2018). Cell cycle heterogeneity directs the timing of neural stem cell activation from quiescence. Science *360*, 99-102.

Park, S., Gonzalez, D.G., Guirao, B., Boucher, J.D., Cockburn, K., Marsh, E.D., Mesa, K.R., Brown, S., Rompolas, P., Haberman, A.M., *et al*. (2017). Tissue-scale coordination of cellular behaviour promotes epidermal wound repair in live mice. Nat Cell Biol *19*, 155-163.

Pastor-Pareja, J.C., Grawe, F., Martin-Blanco, E., and Garcia-Bellido, A. (2004). Invasive cell behavior during Drosophila imaginal disc eversion is mediated by the JNK signaling cascade. Developmental cell *7*, 387-399.

Pastor-Pareja, J.C., Wu, M., and Xu, T. (2008). An innate immune response of blood cells to tumors and tissue damage in Drosophila. Disease models & mechanisms *1*, 144-154; discussion 153.

Pastor-Pareja, J.C., and Xu, T. (2013). Dissecting social cell biology and tumors using Drosophila genetics. Annual review of genetics *47*, 51-74.

Pawlikowski, J.S., Adams, P.D., and Nelson, D.M. (2013). Senescence at a glance. Journal of cell science *126*, 4061-4067.

Perez-Garijo, A. (2018). When dying is not the end: Apoptotic caspases as drivers of proliferation. Seminars in cell & developmental biology *82*, 86-95.

Perez-Garijo, A., Fuchs, Y., and Steller, H. (2013). Apoptotic cells can induce non-autonomous apoptosis through the TNF pathway. eLife *2*, e01004.

Perez-Garijo, A., Martin, F.A., and Morata, G. (2004). Caspase inhibition during apoptosis causes abnormal signalling and developmental aberrations in Drosophila. Development *131*, 5591-5598.

Perez-Garijo, A., Shlevkov, E., and Morata, G. (2009). The role of Dpp and Wg in compensatory proliferation and in the formation of hyperplastic overgrowths caused by apoptotic cells in the Drosophila wing disc. Development *136*, 1169-1177.

Perez, E., Lindblad, J.L., and Bergmann, A. (2017). Tumor-promoting function of apoptotic caspases by an amplification loop involving ROS, macrophages and JNK in Drosophila. eLife *6*.

Pinal, N., Calleja, M., and Morata, G. (2019). Pro-apoptotic and pro-proliferation functions of the JNK pathway of Drosophila: roles in cell competition, tumorigenesis and regeneration. Open Biol *9*, 180256.

Pinal, N., Martin, M., Medina, I., and Morata, G. (2018). Short-term activation of the Jun N-terminal kinase pathway in apoptosis-deficient cells of Drosophila induces tumorigenesis. Nature communications *9*, 1541.

Qi, S., and Calvi, B.R. (2016). Different cell cycle modifications repress apoptosis at different steps independent of developmental signaling in Drosophila. Mol Biol Cell *27*, 1885-1897.

Ramet, M., Lanot, R., Zachary, D., and Manfruelli, P. (2002). JNK signaling pathway is required for efficient wound healing in Drosophila. Developmental biology *241*, 145-156.

References

Repiso, A., Bergantinos, C., and Serras, F. (2013). Cell fate respecification and cell division orientation drive intercalary regeneration in Drosophila wing discs. Development *140*, 3541-3551.

Restall, I.J., Parolin, D.A., Daneshmand, M., Hanson, J.E., Simard, M.A., Fitzpatrick, M.E., Kumar, R., Lavictoire, S.J., and Lorimer, I.A. (2015). PKCiota depletion initiates mitotic slippage-induced senescence in glioblastoma. Cell Cycle *14*, 2938-2948.

Ritschka, B., Storer, M., Mas, A., Heinzmann, F., Ortells, M.C., Morton, J.P., Sansom, O.J., Zender, L., and Keyes, W.M. (2017). The senescence-associated secretory phenotype induces cellular plasticity and tissue regeneration. Genes & development *31*, 172-183.

Ryoo, H.D., Gorenc, T., and Steller, H. (2004). Apoptotic cells can induce compensatory cell proliferation through the JNK and the Wingless signaling pathways. Developmental cell *7*, 491-501.

Sandoval-Guzman, T., and Currie, J.D. (2018). The journey of cells through regeneration. Current opinion in cell biology *55*, 36-41.

Santabarbara-Ruiz, P., Lopez-Santillan, M., Martinez-Rodriguez, I., Binagui-Casas, A., Perez, L., Milan, M., Corominas, M., and Serras, F. (2015). ROS-Induced JNK and p38 Signaling Is Required for Unpaired Cytokine Activation during Drosophila Regeneration. PLoS genetics *11*, e1005595.

Schubiger, G. (1971). Regeneration, duplication and transdetermination in fragments of the leg disc of Drosophila melanogaster. Developmental biology *26*, 277-295.

Schuster, K.J., and Smith-Bolton, R.K. (2015). Taranis Protects Regenerating Tissue from Fate Changes Induced by the Wound Response in Drosophila. Developmental cell *34*, 119-128.

Shlevkov, E., and Morata, G. (2012). A dp53/JNK-dependant feedback amplification loop is essential for the apoptotic response to stress in Drosophila. Cell Death Differ *19*, 451-460.

Sluss, H.K., Han, Z., Barrett, T., Goberdhan, D.C., Wilson, C., Davis, R.J., and Ip, Y.T. (1996). A JNK signal transduction pathway that mediates morphogenesis and an immune response in Drosophila. Genes & development *10*, 2745-2758.

Smith-Bolton, R.K., Worley, M.I., Kanda, H., and Hariharan, I.K. (2009). Regenerative growth in Drosophila imaginal discs is regulated by Wingless and Myc. Developmental cell *16*, 797-809.

Storer, M., Mas, A., Robert-Moreno, A., Pecoraro, M., Ortells, M.C., Di Giacomo, V., Yosef, R., Pilpel, N., Krizhanovsky, V., Sharpe, J., *et al*. (2013). Senescence is a developmental mechanism that contributes to embryonic growth and patterning. Cell *155*, 1119-1130.

Sun, D., and Buttitta, L. (2017). States of G0 and the proliferation-quiescence decision in cells, tissues and during development. The International journal of developmental biology *61*, 357-366.

Sun, G., and Irvine, K.D. (2011). Regulation of Hippo signaling by Jun kinase signaling during compensatory cell proliferation and regeneration, and in neoplastic tumors. Developmental biology *350*, 139-151.

Sun, G., and Irvine, K.D. (2013). Ajuba family proteins link JNK to Hippo signaling. Sci Signal *6*, ra81.

Sun, G., and Irvine, K.D. (2014). Control of growth during regeneration. Current topics in developmental biology *108*, 95-120.

Sustar, A., Bonvin, M., Schubiger, M., and Schubiger, G. (2011). Drosophila twin spot clones reveal cell division dynamics in regenerating imaginal discs. Developmental biology *356*, 576-587.

Uchida, S., Yoshioka, K., Kizu, R., Nakagama, H., Matsunaga, T., Ishizaka, Y., Poon, R.Y., and Yamashita, K. (2009). Stress-activated mitogen-activated protein kinases c-Jun NH2-terminal kinase and p38 target Cdc25B for degradation. Cancer Res *69*, 6438-6444.

Uhlirova, M., and Bohmann, D. (2006). JNK- and Fos-regulated Mmp1 expression cooperates with Ras to induce invasive tumors in Drosophila. The EMBO journal *25*, 5294-5304.

Ursprung, H. (1959). Fragmentation and radiation experiments to determine the determination and fate map of the Drosophila genital disc. Roux's Arch Dev Biol *151*, 501-558.

Wang, Y., Antunes, M., Anderson, A.E., Kadrmas, J.L., Jacinto, A., and Galko, M.J. (2015). Integrin Adhesions Suppress Syncytium Formation in the Drosophila Larval Epidermis. Current biology : CB *25*, 2215-2227.

Wells, B.S., Yoshida, E., and Johnston, L.A. (2006). Compensatory proliferation in Drosophila imaginal discs requires Dronc-dependent p53 activity. Current biology : CB *16*, 1606-1615.

Worley, M.I., Alexander, L.A., and Hariharan, I.K. (2018). CtBP impedes JNK- and Upd/STAT-driven cell fate misspecifications in regenerating Drosophila imaginal discs. eLife *7*.

Worley, M.I., Setiawan, L., and Hariharan, I.K. (2012). Regeneration and transdetermination in Drosophila imaginal discs. Annual review of genetics *46*, 289-310.

Wu, M., Pastor-Pareja, J.C., and Xu, T. (2010). Interaction between Ras(V12) and scribbled clones induces tumour growth and invasion. Nature *463*, 545-548.

Yoo, S.K., Pascoe, H.G., Pereira, T., Kondo, S., Jacinto, A., Zhang, X., and Hariharan, I.K. (2016). Plexins function in epithelial repair in both Drosophila and zebrafish. Nature communications *7*, 12282.

Zeitlinger, J., and Bohmann, D. (1999). Thorax closure in Drosophila: involvement of Fos and the JNK pathway. Development *126*, 3947-3956.

Acknowledgements

I am extremely grateful to all the people who have accompanied me through this wonderful journey.

Thank you Anne for the giving me the opportunity to join your lab. Thanks for your continuous support, for keeping your door always open, and for constantly contributing with innovative and challenging ideas. One of the most important things I learned from you is that sometimes quick-and-dirty is also an option. Besides your scientific support, you also contributed to create the "Classen lab culture", which has been very important to me.

Thanks to all the lab in Munich – Addie, Christina, Isabelle, Marco, Ramya, Vanessa – and in Freiburg – Abhay, Carlo, Deepti, Friedericke, Janhvi – for being friends, and not just colleagues (despite what somebody told once at the airport security).

I would like to thank the members of my TAC for their support through the years, and the members of my exam committee, who agreed on reading and evaluating this thesis. Thanks also to Mirka Uhlirova for collaborating on the G2 stalling project. I also acknowledge the support of IMPRS-LS graduate program, and the imaging and flow cytometry facilities at LMU, ZBSA and MPI-IE for technical help.

Thanks to my family, for your support despite the distance and especially for giving me the opportunity to do what I like most. I feel really privileged.

And most importantly, thank you Martina for always being by my side.

Curriculum vitae

Andrea Cosolo

EDUCATION

2013 – 2019   **PhD in Biology** | Ludwig Maximilians University, Munich (Germany)

2010 – 2012   **Master's Degree in Medical Biotechnology** *summa cum laude* | University of Udine (Italy)

2007 – 2010   **Bachelor's Degree in Biotechnology** *summa cum laude* | University of Udine (Italy)

PUBLICATIONS

Cosolo, A., Jaiswal, J., Csordas, G., Grass, I., Uhlirova, M., & Classen, A. K. (2019). JNK-dependent cell cycle stalling in G2 promotes survival and senescence-like phenotypes in tissue stress. Elife, 8. doi:10.7554/eLife.41036

La Fortezza, M., Grigolon, G., Cosolo, A., Pinduyrin, A., Breimann, L., Blum, H., van Steensel, B., Classen, A. K. (2018). DamID profiling of dynamic Polycomb-binding sites in Drosophila imaginal disc development and tumorigenesis. Epigenetics Chromatin, 11(1), 27. doi:10.1186/s13072-018-0196-y

La Fortezza, M., Schenk, M., Cosolo, A., Kolybaba, A., Grass, I., & Classen, A. K. (2016). JAK/STAT signalling mediates cell survival in response to tissue stress. Development, 143(16), 2907-2919. doi:10.1242/dev.132340

AWARDS AND FELLOWSHIPS

Prize for Best Poster European Drosophila Research Conference 2015

Prize for Best Poster IMPRS-LS symposium 2015

IMPRS-LS member International Max Planck Research School, class of 2013